UNIVERSITE DE LIMOGES

ECOLE DOCTORALE SCIENCES ET INGENIERIE POUR L'INFORMATION

FACULTE DES SCIENCES ET TECHNIQUES

Année 2011 Thèse N° 67.2011

THESE

pour obtenir le grade de

DOCTEUR DE L'UNIVERSITÉ DE LIMOGES

Spécialité : "Electronique des Hautes Fréquences, Photonique et Systèmes"

présentée et soutenue par

Sylvain JOLIVET

le 06 Décembre 2011

Limitations et Opportunités des Circuits Actifs pour la Réalisation d'un Filtrage RF Haute Performance et Accordable en Fréquence pour les Récepteurs TV

Thèse dirigée par Bernard JARRY et Julien LINTIGNAT

JURY

M. Raymond QUERE, Professeur à l'Université de Limoges – XLIM	Président
M. Hervé BARTHELEMY, Professeur à l'Université Sud Toulon Var – IM2NP	Rapporteur
M. Eric RIUS, Professeur à l'Université de Bretagne Occidentale – Lab-STICC	Rapporteur
M. Philippe EUDELINE, Directeur Technologie et Innovation – Thales Air Systems	Examinateur
M. Didier LOHY, Directeur Technologie et Innovation – NXP	Examinateur
M. Sébastien AMIOT, Architecte Circuits RF, Ingénieur Senior Principal – NXP	Examinateur
M. Bernard JARRY, Professeur à l'Université de Limoges – XLIM	Examinateur
M. Julien LINTIGNAT, Maître de Conférence à l'Université de Limoges – XLIM	Examinateur
M. Stéphane BILA, Chargé de Recherche CNRS **–** XLIM	Invité

A ma femme Vanessa,

A mes parents, A mon frère,

Acknowledgments

En préambule à ce mémoire, je souhaite adresser ici tous mes remerciements aux personnes qui m'ont apporté leur aide et leur soutien, et qui ont ainsi contribué à l'élaboration de ce mémoire.

En particulier, je remercie sincèrement Didier Lohy de m’avoir permis de poursuivre mes études d’ingénieur en microélectronique par une thèse de doctorat CIFRE au sein de la BL TV Front-End de NXP Semiconductors Caen. Je souhaite également adresser mes remerciements à mes directeurs de thèse Bernard Jarry et Julien Lintignat du laboratoire XLIM de Limoges pour les discussions que j’ai pu avoir avec eux et leurs suggestions. Je tiens aussi à remercier Sébastien Amiot d’avoir accepté de superviser mes travaux de thèse à NXP, ainsi que pour ses conseils et ses remarques pertinentes qui m’ont permis de progresser tant sur le plan technique que rédactionnel tout au long de ces trois années.

Par ailleurs, j’adresse également mes remerciements à Hervé Barthélémy et Eric Rius pour avoir accepté d’être rapporteur de cette thèse, ainsi qu’à Raymond Quéré, Philippe Eudeline et Stéphane Bila pour leur participation au jury.

Un grand Merci à Olivier Crand et à Simon Bertrand pour leur support technique et leur bonne humeur. Je n’oublierais pas non plus votre précieuse contribution au tape-out du filtre de Rauch sur silicium. Merci aussi aux collègues de bureau pour leur gentillesse et leur humour : Xavier Pruvost, Markus Kristen, Samuel Cazin, Dominique Boulet, Patrick Attia et la HDMI-team. Puisqu’il me serait difficile de citer tout le monde, je remercie la BL TV Front-End dans son ensemble pour l’accueil chaleureux que j’ai reçu. Ces trois années parmi vous sont passées bien vite.

J’ai aussi une pensée particulière pour mes bons collègues de thèse Amandine Lesellier, Esteban Cabanillas et Nico Prou. Merci pour votre bonne compagnie, ce fut un plaisir de travailler à vos côtés ! Merci également à l’Ancien, tes sages conseils ont été une source d’inspiration.

J'adresse mes plus profonds remerciements à mes parents Chantal et Philippe qui m'ont toujours soutenu et incité à persévérer au cours de cette thèse. Grâce à vous ces efforts ont payé. Ce manuscrit vous est dédié, ainsi qu’à Simon. Merci à toi d’avoir pris le temps de relire mon mémoire.

Enfin Merci à toi Vanessa du fond du cœur pour m’avoir supporté pendant ces trois années. Merci pour ton amour et pour ta patience, merci pour ton soutien sans faille et pour tes encouragements dans les moments de doute. Tu m’as aussi communiqué tes propres qualités de rigueur et d’amour du travail bien fait. Ce manuscrit te doit beaucoup et ne serait pas ce qu’il est sans toi.

Summary

French Introduction

Les signaux TV sont transmis de manière analogique. Une modulation, soit analogique ou digitale, de ces signaux leur permet de porter le codage notamment des pixels, de la couleur et du son. La présente thèse se place dans le cadre la réception de signaux transmis par voie terrestre et par câble, ce qui représente un spectre fréquentiel s'étalant de 42 à 1002MHz par canaux d'une largeur de 6 à 8MHz selon le standard utilisé.

La réception des signaux TV est constituée de deux étapes. D'abord la réception du signal RF, qui nécessite l'amplification du signal et le filtrage d'un canal désiré parmi tous ceux reçus. Cette étape doit limiter au maximum les dégradations supplémentaires du signal. Cela signifie que cette étape doit être réalisée avec un faible bruit pour pouvoir recevoir des signaux de faible puissance, et une forte linéarité pour être capable de recevoir le canal désirés malgré la présence d'interféreurs forts. Ces contraintes de dynamique se retrouvent sur chacun des blocs qui constituent le récepteur TV. Son rôle est donc de fournir le canal désiré le plus propre possible pour réaliser la démodulation, qui est la seconde étape, dans de bonnes conditions. Toute dégradation du signal peut en effet mener à des erreurs de démodulation, comme un pixel affiché dans une mauvaise couleur sur l'écran de télévision par exemple.

Aujourd'hui, l'architecture des récepteurs TV est constituée d'un amplificateur faible bruit (LNA) suivi d'un mélangeur pour pouvoir filtrer le canal désiré à plus basse fréquence. Cela permet de filtrer le canal de manière plus précise. Cependant, un filtrage RF est aussi nécessaire pour assurer la qualité de la réception, protéger le mixeur et réaliser un premier filtrage du spectre reçu. Pour relâcher ses contraintes en termes de dynamique, le filtre RF peut être placé entre le LNA et le mélangeur, pourvu que le LNA soit assez performant. En plus de bonnes performances en bruit et en linéarité, le filtre RF doit être accordable en fréquence pour pouvoir être centré sur le canal désiré partout dans la bande 42 – 1002MHz. Il doit également être sélectif pour réaliser un premier filtrage des signaux non-désirés forts qui peuvent dégrader la qualité de la réception.

Ces signaux peuvent être de trois natures différentes. Il s'agit d'abord de rejeter les fréquences d'harmoniques impaires. En effet, le mélangeur utilise un oscillateur local à signal carré et provoque la conversion à basse fréquence des harmoniques impaires du spectre RF reçu. D'autre part, les canaux adjacents au canal désirés doivent être atténués dès le début de la chaîne de réception pour assurer la compatibilité avec les standards internationaux comme l'ATSC A/74. Enfin, les signaux non-TV situés dans la bande 42 – 1002MHz doivent aussi être rejetés. On peut citer comme exemple les signaux FM ou TETRA.

Habituellement, des résonateurs LC assurent sur ce filtrage RF. Pour ce faire, ils utilisent des varactors ou des bancs de capacités mis en parallèle d'inductance. Cependant, atteindre le bas de la bande VHF à 42MHz nécessite l'utilisation de valeurs d'inductance d'environ 100nH. Alors, l'intégration de ces inductances sur silicium s'avère compliquée. De plus, les inductances en composants discrets ou intégrées sur silicium sont soumises à des

couplages électromagnétiques qui peuvent dégrader les performances requises. Ces inductances limitent aujourd'hui l'intégration totale du récepteur TV sur silicium.

C'est pourquoi l'étude se concentre sur un filtrage uniquement actif, ne comportant pas d'inductance. Il s'agit d'étudier les performances de ce type de circuit ainsi que leurs limitations et les opportunités technologiques qui peuvent se présenter. Cela nous a mené à poser la problématique suivante :

Limitations et Opportunités des Circuits Actifs pour la Réalisation d'un Filtrage RF Haute Performance et Accordable en Fréquence pour les Récepteurs TV

I. Introduction to TV tuners and to RF Filtering

I.1 TV Signals Transmission

I.1.a Video Signal Transmissions

I.1.a.i Image Generation

A TV screen consists in several thousands of pixels associated together on a rectangular panel. Each pixel is made of three photo-emittive cells, each covered by a different colored filter: a red, a green and a blue one. Using the additive colors principle, depicted on Figure 1, the screen is able to display a colored picture. This coding of colors may rely, for instance, on three colors. This is called RGB coding, for Red-Green-Blue.

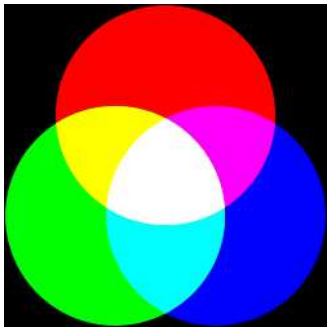

Figure 1. Additive colors principle

I.1.a.ii Transmission of a TV Signal – Example of Analog Modulation

As it may be seen on Figure 2, to transmit a TV signal, the RGB coding of the picture is multiplexed with sound, synchronization signals and teletext pieces of information. This complete TV signal is then modulated, in order to be adapted to the transmission medium, and emitted through electromagnetic waves or cable.

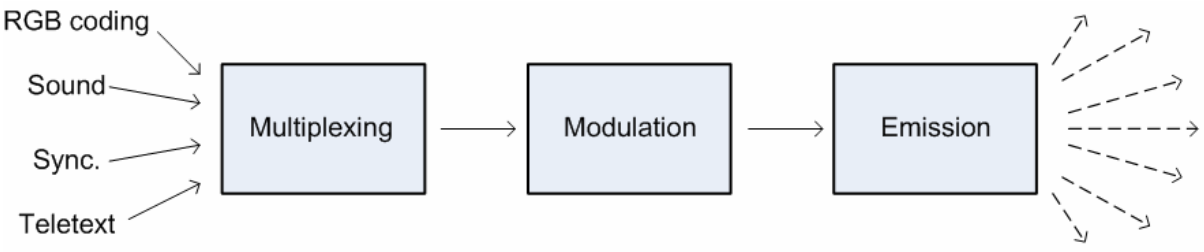

Figure 2. From picture coding to signal emission

I.1.b Modulation

Modulation is the principle of a signal transmission. As explained in [I.1], modulation is required in both wired and wireless system. Indeed, coaxial cables shielding is better at high frequencies whereas for wireless communications, the size of the antenna should be a significant fraction of the wavelength to realize a sufficient gain. Depending on the nature of the source signal, *i.e.* whether it is analog or digital, the modulation is different but it usually consists in a high-frequency carrier modulated by the useful signal.

I.1.b.i Analog modulations

Most common analog modulations are AM, PM and FM, which respectively stand for amplitude, phase and frequency modulation. Assuming a high frequency signal *S(t)* of the form

$$S(t) = A(t)\cos\left(\omega_c t + \Phi(t)\right), \tag{I.1}$$

amplitude modulation actually consists in replacing *A(t)* by the original signal

$$A(t) = A\left(1 + M\cos\left(\omega_m t\right)\right). \tag{I.2}$$

Time and frequency representations of AM modulations are depicted in Figure 3:

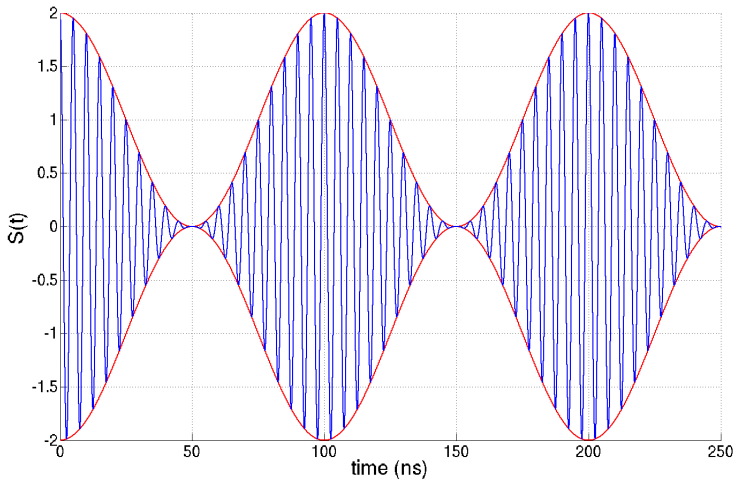

Figure 3. Time representation of an AM modulation

Phase and frequency modulations consist in modulating respectively the phase $\Phi(t)$ and ω_c in *S(t)* shown in Equation (I.1). The time representation of an FM modulation is illustrated in Figure 4. It is worth noticing that the PM modulation of a sine wave, which is the particular case observed in Figure 4, gives the same results as the FM modulation.

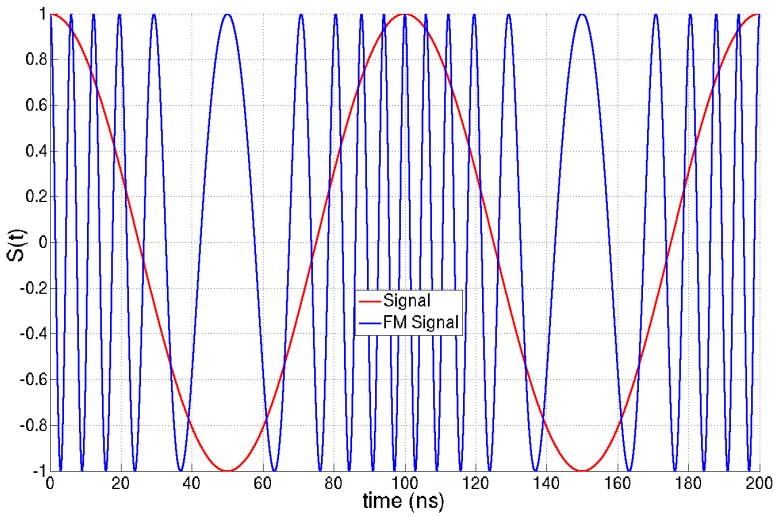

Figure 4. Time representations of an FM modulation

I.1.b.ii Digital modulations

In digital systems, the carrier is modulated by a digital baseband signal. Modulations similar to the analog ones are possible, modulating the amplitude (ASK for Amplitude Shift Keying), the phase (PSK for Phase Shift Keying) or the frequency (FSK for Frequency Shift Keying). Time representations of such modulations are given in Figure 5.

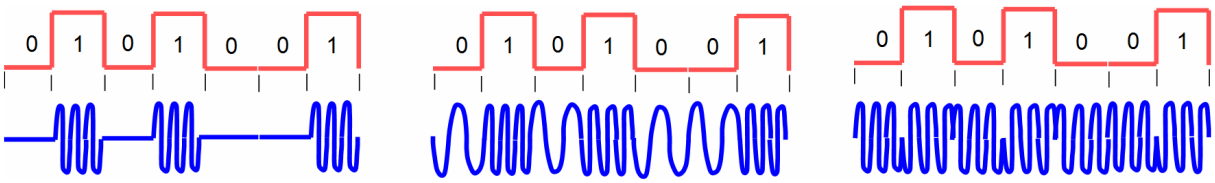

Figure 5. ASK (a), FSK (b) and PSK (c) modulations

In many applications, the binary data stream is divided by sets of two (or more) bits and is modulated using a single carrier. As said in [I.1], this is possible because sine and cosine are orthogonal functions so each set of two bits has a single representation in this space. Such modulation is called IQ modulation, I and Q standing for In-phase and Quadrature-phase.

The major advantage of IQ modulation is that symbol rate becomes half the bit rate. Hence, the required bandwidth is divided by two, which makes it a very popular solution.

As it may be seen in Figure 6, assuming X and Y are two simultaneous bits forming a set and ω_c is the carrier frequency, the output *S(t)* is then:

$$S(t) = X\cos(\omega_c t) + Y\sin(\omega_c t)). \qquad \text{(I.3)}$$

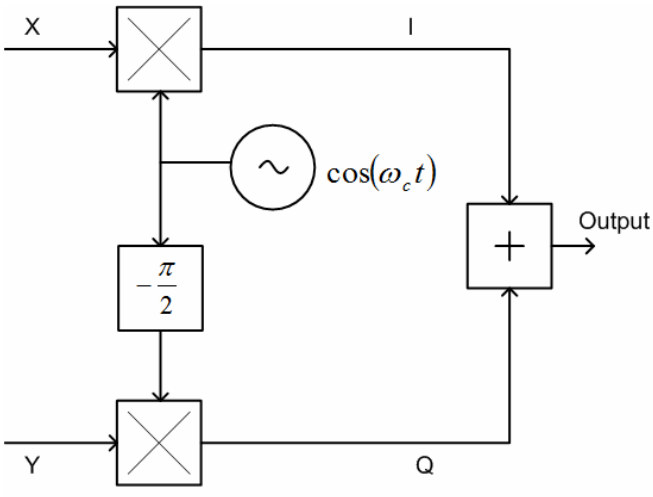

Figure 6. I-Q modulation

Nowadays, most used IQ modulations are QAM and QPSK. QAM actually consist in coding the signal with different amplitudes: for instance, +A and –A for each I and Q path. Such coding is called 4QAM. PSK uses phase to code the signal, as depicted in Figure 7 for example.

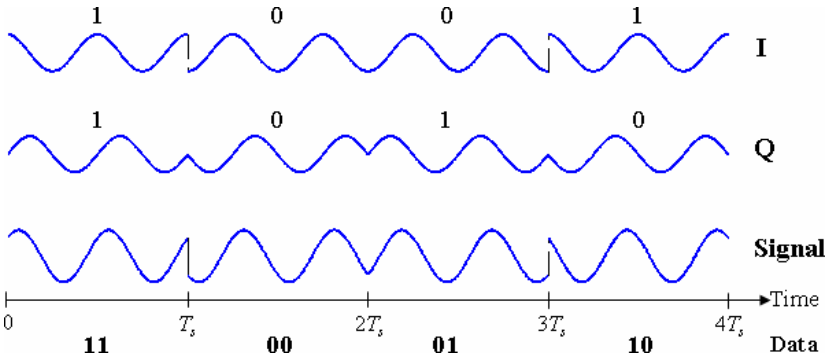

Figure 7. Time representations of I, Q and output signals using a 4PSK modulation

More complex modulations using more bits per symbol are also used, such as 256QAM or even 1024QAM. It is also possible to use combine both modulation types in a 16APSK modulation.

These modulations can be described in a Quadrature-phase versus In-phase graph, as illustrated in Figure 8. These graphs are called ***constellations***.

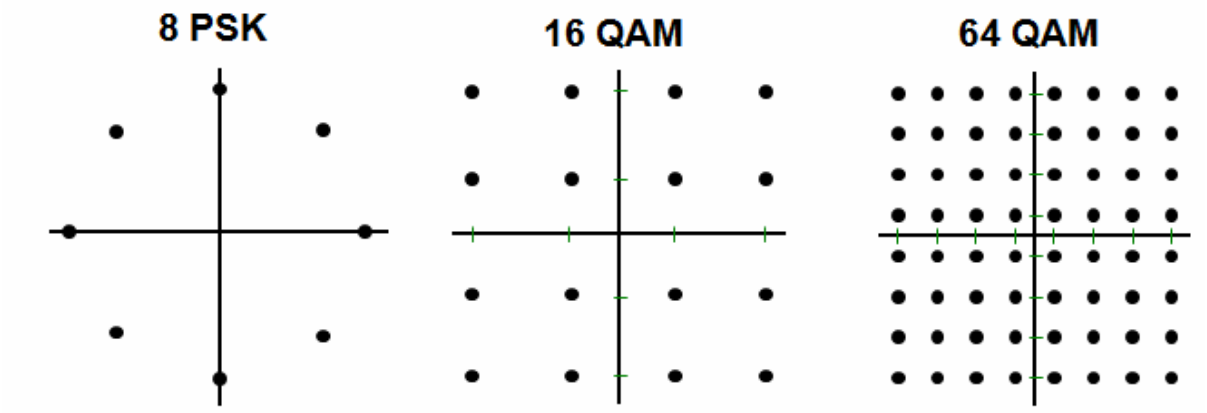

Figure 8. 8PSK (a) , 16QAM (b) and 64QAM (c) constellations

I.1.b.iii Analog and Digital Standards

For compatibility and interoperability reasons, all TV transmissions depend on standards. These standards aim at specifying how TV transmissions take place, and in particular they define operating frequencies, channel bandwidths, allowed emission power levels, modulation types, picture formats... Emitted signals are based on either an analog or a digital modulation.

Analog signals mainly use three different standards: ***NTSC***, ***PAL*** and ***SECAM***. These standards, used since the beginning of color TV transmissions, are less and less broadcasted since the quality of the reception is strongly related to the reception power level.

The past ten years have seen the progressive emergence of digital TV. One of its advantages is that the quality of the reception is not related to the power level: it only requires a threshold power level to operate in good conditions. Above the threshold power level, the quality of the reception felt by the end-user becomes independent of the received power. This

makes the covering of a large territory easier and less expensive. Indeed, single frequency networks (known as SFNs) become possible due to the ability to treat echoes of digital modulations.

Furthermore, up to eight single definition programs can be packed in a single TV channel with the MPEG-2 norm, where only one analog program was emitted before. This evolution drastically reduced channels broadcasting costs. Digital standards are also able to handle more advanced compression formats like MPEG-4, which allow the use of high-definition picture and sound formats.

There are four main digital standards across the world, as it may be seen in Figure 9 for terrestrial signals: ***ATSC*** for Northern America, ***ISDB*** for Brazil and Japan, ***DMB*** for China and finally, ***DVB*** for Europe, Australia, India and Russia.

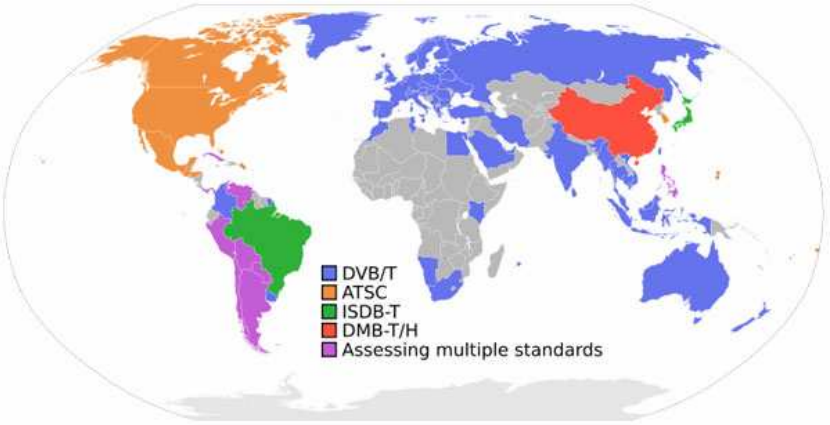

Figure 9. Used digital Standard According to Countries

In France for instance, the analog switch-off has already taken place: only digital TV is broadcasted. However, it has not yet taken place everywhere in the world. The coexistence of analog and digital standards will still last for more than a decade in some countries. Hence, this has to be taken into account when designing the TV receiver.

I.1.c Satellite, Cable & Terrestrial spectra

I.1.c.i TV Transmission Modes

Broadcasted TV signals can be transmitted by three different means, corresponding to three different reception modes: cable, satellite and terrestrial.

Some TV transmissions take place using ***cable networks***.

Satellite transmissions actually consist in transmitting the TV electromagnetic waves by a satellite between the emitting and the reception parabolas, as illustrated in Figure 10.

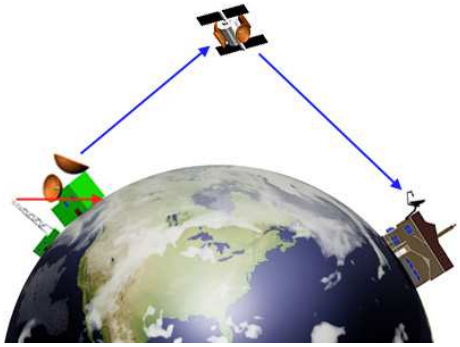

Figure 10. Satellite TV transmissions

Terrestrial transmissions correspond to TV signals emitted with the help of several antennas located everywhere in a country. To pick up these electromagnetic waves, an antenna has to be located on the roof of the house.

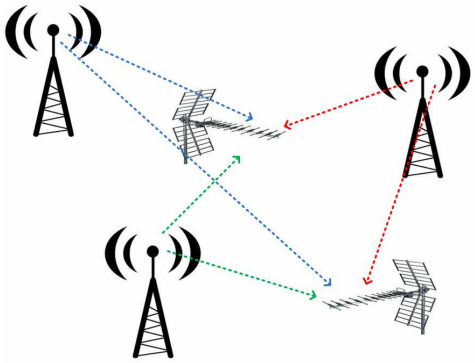

Figure 11. Terrestrial TV transmissions

All these TV signals have their own specificities and have to be studied, to specify as accurately as possible the TV receiver requirements. Only cable and terrestrial signals are considered in the following. Satellite reception does not enter the scope of study of the present PhD thesis because of their different constraints.

I.1.c.ii Cable spectrum

The cable spectrum is fully loaded and covers frequencies from 45 to 1002MHz, with channel bandwidths between 6 and 8 MHz according to the standard.

It is worth adding that both digital and analog signals coexist. However, the cable operator determines a power at which all channels are transmitted. Thus, all channels are received with almost the same power level, as shown on Figure 12 [I.2].

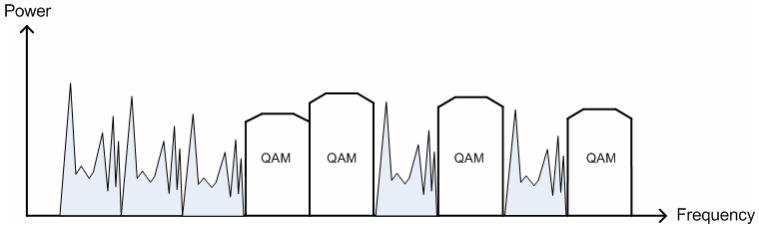

Figure 12. Cable TV Spectrum

I.1.c.iii Terrestrial spectrum

First of all, the terrestrial spectrum is divided into several TV sub-bands, as depicted in Figure 13. These TV sub-bands have to coexist with non-TV bands, like the CB[1], the FM[2] bands (88-108MHz), TETRA[3] or GSM[4]. These signals act as interferers which may degrade the quality of the reception and have to be filtered out by the TV tuner.

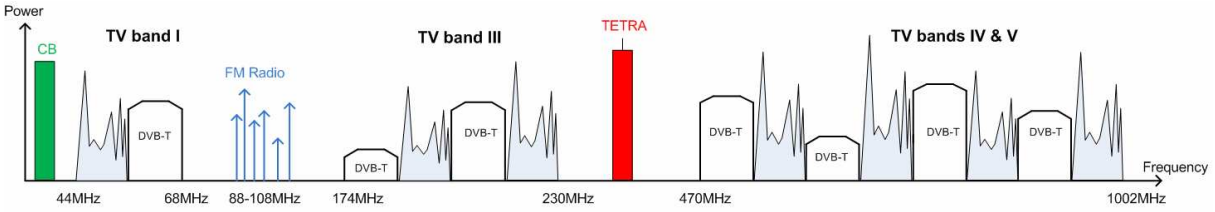

Figure 13. Terrestrial TV Spectrum

As said previously, in the countries where the analog switch-off has not yet taken place, digital and analog signals still coexist. Figure 14 illustrates the TV spectrum received in Caen before the analog switch-off. Signals from three antennas are received simultaneously: Caen, Le Havre and Mont-Pinçon. Since the received power depends on the distance between the emitting and the receiving antennas, a weak desired signal received from a far-away antenna can coexist with a strong unwanted interferer emitted very close to the reception antenna. Hence, the TV tuner should be able to handle signals having power differences which can go up to 57dB according to *ATSC A/74* requirements [I.3].

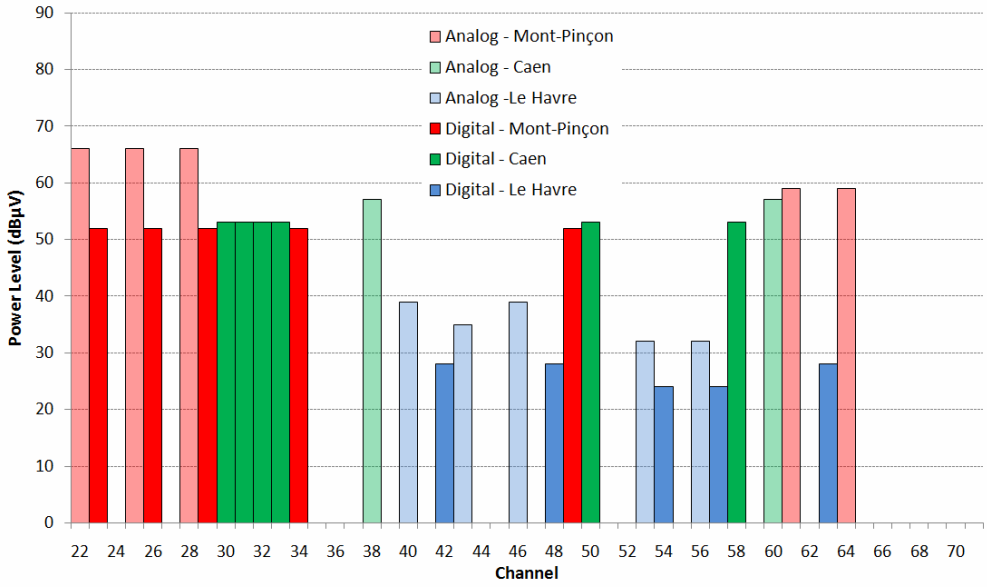

Figure 14. Terrestrial TV spectrum in Caen (before analog switch-off)

[1] CB, standing for *Cell Broadcast*, is a mobile radio standard used for the delivery of messages to multiple users in a specified geographical area.
[2] FM, standing for *Frequency Modulation*, is a broadcast technology used by radio stations.
[3] TETRA, standing for *Terrestrial TRuncked Radio*, is a mobile radio standard designed for use by government agencies or emergency services.
[4] GSM, standing for *Global System for Mobile Communications*, is a standard used for cellular networks.

The transmission of the signal through several paths can also be a drawback. Indeed, before being received with a single antenna, terrestrial signals are subject to multipath propagation and also to echoes, especially in mountain areas. Degradation and delay of the signal due to these phenomena may cause interferences between one transmitted symbol and its subsequent symbols, thus degrading their correct detection. This phenomenon is called ***intersymbol interferences*** (ISI) and may strongly degrade the reception of the signal. To reduce the impacts of ISI, more complex modulations than those previously described are used, such as multiple carriers (COFDM) or modulations which eliminate spectral redundancies (8VSB).

I.1.d General Description of a TV Receiver

The receiver is an essential piece in a television. Composed of a tuner and a demodulator, it allows the conversion of the RF television transmission into audio and video signals, which can further be processed to produce sound and to display colored pictures. This is illustrated in Figure 15. Hence, people are able to select a TV channel.

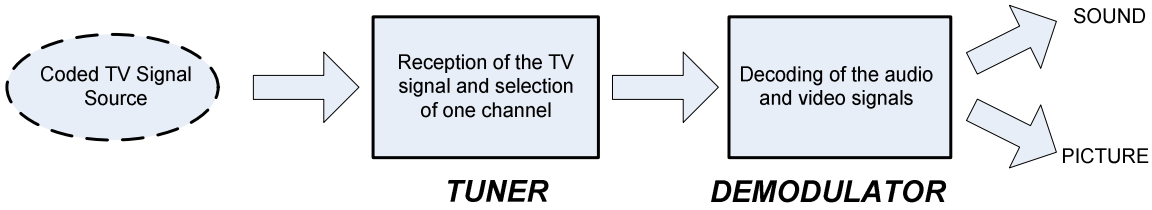

Figure 15. TV reception chain

In more details, the RF television signal is first received and processed by the tuner, to select one channel within the spectrum. This front-end part of the receiver has to transmit the cleanest possible signal to the input of the demodulator, without introducing degradation nor interferences with other channels. Indeed, distortions or degradation of the wanted TV signal may result in demodulation errors leading to wrong pixel colors on the TV screen.

That is why very high performances are required for the tuner. It has to deal with the received broadband RF signal. As explained in more details further, the signal has then to be downconverted from RF frequencies to lower frequencies, and finally, the tuner has to filter the wanted channel, so that only one is transmitted to the demodulator. Besides, all these steps have to be performed with as little degradation of the signal as possible.

From this, three main characteristics of the TV tuner can be highlighted. It has to be:
- ***sensitive***, in order to be able to receive even weak wanted signals;
- ***selective***, so that unwanted interferers are strongly rejected;
- ***accurate***, to return the exact emitted signal.

I.1.e Broadband Reception Systems

Figure 16 describes the frequency ranges of terrestrial signals and of other radio communications such as UMTS[5], GSM or WLAN[6]. Their differences make the receiver systems associated to each to be sorted into three main categories.

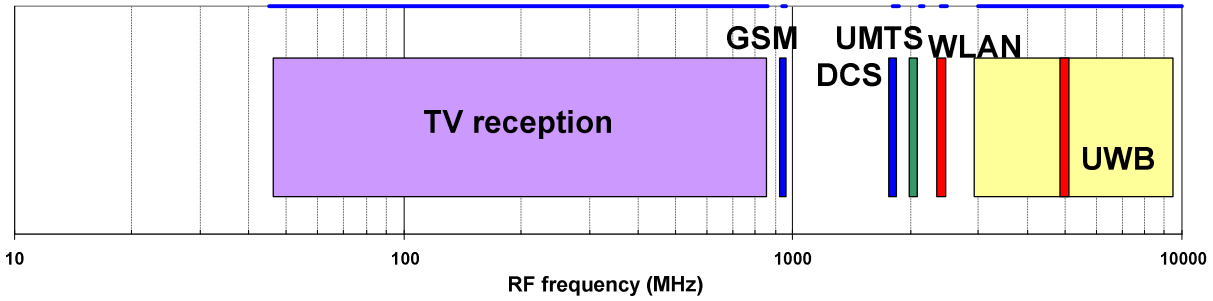

Figure 16. Coexistence of standards in the off-air spectrum

I.1.e.i Narrowband Systems

Narrowband refers to a situation in radio communications where the bandwidth of the message does not significantly exceed the channel's coherence bandwidth. It is a common misconception that narrowband refers to a channel which occupies only a "small" amount of space on the radio spectrum. GSM or UMTS receivers can be quoted as examples of narrowband systems.

I.1.e.ii Wideband Systems

In communications, wideband is a relative term used to describe a wide range of frequencies in a spectrum. A system is typically described as wideband if the message bandwidth significantly exceeds the channel's coherence bandwidth. This is the case of UWB receivers.

I.1.e.iii Broadband Systems

Broadband in telecommunications is a term which refers to a signaling method which includes or handles a relatively wide range of frequencies which may be divided into channels or frequency bins. The terrestrial TV spectrum spreads from 45 to 862MHz, therefore covering nearly 5 frequency octaves, and channels occupy a bandwidth varying between 6 and 8MHz. These signals can be qualified as broadband.

Being able to receive any channel within the broadband terrestrial or cable spectrum with high performances is the challenge that TV tuners have to face. To answer this challenge, the architecture of the tuner is optimized and its specifications are very tight.

[5] UMTS, standing for *Universal Mobile Telecommunications System*, is a third generation mobile cellular technology for networks based on the GSM standard

[6] WLAN, standing for *Wireless Local Area Network*, links two or more devices by a wireless means like the IEEE 802.11 standard, also called Wi-Fi.

I.2 TV Receivers Architecture & Specifications

I.2.a TV Tuner Architecture

As said before and as in most receivers, the signal is first amplified by a LNA before being mixed, as shown in Figure 17. The mixing stage actually consists in multiplying two signals. Let's consider the RF signal and the LO (which stands for Local Oscillator) one, assuming that both are sine wave signals, mixed by a linear system:

$$\cos(\omega_{RF}t)\cos(\omega_{LO}t) = \frac{1}{2}\left(\cos((\omega_{RF} - \omega_{LO})t) + \cos((\omega_{RF} + \omega_{LO})t)\right). \quad \text{(I.4)}$$

Hence, the RF signal is actually translated to lower frequency by the LO signal. Two new frequencies then come out:

- $\omega_{RF} - \omega_{LO}$, called IF frequency, which is the useful frequency;
- $\omega_{RF} + \omega_{LO}$, called image frequency which has to be rejected.

Depending on the value of the intermediate frequency (IF) $f_{IF} = f_{RF} - f_{LO}$, receivers are called IF, low-IF or even ZIF (which stands for Zero-IF) when the signal is directly converted to baseband.

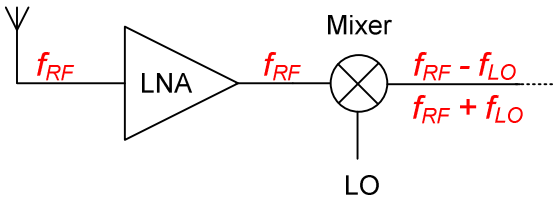

Figure 17. RF receiver front-end simplified architecture

As it may be seen on Figure 18, once the signal is converted to IF, the wanted channel is filtered. It is a very selective and sharp filter so that only this channel remains among the entire received spectrum. Then, an analog-to-digital conversion of the channel is performed by an ADC in order to provide the signal to be demodulated.

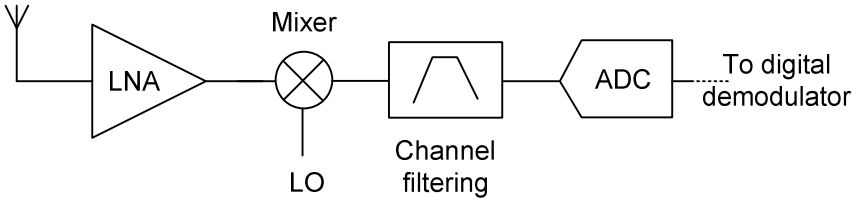

Figure 18. TV receiver architecture

One might wonder why this tuner architecture is necessary. Indeed, a simpler concept would be designed with an analog-to-digital converter (ADC) much closer to the antenna. However, such an ADC would require very high sampling rate and resolution to be designed, since two billion samples per second are needed [I.2] to convert up to 1GHz. Though this type of architecture is emerging to handle cable TV signals [I.4], the presence of very high power differences between channels still prevents from using it for terrestrial applications.

I.2.b TV Tuner High Performance Specifications

I.2.b.i Low noise

As explained in APPENDIX A, noise is a random fluctuation of energy which can be found in all electronic circuits. In the case of an RF receiver, a high noise level results in an undesirable signal that masks or degrades the useful signal, as illustrated on Figure 19 by a noisy sine wave.

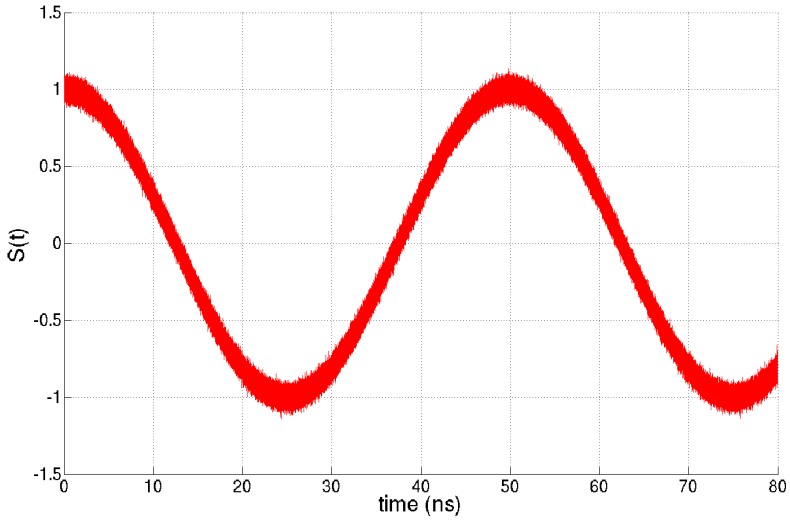

Figure 19. Noise added to a sine signal

A noisy reception chain makes the wanted signal be degraded. Hence, it becomes more difficult to finally demodulate in good conditions and the number of errors may increase. To decrease demodulation errors, noise has to be as low as possible compared to the wanted signal. This is expressed by a signal-to-noise ratio (SNR) that should be high enough at the input of the demodulator. This is one of the specifications for the TV tuner. On Figure 20 are shown two 16QAM constellations drawn for two different SNR. It clearly shows that noise random fluctuations on the desired signal can lead to decision errors on bit values.

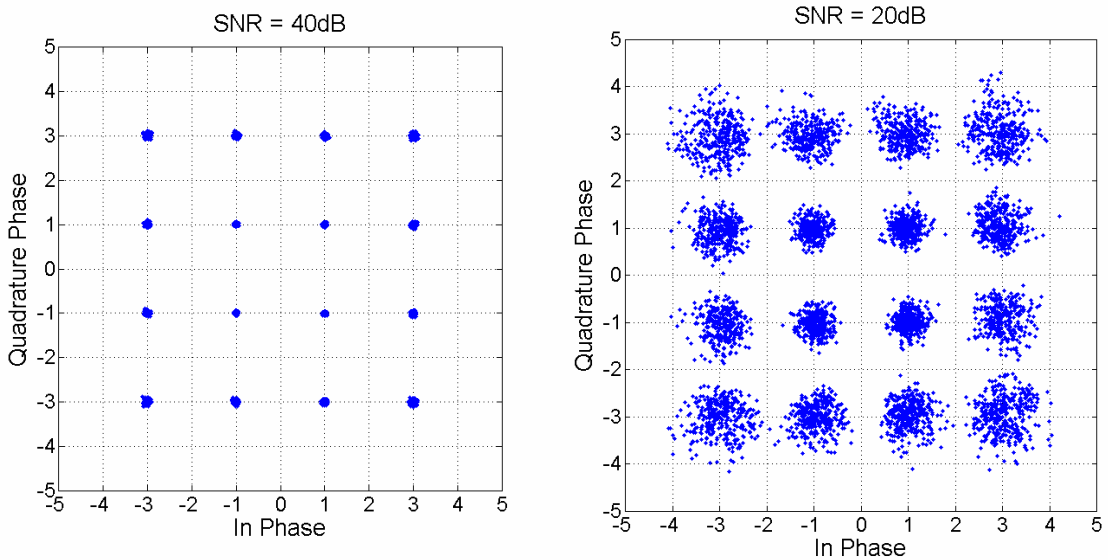

Figure 20. 16QAM constellations for two different SNR

Figure 21 illustrates the uncoded BER, which stands for Bit Error Rate, versus the E_s/N_0, which is the energy of a symbol E_s normalized to the noise power N_0, in the case of a 16 QAM modulation. Assuming that the symbol and the sampling periods are equal, E_s/N_0 then corresponds to the SNR.

The required BER depends on the communication system. However, this figure shows that BER strongly depends on the SNR. To reach bit error rates of 10^{-4} or 10^{-5}, SNR of 18 to 20dB are needed. Besides, it is worth pointing out that a 1dB variation at these SNRs leads to a factor 10 variation on the BER. Hence, noise is a very critical issue in our applications.

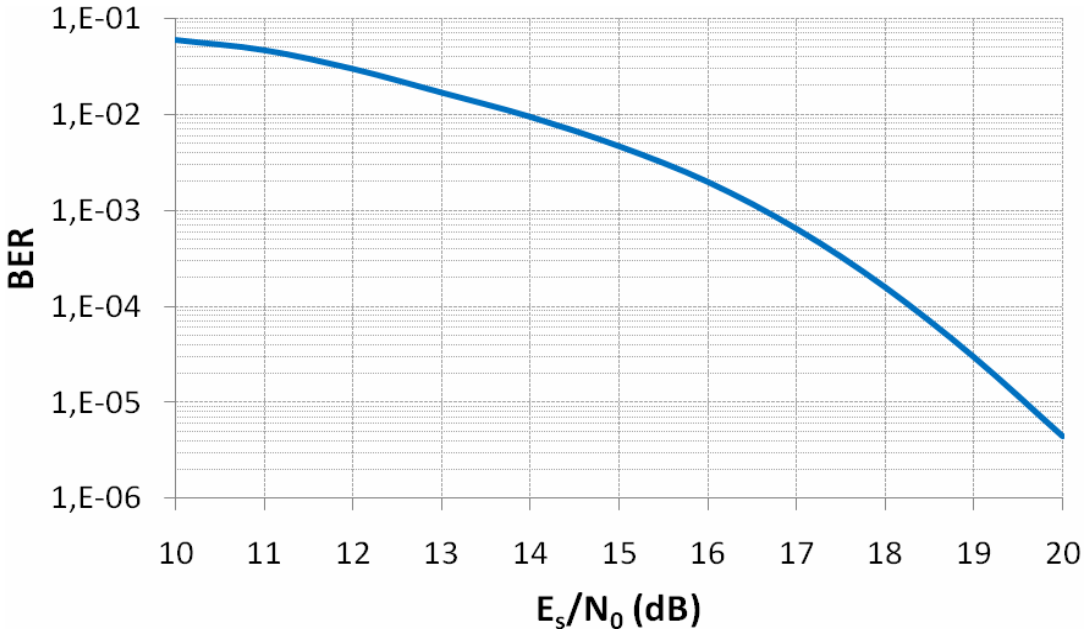

Figure 21. BER versus E_s/N_0 in case of a 16QAM modulation

As explained in APPENDIX A, the noise factor (or the noise figure) is a way to measure the degradation of the SNR by a system between its input and its output. Applying ***Friis' formula*** to a receiver system made of a LNA of gain G_{LNA} and of noise factor F_{LNA}, and considering the noise factor of the rest of the receiver chain F_{rest}, it can be written that:

$$F_{receiver} = F_{LNA} + \frac{F_{rest} - 1}{G_{LNA}}. \qquad \text{(I.5)}$$

Thus, the receiver noise factor is strongly dependent on the noise and the gain of the first stage LNA. To get a very low $F_{receiver}$, it is required to have a high gain with a very low noise factor, and this stage is performed by an LNA. When F_{LNA} is low while G_{LNA} is high, the noise constraints over the rest of the receiver chain, described by the noise factor F_{rest}, can be relaxed.

I.2.b.ii High linearity

Although components such as amplifiers are considered as linear elements for small signals, they actually have non-linear characteristics. When dealing with large signals, distortion phenomena like compression or intermodulation occur and may strongly degrade the wanted signal. The theory about distortions and its effects are discussed more extensively in APPENDIX B. Figure 22 shows the degradation of a since wave due to second order distortion (a) and to third and fifth order distortion (b).

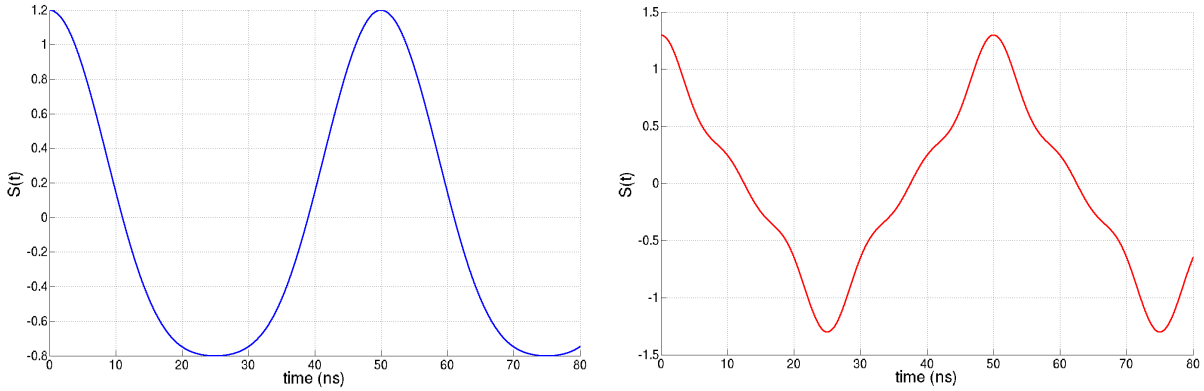

Figure 22. Second order (a) and Third and Fifth order (b) distortion of a sine wave

References [I.5 and I.6], written by *Charles Rhodes*, highlight how crucial the linearity of the TV receivers is. It demonstrates that nearly all interferences are due to third order non-linearity of the receiver when overloaded. Indeed, the receiver is then subject to multiple distortion products which may fall in the desired channel, as described in Figure 23. Thus, like noise, intermodulation products falling can mask and degrade the wanted signal.

To describe the degradation of the signal by noise as well as non-linearities, a factor similar to the SNR is often used. It is called SNIR, standing for ***Signal to Noise plus Interference Ratio***.

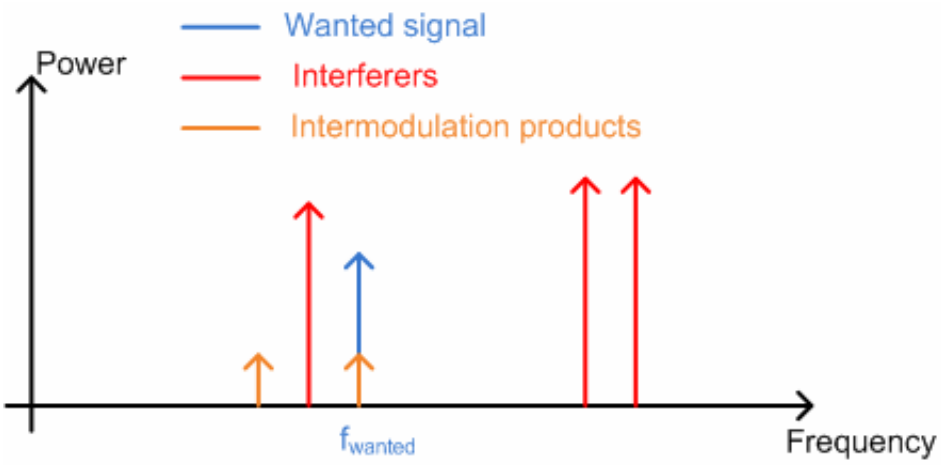

Figure 23. Intermodulation products interfering with a desired signal

I.2.b.iii Specifications of the Tuner

To increase the above defined SNIR at the demodulator input, the TV tuner aims at handling large signal swings while being as linear and as low noise as possible. This linearity versus noise trade-off is called ***dynamic range*** in the following. The specifications of the tuner are presented in Table 1. As said, to be used for cable and terrestrial signals, it has to cover the 42 – 1002 MHz band.

Specifications are set so that NF has to be kept below 6.5dB for the entire tuner. In terms of linearity, IIP3 of 11dBm is targeted, which corresponds to 120dBµV on 75Ω impedance often used for TV context.

Table 1. Tuner Specification Requirements

Frequency Range (MHz)	45 - 1002
NF (dB)	6.5
IIP3 (dBm)	11
IIP2 (dBm)	31
Maximum input Power (dBm)	As large as possible

I.3 RF Filter Specifications

I.3.a TV Tuner Bloc Specifications

The required specifications on the tuner involve several requirements over each bloc constituting the TV tuner. First, let's consider a front-end composed of a LNA and a mixer, to better understand the roles of each.

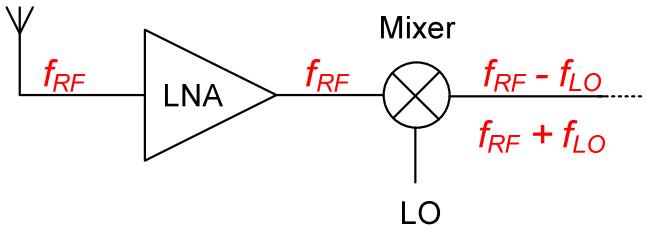

Figure 24. Front-end part of the TV tuner

I.3.a.i Constraints on the LNA

As explained previously, the broadband LNA is the essential stage to lower the tuner noise figure. This LNA has to be very low noise and its gain has to be large. It also has to ensure a good impedance matching to the antenna, so that there is almost no loss of power between the antenna and the tuner. This is specified with return loss that should be lower than 8dB.

To increase the second-order linearity of the tuner, it is worth using differential mode over the entire tuner chain. However the use of a front-end balun for the single to differential conversion shows two major drawbacks. Indeed, a balun consists of inductances which are both sensitive to the electromagnetic environment and difficult to integrate. That is why the architecture makes use of a front-end single-to-differential LNA.

I.3.a.ii Constraints on the Mixer

In the case of TV tuners, a squared LO signal is preferred to handle mixing (see Figure 25) since abrupt switching characteristics enable to lower noise. However, the frequency spectrum of such a signal is made off many non-negligible odd harmonics as depicted on Figure 26:

$$\cos(\omega_{LO}t)+\cos(3\omega_{LO}t)+\cos(5\omega_{LO}t)+... \quad \text{(I.6)}$$

The mixing of the RF signal and the squared LO leads to:

$$\cos(\omega_{RF}t)[\cos(\omega_{LO}t)+\cos(3\omega_{LO}t)+\cos(5\omega_{LO}t)+...] \quad \text{(I.7)}$$

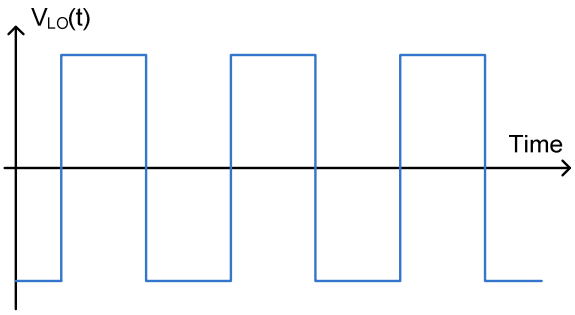

Figure 25. LO time evolution

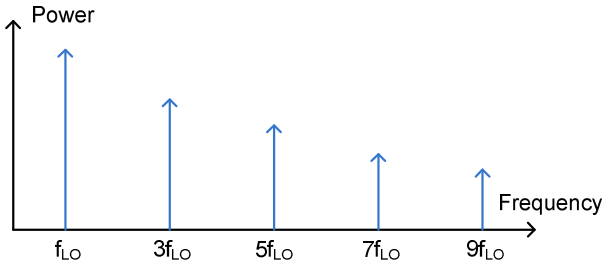

Figure 26. LO frequency spectrum

Developing previous expression:

$$\cos((\omega_{RF} \pm \omega_{LO})t) + \cos((\omega_{RF} \pm 3\omega_{LO})t) + \cos((\omega_{RF} \pm 5\omega_{LO})t) + \ldots \quad \text{(I.8)}$$

As said, the IF frequency is defined as:

$$\omega_{IF} = \omega_{RF} - \omega_{LO} \quad \text{(I.9)}$$

Now, the RF signal is not only made of the wanted channel, but it is also composed of other RF unwanted signals that may be located so that following relations are verified:

$$\omega_{IF} = \omega_{RF3} - 3\omega_{LO} \quad \text{(I.10)}$$

$$\omega_{IF} = \omega_{RF3} - 5\omega_{LO} \quad \text{(I.11)}$$

This leads to the downconversion of odd harmonics to IF, as it is depicted in Figure 27.

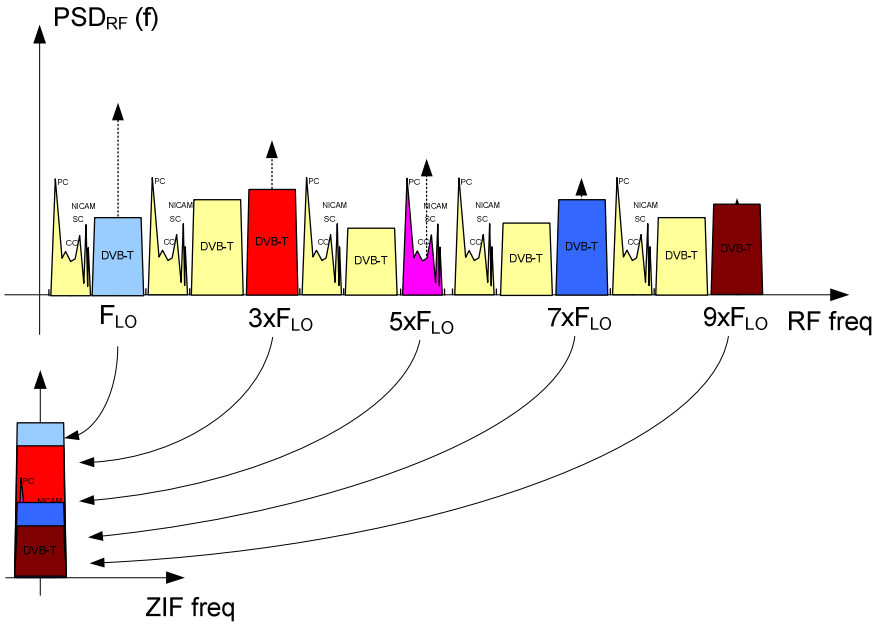

Figure 27. Downconversion of LO harmonics to IF

Therefore, a certain harmonic rejection level is required so that the wanted signal is not corrupted by these harmonics.

I.3.b Roles of RF Selectivity

At first sight, a LNA and a mixer are sufficient to get the reception functionality. Nevertheless, in case of TV receivers, the architecture has to be optimized in order to reach the required high RF performances. In particular, RF selectivity is essential to relax the constraints on the LNA and on the mixer. Moreover, this RF filtering is a strong asset to be able to keep the tuner performances in the presence of strong interferers, when handling terrestrial TV signals.

Within the tuner, the RF filter can be located between the LNA and the mixer, if the LNA presents high enough performances, as illustrated in Figure 28. As said previously, it has to be ***frequency tunable***, so as to be centered on the wanted channel. The central frequency of the filter has to be tunable over the 45-1002MHz band, in order to be used both for cable and terrestrial receivers.

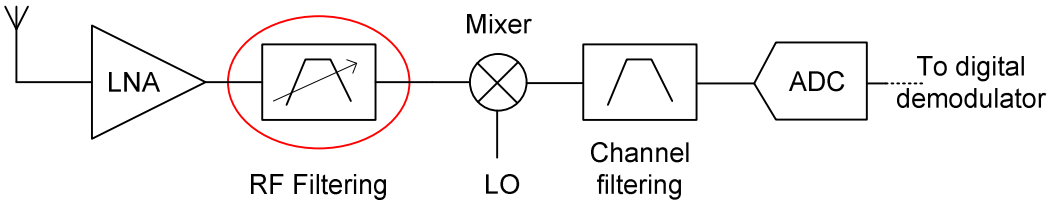

Figure 28. TV tuner architecture

As said before, when mixing the RF signal with the LO frequency, the harmonic frequencies of the LO are also downconverted to IF. Hence, a certain rejection of these harmonics is required. To relax the constraints over the mixer stage, ***the RF filter rejects all harmonic frequencies*** by a certain amout. It allows the relaxation of the constraints on the harmonic-rejection mixer located after the filter.

Even though a low-pass filter would be enough to reject harmonics, the ***bandpass*** character of the filter has two main assets. First, a bandpass filter is able to ***protect the mixer from strong unwanted interferers***. Indeed, in case of the reception of a weak wanted signal, the RF filter has to reject all unwanted signals as high as possible, on both sides of the central frequency. For this matter, the RF filter would have been even more efficient if it was connected directly at the antenna, also protecting the LNA. However, the frequency tuning while keeping a good matching to the antenna appears difficult. Besides, from Friis' formula, it would require a very low noise filtering, which is hard to achieve.

The second asset of a bandpass RF filtering is the ***rejection of adjacent channels***. This is a crucial feature to meet international norms such as *ATSC A/74* or the *Nordig Unified*. These norms require a certain adjacent channels rejections from the front-end part of the tuner, called protection ratios. These may be seen on Figure 29, which summarizes the wanted protection ratios according to various standards [I.3, I.7 and I.8] as a function of the position of the unwanted channel. An RF selectivity stage allows reaching these adjacent channels rejection specifications.

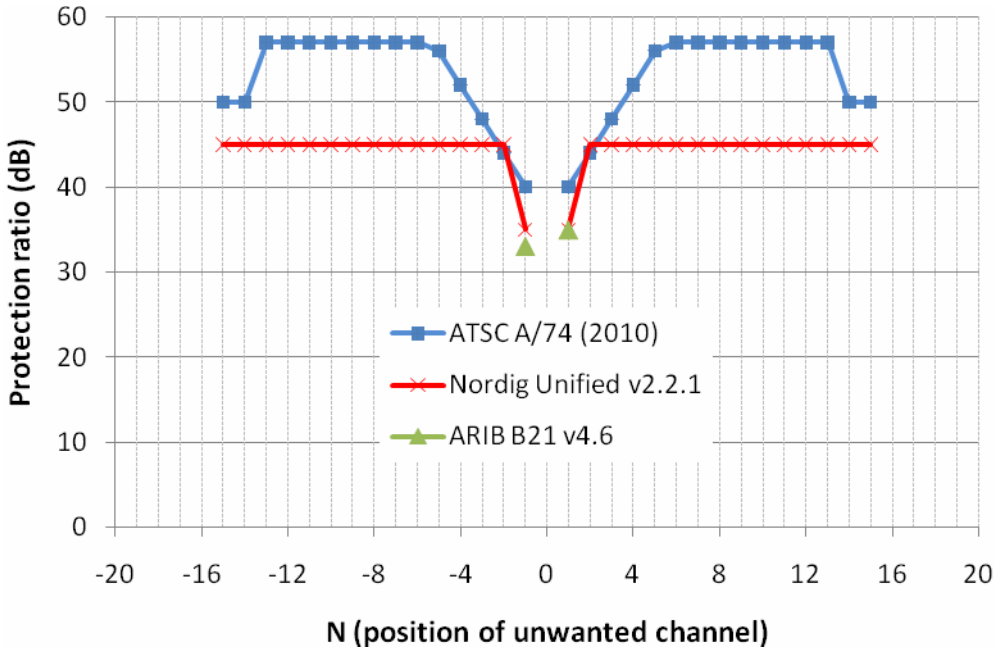

Figure 29. Protection ratios for different standards

These adjacent channel rejection requirements can even become more stringent in the coming years. Indeed, with the analog switch-off, frequency bands formerly occupied by analog TV become free. They are called *white spaces*. These frequency allocations may be used in the future for various purposes such as home wireless LAN for instance. Thus, their emitting power and frequencies could become a problem if TV tuners are not selective enough.

Furthermore, the LTE, standing for Long Term Evolution, which is the most recent GSM/UMTS norm, is looking for emitting within the 800-900MHz range. Since mobile communications require high emitting powers, this may cause interference from mobile service base stations and handsets overloading the sensitive TV tuner front end circuitry, preventing existing viewers from seeing a picture [I.9].

Such a filter has also to be ***accurately centered*** on 6 to 8 MHz large channels. That is to say that frequency calibration has to be taken into account when designing the filter, through a way of correcting the central frequency if it deviates from the wanted one. Moreover, the frequency tuning range has to be divided in ***frequency steps*** which are 6MHz maximum in order to be able to center the filter on all the different channels, as depicted in Figure 30.

Figure 30. Maximum frequency step of the filter

This RF filtering is a ***first step of selectivity***. It does not aim at selecting sharply only one channel with high RF performances. This sharp filtering is performed after downconversion to IF, to take advantage of working at lower frequencies. However, the RF filtering has other assets which are essential to reach the high performances required by the TV tuner.

I.3.c Selectivity Specifications

Selectivity specifications are summarized in Table 2. As said, both high selectivity and broadband tunability are required. Specifications on adjacent channels rejection are set on most critical points (N±5 and N±6 from *ATSC A/74*). Thus, it enables to get a shape for the filtering which rejects all other adjacent channels sufficiently. Note that, in the following, H3 and H5 respectively stand for the third order and the fifth order harmonic frequencies.

Table 2. Selectivity Specifications

Filter Tuning Range (MHz)	45 – 1002
H3 & H5 rejection (dB)	25 for both
N±5 & N±6 rejection (dB)	5 & 6
Non-TV bands rejection (dB)	15
Power rejection on the whole spectrum (dB)	10

I.3.d Abacus

Several abacuses can be drawn from the above specifications, as illustrated in Figure 31 and Figure 32. It is worth noticing that, at low frequencies, adjacent channels are rejected more than specified when reaching the specifications in terms of harmonic frequencies filtering. This latter constraint is thus the most difficult one to achieve. On the contrary, at high frequencies, harmonics get more far-away from the wanted signal. However, adjacent channels are still located at N±5 and N±6 become more difficult to filter out since it requires a high selectivity.

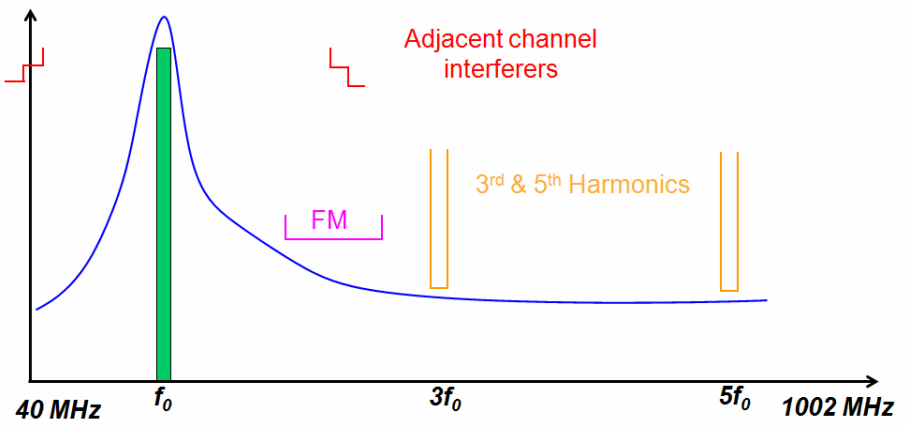

Figure 31. Low frequency abacus

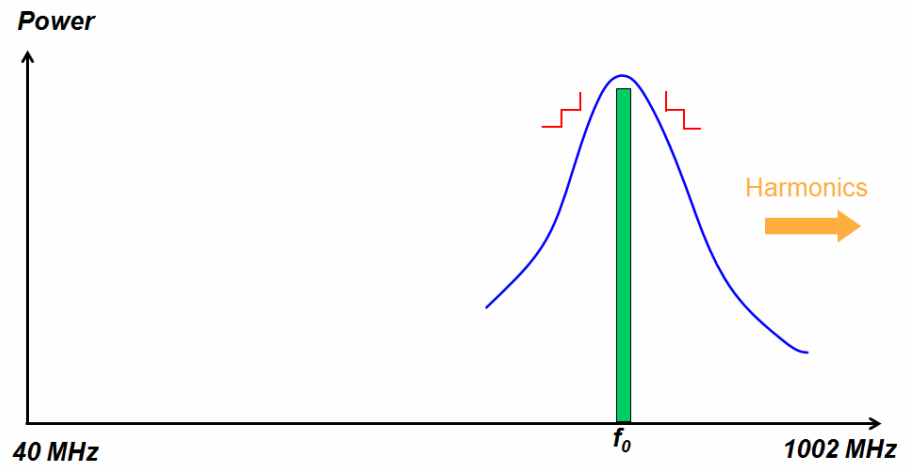

Figure 32. High frequency abacus

Above 870MHz, there are no more terrestrial channels so adjacent channels rejection specifications can be relaxed. However, a high selectivity is still required to face any interferer like the GSM frequencies.

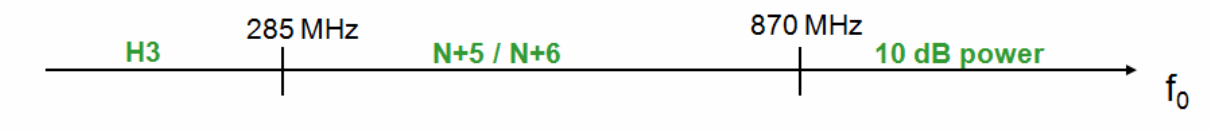

Figure 33. Hardest rejections to reach according to the central frequency

I.3.e RF Performances Specifications

As said, RF specifications on the entire tuner involve RF specifications on each bloc constituting its architecture. Targets on noise and on linearity are summarized in Table 3. Input-referred intercept points were specified to get rid of the filter gain. However, a gain close to unity is targeted.

Table 3. RF Performances Specifications

NF (dB)	10
IIP3 (dBm)	11
IIP2 (dBm)	31
Gain (dB)	~ 0

I.4 Technological Trend of RF Selectivity

I.4.a RF filtering integration history

Since the beginning of TV, TV tuners have known several technological evolutions. Up to the years 2000, they were referred as ***can tuners***. [I.10] Indeed, they were made of active components as well as hundreds of passive external components, mounted together on a board [I.11]. The whole was encapsulated inside a metal shield enclosure, the can, in order to protect the tuner from the electromagnetic fields present in the environment. Furthermore, these can tuners had an architecture making use of several bandpass filtering stages, associated to a very selective Surface Acoustic Wave (SAW) filter located in the IF path. These features strongly immunize can tuners from all kinds of interferers and provide a very important adjacent filtering before the LNA. As illustrated in Figure 34, RF filtering was handled by means of several air coils, manually tuned, in parallel of high voltage varicaps.

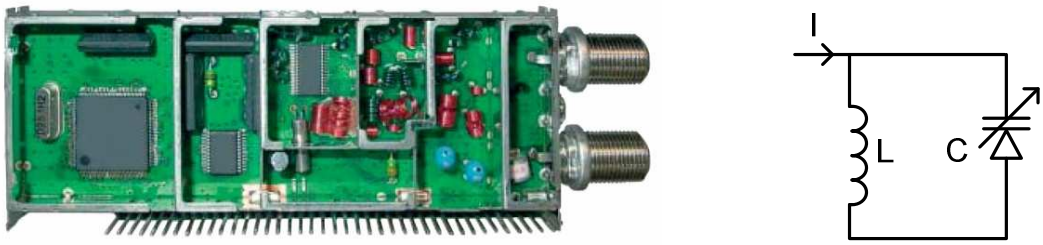

Figure 34. Can tuner (a) and its RF filtering (b)

In 2007, ***first silicon tuners*** were designed, like the NXP TDA 18271 (see Figure 35). As explained in [I.10], the development lag of TV tuners behind all other TV developments highlights that silicon tuners have difficult challenges to overcome. This major technological step allowed the emergence of new functionalities and applications. Indeed, a silicon tuner has become multi-standard while can tuners were aimed at receiving only one single standard. In addition, silicon tuners show higher integration, lower power consumption, better thermal behaviour and better reliability. The emergence of multiple tuners integrated on a same chip also allows digital video recording or picture-in-picture applications. [I.12]

Silicon tuners integrate almost all TV tuner functions on silicon. However, RF filtering was still handled by discrete inductors in parallel of discrete varactors. The whole was integrated within a package as it may be seen in Figure 35 [I.13].

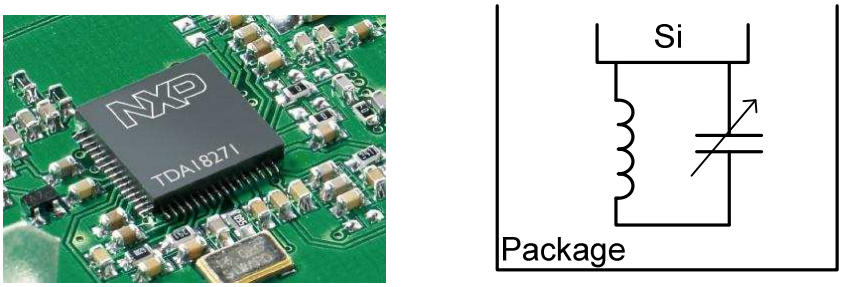

Figure 35. NXP TDA18271 (a) and its RF filtering (b)

Newest silicon tuners generations, like NXP TDA 18272 (Figure 36) and 18273, use switched capacitors banks which enable a higher, though still partial, on-chip integration of the RF filtering.

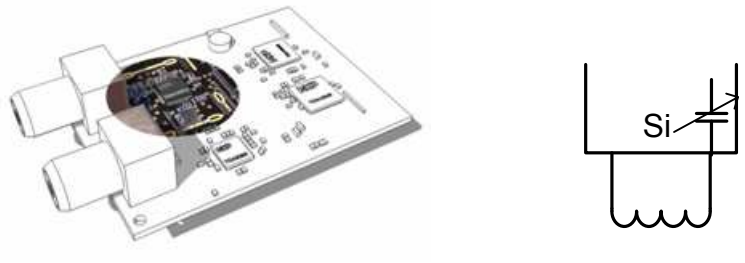

Figure 36. NXP TDA18272 (a) and its RF filtering (b)

I.4.b Opportunities & Limitations of active circuits

Today, silicon tuners like the one shown on Figure 36 are integrated in a can, further integrated on a TV board. Comparable to the metal enclosure of can tuners, this shielding protects the TV tuner from electromagnetic perturbations coming from other components or from the environment itself. Indeed, the inductors of RF filters are mounted on a board and these coils act as antennas which catch electromagnetic signals. Electromagnetic coupling may degrade the performances of the RF selectivity, and so the performances of the tuner.

In the coming years, the technological trend is to mount TV tuners directly on the TV board, among thousands of other components. Hence, without shielding blocking all electromagnetic perturbations, the TV tuner has to be as less sensitive as possible to its environment. This is the first reason of studying the opportunities and the limitations of a fully-active, inductorless, RF selectivity.

Furthermore, discrete inductors currently used show some other drawbacks like the spread on their values. Hence, a fully-active solution would lead to a very flexible solution with no external components and being immune to electromagnetic couplings, leading to a next generation of TV tuners.

In addition, studying fully-active filters will lead to the study of its technological aspects. Indeed, is CMOS or BiCMOS better to realize such a filter? In case of a CMOS filter, is there a technological node below which the filter becomes less selective? Moreover, is it possible to take advantage of the smaller $R_{on}C_{off}$ product of advanced-node MOS switches? There are many questions that need to be answered once going about fully-active filtering.

I.5 Answering the Problematic of the PhD Thesis

Taking into account all the various issues that were previously described, it has been decided that this PhD thesis will address the following innovative problematic:

Limitations & Opportunities of Active Circuits for the Realization of a High Performance Frequency Tunable RF Selectivity for TV Tuners

In the present manuscript, Chapter II describes the challenges and the state-of-the-art of RF filtering, first considering passive LC filtering solutions before dealing with active solutions. From the literature analysis, Gm-C filters appear as the most appropriate solution and are studied more deeply in Chapter III. Gm-C filter simulations are described therein. Chapter IV deals with another active solution, a Rauch filter, which is based on a voltage amplifier. This allows a promising enhancement of the dynamic range, which has been confirmed by measurements on a test-chip. The performances of Gm-C and Rauch filters are then compared in Chapter V. Chapter VI concludes and proposes some perspectives to this work.

I.6 References

[I.1] B. Razavi, *RF Microelectronics*. Prentice-Hall, 1998.

[I.2] A. Wong and J. Du Val, "Silicon TV tuners poised to replace cans", *RF design*, pp.22-28, Oct-2005.

[I.3] "ATSC Recommended Practice: Receiver Performance Guidelines", Document A/74, 2010.

[I.4] K. Doris and E. Janssen, "Multi-Channel Receiver Architecture and Reception Method," U.S. Patent WO 2010/055475 A120-2010.

[I.5] C. W. Rhodes, "New Challenges to Designers of DTV Receivers Concerning Interference," *Consumer Electronics, IEEE Transactions on*, vol. 53, no. 1, pp. 72-80, 2007.

[I.6] C. W. Rhodes, "Interference to DTV Reception due to Non-Linearity of Receiver Front-Ends," *Consumer Electronics, IEEE Transactions on*, vol. 54, no. 1, pp. 58-64, 2008.

[I.7] "NorDig Unified Requirements for Integrated Receiver Decoders for use in cable, satellite, terrestrial and IP-based networks", NorDig Unified version 2.2.1, November 24, 2010.

[I.8] Association of Radio Industries and Businesses, "Receiver for Digital Broadcasting, ARIB Standard (Desirable Specifications)", ARIB STD-B21 Version 4.6, March 14, 2007.

[I.9] Digitag report, "UHF Interference Issues for DVB-T/T2 reception resulting from the Digital Dividend", 2010.

[I.10] A. Wong and J. Du Val, "Silicon TV tuners poised to replace cans", *RF design*, pp.22-28, Oct-2005.

[I.11] Brian D. Mathews, "The end of region-specific designs?", ECNmag.com, November 2007.

[I.12] A. Wong, "Silicon TV Tuners Will Replace Cans Tuners as Transistors Replaced the Vacuum Tube", ADEAD White Paper, 2005.

[I.13] M. Bouhamame et al., "Integrated Tunable RF Filter for TV Reception [42MHz..870MHz]," presented at the Electronics, Circuits and Systems, 2007. ICECS 2007. 14th IEEE International Conference on, 2007, pp. 837-840.

II. Challenges of RF Selectivity

Following chapter is dedicated to the challenges of RF selectivity. It objective is to find which filter topology best fulfills the specified requirements of TV receivers. It also provides a comparison of the performances of different filter topologies and structures that may be found in the literature. Their opportunities and limitations from a technological point of view will also be assessed.

II.1 Comparison of the Possible Topologies

II.1.a Possible Topologies

There are several ways to fit the previously described abacus and this chapter aims at determining which one suits the best to fulfil the required specifications. From a mathematical point of view, it consists in finding transfer function parameters (order and coefficients) which allow achieving the desired selectivity requirements as well as an easy frequency tuning.

Equation (II.1) shows a transfer function in Laplace domain of order $\max\{n,m\}$, where *m* corresponds to the number of poles of *H(s)* and *n* to its number of zeros. α_i and β_i are called coefficients of this transfer function.

$$H(s)=\frac{\alpha_n s^n+...+\alpha_1 s^1+\alpha_0 s^0}{\beta_m s^m+...+\beta_1 s^1+\beta_0 s^0} \qquad \text{(II.1)}$$

It is worth pointing out that a high order transfer function k_t means a high number of reactive elements k_r to implement the circuit since $k_r \geq k_t$. For high order filters, frequency and selectivity tuning may become difficult to handle since several components values would have to be tuned. That is why a low order is preferred.

In this chapter II.1, several topologies of filters are assessed in order to find which one suits the best to fulfil the required specifications.

II.1.b Low-pass Topologies

II.1.b.i General Principle

A first order RC low-pass filter [II.1] actually consists in a resistor associated to a capacitor as depicted in Figure 37. Another first order low-pass filter can also be obtained using an inductor and a resistor, which is known as an RL low-pass filter. For both, high frequencies are cut by the reactive element.

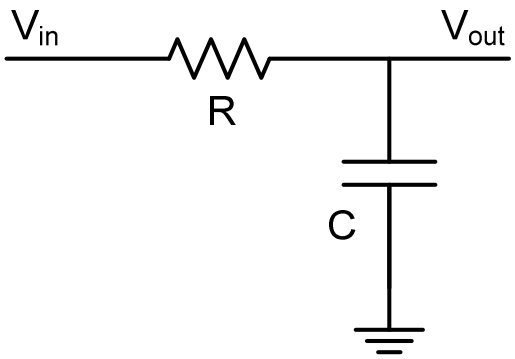

Figure 37. First order RC low-pass filter

As only one reactive element is present, this is a first order filter. The transfer function of this RC circuit in Laplace domain is given by:

$$H_{LPF}(s) = \frac{1}{1 + \frac{s}{2\pi f_c}}, \tag{II.2}$$

where f_c is the cut-off frequency

$$f_c = \frac{1}{2\pi RC} \tag{II.3}$$

For an RL low-pass filter, the transfer function has the same form. The difference relies in the cut-off frequency definition which depends on L and R in this case. To obtain a frequency tunable filter, the cut-off frequency has to be made adaptable by modifying the value of the elements of the circuit.

It is worth noticing that, for a first order low-pass filter, the transfer function is $\frac{1}{\sqrt{2}}$ at f_c. Hence, if the filter is centered so that $f_c = f_{wanted}$, then adjacent channels located at lower frequencies are less rejected than the desired channel. This property is true for all low-pass filters. Figure 38 depicts a first order low-pass filter when tuning its cut-off frequency. Figure 39 illustrates its adjacent channels and its harmonics rejections.

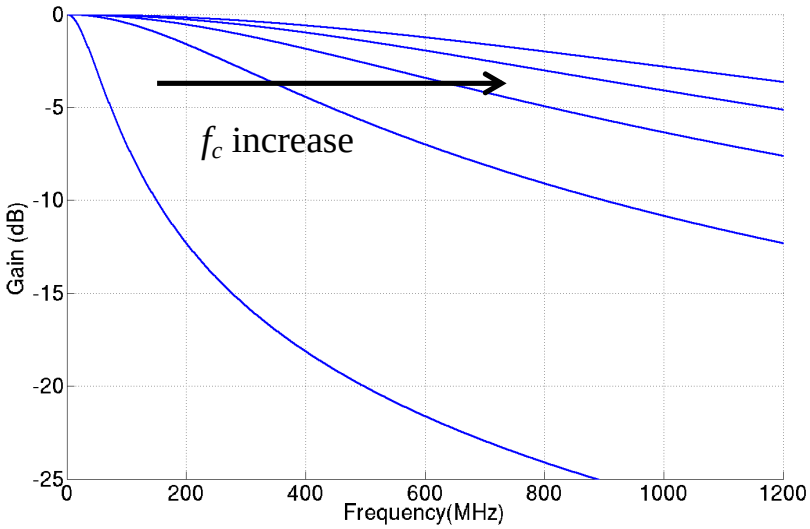

Figure 38. Cut-off frequency tunability of a first order low-pass filter

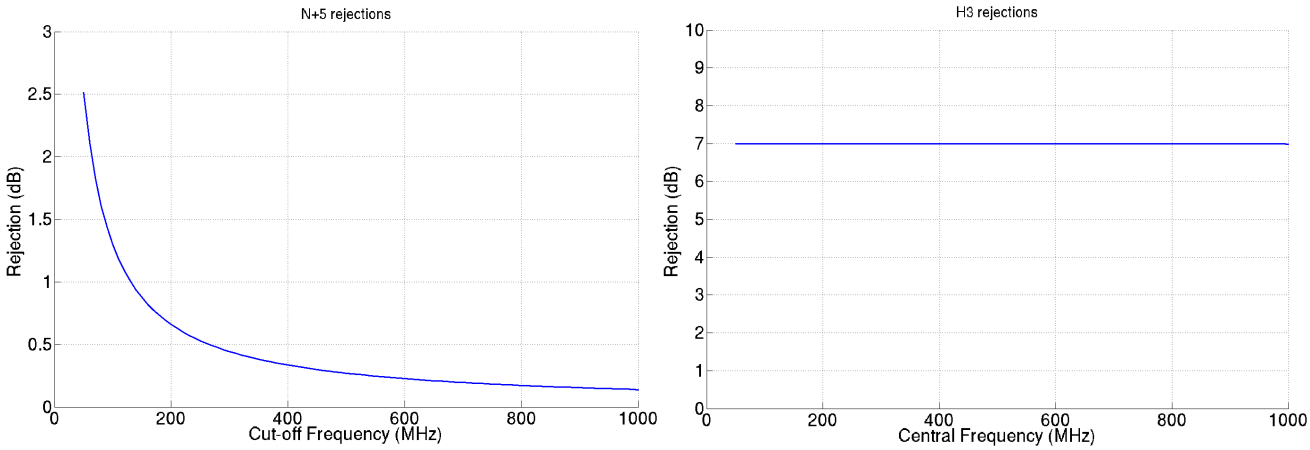

Figure 39. H3 and N+5 rejections of a first order low-pass filter

A higher order low-pass filter can be obtained increasing the number of poles in the transfer function by the addition of reactive elements in the circuit. Figure 40 presents second order low-pass filters built either cascading two RC first order filters or combining an inductor to a capacitor.

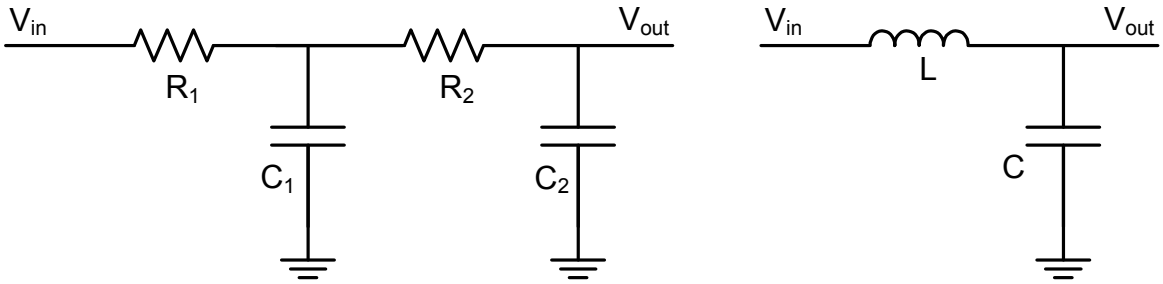

Figure 40. Second order RC and LC low-pass filters

The transfer function of a second order filter is then given by the formulas:

$$H_{LPF\,2}(s) = \frac{\alpha}{(s-p_1)(s-p_2)} = \frac{1}{1+\beta_1 s+\beta_2 s^2}, \qquad \text{(II.4)}$$

α being a constant. Such filter allows getting a steeper slope in order to reject harmonics more strongly as depicted in Figure 41 and Figure 42.

For second order (and more) filters, different topologies may be used, as illustrated in Figure 43, corresponding to different sets of coefficients β_is in the transfer function [II.2]. These topologies, known as Chebychev, elliptic or Butterworth filters, enable to get a flatter passband or a steeper slope (see Figure 43). Their rejections are plotted in Figure 44. Though elliptic filters show higher rejections, it is worth adding that this kind of filter uses one reactive element more than the other two filters, which creates a transmission zero (notch).

For instance, the normalized transfer function of a second order Butterworth low-pass filter is given by:

$$H_{Butterworth\,2}(s) = \frac{1}{1+\sqrt{2}s+s^2}. \qquad \text{(II.5)}$$

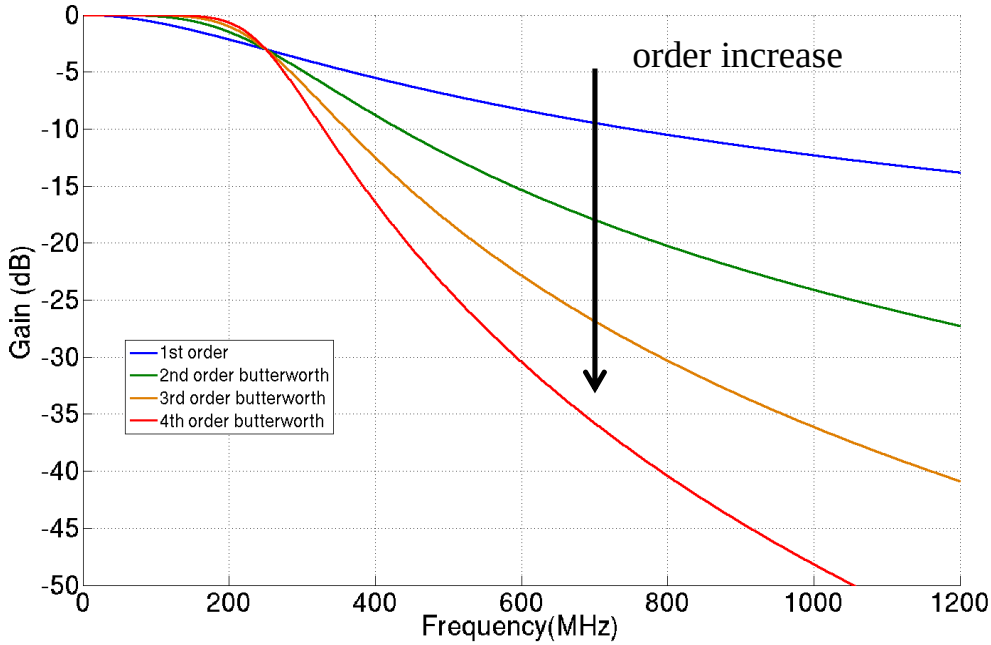

Figure 41. Impact of the Low-pass Filters Transfer Function Order

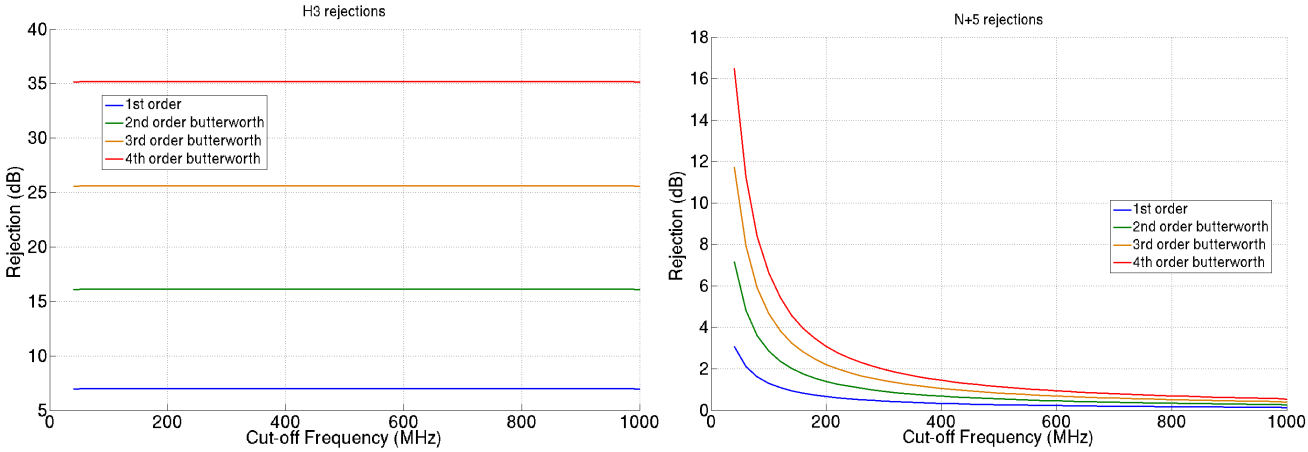

Figure 42. H3 and N+5 rejections according to the order

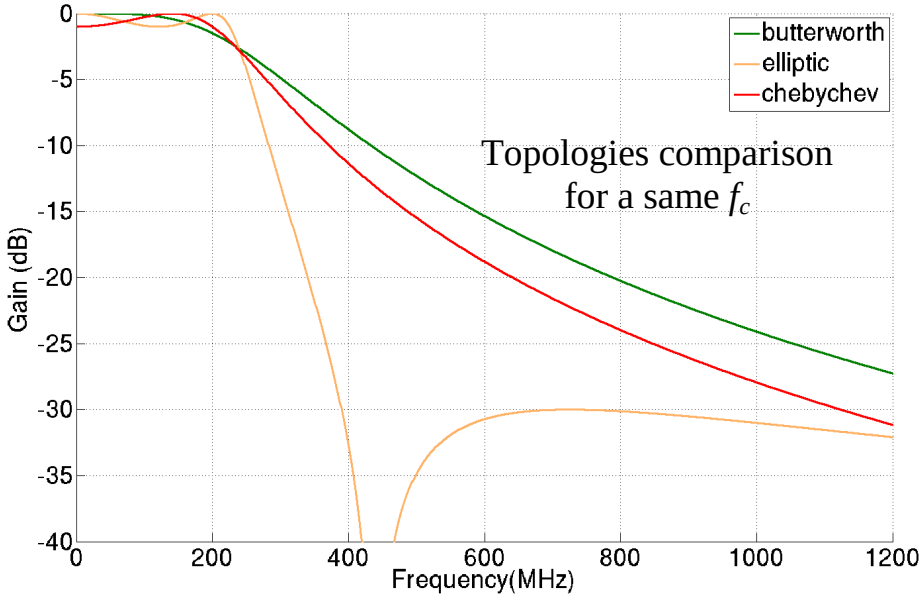

Figure 43. Second order Low-pass Filters Topologies

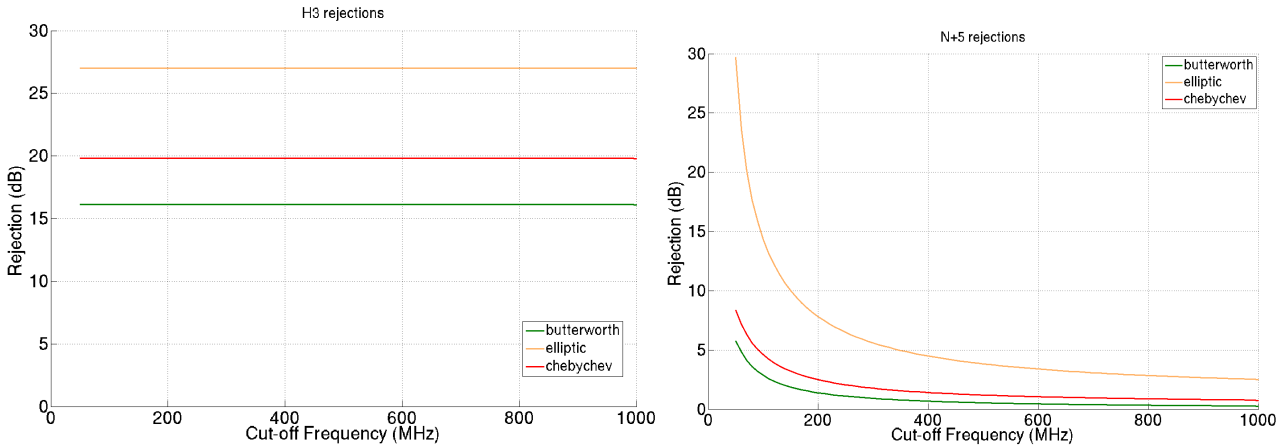

Figure 44. H3 and N+5 rejections according to the second order topology

II.1.b.ii Assessment of the Topology

The major advantage of low-pass filters is their ability to reject harmonic frequencies. For a given filter, the rejection of harmonic frequencies remains constant while tuning the cut-off frequency, as it may be observed in Figure 42.

However, as it may also be seen in Figure 42, first and second order filters do not reach the desired 20dB H3 and H5 rejection. A third order is then required, meaning at least three reactive elements. Tuning the cut-off frequency by tuning the reactive elements values while keeping a constant set of coefficient in the transfer function may become difficult as well.

This graph in Figure 42 also highlights the poor adjacent channels rejection of low-pass filters, especially when reaching high frequencies: less than 1dB rejection of the N+5 at 500MHz., even for third order topologies Furthermore, adjacent channels located below the cut-off frequency are amplified by up to 3dB.

II.1.c Bandpass Topologies

II.1.c.i Low-Pass to Bandpass Transformation

Regardless of the order, a bandpass filter [II.1] can be obtained from a low-pass filter by means of the following transformation:

$$s \to \frac{s^2 + \omega_0^2}{s.BW_\omega}, \tag{II.6}$$

where BW_ω is the -3dB bandwidth

$$BW_\omega = \omega_2 - \omega_1, \tag{II.7}$$

expressed in pulsation, and $\omega_{0\ is}$ the resonant pulsation:

$$\omega_0^2 = \omega_1 \omega_2, \tag{II.8}$$

In these formulas, ω_1 and ω_2 are pulsations which enable to build the bandpass filter characterizing its passband and stopbands.

The low-pass to band-pass transform consists in replacing inductors in the circuit by a series combination of inductor and capacitor, and capacitors by a parallel combination of inductor and capacitor [II.3], as it may be seen in Figure 45.

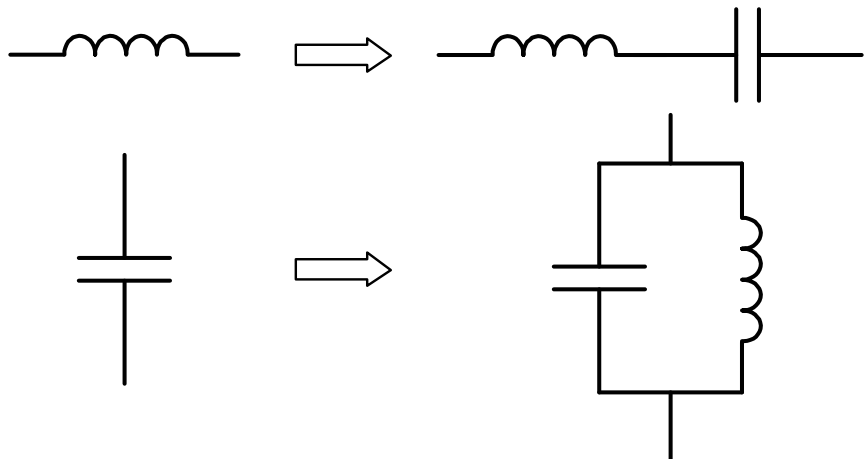

Figure 45. Low-pass to Bandpass Transformation

Hence, the transfer function of a second order bandpass filter in Laplace domain has the following form [II.1]:

$$H_{BPF}(s) = \frac{1}{1 + Q\left(\frac{s}{\omega_0} - \frac{\omega_0}{s}\right)}. \tag{II.9}$$

This filter presents a resonance at a frequency, called ***central frequency***, determined by the reactive elements of the circuit:

$$f_0 = \frac{1}{2\pi\sqrt{LC}}. \tag{II.10}$$

Q is a term called ***quality factor***, studied in more details later on, given by the formula:

$$Q = \frac{f_0}{BW_f} \tag{II.11}$$

Figure 46 illustrates the transfer function gain versus frequency for given parameters. As expected, the transfer function presents a bandpass characteristic.

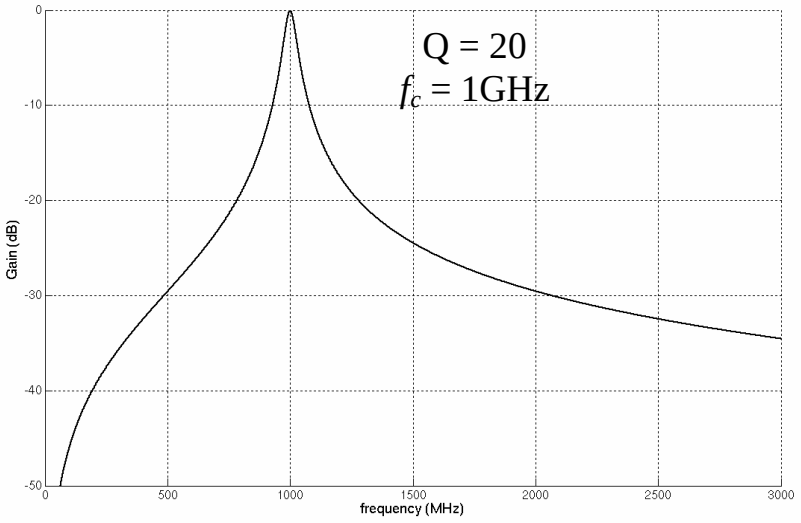

Figure 46. Bandpass Filter Transfer Function

From the RC and the LR first low-pass filters, two main second order bandpass filters are derived. First one, derived from the RC low-pass, is a parallel resonator made of an inductor *L* with its series losses R_s, in parallel of a capacitor *C*, as shown in Figure 47. The equivalent admittance of such a circuit is minimal at the resonance frequency. Hence, the output voltage gets higher at the resonant frequency. It is called a ***voltage resonance***.

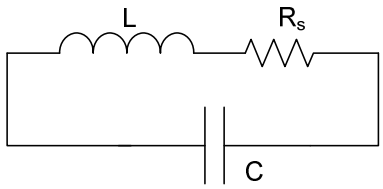

Figure 47. RLC resonator with parallel capacitor

Derived from an LR low-pass, the circuit depicted in Figure 48 is composed of a series resonator. Indeed, the resonance is reached when the equivalent impedance is minimal. The resonance happens when the output voltage gets minimal, and so, when the current get maximal. This is called a ***current resonance***.

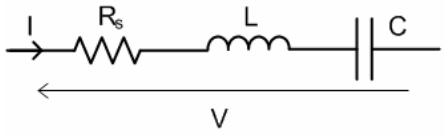

Figure 48. Series LC resonator assuming series loss

II.1.c.ii Quality Factor

From the formula of Q previously given, it may be observed that the higher the Q, the more selective the filter. Indeed, if a non-lossy filter is assumed, such as an ideal LC resonator, this leads to an infinite Q-factor, meaning a zero bandwidth.

The quality factor Q_L of a non-ideal inductor can also be defined as:

$$Q_L = \frac{\omega_0 L}{R_s}, \tag{II.12}$$

with R_s being the series losses of this inductor.

By means of a series to parallel transformation, this circuit can be converted into a parallel resonator. Then, a parallel to L and C resistance R_p appears which is computed as follows:

$$R_p = (Q_L^2 + 1)R_s \tag{II.13}$$

This leads to the following circuit:

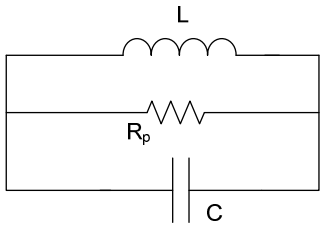

Figure 49. RLC parallel circuit

Let's compute the quality factor of this circuit:

$$Q_0 = \frac{R_p}{\omega_0 L}. \tag{II.14}$$

Replacing with previous equations, we get:

$$Q_0 = \frac{(Q_L^2 + 1)R_s}{\omega_0 L}. \tag{II.15}$$

Now,

$$Q_0 = Q_L + \frac{1}{Q_L} \approx Q_L \text{ with } Q_L >> 1 \tag{II.16}$$

If it is considered that the Q-factor of the inductor is above 10, then the latter equation can be obtained. It demonstrates how crucial it is to use high-Q inductors since the quality factor of the filter is directly the one of the inductor.

II.1.c.iii Difference Between BPF and a Combination of HPF and LPF

The combination of a first low-pass filter with a first order high-pass filter also creates a second order bandpass filtering. A high-pass transfer function may be obtained from a low-pass one by means of the following transformation [II.3]:

$$s \rightarrow \frac{\omega_{HPF}}{s}. \tag{II.17}$$

Considering ω_1 as cut-off frequency, this leads to:

$$H_{HPF}(s) = \frac{s}{1 + \frac{s}{\omega_1}} \tag{II.18}$$

This corresponds to inverting capacitors and inductors in the circuit (see Figure 50), and to modify their value according to the transformation.

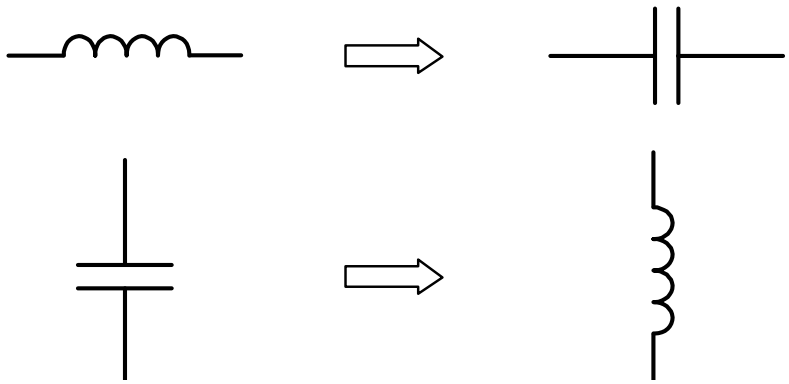

Figure 50. Low-pass to High-pass Transformation

Combining low-pass (with ω_2 as cut-off frequency) and high-pass topologies, it leads to the following bandpass filter transfer function:

$$H_{BPF}(s) = H_{LPF}(s).H_{HPF}(s) = \frac{s}{1 + s\left(\frac{1}{\omega_1} + \frac{1}{\omega_2}\right) + \frac{s^2}{\omega_1 \omega_2}}. \tag{II.19}$$

Assuming

$$Q = \frac{\sqrt{\omega_1 \omega_2}}{\omega_1 + \omega_2} \text{ and } \omega_0 = \sqrt{\omega_1 \omega_2}, \tag{II.20}$$

this gives:

$$H_{BPF}(s) = \frac{1}{1 + jQ\left(\frac{s}{\omega_0} - \frac{\omega_0}{s}\right)}. \tag{II.21}$$

Thus, Q is maximum when $\omega_1 = \omega_2$ and this gives $Q_{\max} = \frac{1}{2}$. The combination of a low-pass and a high-pass filter gives a bandpass filter, but this filter has a selectivity limited to $\frac{1}{2}$. Figure 67, shown further, underlines that such selectivity is not enough to reach the RF selectivity specifications.

II.1.c.iv Assessment of the Topology

The main advantage of the bandpass filter topology is its ability to reach a smaller bandwidth than a combination of a low-pass and a high-pass filters. Based on only two reactive components for a second order filter, the selectivity can be adjusted to whatever -3dB

bandwidth, tuning the quality factor of the filter. This kind of filter is very attractive for both adjacent channels and harmonic frequencies rejections.

Higher order bandpass filters enable to reach higher rejections, as depicted in Figure 51 and Figure 52, at the cost of the use of more reactive elements.

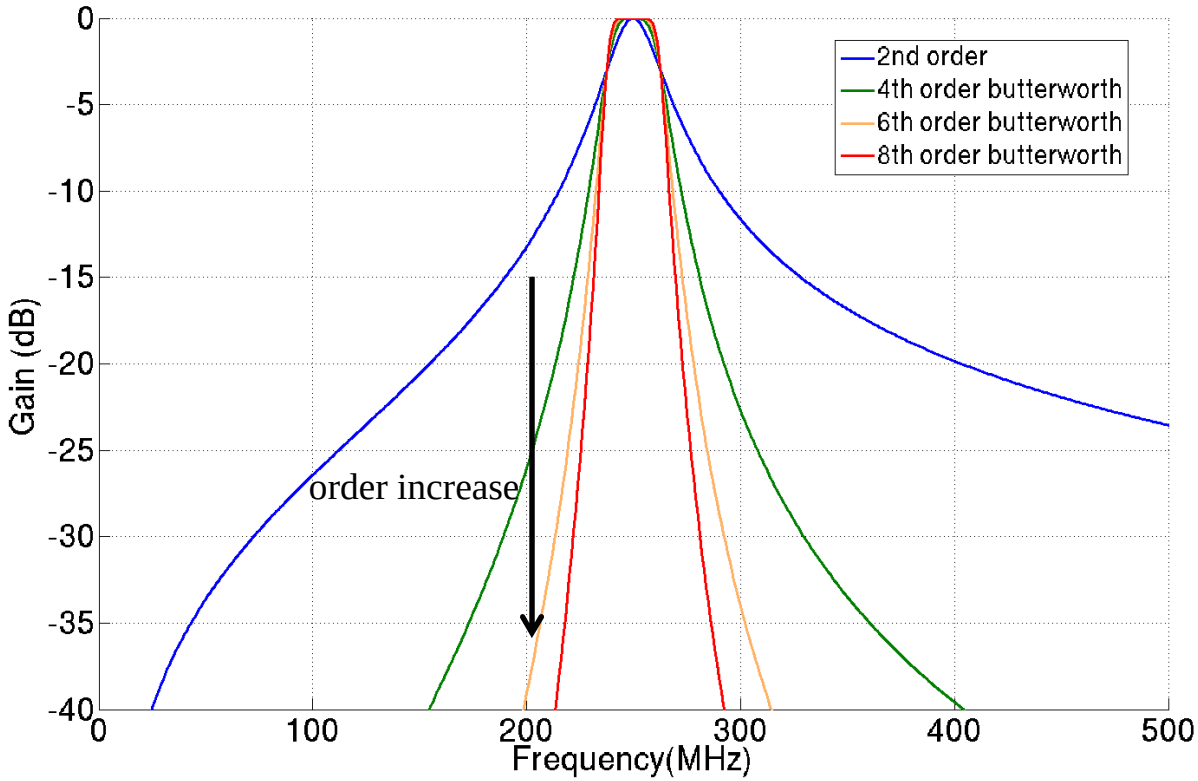

Figure 51. Impact of the Bandpass Filters Transfer Function Order

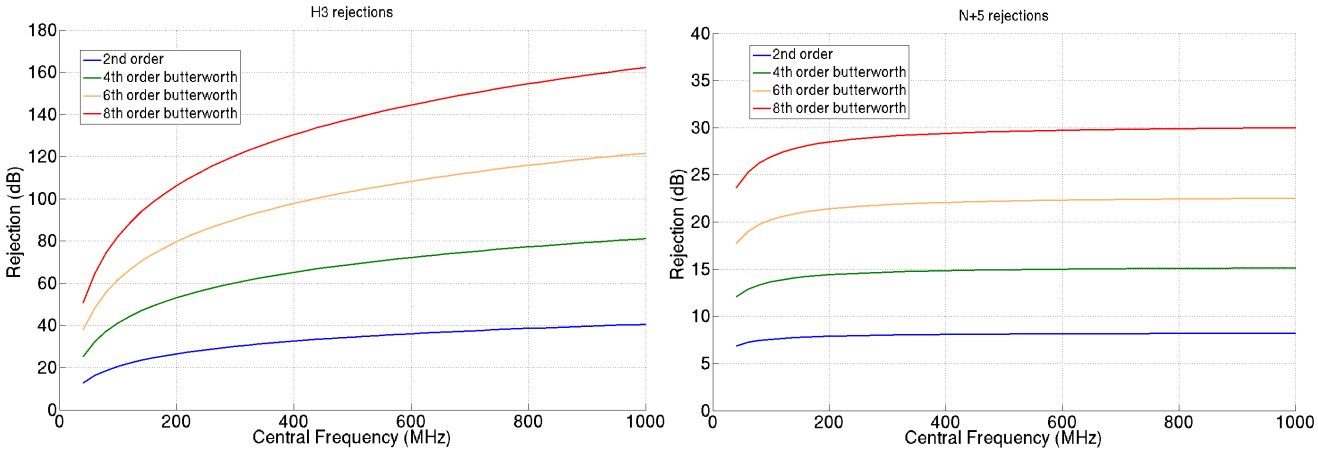

Figure 52. H3 and N+5 rejections according to the order

In case of high order bandpass filters, some particular associations of transfer function coefficients can be achieved [II.2]. Such filter aims at getting the flatter passband (*Butterworth* topologies) or the steeper roll-off allowing some ripple in the passband or in the stopband (*Chebychev type I or II* filters). Some filters present an equalized ripple in the passband and in the stopband and also have the fastest transitions. These filters are known as *elliptic*. A comparison between these filters is performed in Figure 53 and Figure 54.

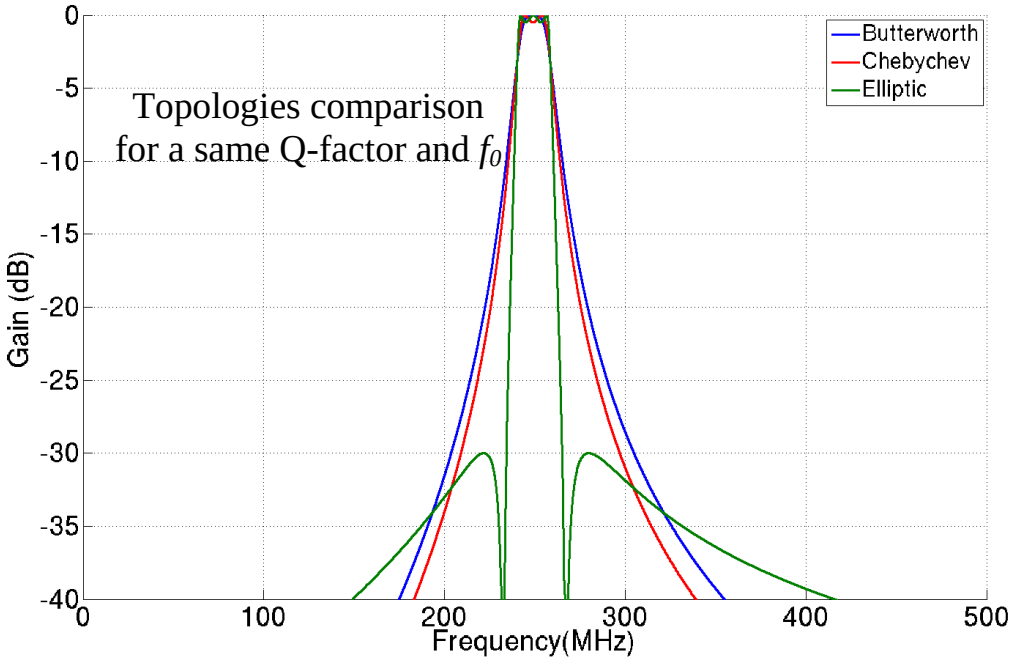

Figure 53. Comparison of fourth order bandpass filters

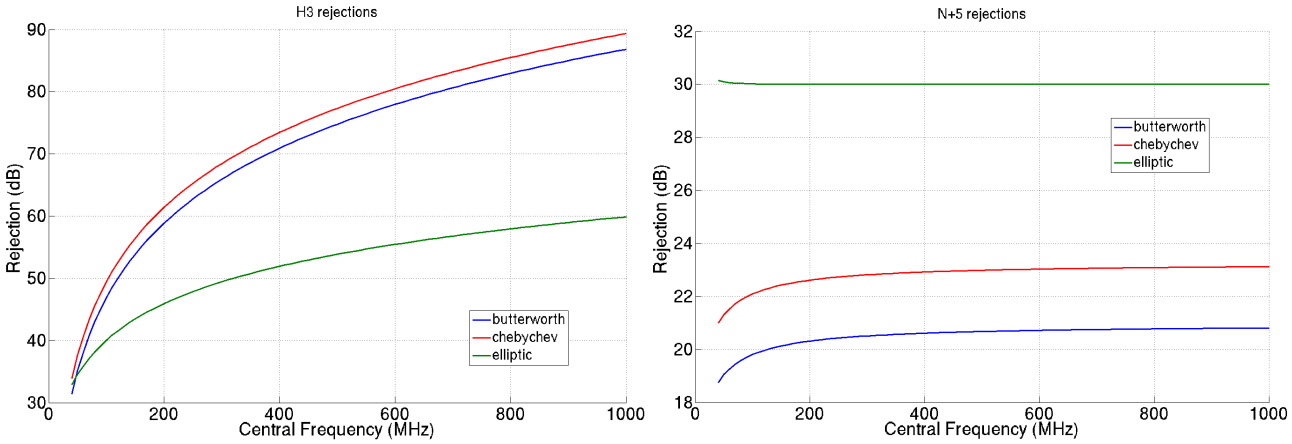

Figure 54. H3 and N+5 rejections according to the fourth order topology

Despite a higher selectivity than second order bandpass, these filters are constituted with four or more reactive elements, leading to a more complex circuit. In particular, the frequency tuning requires keeping the sets of coefficient of the transfer function constant, as said for low-pass high order filters. As explained, to minimize the number of reactive elements in the circuit, a second order bandpass filter is preferred to higher order bandpass filters.

Furthermore, Figure 55 depicts the use of a second order bandpass filters tuned in frequency at constant Q-factor or at a constant-BW, and the achieved rejections are in line with the order of magnitude of the required specifications.

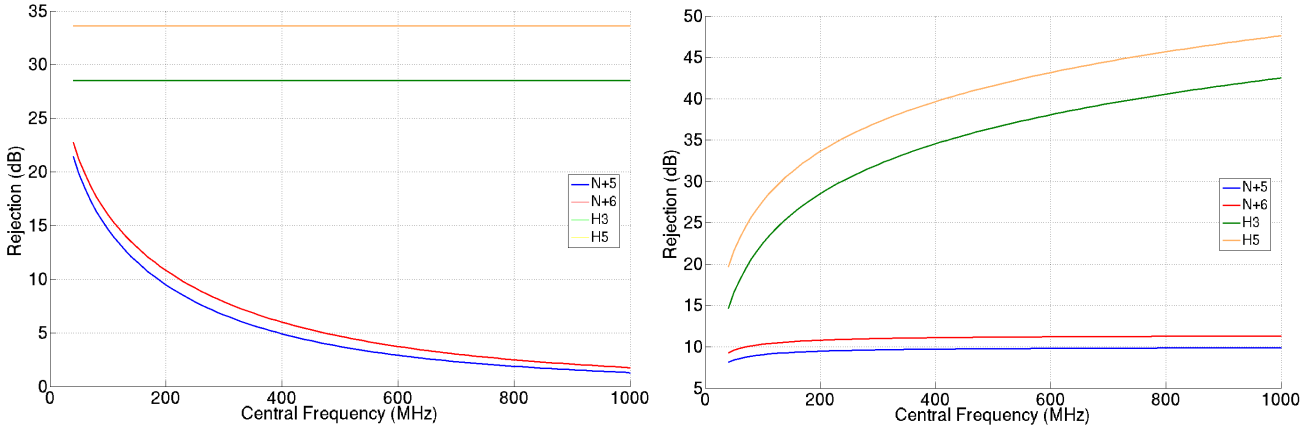

Figure 55. Rejections of a constant Q (Q=10) and constant BW (BW=20MHz) second order bandpass filter

II.1.d Double Notch Topologies

Another possible topology has been studied, consisting in two cascaded notch filters creating a selective bandwidth as illustrated in Figure 58. Once again, the transfer function of a single notch filter can be obtained from the low-pass transfer function by means of the following transformation:

$$s \rightarrow \frac{s.BW_{\omega}}{s^2 + \omega_0^2}, \tag{II.22}$$

where BW_{ω} is the filter stopband bandwidth.

This leads to the following transfer function of a double notch, considering their quality factor:

$$H_{DNF}(s) = \frac{s^2 + \omega_1^2}{\omega_1^2 + \frac{s\omega_1}{Q_1} + s^2} \cdot \frac{s^2 + \omega_2^2}{\omega_2^2 + \frac{s\omega_2}{Q_2} + s^2}. \tag{II.23}$$

The low-pass to notch transformation [II.3] corresponds to the transformation of the passive elements of the circuit given in Figure 56:

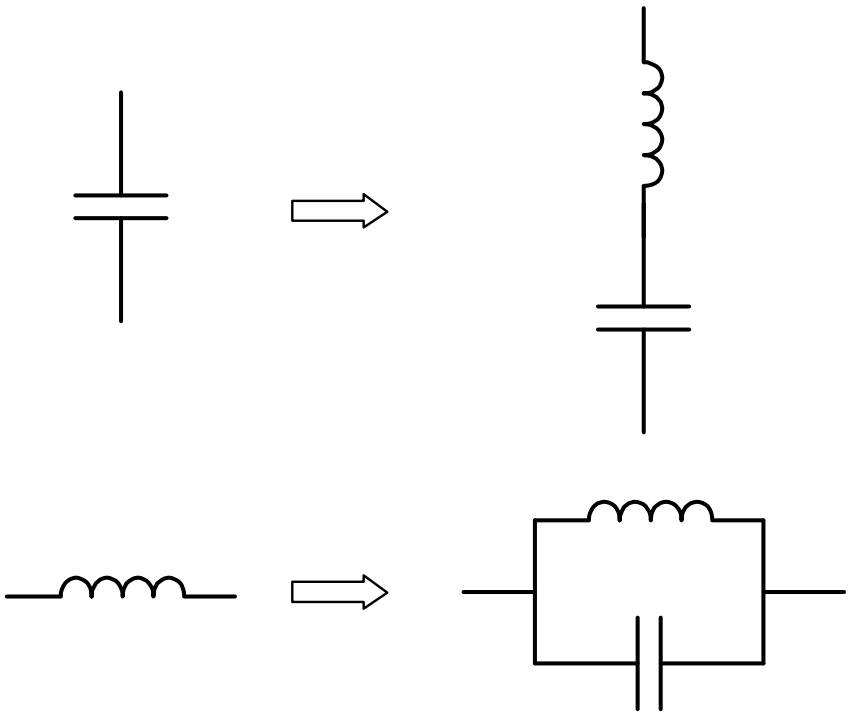

Figure 56. Low-pass to Notch Transformation

Hence, a possible implementation of such a filter is given in Figure 57. Figure 58 shows that, although it can reject close adjacent channels, this solution requires a low pass filtering of harmonic frequencies as well as a high pass filter for the rejection of low frequency interferers.

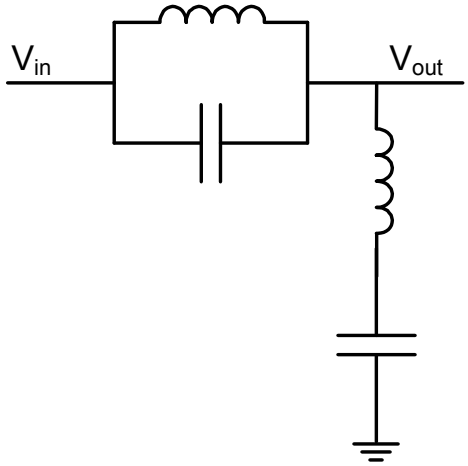

Figure 57. Double Notch Filter schematic

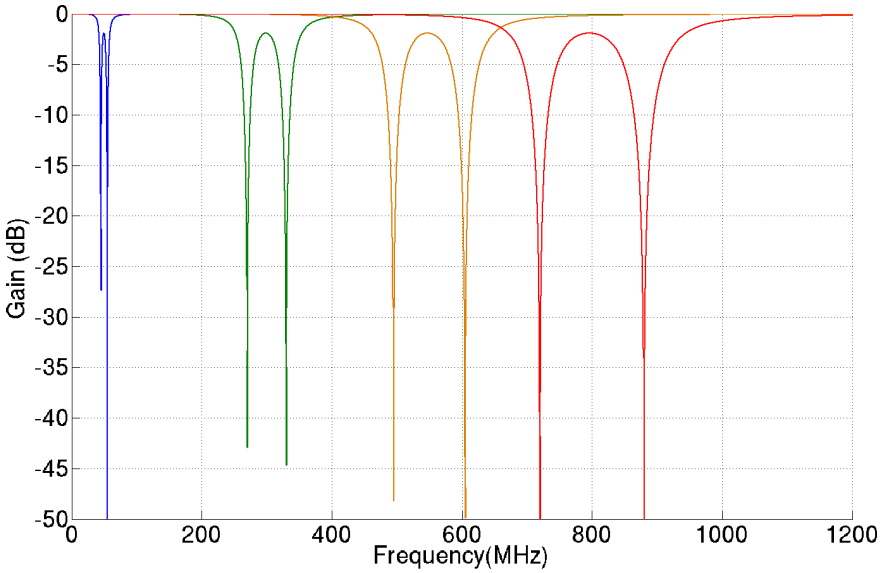

Figure 58. Double Notch Filtering

II.1.e Comparison of the Topologies

The previously studied topologies are compared in Table 4. The table summarizes the different advantages and drawbacks of each solution.

Table 4. Comparison of the Topologies

Topology	Advantages	Drawbacks
Low-pass	Harmonics rejection for order>3	Adjacent channels rejection above f_c
Bandpass	Selectivity depends on Q Harmonics rejection for order>2 Adjacent channel rejection for order>2	
Double notch	Adjacent channel rejection Frequency tuning	Harmonics rejection

From this, the bandpass filtering can be considered as the most appropriate solution since it is able to attenuate both harmonics and adjacent channels. The Q-factor also appears as a strong advantage in order to reject interferers in a controlled way. Moreover, a second order bandpass filter is sufficient to reach the specifications given in introduction, while higher order filters are required for the low-pass. This enables the minimization of reactive components.

That is why the second order bandpass topology has been chosen to handle the RF selectivity.

II.2 Passive LC Second Order Bandpass Filtering

II.2.a Frequency Tunability

As explained before, cable and terrestrial TV bands cover a range from 45MHz up to 1002MHz. Given f_0 formula, some relations and orders of magnitude for L and C can be deduced. It has to be kept in mind that usual integrated capacitances in microelectronics vary between 10fF and 100pF. According to the technology, inductors may be integrated on silicon as well. However, above some tens of nano-Henrys, a spiral inductor becomes too large and so very costly in terms of silicon on-chip space. Hence, it is not efficient to integrate 50nH or more, which are values needed to reach the bottom of the TV bands in VHF low.

To achieve a frequency sweep of the central frequency by steps smaller than a channel width of 6MHz as explained in introduction, the value either of the inductance or of the capacitance, or even both of them, has to be changed gradually.

Technically, it is not optimum to switch inductors. Indeed, parallel switching of inductors, as described in Figure 59.a, requires even higher inductance values since N parallel inductances L are equivalent to a value of inductance of $\frac{L}{N}$. The addition of inductors in series, depicted in Figure 59.b, is efficient in terms of inductance values. However, a large difference of quality factor happens between L_{max} and L_{min}. L_{min} is made of a small inductance value in series with several switches R_{on} in series, while L_{max} is constituted of a large inductance value with no switch R_{on} in series.

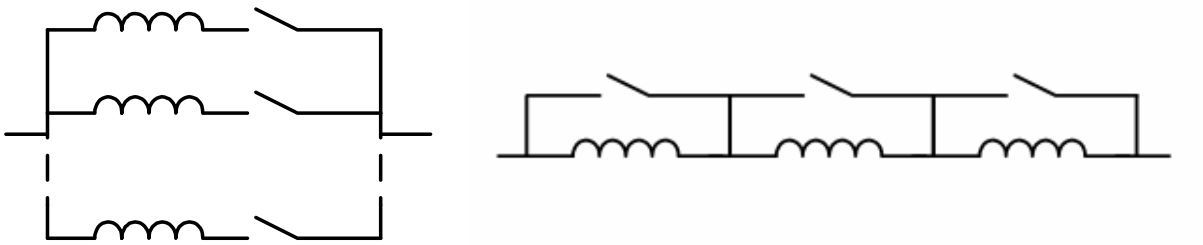

Figure 59. a) parallel inductors switching, b) series inductors switching

Capacitance values can be tuned by different means. The two most popular techniques are the varactor (Figure 60.a) and the capacitor bank (Figure 61.a). The varactor, which actually is a reverse-biased varicap diode with a voltage V_b, has a capacitance C_d which depends on the voltage bias, as it may be seen in Figure 60.b.

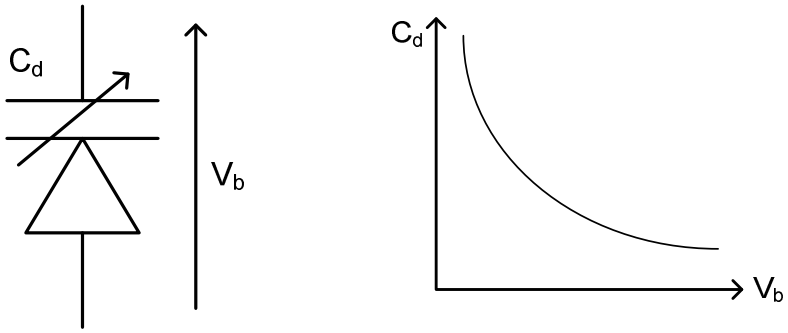

Figure 60. a) Varactor symbol, b) C(V) curve of a varactor

The capacitors bank is made of several capacitors in parallel that can be switched-on, as illustrated in Figure 61, so that a capacitance is added to the initial capacitance. This is a very efficient way of synthesizing a tunable capacitance since the switchable capacitance can have a same quality factor (tuned by the R_{on} of the switches).

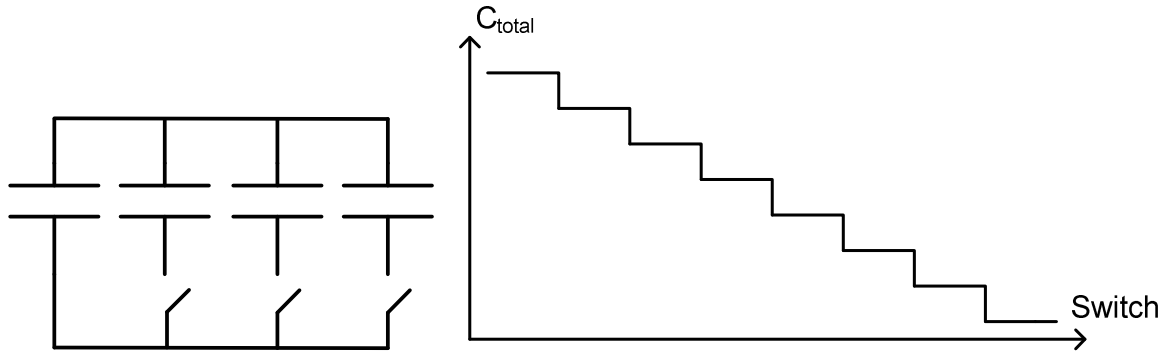

Figure 61. a) Capacitors banks, b) Capacitance evolution of a capacitors bank

Figure 62 shows the value of the central frequency given in Equation (II.10) when varying the capacitance value. This graph is plotted for different inductance values.

It is interesting to notice the great dependency of f_0 for small C values and large L values. Hence, it means that the filter f_0 is very sensitive to capacitance values. Since capacitances are small, such a filter may be difficult to centre accurately at a given frequency. It may also be very sensitive to capacitive parasitics. Moreover, it requires very large capacitances to reach low frequencies.

Hence, this graph underlines the L versus C values trade-off and highlights the difficulty of having a single LC filter for the whole 45-1002MHz band.

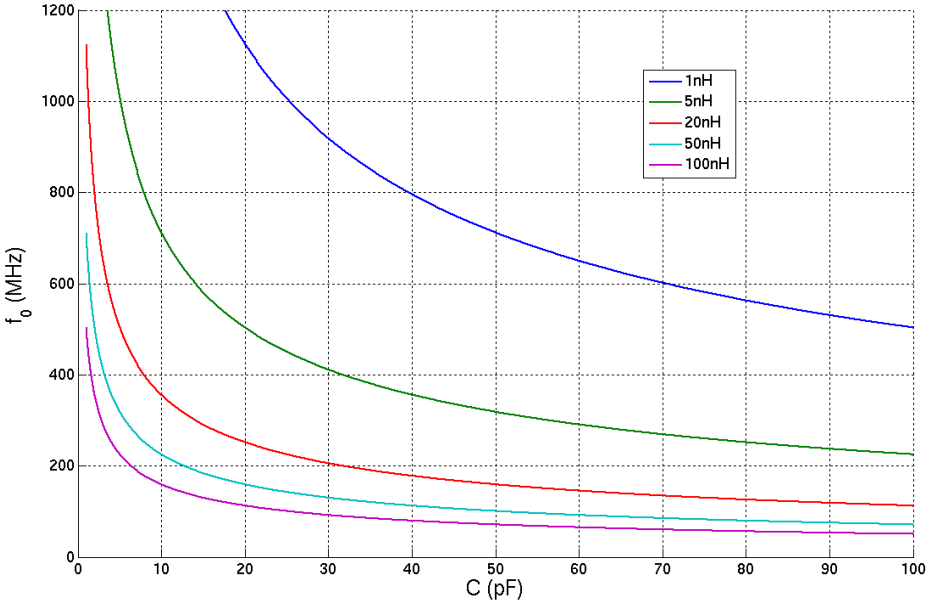

Figure 62. Central frequency versus C for various L values

A possible solution is to split the whole TV band into several sub-bands. Each sub-band may use a different inductor and then switch capacitors to sweep the entire frequency range. One can imagine the use of 100nH in VHF low, 10nH in the mid-band and 1nH for the UHF bands.

In particular, this is very interesting in terms of silicon area for the low-end of the TV band. Indeed, capacitors get smaller when increasing the inductance value while keeping the central frequency constant. Furthermore, for a given inductor value, the tuning range of the filter is proportional to the ratio between the square roots of the capacitances:

$$\frac{f_{\max}}{f_{\min}} \propto \sqrt{\frac{C_{\max}}{C_{\min}}}. \tag{II.24}$$

Using several inductors is a good way of keeping capacitances ratios acceptable for integration. Nevertheless, this method requires additional pins on the chip packaging.

II.2.b Selectivity Tunability

Positioning the central frequency of the filter is one step. A second one consists in getting the desired selectivity, *i.e.* the desired Q-factor. In the following a parallel RLC circuit is considered, with a 10nH inductor and a variable capacitance.

It has been previously explained that, in an LC filter, the bandwidth and the Q-factor are determined by either series or parallel losses. In general, series losses R_s come from the inductor, often implemented by a long resistive spiral wire. Capacitors mainly bring parallel losses R_p, due to a small current flowing through the non-ideal insulator. This results in an equivalent RLC circuit, depicted in Figure 63.

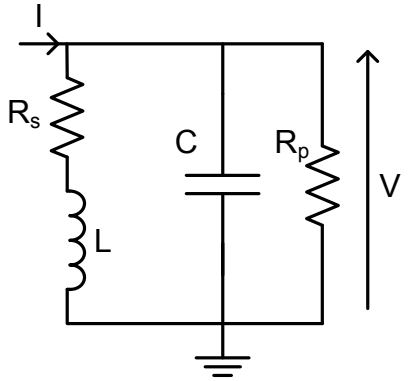

Figure 63. Equivalent RLC circuit

Furthermore, the LC filter presents different behaviour depending on the major contributor between R_p and R_s. To be able to compare these two contributors, the series resistance R_s is transformed into an equivalent parallel resistance $R_{s//}$ as follows:

$$R_{s//} = R_s\left(1+Q^2\right), \tag{II.25}$$

where Q is the quality factor of the resonant circuit.

Hence, the circuit is said R_p-limited if $R_p<R_{s//}$, since parallel losses from the capacitor are dominant. On the contrary, if $R_p>R_{s//}$, the circuit is said R_s-limited and series losses from the inductor are considered as the major source of losses of the filter.

As it may be seen in Figure 64, an R_p-limited filter will give a constant gain frequency sweep when tuning the capacitance. One can also notice that the Q-factor decreases with frequency. Indeed, the quality factor of the parallel circuit is then defined as:

$$Q_{//} = R_p \sqrt{\frac{C}{L}} \tag{II.26}$$

while higher frequencies are reached with smaller capacitances.

However, most of the time, LC resonators are R_s-limited because of the poor Q-factors of discrete or of on-chip inductors. Such a filter presents a constant bandwidth when sweeping the frequency with the capacitance. The quality factor of this resonant circuit is given by:

$$Q_s = \frac{1}{R_s} \sqrt{\frac{L}{C}} \tag{II.27}$$

Then, the bandwidth becomes independent from the tuning capacitance C:

$$BW = \frac{f_0}{Q_s} = \frac{1}{2\pi\sqrt{LC}} R_s \sqrt{\frac{C}{L}} = \frac{R_s}{2\pi L} \tag{II.28}$$

Another particularity of this R_s-limited circuit is that gain strongly increases with frequency, due to the increase of the Q-factor, as illustrated in Figure 64.

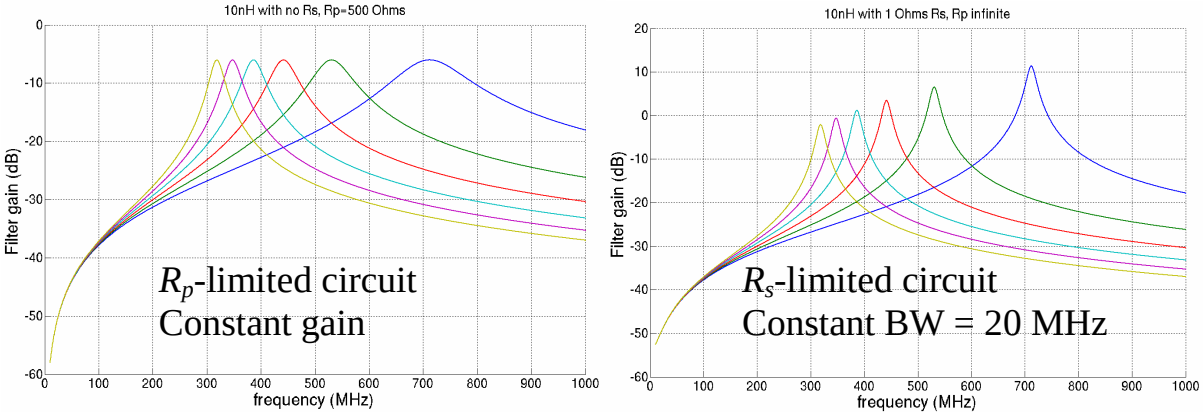

Figure 64. R_p-limited (a) and R_s-limited LC filter when sweeping the capacitance

The large gain increase of an R_s-limited filter can be handled by the decrease of the current I flowing through the resonator, by means of a reduced input transconductance g_m, as shown in Figure 65. This compensates for the gain increase but this will also result in a filter with lower noise performances. Dividing the whole tuning range in sub-bands is another good solution to limit the gain increase to a certain amount.

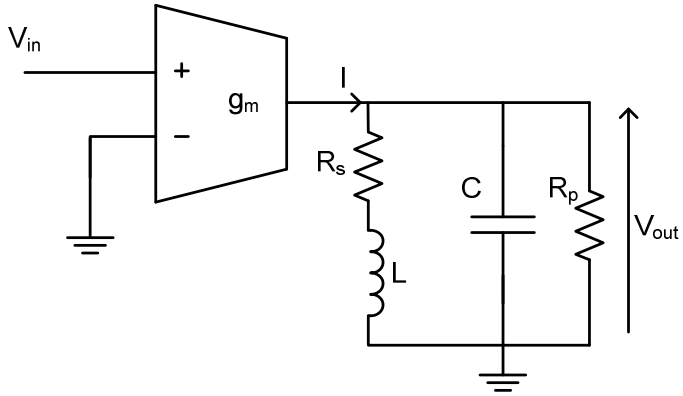

Figure 65. Current-fed resonating circuit

II.2.c Second Order Bandpass Filter for TV Tuners Specifications

Assuming a second order bandpass filter topology, the specifications previously set on the RF selectivity stage can be converted in terms of filter bandwidth and Q-factor. Figure 66 depicts these two parameters as a function of the filter central frequency.

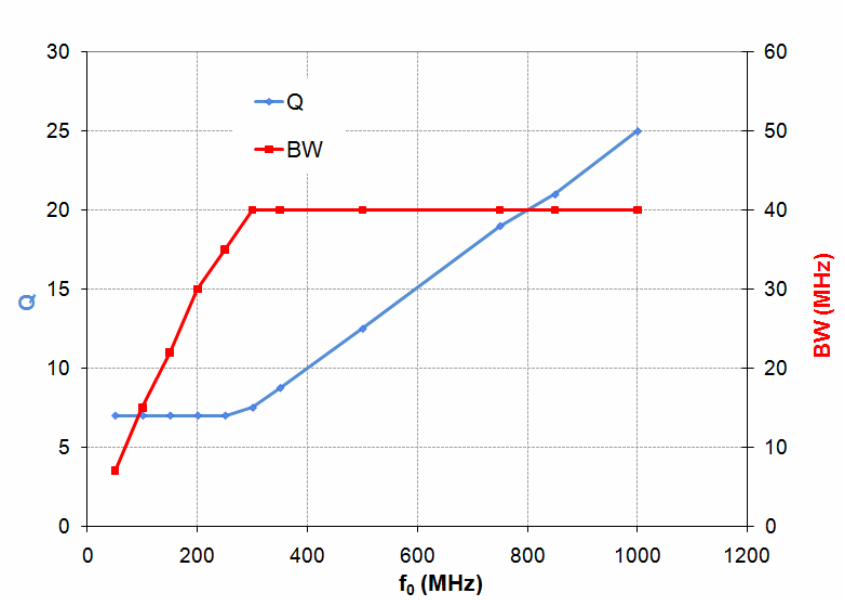

Figure 66. Q and BW versus central frequency from specifications

Hence, at low frequencies where harmonic rejections are dominant, it means a constant-Q rejection to reach the minimal rejection of H3. Aadjacent channels become the most stringent specification to fulfil. Then, a constant-BW rejection is required to reach the minimal rejection of the adjacent channels.

Figure 67 describes the N±5 channel and the third harmonic rejection versus the filter central frequency, for various Q-factors. This figure highlights how selective a filter should be to reject adjacent channels as high as specified.

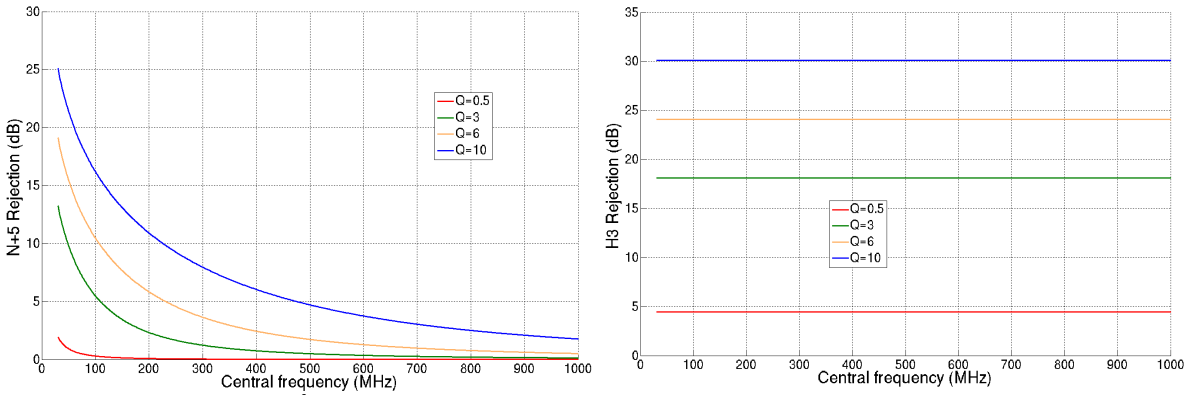

Figure 67. N+5 (a) and 3rd harmonic (b) rejection versus the filter central frequency for various Q-factors

II.2.d Passive LC Filters from the Literature

It has previously been demonstrated that for our application, the most interesting passive LC filters are second order bandpass filters, sometimes cascaded to obtain a higher order filter. As explained, they are mostly based on a parallel LC resonator, often referred as an LC tank. According to the inductor nature, papers can be sorted into two main categories:

- Discrete inductor based filters
- On-chip inductor based filters

The performances of several passive LC filters are summarized in a table that may be found in APPENDIX C. Among them, the most recent one [II.4] describes two cascaded first order passive LC filters, as shown in Figure 68. Figure 68 also describes how frequency and gain tuning is realized. The two LC tanks are fed in current by transconductances having a built-in first order low-pass filter which allows higher harmonic frequencies rejections. The 130MHz to 1GHz band is divided into two sub-bands. The higher inductance value is realized by means of an off-chip inductor while parasitic inductances from PCB traces and bonding wires realize a small inductance value, as depicted in Figure 69.

This filter exhibits in band 18dB NF and 20dBm IIP3, for a Q-factor of 5 as it may be seen in Figure 70. The strong asset of this filter is the harmonic rejection which is higher than 36dB over the whole tuning range.

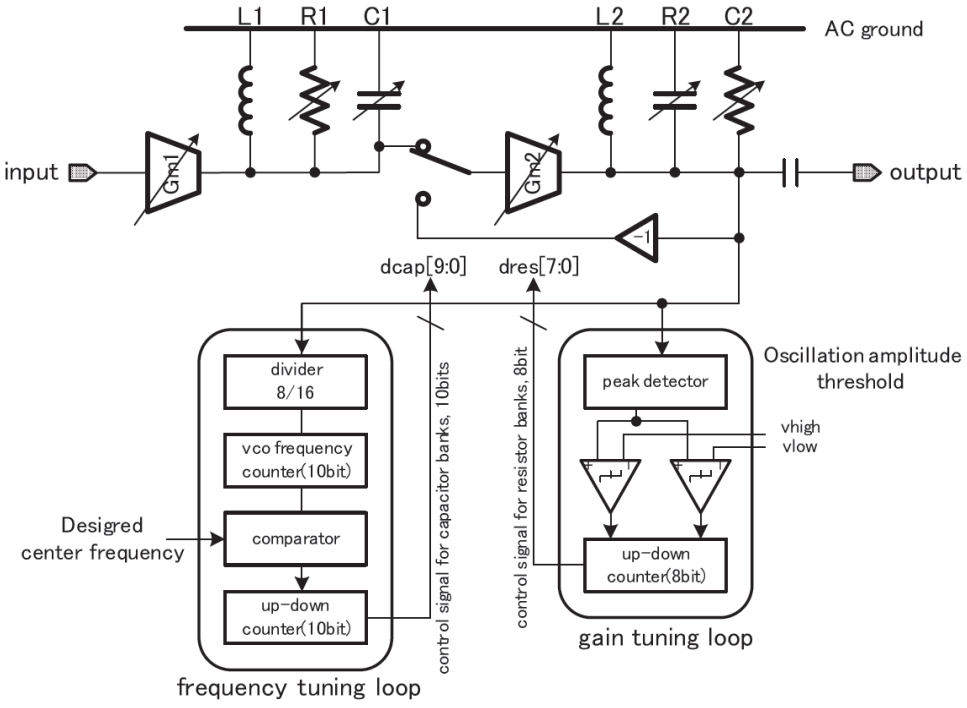

Figure 68. Cascade of two second order bandpass filter

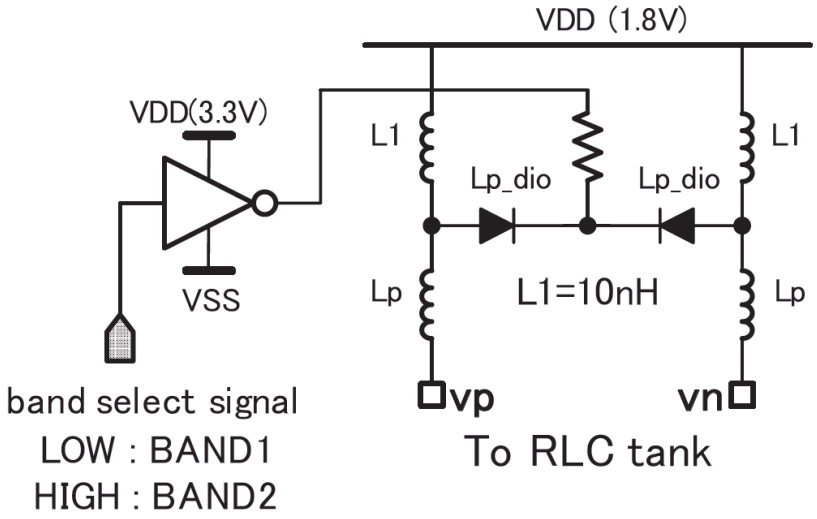

Figure 69. Band Switching

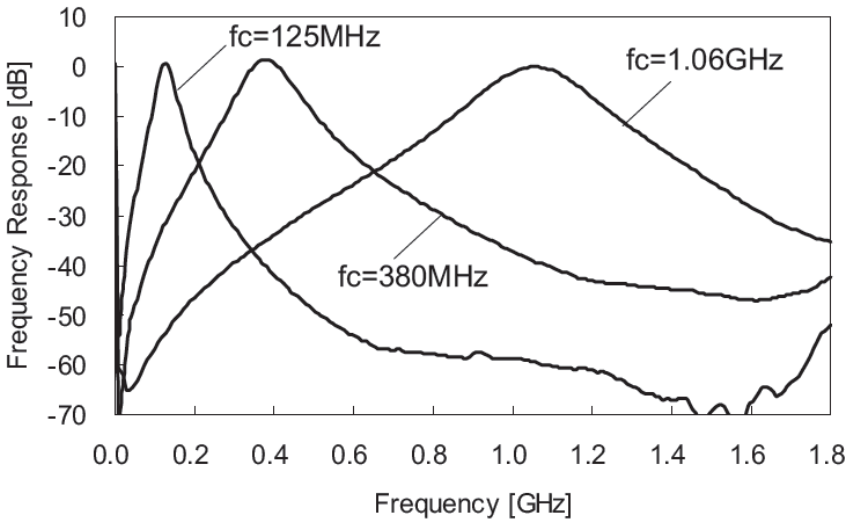

Figure 70. Filter frequency response

II.3 Towards a Fair Figure-of-Merit

II.3.a Required Parameters to Handle a Fair Comparison

To be able to compare the performances of the various structures of RF filters (passive LC, Gyrator-C, Gm-C, n-path filters or else) that may be found in the literature, a common reference figure is needed. This figure, called figure-of-merit (FOM), should take into account all parameters related to the specifications discussed in introduction, which are:

- RF dynamic range: ***linearity*** and ***noise***;
- ***Frequency tuning range***;
- Selectivity: ***quality factor***, harmonics and adjacent channels rejections;
- ***Maximum working frequency***.

Some other aspects might as well be taken into account, such as the ***process variations***, the ***gain*** at the central frequency or even the ***area*** occupied by the circuit.

II.3.b Study of the Figures-of-Merit Found in the Literature

Let's have a look at some FOMs found in the literature. In [II.5], *K. Kwon et al*, a FOM for linear and low-noise low-pass filters is presented. Their FOM is the following:

$$FOM = \frac{OIP3.f_{\max}.TR.N}{(F-1)P_{dc}} \tag{II.29}$$

where F is the noise factor, P_{dc}/N is the power consumption per pole and *TR* is the frequency tuning range.

The quality factor of the filter, for a band-pass, is an important parameter to consider and is not taken into account in this FOM. Although too high power consumption would be an issue, it is not a primary specification since TV is not a portable application. Input parameters would also be preferred because of their independence of the filter gain.

Another FOM is introduced in [II.6]. After having described a passive band-pass filter, F. Dülger et al. have introduced the following figure-of-merit, which is taken in dB:

$$FOM_{dB} = \frac{N.SFDR.f_0.Q}{P_{dc}} \tag{II.30}$$

where P_{dc}/N is still the power consumption by pole, *SFDR* is the Spurious Free Dynamic Range.

However, this FOM does not take into account the frequency tunability. There is reference neither to linearity nor to noise in this figure, which makes this FOM not suitable for the previously described purposes.

Another paper [II.7] provides a FOM but here again no mention is made about linearity or noise:

$$FOM = \log\left(\frac{f_0 N}{P_{dc}}\right) \tag{II.31}$$

This FOM is plotted versus $\frac{f_{\max}}{f_{\min}}$.

II.3.c Proposed Figure-of-Merit

To be sure to use a suitable figure-of-merit, a new FOM is introduced, taking into account all the parameters that have been mentioned previously.

$$FOM = 10^{\frac{IIP3-NF}{10}} . Q_{moy} . f_{\max} . TR \tag{II.32}$$

where $TR = \frac{f_{\max}}{f_{\min}}$ is the tuning range.

This FOM can also be normalized to the power consumption.

II.4 Active Filtering Solutions

From the literature, it comes out that Gyrator-C and Gm-C are the most used techniques to handle fully active RF filtering. Since they are continuous-time filters with no discretisation of the signal, they are well matched for current NXP tuner architectures. This chapter aims at describing their principle and the state-of-the-art of these techniques. Other solutions, which are emerging techniques, are studied later in this manuscript.

II.4.a Gyrator-C Filtering

II.4.a.i Gyrator General Principle

The gyrator is the most popular structure to handle active RF bandpass filtering. Its principle consists in ***synthesizing an inductive behaviour*** by means of two transconductors in the configuration depicted in Figure 71.

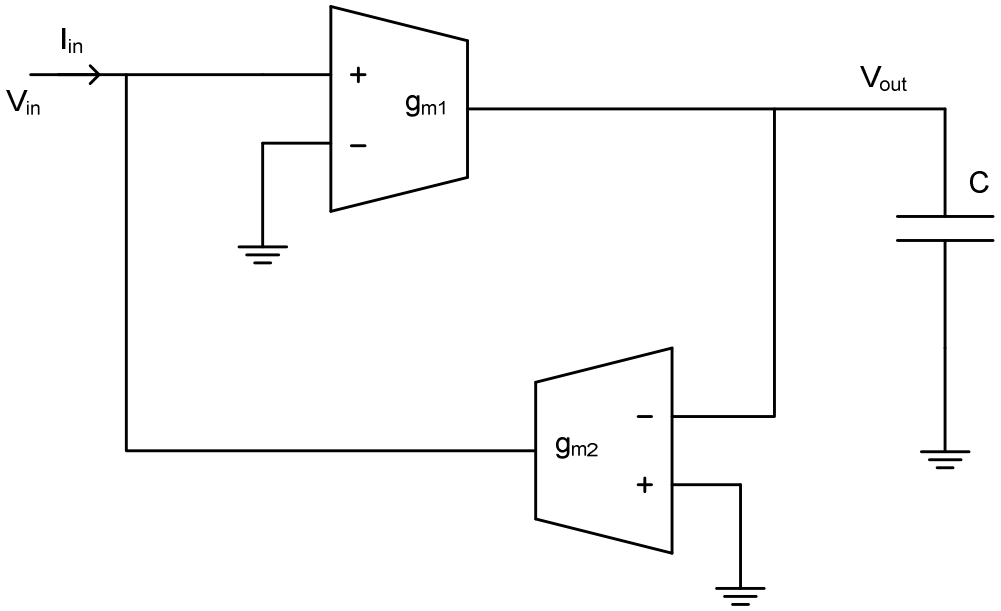

Figure 71. Gyrator configuration

To find the equivalent impedance of this load, first steps of computation give:

$$\begin{cases} g_{m1}V_{in} = jC\omega V_{out} & \text{(III.33)} \\ I_{in} = g_{m2}V_{out} & \text{(III.34)} \end{cases}$$

From these two equations, one gets:

$$Z_{in} = \frac{V_{in}}{I_{in}} = j\omega\left(\frac{C}{g_{m1}g_{m2}}\right). \quad \text{(III.35)}$$

Hence, the input impedance Z_{in} of this load shows an inductive behaviour, with an effective inductance L_{eff} given by:

$$L_{eff} = \frac{C}{g_{m1}g_{m2}}. \quad \text{(III.36)}$$

A parallel self resonating circuit is then obtained considering a parallel capacitor C_p to the gyrator. This leads to a resonant frequency given by:

$$\omega_0 = \sqrt{\frac{g_{m1}g_{m2}}{CC_p}}. \qquad \text{(III.37)}$$

A filter using a gyrator as a resonant element is called in the literature a Gyrator-C filter.

Figure 72 depicts a fourth order high-pass filter. The equivalent gyrator-C filter is obtained transforming the inductors of the circuit into gyrators.

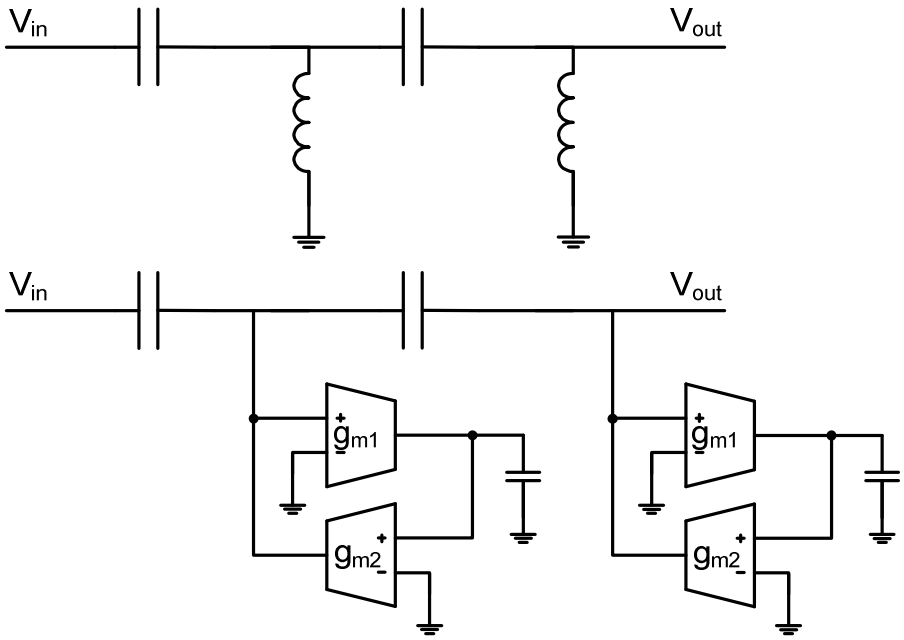

Figure 72. Synthesis of a filter using gyrators

II.4.a.ii Impact of Real Elements

Though previous transconductances were considered as ideal, imperfections appear when implementing the design. It can be either an input capacitance (for instance the C_{gs} of a MOS realizing the g_m) or a non-infinite output resistance. This leads to the schematic shown in Figure 73, where C_2 takes into account the real model of the transconductance as well as the internal node capacitance of the gyrator.

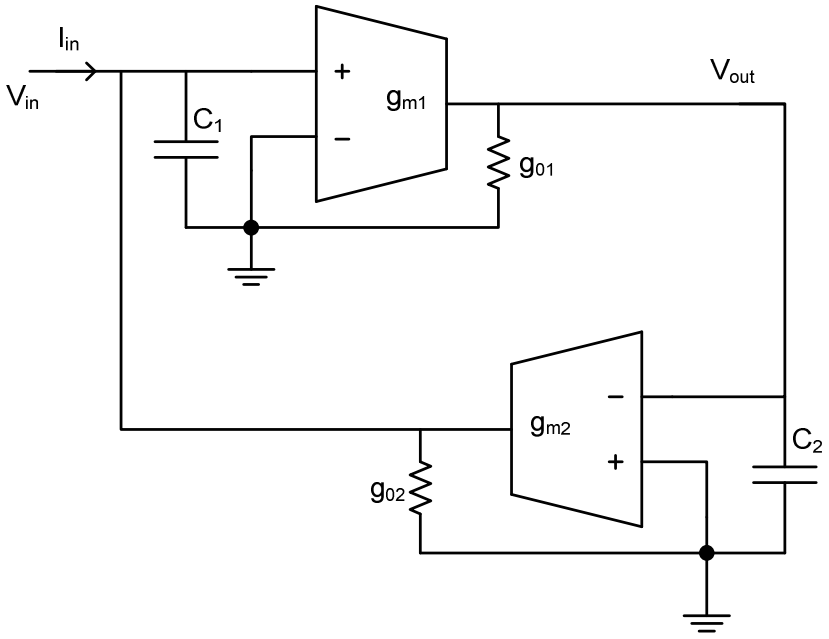

Figure 73. Gyrator with real transconductances

The electrical analysis of the circuit leads to:

$$V_{in} = \frac{I_{in} - g_{m2} V_{out}}{g_{o2} + jC_1\omega} \tag{III.38}$$

and

$$V_{out} = \frac{g_{m1} V_{in}}{g_{o1} + jC_2\omega}. \tag{III.39}$$

By combining the last two equations, one gets the equivalent admittance:

$$Y_{in} = \frac{I_{in}}{V_{in}} = \frac{1}{\frac{g_{01}}{g_{m2} g_{m1}} + j\omega \frac{C_2}{g_{m2} g_{m1}}} + (g_{02} + j\omega C_1) \tag{III.40}$$

This admittance formula is similar to the one of a parallel resonant RLC filter, as depicted in Figure 74. By identification, its different parameters can be determined: inductance, parallel and series resistance and capacitance.

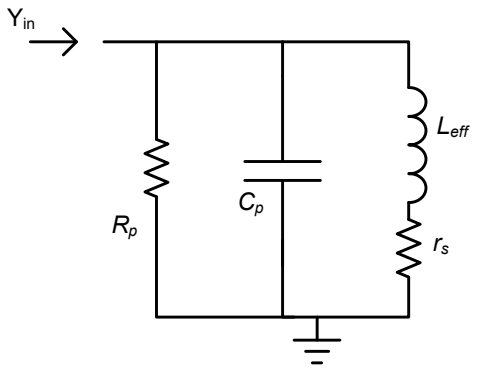

Figure 74. Parallel equivalent circuit

This gives the following values for the equivalent RLC parameters:

$$\begin{cases} L_{eff} = \dfrac{C_2}{g_{m1} g_{m2}} & \text{(III.41)} \\ C_p = C_1 & \text{(III.42)} \\ R_p = \dfrac{1}{g_{02}} & \text{(III.43)} \\ r_s = \dfrac{g_{01}}{g_{m1} g_{m2}} & \text{(III.44)} \end{cases}$$

The resonant frequency and the quality factor are then given by these formulas:

$$\begin{cases} \omega_0 = \sqrt{\dfrac{g_{m1} g_{m2}}{C_1 C_2}} & \text{(III.45)} \\ Q = \dfrac{1}{g_{01}} \sqrt{\dfrac{g_{m1} g_{m2} C_2}{C_1}} & \text{(III.46)} \end{cases}$$

It is worth noticing is that transconductors imperfections create a self-resonant frequency of the gyrator. It means that the gyrator can be used in two ways:

- as a resonant circuit with a central frequency determined by the transconductor imperfections; or
- as an inductor if the working frequency is lower than the gyrator resonant frequency.

II.4.a.iii Single-Ended Structures

A commonly used single-ended Gyrator-C structure is depicted in Figure 75, where the transconductances g_{m1} and g_{m2} are realized by means of a common source and a common drain MOS transistors. Furthermore, two current sources I_1 and I_2 bias the whole circuit.

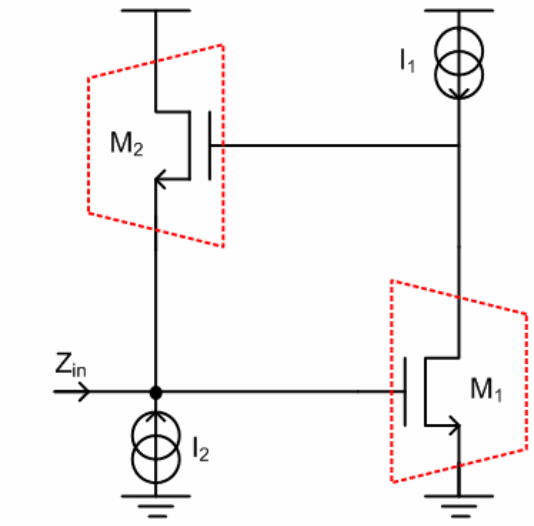

Figure 75. Single-ended gyrator structure

The equivalent impedance of a parallel RLC circuit can be computed. Neglecting drain-source capacitances at first order, one gets:

$$\begin{cases} L_{eff} = \dfrac{C_{gs2}}{g_{m1} g_{m2}} & \text{(III.47)} \\ R_s = \dfrac{g_{01}}{g_{m1} g_{m2}} & \text{(III.48)} \\ C_p = C_{gs1} & \text{(III.49)} \\ R_p = \dfrac{1}{g_{02}} & \text{(III.50)} \end{cases}$$

This structure resonates with the following parameters:

$$\begin{cases} \omega_0 = \sqrt{\dfrac{g_{m1} g_{m2}}{C_1 C_2}} & \text{(III.51)} \\ Q = \sqrt{\dfrac{g_{m1} C_{gs_2}}{g_{m2} C_{gs_1}}} & \text{(III.52)} \end{cases}$$

From these formulas, it comes out that M_1 and M_2 parameters are subject to a compromise. Indeed, to obtain a sufficiently high resonant frequency and to ensure a high quality factor, g_{m2} is required to be high while g_{m1} is kept at a relatively low value. However, in [II.8], a noise analysis is performed and demonstrates that noise voltage is proportional to $\frac{g_{m2}}{g_{m1}}$. The trade-offs and the optimizations of the gyrator are discussed more deeply in next chapter.

A similar structure is described in the literature. It actually relies on the same principle but uses a common source MOS transistor associated to a common gate one, as depicted in Figure 76. This solution aims at obtaining different formulas for R_p and R_s of the equivalent model, which may be useful to reach another trade-off. Indeed, the formulas are then given by:

$$\begin{cases} R_p \approx \dfrac{1}{g_{m1}} & \text{(III.53)} \\ R_s = \dfrac{g_{ds1}}{g_{m1} g_{m2}} & \text{(III.54)} \end{cases}$$

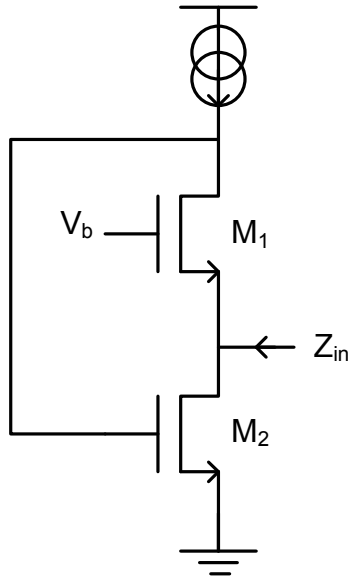

Figure 76. Another single-ended gyrator structure

A possible improvement of the initial structure consists in using a cascode stage in order to increase M_1 output resistance, as it may be seen on Figure 77, based on *R.M. Weng et al.* publication [II.9]. This results in a reduced series resistance. The three current sources enable a large g_m tuning and an independent tuning between g_{m1} and g_{m3} since only I_1 goes through M_3 whereas (I_1+I_3) goes through M_1. Parameters then become less intricate than before.

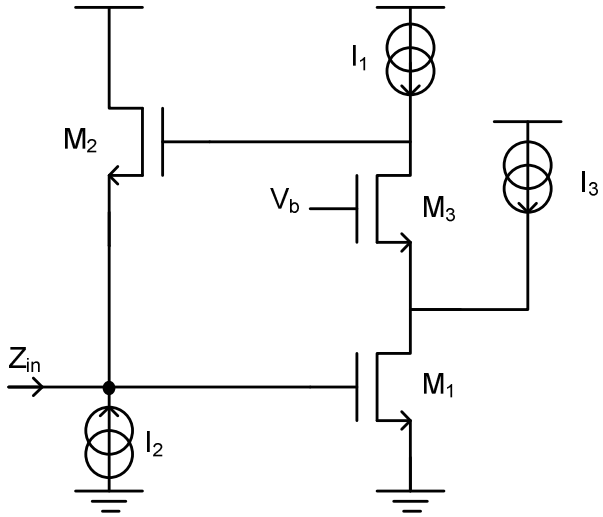

Figure 77. Improved cascoded Gyrator-C

Its RLC equivalent values become:

$$\begin{cases} L_{eff} = \dfrac{C_{gs2}}{g_{m1}g_{m2}} & \text{(III.55)} \\ R_s = \dfrac{g_{01}g_{03}}{g_{m1}g_{m2}g_{m3}} & \text{(III.56)} \\ C_p = C_{gs1} & \text{(III.57)} \\ R_p = \dfrac{1}{g_{02}} & \text{(III.58)} \end{cases}$$

In the literature, negative impedance circuits (NICs) are often added to Z_{in} to circumvent low quality factors issues. Indeed, a negative resistance compensates for the parallel resistance of the overall equivalent RLC circuit, leading to an enhanced quality factor. The NIC usually intrinsically adds a capacitance to the parallel RLC circuit as well, which results in a lowered self-resonant frequency of the Gyrator-C structure.

On Figure 78, C_{nic} and R_{nic} are the capacitance and the negative impedance created by the NIC. Another capacitor C_{tune} can be used in parallel to tune the central frequency, which gives the following formulas.

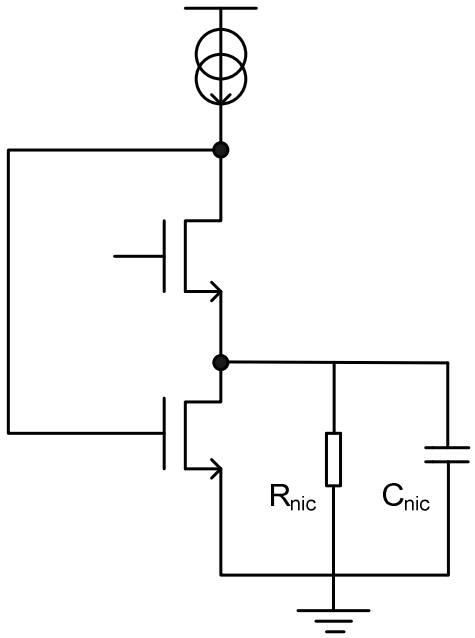

Figure 78. Gyrator-C and NIC

$$\begin{cases} \omega_0 = \dfrac{1}{\sqrt{L_{eff} C}} & \text{(III.59)} \\ C = C_p + C_{nic} + C_{tune} & \text{(III.60)} \end{cases}$$

This gives the following filter quality factor:

$$Q = \frac{R_p R_{nic}}{R_p + R_{nic}} \sqrt{\frac{C}{L}} \qquad \text{(III.61)}$$

The cancellation of the parallel equivalent resistance leads to a pure LC circuit with a ideally infinite Q-factor. The negative impedance circuit can make the structure oscillate if R_{nic} cancels exactly for R_p. However, a partial cancellation of R_p and an accurate control of R_{nic} value may lead to very high Q-factor (R_p+R_{nic} close to zero). In the literature, quality factors superior to 100 and up to 2000 have been published [II.10 to II.14]. Though it may be very attractive for VCOs, stability can then become a critical issue when dealing with an RF filter.

In the literature, self resonant frequencies of Gyrator-C circuits goes from 400MHz up to 2.5GHz and are mainly used for GSM applications. The main issue of these structures is the poor linearity versus noise trade-off. IIP3 of -5dBm downto -30dBm are reported while,

when given, reported noise figures are also very high (see APPENDIX C) since high Q-factors are often targeted. This results in poor RF performances.

II.4.a.iv Differential Structures

Differential transconductors are mainly based on differential pairs as illustrated in Figure 79.

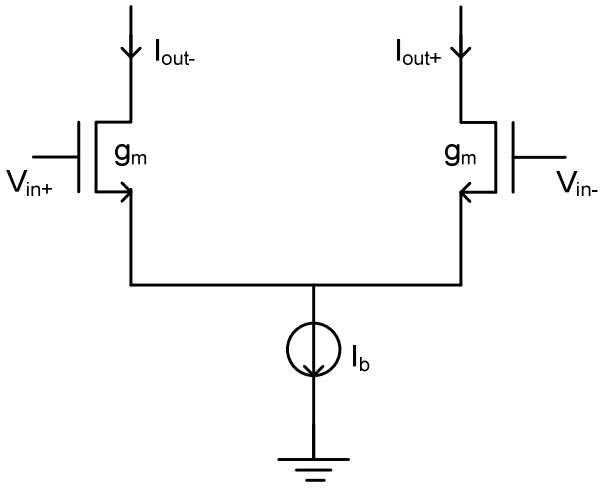

Figure 79. Differential Pair Transconductor

These differential transconductors enable to create a double gyrator, as it may be seen in Figure 80, which is equivalent to a floating inductor, one per path in differential.

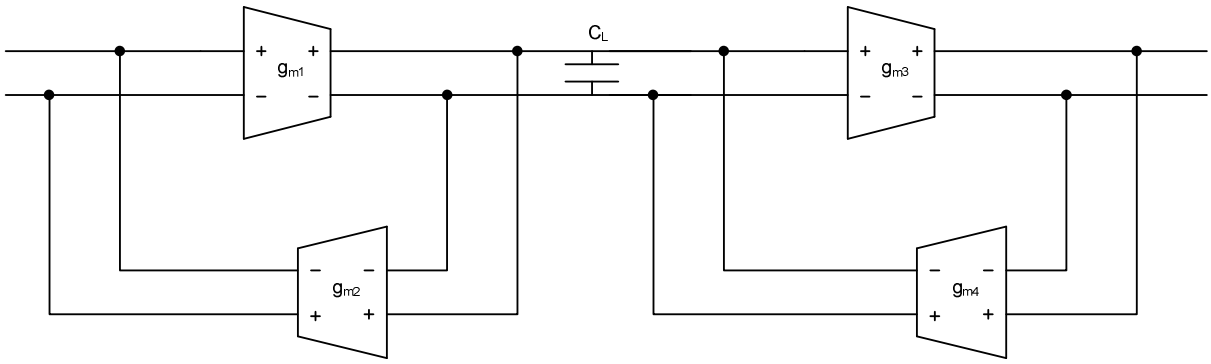

Figure 80. Double Gyrator

II.4.b Gm-C filtering

Gm-C and OTA-C filtering are both based on a similar principle which consists in ***synthesizing a transfer function*** by means of integrators built with Gm-cells or OTAs. As said, Gyrator-C filters consist in emulating an inductive behaviour.

II.4.b.i From Integrators to Transfer Function Synthesis

In the literature, it has been shown [II.15 and II.16] that all continuous time filters can be decomposed into an association of integrators. Thus, combining a few Gm-cell and capacitors, several different filters can be obtained. For instance, a possible way is to transform the circuit in an equivalent LC ladder and to replace inductors by gyrators.

A way to create an integrator is to associate a capacitor to the transconductance. Indeed, the computation of the transfer function has an integrator form:

$$\frac{V_{out}}{V_{in}} = \frac{g_m}{jC\omega}. \qquad \text{(III.62)}$$

Assuming the transconductor non-infinite output resistance r_0, this leads to a lossy integrator as depicted on Figure 81, having the following transfer function.

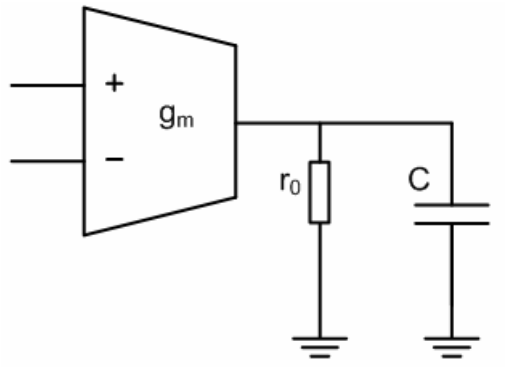

Figure 81. Lossy Integrator

$$\frac{V_{out}}{V_{in}} = \frac{g_m r_0}{1 + jr_0 C\omega} \qquad \text{(III.63)}$$

Hence, the basic cell of these integrators, and so of Gm-C filters, is the Gm-cell. It is a transconductance amplifier which is able to convert an input voltage into an output current with a given gain g_m, called transconductance. The literature deals with both OTAs and Gm-cells when describing integrators. However, an OTA, which stands for Operational Transconductance Amplifier, is regarded as an operational amplifier whose output impedance is very low. As mentioned in [II.15], OTAs transconductance value is almost irrelevant as long as its voltage gain is high. On the contrary, a Gm-cell is a more general term, referring to a voltage-controlled current-source having a well determined transconductance value. That is why the term “OTA-C” filters will be avoided in the following.

In all publications dedicated to Gm-C or OTA-C filters, the basic idea is first to design a transconductor. For our application, we have to associate a few of these transconductors in a way that the transfer function of the circuit corresponds to the desired type of filter. A large number of the second order bandpass topologies are given in [II.17] in a complete study by R.L. Geiger and E. Sánchez-Sinencio.

II.4.b.ii Gm-C Filters in the Literature

One way to synthesize a given transfer function is to find its LC equivalent circuit and then to replace inductors by gyrators and resistors by 1/Gm cells. In this case, Gyrator-C and Gm-C filters are equivalent. This is especially the case for simple transfer function. For more complex transfer function, this synthesis method may not be optimal in terms of number of components.

Figure 82 depicts an LC elliptic third order low-pass filter circuit above its equivalent in a Gm-C structure [II.2]. It may be seen that the inductor has been replaced by a differential double gyrator made of four Gm cells.

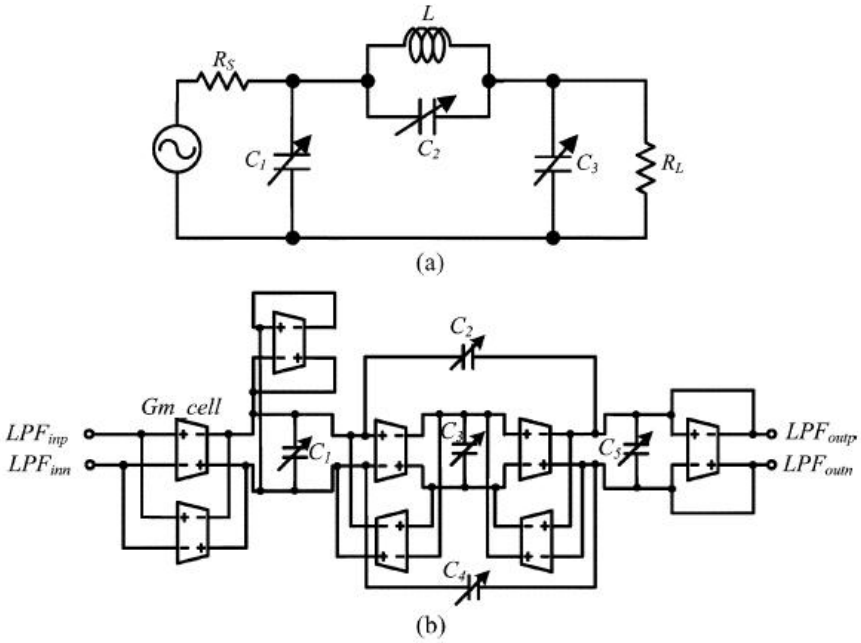

Figure 82. Elliptic 3rd order low-pass filters

Reference [II.7], written by *R.G. Carvajal et al* is one example of a Gm-C tunable filter which is based on a very linear Gm-cell architecture, shown on Figure 83. The structure is quite complex with both common-mode feed-forward and feed-back to ensure a high linearity.

Once this transconductor is designed, several are associated as depicted in Figure 84 to synthesize a second-order bandpass filter. Though this structure can be used over a very wide frequency range, from 300kHz to 32MHz, the complexity of the transconductor limits the use at higher frequencies. It exhibits a good linearity (8 dBm IIP3) but no information about noise is given. Figure 84 shows that the transconductance of the Gm-cells is tunable, by means of V_{tuning}. Hence, the frequency tunability of the filter is achieved by g_m tuning.

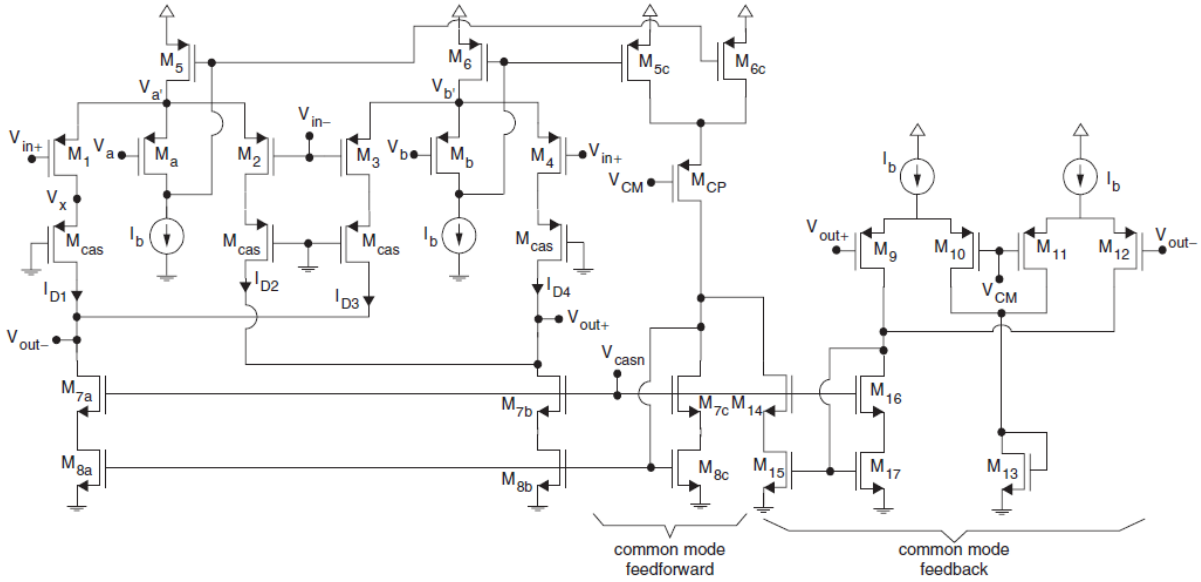

Figure 83. Complete schematic of the transconductor

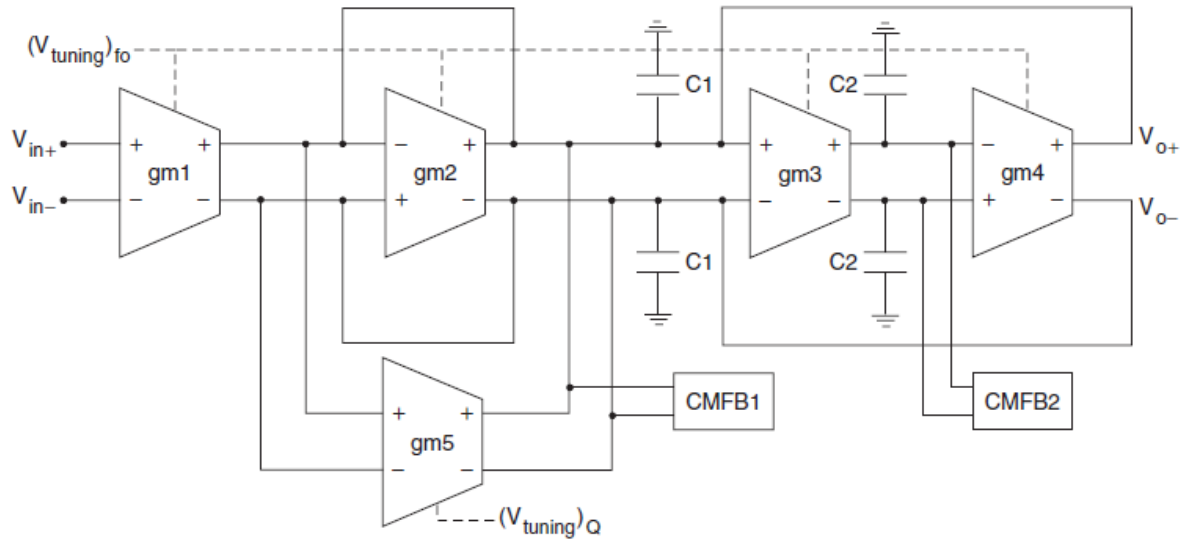

Figure 84. Implementation of the filter

II.4.c Second Order Bandpass Filters

There are several different ways to synthesize a second order bandpass transfer function with Gm-cells. Two first topologies are discussed before presenting the one that will be more detailed later.

II.4.c.i The different possible topologies

In Figure 85 is depicted a first filter [II.17]. The filter transfer function is given by:

$$H(\omega) = \frac{V_{out}}{V_{in}} = \frac{jg_{m3}C_1\omega}{g_{m1}g_{m2} + jg_{m3}C_1\omega - C_1C_2\omega^2} \quad \text{(III.64)}$$

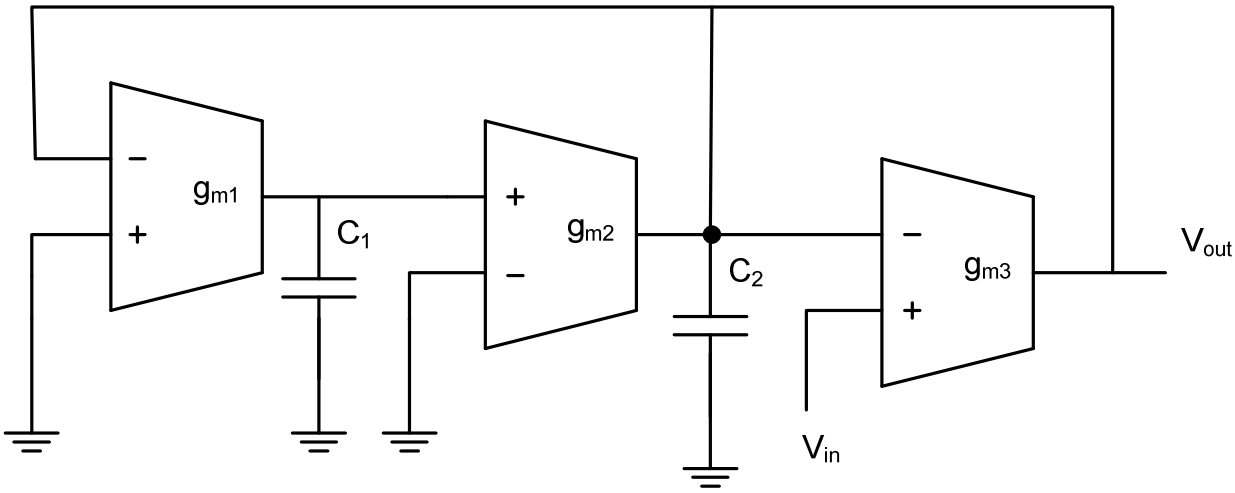

Figure 85. Constant-bandwidth and constant-gain frequency tunable bandpass filter

This leads to the following parameters, assuming $g_{m1} = g_{m2} = g_m$.

$$\begin{cases} \omega_0 = \dfrac{g_m}{\sqrt{C_1C_2}} & \text{(III.65)} \\ Q = \dfrac{g_m}{g_{m3}}\sqrt{\dfrac{C_2}{C_1}} & \text{(III.66)} \end{cases}$$

Thus,

$$BW = \frac{g_{m3}}{C_2} \quad \text{(III.67)}$$

Thus central frequency tunability is achieved, tuning C_1 or g_m values, while keeping a constant bandwidth. However, this structure needs to tune both transconductances and capacitances. That is why it has not been studied more deeply in the following.

Now let's consider a second structure [II.17], depicted on Figure 86:

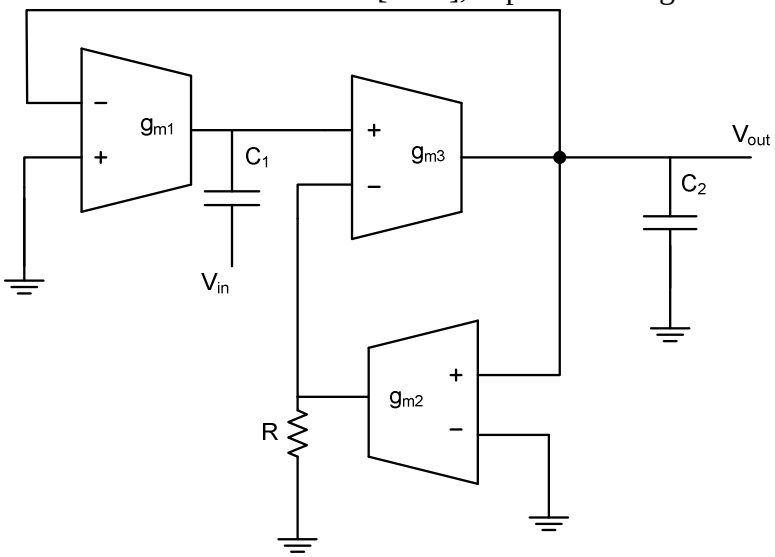

Figure 86. Constant-Q frequency tunable bandpass filter

In this structure, assuming $g_{m1} = g_{m2} = g_m$ leads to the following quality factor, the central frequency being the same as before.

$$Q = \frac{1}{g_{m3} R} \sqrt{\frac{C_2}{C_1}} \qquad \text{(III.68)}$$

A constant-Q move is achievable thanks to g_m tuning or keeping $C_1 = C_2$. However, the *1/R* dependency of *Q* makes this structure noisy but also being strongly subject to temperature and process variation whereas a robust implementation is required for industrialization.

II.4.c.ii Study of a Gm-C Bandpass Filter for TV Tuners

Now let's describe more accurately a Gm-C bandpass filter designed for TV tuners [II.18, II.19 and II.20]. *Y. Sun et al* have proposed a second order bandpass filter architecture, also called biquad in the following, which is then cascaded to obtain a higher order filtering.

The second order Gm-C filter, the basic biquad, is the differential structure depicted in Figure 87. This is the architecture which is chosen and implemented in next chapter. It was chosen to tune only capacitors so as to keep a constant g_m value which is linearized.

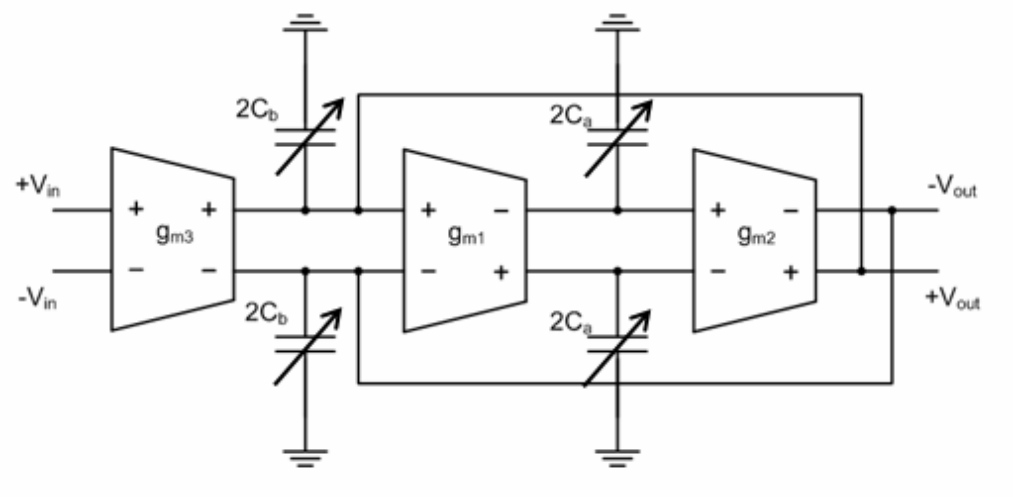

Figure 87. Biquad Schematic

The Gm-cells of this filter are based on a differential pair designed in 130nm CMOS with a common-mode feedback, as illustrated in Figure 88. A constant gm value is obtained and linearized by dynamic source degeneration. Negative resistance have also been added on g_{m1} and g_{m2} to enhance the quality factor. Thanks to three of these Gm-cells, the biquad can be obtained. Cascading four biquads allows the creation of an eighth order bandpass filter.

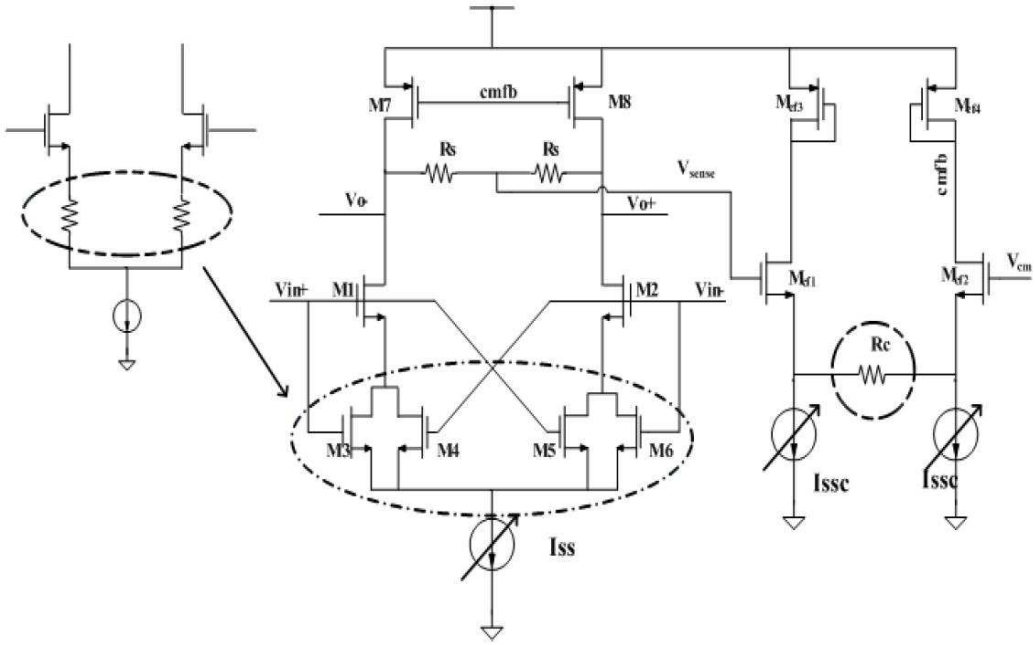

Figure 88. Reported Gm-cell

In [II.18], two filters have been realized, based on this Gm-cell. The first filter operates from 48 MHz to 287 MHz and is an eighth order bandpass filter. It is used to reject harmonic frequencies. The second filter is a second order bandpass filter which operates from 287 MHz till 860 MHz. This second filter is mainly used to reject adjacent channels.

Reference [II.19] describes the use of a single biquad between 50 and 300MHz. The great asset of this structure is the reported power consumption of 7.6mW due to a 1.2V supply voltage. In terms of dynamic range, an IIP3 of 5dBm for a NF of 20dB is reported.

Reference [II.20] is based on the same architecture as the latter filter. However, the two transconductances of the gyrator are tunable. This second degree of tunability allows the enhancement of the tuning range. Frequencies from 48 to 780 MHz are now covered at the cost of reduced linearity and higher noise.

II.4.c.iii Performances Comparison of Gm-C Filters

Many RF bandpass filters, making use of single MOS transistors as transconductors, were previously reported [II.8, II.21]. Operating in the GHz range, they can reach very high Q-factors for a very low power consumption, but with signal distortion and noise. In parallel, the possibility to use an active selectivity for RF front-ends under certain conditions on the LNA (2dB NF and gain limited to 10dB) was shown in [II.22]. The literature also reports on more complex Gm-C filters, used at lower frequencies (40-300MHz), which achieve both interesting RF performances and large tuning range [II.5]. However such filter, with a low-pass structure, does not have an influence on adjacent channels rejection. Finally, as previously described, it has been reported a Gm-C bandpass filter for TV tuners that reaches a good dynamic range while being very low power [II.19]. The performances of these RF filters are summarized in Table 5.

Table 5. Gm-C & Gyrator-C RF Filters

Ref.	[II.8]	[II.21]	[II.22]	[II.5]	[II.19]	**Units**
Type	BPF	BPF	BPF	LPF	BPF	**-**
Mode	single	single	differential	differential	differential	**-**
Freq.	400-1050	500-1300	1900-3800	50-300	50-300	**MHz**
Q	2 to 80	60	40		6	**-**
NF		8.5	18	14	20	**dB**
IIP3	-15	-26		16	4	**dBm**
Power	51	274	10.8	72	7.6	**mW**
Supply		5	1.8	1.8	1.2	**V**
Techno	350	350	180	180	130	**nm**

II.4.d Rm-C Filtering

R_m based filters are very similar to the Gm-cells based ones. As explained previously, a Gm-cell converts a voltage into a current with a certain gain g_m whereas a trans-resistance amplifier converts a current into a voltage with a certain resistive gain R_m, called “trans-resistance”.

A capacitors associated to this trans-resistance amplifier creates a derivator, as depicted in Figure 89, which is essential to synthesize a filter transfer function. Indeed, this leads to a derivative behaviour since:

$$\frac{V_{out}}{\Delta V_{in}} = jR_m C\omega . \qquad \text{(III.69)}$$

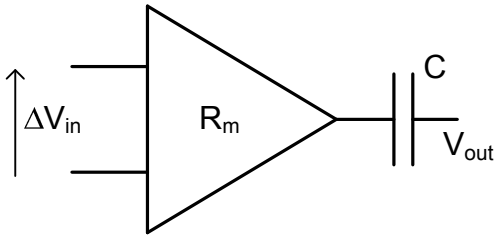

Figure 89. Derivator using an Rm amplifier

Rm-C filters are rarely used above 10MHz because of their frequency limitation. Only two publications were classified in APPENDIX C. In [II.23] *Y. Cheng et al* present an interesting structure, which consists in a CMOS inverted-based Rm-C amplifier that is connected to a capacitor in order to form an Rm-C biquad. A Q-enhancement circuit is added which also helps to adjust the filter operating frequency and gain. The entire circuit is illustrated in Figure 90.

The Rm amplifier is realized with a CMOS inverter with feedback and current-source load. The Q-enhancement is realized thanks to a negative resistance which generates a higher gain, resulting in a higher Q-factor: the higher the gain, the higher the extra-gain given by the positive feedback.

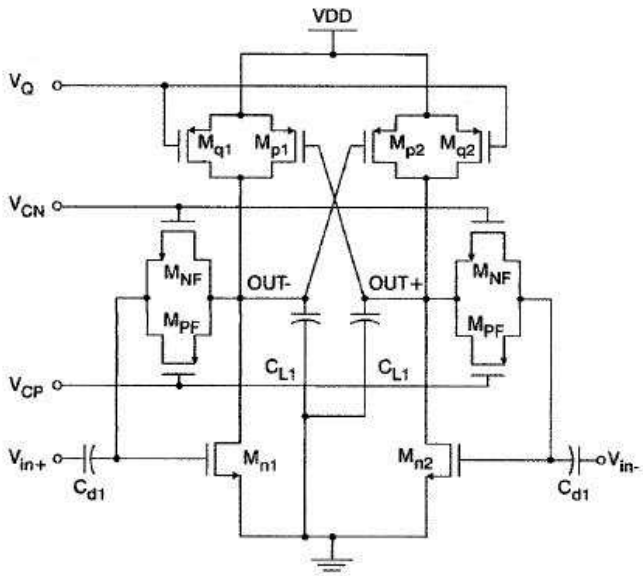

Figure 90. Reported Rm-C filter

As far as the performances are concerned, this structure is tunable between 41 and 178MHz with 20 dB gain. It also achieves a noise figure of 15 dB and an IIP3 of -5 dBm. Further details are given in APPENDIX C.

II.5 Literature Survey

Several papers dealing with active filtering, as well as passive LC filtering, are sorted in tables in APPENDIX C. These tables summarize the performances found in the papers. From these tables, some statistics can also be drawn.

Figure 91 depicts the part of CMOS and BiCMOS based filters in the literature. As it may be seen, more than 90% of them are designed in CMOS.

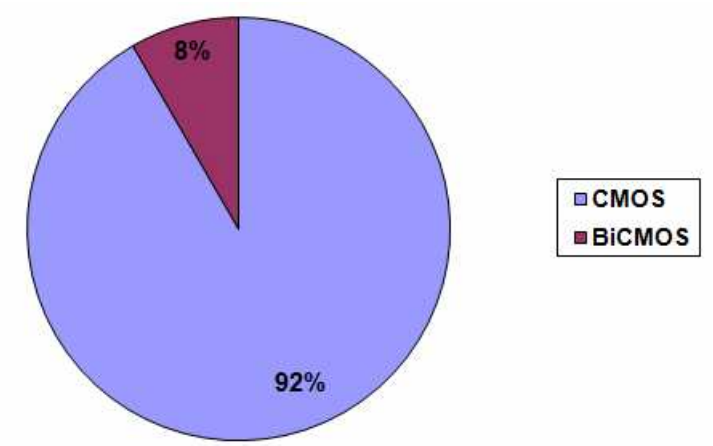

Figure 91. CMOS vs BiCMOS filters

Figure 92 shows which CMOS technology node is used to design the filter. 0.35µm and 0.18µm nodes are the most used. It is worth noticing that even for the analog design of an RF filter, the technological trend goes towards more advanced nodes like 90nm CMOS and even 65nm CMOS as it will be described later on.

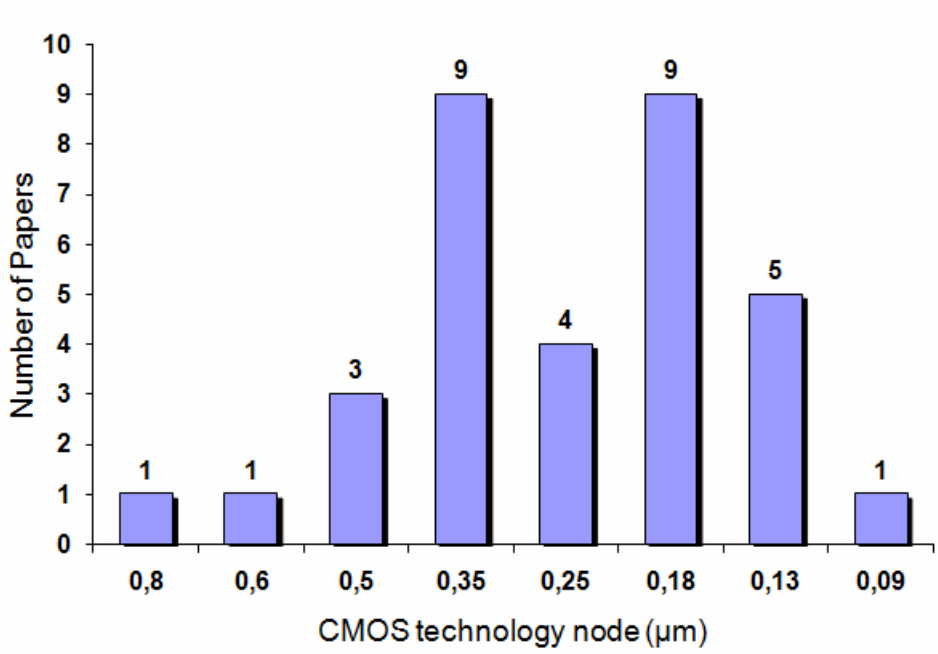

Figure 92. CMOS filter technology node

Figure 93 depicts the RF performances of some filters found in the literature. It does not take into account their quality factor because very few papers mention IIP3, NF and Q at the same time. However, this graph shows how challenging the wanted RF performances are compared to already published filters.

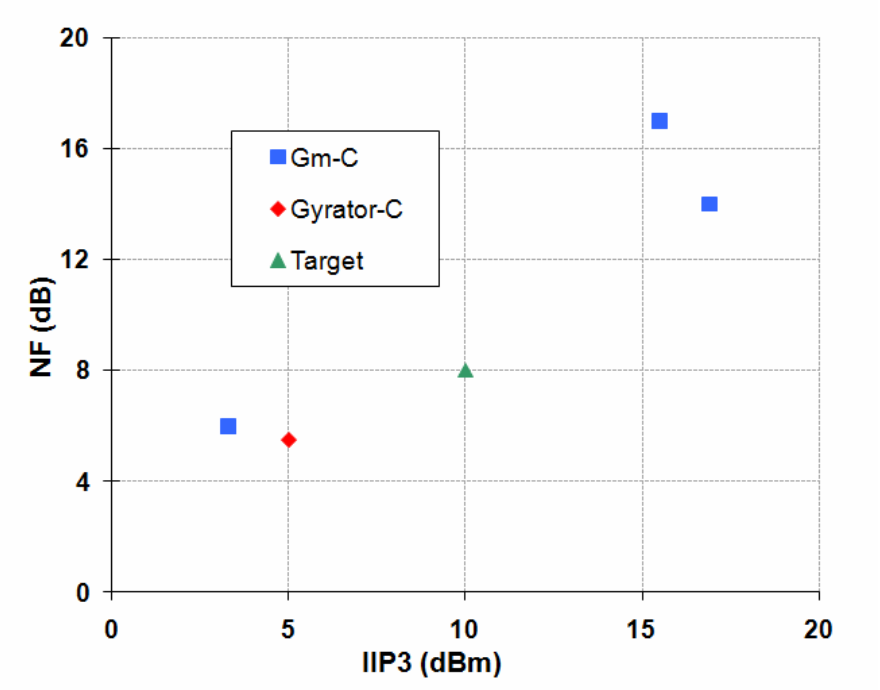

Figure 93. NF versus IIP3 found in the literature

II.6 Technological Opportunities and Limitations

A fully active structure relies on the technological choice of the transistors, but it also relies on the available passive components in the chosen technology.

II.6.a Integrated Passive Components

II.6.a.i Inductors

On-chip inductors are mainly realized as spirals to enhance the inductive effect. However, the planar spiral geometry is far from being solenoidal and ***the inductance does not scale linearly*** with the number of turns. Hence, on-chip inductors often require large silicon space.

The quality factor of such an inductor is limited by series loss due to the resistivity of the metal layer used for the spiral. Thick copper layers can be used to reduce the resistivity and to increase the inductor quality factor. Nevertheless this may require additional masks, so the cost of the final chip is increased. Furthermore, despite copper metal line, on-chip inductors quality factors stay relatively low. This parameter is also strongly dependent on the silicon area. Indeed, the larger the inductor area, the higher the quality factor, but the larger the capacitive parasitics which lower the self resonant frequency.

II.6.a.ii Capacitors

Having a look to the capacitance formula, given by

$$C = \frac{\varepsilon_0 \varepsilon_r S}{t_{ox}}, \tag{III.70}$$

it is worth noticing that it strongly depends on the insulator thickness t_{ox} and on the surface S. To decrease the capacitance area, the insulator thickness has to be decreased. According to the various materials constituting the capacitances, different types can be used. A MOS capacitance (Metal-Oxide-Semiconductor) allows the use of high density capacitances due to a high permittivity coefficient oxide layer, made of TaO_5 for instance. However, they are strongly non-linear and they require a bias. Using additional lithography masks, MIM (Metal-Insulator-Metal) capacitors may be used. Because they use a very thin insulator, MIM capacitances are able to achieve high capacitance values and also show a high density (between 2 and 6fF/µm^2).

II.6.a.iii Resistors

Resistors can be made with various materials according to the wanted resistance value. Very reliable models are required, especially in terms of parasitic and also of process and temperature variations, in order to achieve very stable and robust designs.

II.6.b Transistors

One major opportunity of fully active, therefore transistor based, filtering is the ability to take advantage of technology scaling. ***Higher density*** of integration and smaller consumption thanks to a ***lower supply voltage*** are well known advantages. A more advanced technology node allows using more ***digital gates*** in a same area in order to improve the analog RF performances by means of calibration.

A second advantage of advanced BiCMOS or CMOS nodes is that switches show a ***lower $R_{on}.C_{off}$ constant***, as described in Figure 94 using BSIM4 models. This allows obtaining capacitors banks with smaller non-linear parasitic capacitances for a given on-switch resistance. It is then possible to obtain capacitors with high quality factors, resulting in higher RF performances.

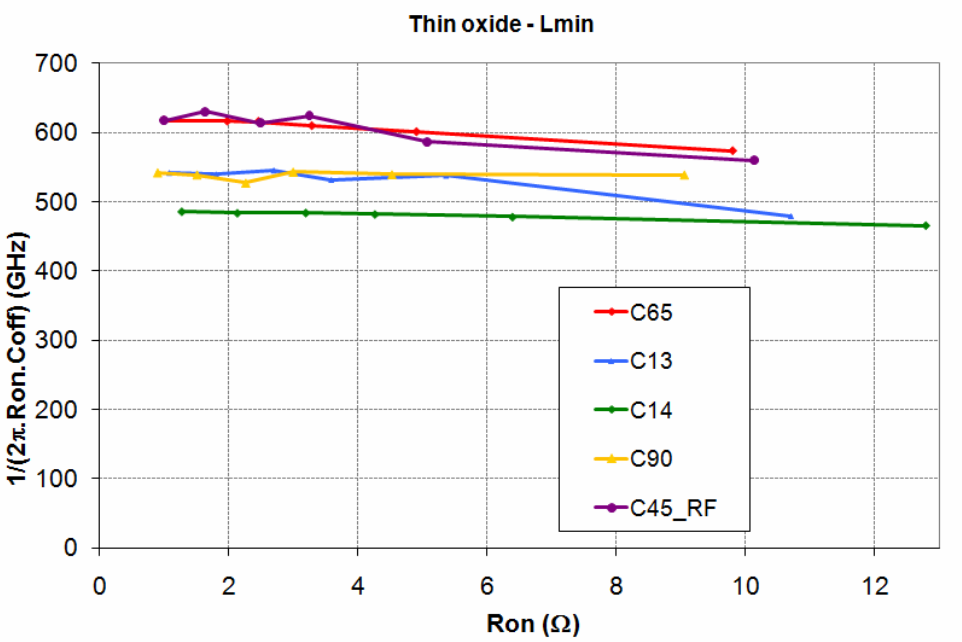

Figure 94. $R_{on}.C_{off}$ constant for different technology nodes

However, advanced CMOS transistors are less able to amplify. Indeed, as depicted in Figure 95, the $\frac{g_m}{I_d}$ ratio for a given $\frac{W}{L}$ decreases with the technology.

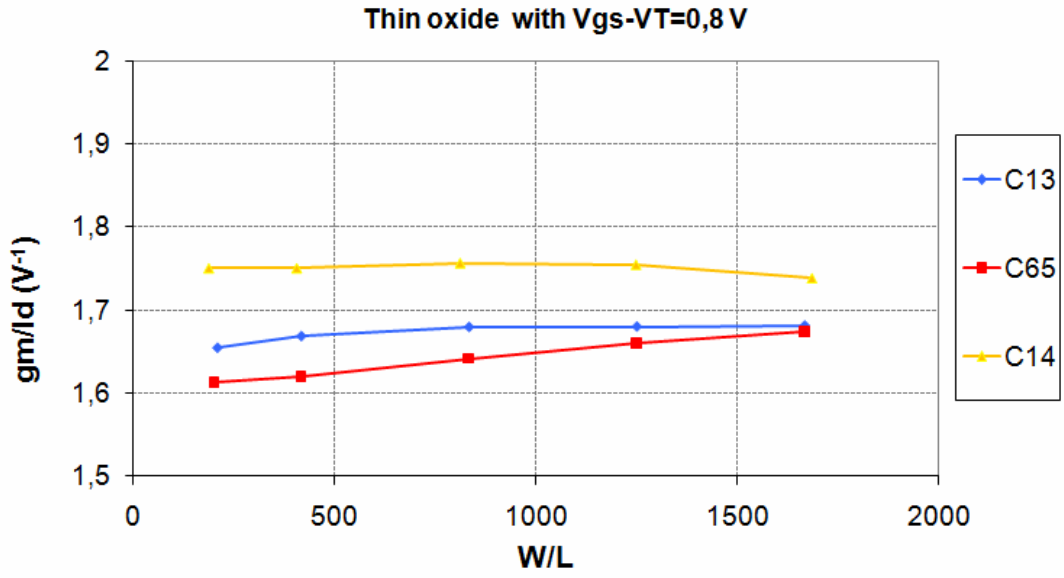

Figure 95. g_m/Id for different technology nodes

Furthermore, in order to realize a transconductor without negative resistance, a large drain-source resistance is needed so as to get a high transconductor voltage gain. Figure 96

depicts this R_{ds} resistance versus the drain current. As it may be found in the literature, the smaller the gate length L, the smaller the drain-source resistance since:

$$R_{ds} = \frac{LU_a}{I_d}, \qquad \text{(III.71)}$$

where U_a is a factor depending on channel-length modulation.

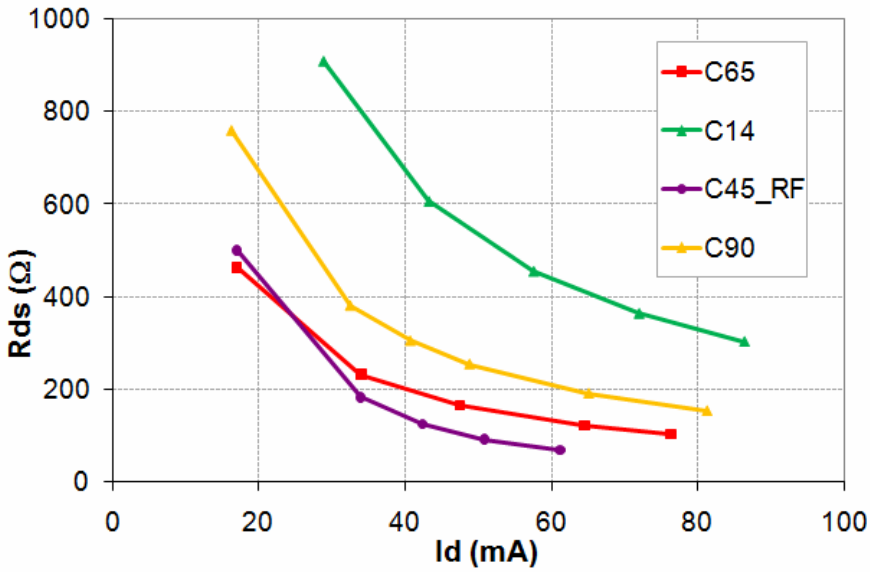

Figure 96. Drain-source resistance versus drain current

As far as intrinsic noise and linearity of CMOS technologies are concerned, it is very difficult to compare one to another. Indeed, it strongly depends on the modeling and its accuracy. Comparing technologies from different founders may lead to misinterpretations.

An important point in comparing technologies is their ability to support high supply voltages by means of thick oxide transistors. Since the RF filter should be able to handle the LNA output swing, a high enough supply voltage is required. Indeed a 1.2V supply in 65nm CMOS would not be sufficient to handle a large swing without distortions. Minimum gate lengths and supply voltages of the various studied technologies are summarized in Table 6.

Table 6. CMOS technologies comparison

	CMOS technology									
Name	**C14**		**C13**		**C90**		**C65**		**C45**	
Provider	*NXP*		*Jazz*		*TSMC*		*TSMC*		*TSMC*	
oxide type	thin	thick	thin	thick	thin	thick	thin	thick	thin	thick
L_{min} (µm)	0,16	0,322	0,12	0,36	0.1	0.28	0,06	0,28	0,04	0,27
Supply (V)	1,8	3,6	1,2	3,3	1.2	2.5	1,2	2,5	1.1	2,5

II.7 Conclusion

As a conclusion, this chapter has demonstrated that the second order bandpass filter topology best fulfils the requirements of TV tuners. Indeed, its efficient central frequency tuning and the possibility to determine accurately either a -3dB bandwidth or a filter quality factor make it a very attractive topology.

Studying the literature allows comparing the performances of various structures. It comes out that Gm-C filters are able to work in the TV operating frequencies while achieving interesting RF performances and tuning range. In the following, this type of filter will be studied more deeply and designed with a high dynamic range focus, in order to determine in a quantitative way which performances are reachable with this type of filter and what are the limitations to this structure.

II.8 References

[II.1] Y. Tsividis and J. O. Voorman, *Integrated continuous-time filters: principles, design, and applications*. IEEE Press, 1993.

[II.2] A. I. Zverev, *Handbook of filter synthesis*. Wiley-Interscience, 2005.

[II.3] I. C. Hunter and I. of E. Engineers, *Theory and design of microwave filters*. IET, 2001.

[II.4] Y. Kanazawa, Y. Fujimoto, and K. Iizuka, "A 130M to 1GHz digitally tunable RF LC-tracking filter for CMOS RF receivers," pp. 469-472, Nov. 2008.

[II.5] Kuduck Kwon, Hong-Teuk Kim, and Kwyro Lee, "A 50–300-MHz Highly Linear and Low-Noise CMOS Gm-C Filter Adopting Multiple Gated Transistors for Digital TV Tuner ICs," *Microwave Theory and Techniques, IEEE Transactions on*, vol. 57, 2009, pp. 306-313.

[II.6] F. Dulger, E. Sanchez-Sinencio, and J. Silva-Martinez, "A 1.3-V 5-mW fully integrated tunable bandpass filter at 2.1 GHz in 0.35-μm CMOS," *Solid-State Circuits, IEEE Journal of*, vol. 38, 2003, pp. 918-928.

[II.7] R. Carvajal, J. Galan, A. Torralba, F. Munoz, and J. Ramirez-Angulo, "1.33 mW, 2 V CMOS continuous-time bandpass filter with two decades of centre frequency tuning range and high Q," *Circuits, Devices and Systems, IEE Proceedings*, vol. 152, 2005, pp. 456-464.

[II.8] Yue Wu, Xiaohui Ding, M. Ismail, and H. Olsson, "RF bandpass filter design based on CMOS active inductors," *Circuits and Systems II: Analog and Digital Signal Processing, IEEE Transactions on*, vol. 50, 2003, pp. 942-949.

[II.9] R. Weng and R. Kuo, "An ω_0-Q Tunable CMOS Active Inductor for RF Bandpass Filters," *Signals, Systems and Electronics, 2007. ISSSE '07. International Symposium on*, 2007, pp. 571-574.

[II.10] Y. Chang, J. Choma, and J. Wills, "The design and analysis of a RF CMOS bandpass filter," *Circuits and Systems, 2000. Proceedings. ISCAS 2000 Geneva. The 2000 IEEE International Symposium on*, 2000, pp. 625-628 vol.2.

[II.11] Zhiqiang Gao, Jianguo Ma, Mingyan Yu, and Yizheng Ye, "A CMOS RF tuning wide-band bandpass filter for wireless applications," *SOC Conference, 2005. Proceedings. IEEE International*, 2005, pp. 79-80.

[II.12] Zhiqiang Gao, Jianguo Ma, Yizheng Ye, and Mingyan Yu, "Large tuning band range of high frequency filter for wireless applications," *Circuits and Systems, 2005. ISCAS 2005. IEEE International Symposium on*, 2005, pp. 384-387 Vol. 1.

[II.13] C. Andriesei, L. Goras, and B. Delacressoniere, “Active RF bandpass filter with wide frequency tuning range,” *Semiconductor Conference, 2008. CAS 2008. International*, 2008, pp. 397-400.

[II.14] C. Andriesei, L. Goras, and F. Temcamani, “Negative resistance based tuning of an RF bandpass filter,” *Circuits and Systems for Communications, 2008. ECCSC 2008. 4th European Conference on*, 2008, pp. 83-86.

[II.15] Y. P. Tsividis, “Integrated continuous-time filter design - an overview,” *Solid-State Circuits, IEEE Journal of*, vol. 29, no. 3, pp. 166-176, 1994.

[II.16] E. Sanchez-Sinencio, R. L. Geiger, and H. Nevarez-Lozano, “Generation of continuous-time two integrator loop OTA filter structures,” *IEEE Transactions on Circuits and Systems*, vol. 35, no. 8, pp. 936-946, Aug. 1988.

[II.17] R.L. Geiger and E. Sánchez-Sinencio, “Active Fitler Design Using Operational Transconductance Amplifiers: A Tutorial,” *IEEE Circuits and Devices Magazine*, Vol.1, pp.20-32, March 1985.

[II.18] Y. Sun, J.-seon Lee, and S.-gug Lee, “On-chip Active RF Tracking Filter with 60dB 3rd-order Harmonic Rejection for Digital TV tuners.” 2008.

[II.19] Y. Sun, C. J. Jeong, I. Y. Lee, J. S. Lee, and S. G. Lee, “A 50-300-MHz low power and high linear active RF tracking filter for digital TV tuner ICs,” presented at the Custom Integrated Circuits Conference (CICC), 2010 IEEE, 2010, pp. 1-4.

[II.20] Y. Sun, C. J. Jeong, S. K. Han, and S. G. Lee, “CMOS on-chip active RF tracking filter for digital TV tuner ICs,” *Electronics Letters*, vol. 47, no. 6, pp. 407-409, Mar. 2011.

[II.21] V. Stornelli, G. Ferri, G. Leuzzi, and A. De Marcellis, “A tunable 0.5-1.3 GHz CMOS 2nd order bandpass filter with 50/spl Omega/ input output impedance matching,” in *Circuits and Systems, 2006. ISCAS 2006. Proceedings. 2006 IEEE International Symposium on*, p. 4 pp.,2006.

[II.22] Zhiqiang Gao, Jianguo Ma, Mingyan Yu, and Yizheng Ye, “A Fully Integrated CMOS Active Bandpass Filter for Multiband RF Front- Ends,” *Circuits and Systems II: Express Briefs, IEEE Transactions on*, vol. 55, no. 8, pp. 718-722, 2008.

[II.23] Y. Cheng, J. Gong, and C. Wu, “New CMOS 2 V low-power IF fully differential Rm-C bandpass amplifier for RF wireless receivers,” *Circuits, Devices and Systems, IEE Proceedings* -, vol. 148, 2001, pp. 318-322.

III. Gm-C Filtering

III.I Theoretical Study

III.1.a Structure of the Gm-C Bandpass Filter

As mentioned in previous chapter, the following fully-differential Gm-C bandpass filter is considered for its analogy with a current-fed parallel LC resonator [III.1]. Indeed, it is composed of an input transconductor g_{m3}, which converts input voltage into an output current and sets the voltage gain of the filter. This current then flows through variable capacitors C_b and a gyrator synthesizing an inductance, made of transconductors g_{m1} and g_{m2}, and capacitors C_a, as depicted in Figure 97.

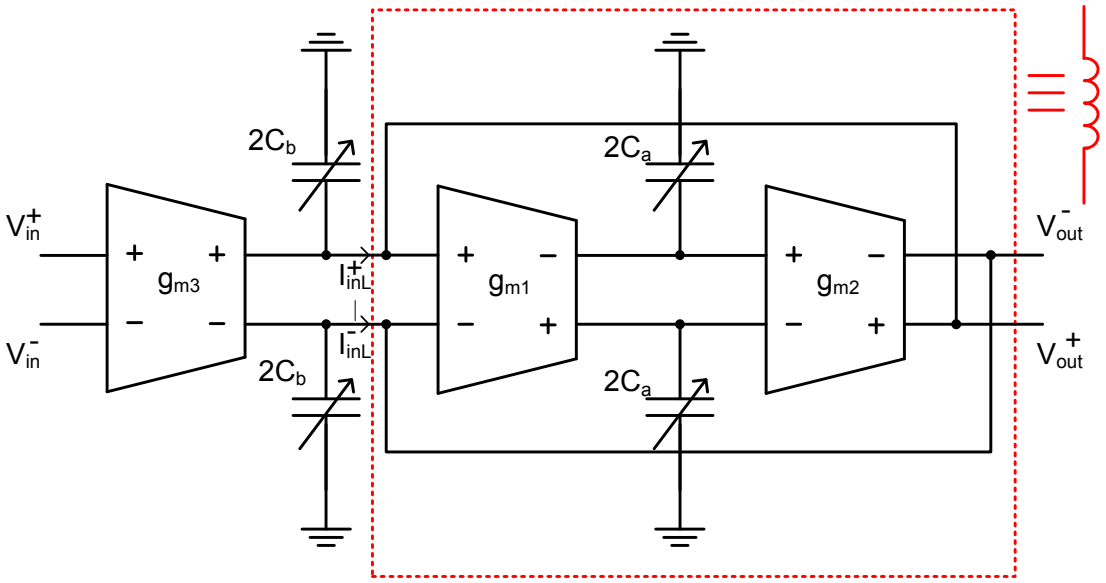

Figure 97. Proposed Differential Gm-C Filter

Considering transconductors imperfections, the capacitive parasitics of all transconductors can be incorporated into either C_a or C_b to simplify the model. However, each Gm-cell also has a non-infinite output impedance that will be called r_0 in the following. It will be considered r_0 for g_{m1} and the same r_0 in common for g_{m2} and g_{m3} to simplify computations. Its RLC equivalent can be deduced and gives the following schematic illustrated in Figure 98.

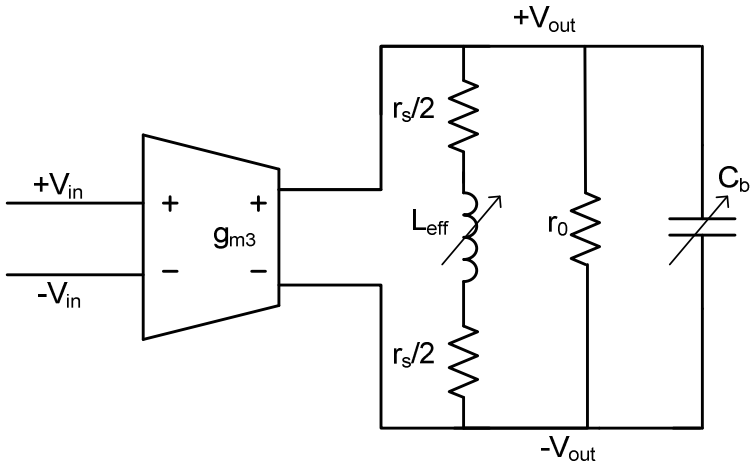

Figure 98. Equivalent RLC resonator

As discussed in the previous chapter, in Figure 98, it is assumed that $L_{eff} = \frac{C_a}{g_{m1} g_{m2}}$ and $r_s = \frac{1}{r_0 g_{m1} g_{m2}}$.

A first computation step gives:

$$g_{m3} V_{in} = V_{out} \left(\frac{1}{r_0} + \frac{1}{jL_{eff}\,\omega + r_s} + jC_b \omega \right) \tag{III.1}$$

Hence, the filter transfer function can be deduced:

$$H(j\omega) = \frac{V_{out}}{V_{in}} = \frac{g_{m3}(jL_{eff}\,\omega + r_s)}{\frac{r_s}{r_0} + 1 + j\frac{\omega}{r_0}\left(L_{eff} + r_s r_0 C_b\right) - \omega^2 L_{eff} C_b} \tag{III.2}$$

Such a filter resonates at a central frequency

$$f_0 = \frac{1}{2\pi} \sqrt{\frac{g_{m1} g_{m2} + \frac{1}{r_0^2}}{C_a C_b}} \tag{III.3}$$

with a quality-factor set to

$$Q = r_0 \frac{\sqrt{C_a C_b \left(\frac{1}{r_0^2} + g_{m1} g_{m2} \right)}}{C_a + C_b}. \tag{III.4}$$

It is worth noticing that tunable capacitors C_a correspond to an equivalent tunable inductor L_{eff}. While passive inductor – varying capacitor resonator leads to a central frequency proportional to $1/\sqrt{C}$, here it is possible to tune both L_{eff} and C provided that C_a and C_b are proportional. f_0 then becomes proportional to $1/C$. This is a very interesting property for a tunable filter since it results in a larger tuning range for a same capacitance ratio:

$$\frac{f_{\max}}{f_{\min}} \propto \frac{C_{\max}}{C_{\min}}. \tag{III.5}$$

That is why in the following, it is assumed $C_a = C_b = C$. Moreover, when only tuning C_b, it leads to a filter gain increasing with frequency, because Q increases as well, whereas tuning both capacitors makes the gain remain constant.

This structure also permits to achieve a constant-Q frequency sweep because Q then becomes constant, independent from C since:

$$Q = \frac{r_0}{2} \sqrt{\frac{1}{r_0^2} + g_{m1} g_{m2}}. \tag{III.6}$$

As previously mentioned, this allows rejecting harmonic frequencies in a constant way.

III.1.b Linearity Considerations

The fully-differential equivalent topology of this circuit is considered. This configuration allows neglecting second order distortion as a first approximation. Furthermore, for each transconductor $G_{m,i}$, the output differential current $I_{out,i}$ is given by:

$$I_{out,i} = g_{mi} V_{in} + g''_{mi} V_{in}^3 . \qquad \text{(III.7)}$$

The transfer function of the schematic can be computed, since the type of solution expected is:

$$V_{out} = \alpha V_{in} + \beta V_{in}^3 , \qquad \text{(III.8)}$$

These α and β coefficients can then be obtained. The differential current in the gyrator I_{inL} gives the following relation:

$$I_{inL} = g_{m2}\left(\frac{r_0}{1+jr_0C_a\omega}\left(g_{m1}V_{inL} + g''_{m1}V_{inL}^3\right)\right) + g''_{m2}\left(\frac{r_0}{1+jr_0C_a\omega}\left(g_{m1}V_{inL} + g''_{m1}V_{inL}^3\right)\right)^3 \qquad \text{(III.9)}$$

Limiting to the third order terms, Equation (III.9) becomes:

$$I_{inL} = \frac{g_{m1}g_{m2}r_0}{1+jr_0C_a\omega}V_{inL} + \left(g_{m2}\frac{g''_{m1}r_0}{1+jr_0C_a\omega} + g''_{m2}\left(\frac{g_{m1}r_0}{1+jr_0C_a\omega}\right)^3\right)V_{inL}^3 , \qquad \text{(III.10)}$$

Keeping first and third order terms, the current of the gyrator can be written as:

$$I_{inL} = \frac{g_{m1}g_{m2}r_0}{1+jr_0C_a\omega}V_{inL} + g_{m2}\frac{g''_{m1}r_0}{1+jr_0C_a\omega}V_{inL}^3 , \qquad \text{(III.11)}$$

Now, assuming

$$V_{out} = V_{inL} , \qquad \text{(III.12)}$$

this results in

$$g_{m3}V_{in} + g''_{m3}V_{in}^3 = I_{inL} + V_{out}\frac{1+jr_0C_b\omega}{r_0} = \frac{g_{m1}g_{m2}r_0}{1+jr_0C_a\omega}V_{out} + \left(g_{m2}\frac{g''_{m1}r_0}{1+jr_0C_a\omega} + g''_{m2}\left(\frac{g_{m1}r_0}{1+jr_0C_a\omega}\right)^3\right)V_{out}^3 + V_{out}\frac{1+jr_0C_b\omega}{r_0} \qquad \text{(III.13)}$$

Since the solution is of the type:

$$V_{out} = \alpha V_{in} + \beta V_{in}^3 . \qquad \text{(III.14)}$$

Replacing:

$$g_{m3}V_{in}+g''_{m3}V_{in}^3=\frac{g_{m1}g_{m2}r_0}{1+jr_0C_a\omega}\left(\alpha V_{in}+\beta V_{in}^3\right)+\left(g_{m2}\frac{g''_{m1}r_0}{1+jr_0C_a\omega}+g''_{m2}\left(\frac{g_{m1}r_0}{1+jr_0C_a\omega}\right)^3\right)\left(\alpha V_{in}+\beta V_{in}^3\right)^3+\left(\alpha V_{in}+\beta V_{in}^3\right)\frac{1+jr_0C_b\omega}{r_0} \quad \text{(III.15)}$$

Thus, this leads to:

$$\boxed{\alpha=\frac{g_{m3}}{\frac{g_{m1}g_{m2}r_0}{1+jr_0C_a\omega}+\frac{1+jr_0C_b\omega}{r_0}}}, \quad \text{(III.16)}$$

which corresponds to the ***gain of the filter transfer function***.

The second equation gives:

$$g''_{m3}=\beta\frac{g_{m1}g_{m2}r_0}{1+jr_0C_a\omega}+\left(g_{m2}\frac{g''_{m1}r_0}{1+jr_0C_a\omega}+g''_{m2}\left(\frac{g_{m1}r_0}{1+jr_0C_a\omega}\right)^3\right)\alpha^3+\beta\frac{1+jr_0C_b\omega}{r_0} \quad \text{(III.17)}$$

Hence,

$$\beta=\frac{g''_{m3}-\left(g_{m2}\frac{g''_{m1}r_0}{1+jr_0C_a\omega}+g''_{m2}\left(\frac{g_{m1}r_0}{1+jr_0C_a\omega}\right)^3\right)\alpha^3}{\frac{g_{m1}g_{m2}r_0}{1+jr_0C_a\omega}+\frac{1+jr_0C_b\omega}{r_0}} \quad \text{(III.18)}$$

This finally gives:

$$\boxed{\beta=\frac{g''_{m3}\left(\frac{g_{m1}g_{m2}r_0}{1+jr_0C_a\omega}+\frac{1+jr_0C_b\omega}{r_0}\right)^3-\left(g_{m2}\frac{g''_{m1}r_0}{1+jr_0C_a\omega}+g''_{m2}\left(\frac{g_{m1}r_0}{1+jr_0C_a\omega}\right)^3\right)g_{m3}^3}{\left(\frac{g_{m1}g_{m2}r_0}{1+jr_0C_a\omega}+\frac{1+jr_0C_b\omega}{r_0}\right)^4}}, \quad \text{(III.19)}$$

which corresponds to the ***third order non-linear term***.

Determining by design the achievable IIP3 of all transconductors leads to the various g_{mi3}, thanks to the formula:

$$g''_{mi}=\frac{4}{3}.g_{mi}.10^{IIP3}. \quad \text{(III.20)}$$

β and α can thus be computed and this gives the achievable IIP3 of the filter.

Assuming an ideal input transconductor Gm3, it is possible to plot an abacus of the linearity of the filter versus the linearity of Gm2, for various Gm1 linearity levels. Gm1 and Gm2 have been set to a common same value for the plot.

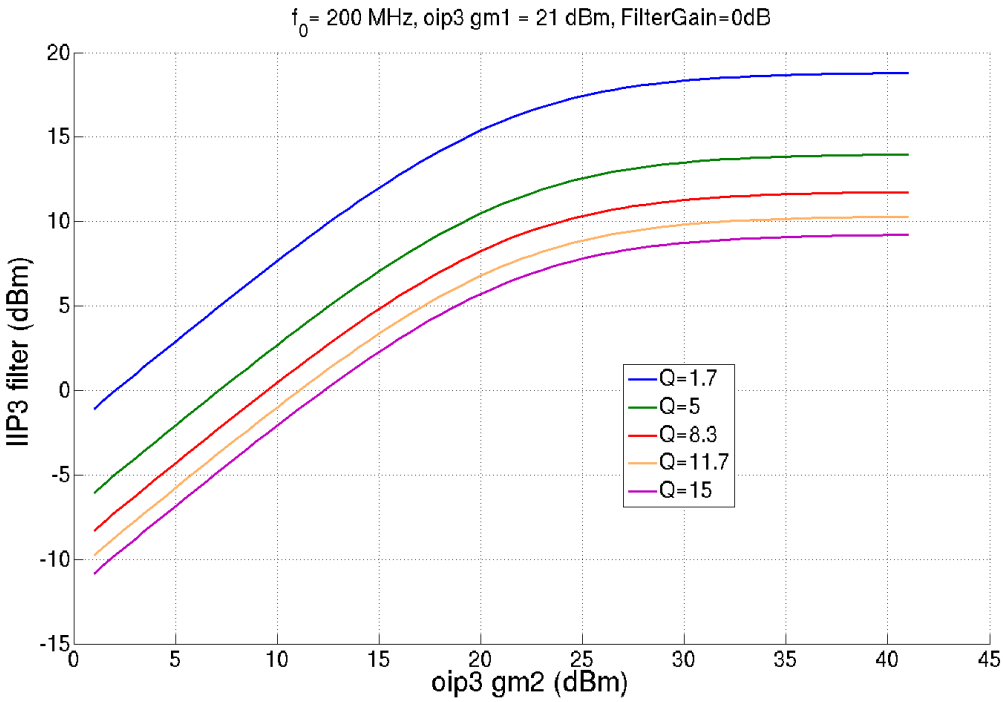

Figure 99. Filter Linearity versus Gm linearity

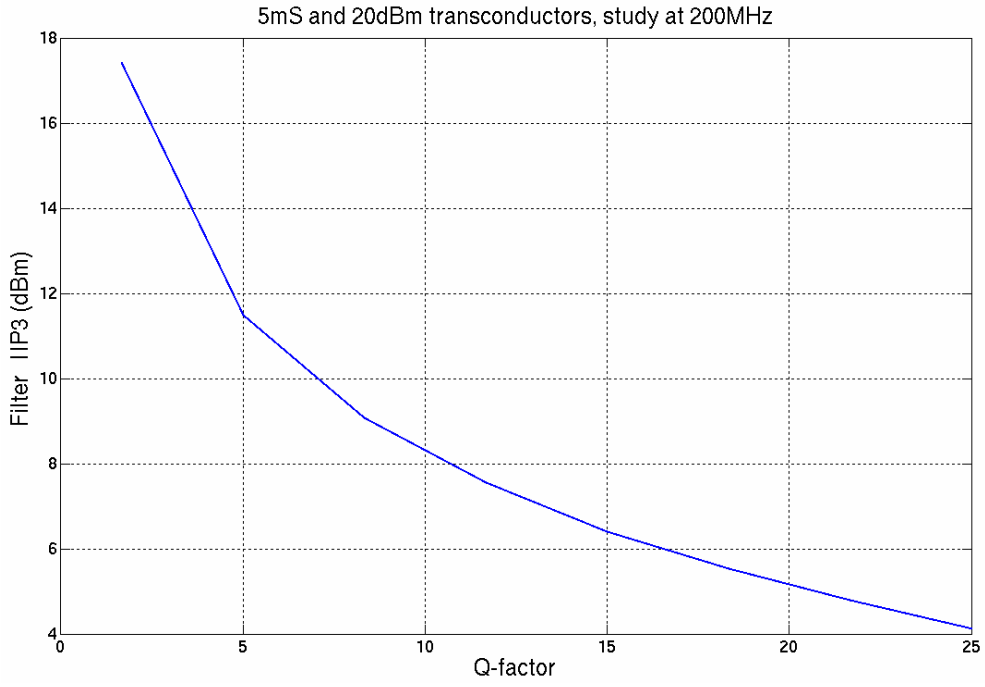

Figure 100. Filter Linearity versus Q-factor

Figure 99 and Figure 100 show that linearity is intrinsically strongly degraded by the gyrator. For instance, if both transconductors have 20dBm OIP3, filter linearity will reach 10dBm IIP3 for a filter Q-factor of 5. And the higher the Q-factor, the stronger this degradation.

Indeed, this phenomenon is due to a peaking voltage $V_{peaking}$ at the internal node of the gyrator, which depends on g_{m1} voltage gain. Increasing r_0 leads to an increase of the voltage gain of g_{m1} and so the peaking. This finally reduces the linearity of the filter since g_{m2} has then to handle a strongly amplified signal.

Linearity performances depend on gain distribution g_{m1}/g_{m2}. Indeed, one can enhance linearity amplifying more on g_{m2} and less on g_{m1}, for a $g_{m1}.g_{m2}$ product kept constant, in order to decrease g_{m1} voltage gain for a given r_0 value. However, according to Friis formula, this results in higher noise, which is also critical in such a structure. Thus $g_{m1}=g_{m2}$ in the following.

The peaking transfer function can be computed and this gives the following equation:

$$H_a(j\omega) = \frac{V_{peaking}}{V_{in}} = \frac{g_{m1}g_{m3}r_0^2}{1 + g_{m1}g_{m2}r_0^2 + jr_0(C_a + C_b)\omega - r_0^2\omega^2 C_a C_b} \qquad \text{(III.21)}$$

Based on the latter equation, Figure 101 illustrates that amplifying more on g_{m2} would lead to a lower peaking voltage at the internal node. Though linearity is enhanced, as it may be observed in Figure 102, noise is thus degraded. Indeed, amplifying less on the first stage means being more subject to noise for the signal (Friis' formula in APPENDIX A).

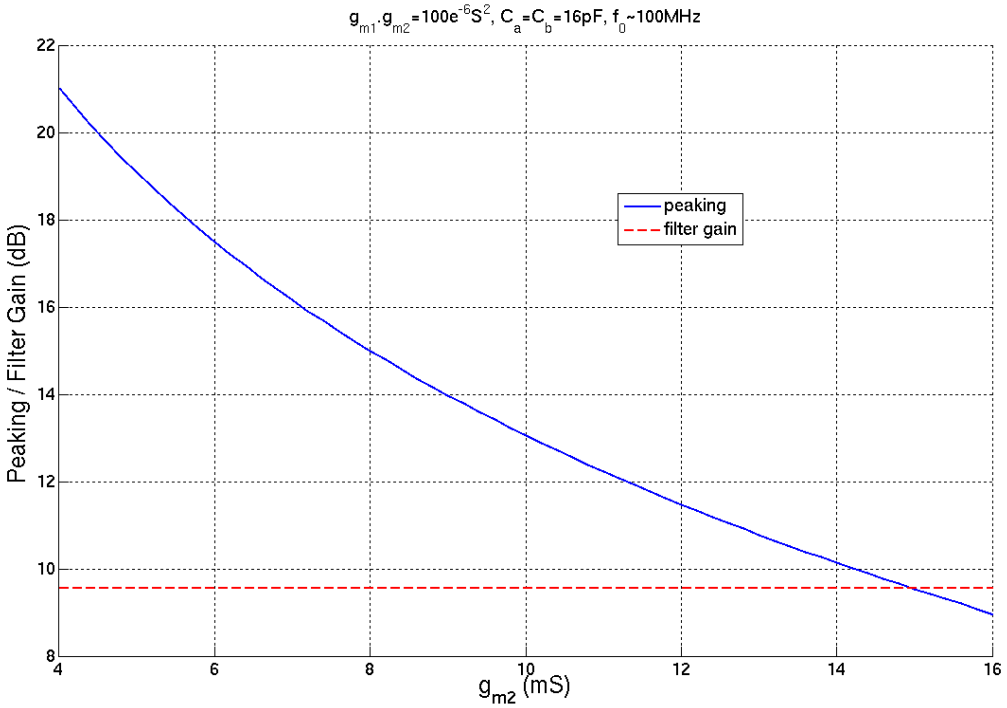

Figure 101. Voltage Peaking at the Gyrator Internal Node

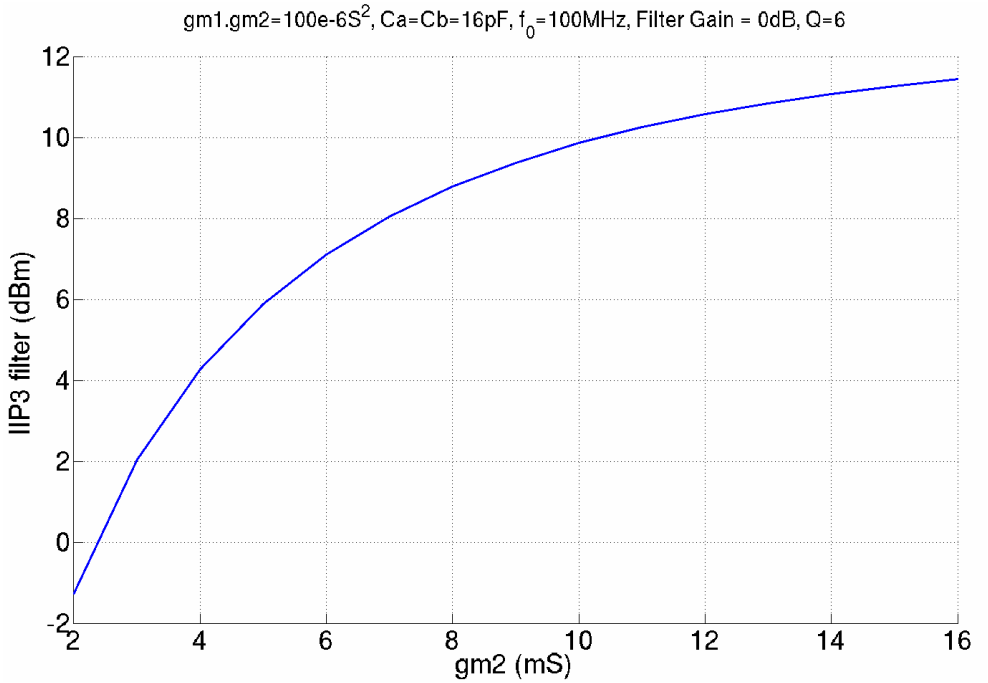

Figure 102. Linearity of the filter versus gm2

Based on Figure 99 and the specifications of the TV tuner RF filter stage, Gm-cells are chosen with linearity levels ***higher than 20dBm OIP3*** and a ***moderate voltage gain (around 22dB) so as to get a moderate filter quality factor***. It allows avoiding the linearity degradation due to the voltage peaking at the gyrator internal node. This is illustrated on Figure 99 where the 10dBm linearity of the filter is reached for 20dBm transconductors and a Q-factor of 5.

III.1.c Noise Considerations

From the RLC equivalent circuit, depicted in Figure 98, it can be demonstrated that the output noise power at f_0 is proportional to Q^2 [III.2]. Indeed, the equivalent admittance Y_{eq} at the output of the transconductor Gm3 is:

$$Y_{eq} = \frac{j\omega L_{eff} + r_s + r_0 + j\omega C_b r_0 \left(j\omega L_{eff} + r_s\right)}{r_0 \left(j\omega L_{eff} + r_s\right)} = \frac{1 + j\dfrac{\omega}{\omega_0 Q} + \left(j\dfrac{\omega}{\omega_0}\right)^2}{\dfrac{j\omega L_{eff} + r_s}{1 + \dfrac{r_0}{r_s}}} \qquad \text{(III.22)}$$

For $\omega = \omega_0$, Y_{eq} becomes inversely proportional to Q:

$$Y_{eq}\left(\omega = \omega_0\right) = \frac{1}{Q} \frac{j\left(1 + \dfrac{r_0}{r_s}\right)}{j\omega L_{eff} + r_s}. \qquad \text{(III.23)}$$

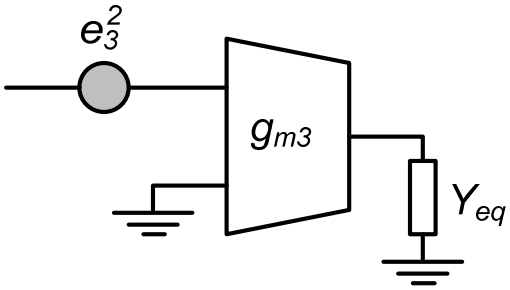

Figure 103. Output noise power computation

Therefore, the total output noise power of this circuit is given by

$$\overline{V_{n,out}^2} = \frac{g_{m3}^2 e_3^2}{Y_{eq}^2}, \tag{III.24}$$

where e_3^2 is Gm3 noise power, as it may be seen in Figure 103. Hence, noise strongly increases as soon as Q increases. On Figure 104 is illustrated the output noise power of the filter versus frequency for different Q factors. Figure 105 clearly underlines the relation between output noise power and Q.

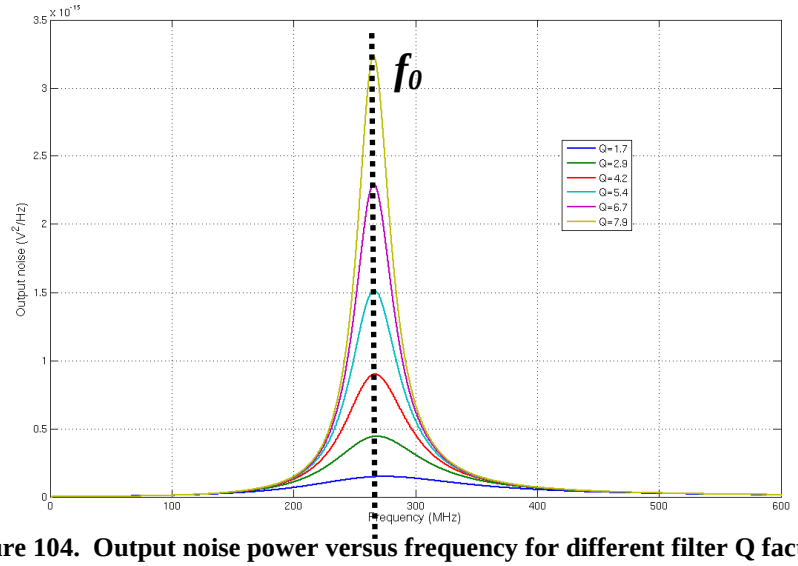

Figure 104. Output noise power versus frequency for different filter Q factors

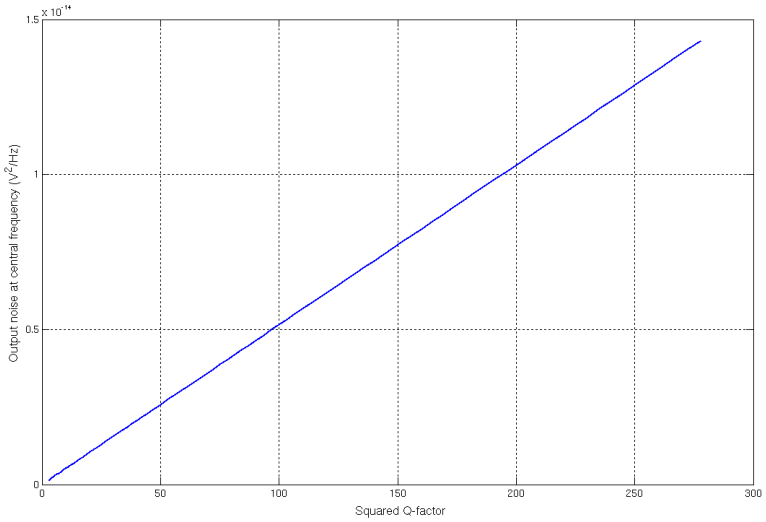

Figure 105. Output noise power versus Q^2

Furthermore, a Gm-C circuit is not a passive RLC circuit since its elements are active and so presents higher noise than passive devices. This explains why the noise of each Gm-cell constituting the filter has to be lowered as much as possible.

For these reasons, it has been chosen to use a ***moderate Q*** of a few units so as to optimize the trade-off linearity versus noise. The choice also involves working on Gm-cells to lower their noise.

III.1.d Focus on VHF Bands

Previous linearity and noise studies have highlighted the high Q-factor dependency of the performances. While in UHF a more demanding selectivity is required to reject adjacent channels, signal would undergo strong distortion and degradation. However, for the VHF range, Q-factor of 4 can be interesting for harmonics filtering since they all are rejected above 20dB, as it may be seen in Figure 106. In addition, adjacent channels located at N±5 and N±6 are rejected on both sides of the filter central frequency. At the low end of the TV band, these channels are rejected by more than 14dB. Hence, the study is focused on VHF bands where moderate Q-factors, like a Q of 4, offer an interesting trade-off in terms of RF performances versus selectivity.

Furthermore, inductors used in VHF cannot be integrated whereas on-chip spirals can help the integration of the UHF filtering. That is why the study has been focused first on the VHF bands.

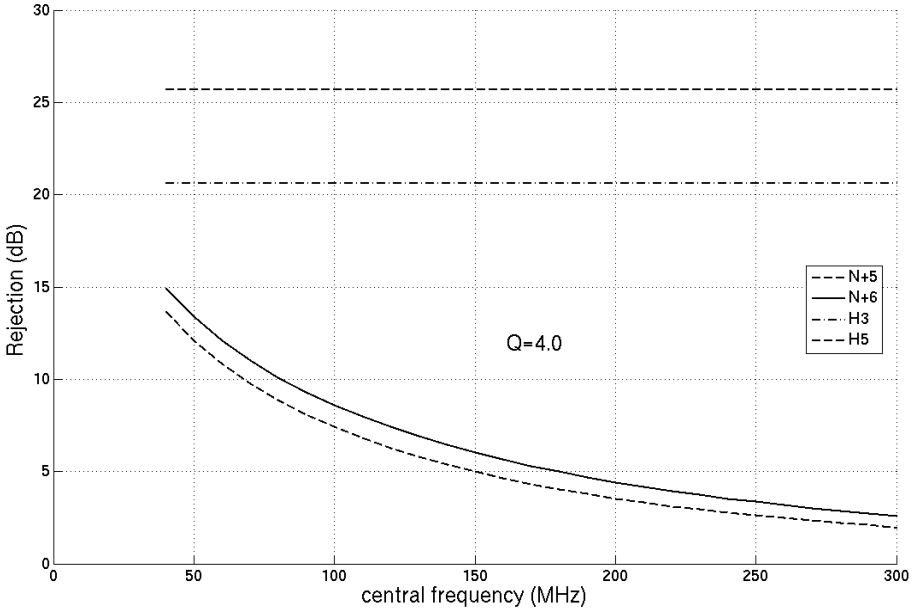

Figure 106. Filter Rejections for Q=4

III.1.e Introduction to Transconductors Optimizations

As discussed previously, the dynamic range of the filter is directly related to the dynamic range of its inner transconductors. Hence, all three transconductors have to be optimized. This section studies the Gm-cells limitations to find an optimal trade-off in terms of linearity and noise. This study has to be performed to reach the specifications both in terms of frequency tuning range and of selectivity.

To optimize the Gm-cell bloc, it is considered a simplified Gm-cell with an active load, regulated by a common-mode feedback (CMFB) [III.3], as described in Figure 107. The bias of the differential pair ensures that $g_{m1} = g_{m2}$ and $g_{m3} = g_{m4}$. Hence, the transconductance g_m of this Gm-cell is given by:

$$g_m = g_{m1} = g_{m2}\,. \tag{III.25}$$

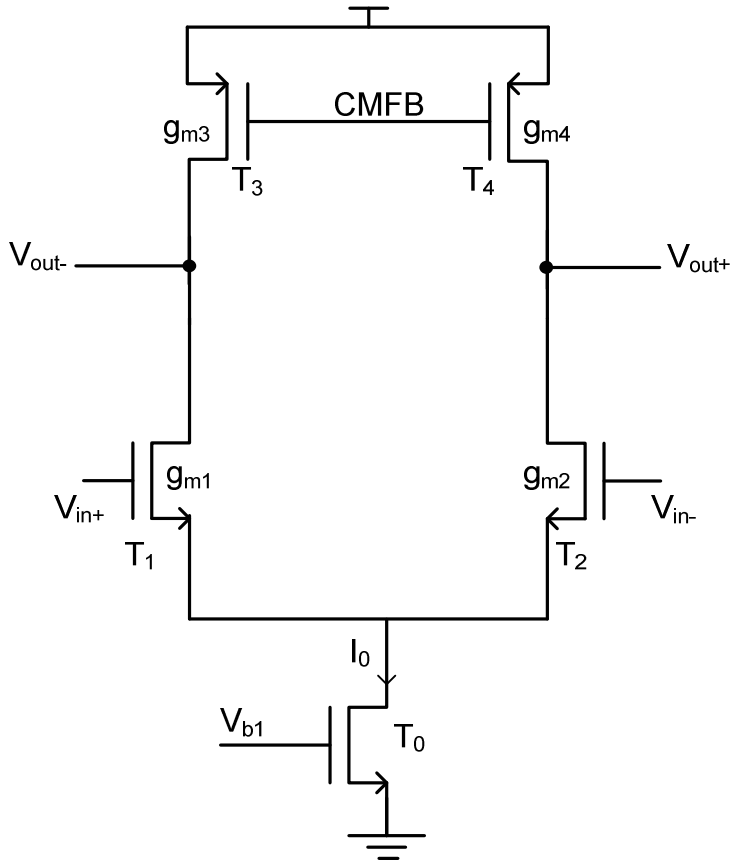

Figure 107. Differential transconductor

As detailed in APPENDIX D, the transconductance g_m of such a differential pair is given by:

$$g_m \approx \beta\left(V_{GS} - V_{th}\right) = \frac{I_0}{\left(V_{GS} - V_{th}\right)}, \tag{III.26}$$

with V_{GS}-V_{th} being the input voltage on either T_1 or T_2, and with

$$\beta = \mu C_{ox}\,\frac{W}{L}\,. \tag{III.27}$$

In terms of noise, the Flicker noise which exhibits a $1/f$ dependency is neglected as a first order approximation since TV bands are located above 45MHz. Hence, transconductor input-referred noise power is proportional to $1/g_m$ [III.4]:

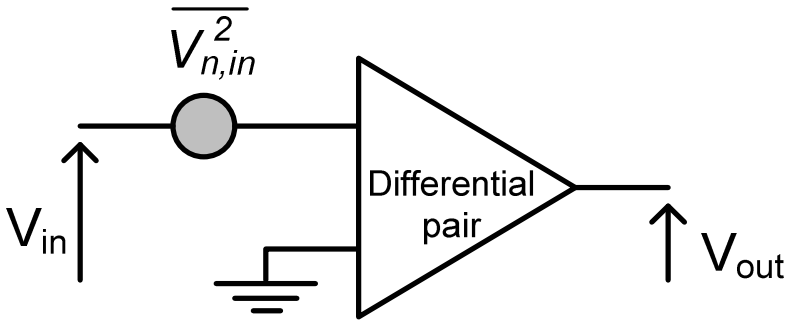

Figure 108. Input referred noise power

$$\overline{V_{n,in}^2} \approx 8kT\left(\frac{2}{3g_{m1}} + \frac{2g_{m3}}{3g_{m1}^2}\right) \propto \frac{\lambda}{g_{m1}}\left(1 + \frac{g_{m3}}{g_{m1}}\right). \qquad \text{(III.28)}$$

λ being a constant term, k being the Boltzman constant and T the temperature.

This means that the higher the transconductance (g_{m1}) values, the lower the noise of the Gm-cell. However, they suffer from non-linearity, as shown in Figure 109. Indeed this figure describes the g_m versus the input voltage for a same current and various transistor sizes which increase the transconductance. From this graph it is clear that high transconductances have to be improved using linearization techniques.

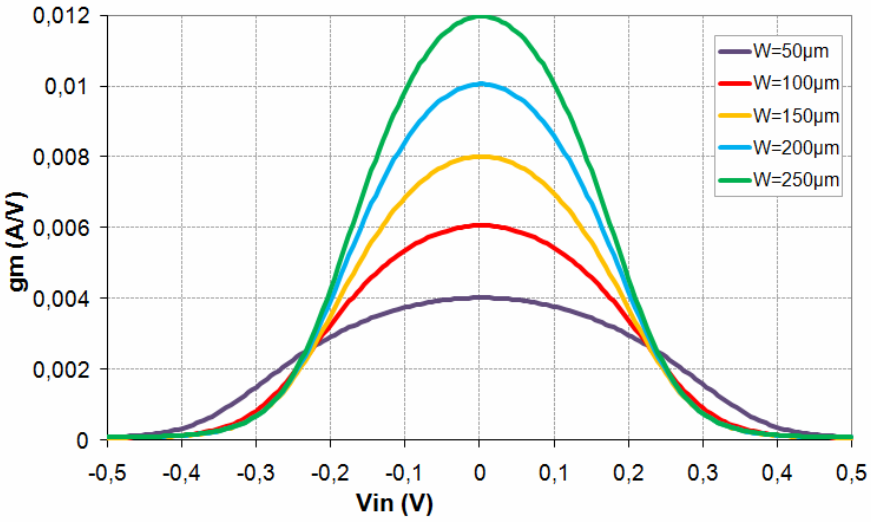

Figure 109. Transconductance non-linearity at constant current, varying the W/L ratio

Furthermore, the choice of high transconductance values means the use of high capacitances to be able to reach the low end of the TV bands since $f_0 \approx \frac{g_m}{2\pi C}$, as shown in Figure 110. In an advanced CMOS technology, large capacitors integration are not suitable for an optimum die area.

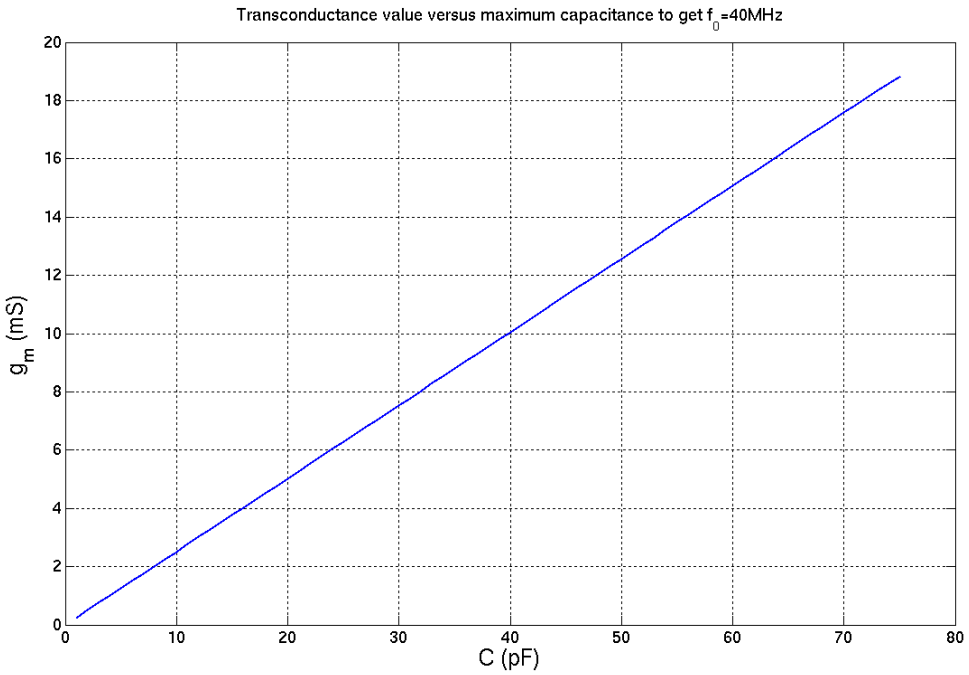

Figure 110. g_m value versus C values to reach the low end of the TV band

Hence, the choice of the transconductance value g_m is particularly critical. The use of low g_m values means a high filter noise. On the contrary, the use of a too high g_m would result in the use of larger capacitors to reach 45MHz and in a poor linearity. To limit C_{max} to less than 50pF, g_m specification is limited to 13mS. That is why we specify that the ***transconductance value should be as high as possible***, in the limit of 13mS, ***and fulfil the 20dBm linearity level*** previously discussed.

Furthermore, the voltage gain $g_m.r_0$ has to be high enough to reach the desired filter quality factor. If r_0 is too low, most of the output current flows through it and not through the capacitance, degrading the functionality of the filter. Indeed, it has been shown previously that for Gm-cells with r_0 as output resistance and $g_{m1}=g_{m2}=g_m$, the quality factor is given by the formula:

$$Q = \frac{r_0}{2}\sqrt{\frac{1}{r_0^2} + g_m^2}\ . \qquad \text{(III.29)}$$

Hence, this gives the required r_0 value:

$$r_0 = \frac{\sqrt{(2Q)^2 - 1}}{g_m}\ . \qquad \text{(III.30)}$$

Table 7 summarizes the specifications set on the design of the transconductors.

Table 7. Specifications of the Transconductor Design

Parameter	Value	Trade-off
g_m	g_m < 13 mS	Noise vs linearity
$g_m.r_0$	22.5 dB	Q vs linearity & noise
C_{max}	< 50 pF	Silicon area vs frequency tuning range
IIP3	> 20 dBm	g_m value vs noise

III.2 Transconductors Linearization Techniques

To handle this tight dynamic range, it is clear that transconductors need to be very linear while being as low noise as possible.

III.2.a Introduction to linearization techniques

The literature reports many different techniques to linearize transconductors g_m. Among them:

- ***Transistor current increase*** and reduce W/L to keep gm constant
- ***Active or passive feedback***, like the well known source/emitter degenerations. Dynamic source degeneration enters in this category.
- ***Unbalanced differential pairs***
- ***Derivative superposition***

Other linearization techniques are also reported in the literature like ***feedforward***, ***predistortion*** which is often used for power amplifiers and actually consist in distorting the input signal before the amplifier so that it is the inverse of the amplifier non-linearity [III.5], or ***second order intermodulation injection*** [III.6] which requires two mixing stages. However these techniques are not discussed in the following. Their complexity does not make them attractive solutions to handle the required transconductor high dynamic range.

III.2.b Transistor Current Increase Technique

Increasing current in a differential pair, reducing the W/L of its transistors T_1 and T_2 to keep its g_m at a certain value, helps to improve linearity.

Indeed, in [APPENDIX D], it is demonstrated that for a MOS differential pair, the linearity V_{IP3} is a function of the input voltage $V_{GS} - V_T$:

$$V_{IP3} = 4\sqrt{\frac{2}{3}}(V_{GS} - V_T). \tag{III.31}$$

Now, this can also give, as a function of the drain current I_d:

$$IP3 = 4\sqrt{\frac{2}{3}}\frac{I_d}{g_m}. \tag{III.32}$$

Hence, the third order intercept point is increased when current is increased while keeping the transconductance constant.

However, the risk is to have a very high current in a small transistor and to overcome the design manual limitations. The transistor may then act as a fuse. Besides, the linearity

levels reached with this technique are still poor, as it may be observed in Table 8, and very high currents are needed to reach high g_m values.

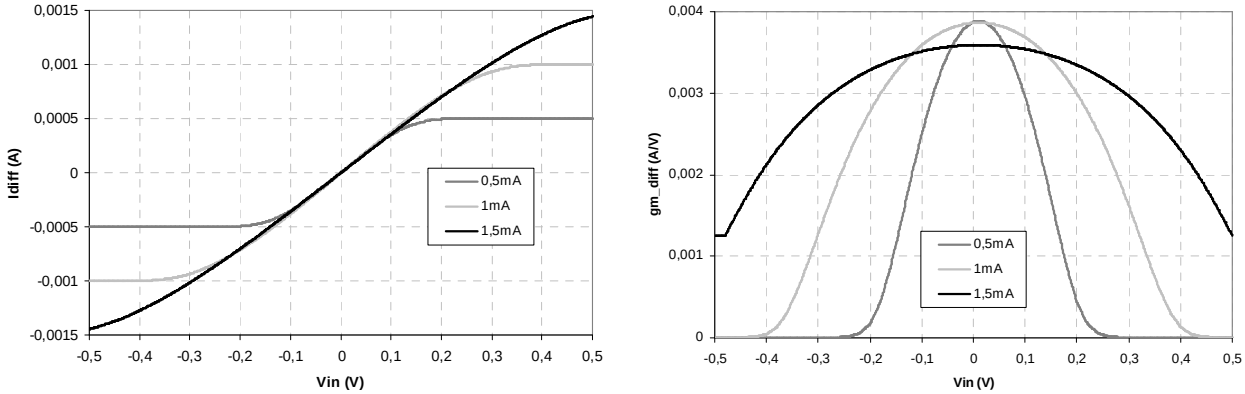

Figure 111. Linearization of the transconductance by current increase

III.2.c Active and Passive Source Degeneration Technique

The principle of active and passive source degeneration (or emitter when dealing with BiCMOS technologies) is to use an active or a passive device, connected to the source of the MOS transistor to linearize the transconductance gain. In this configuration, illustrated in Figure 112, the impedance Z_{deg} acts as a local feedback.

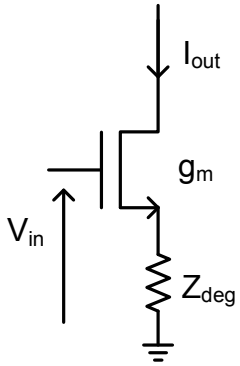

Figure 112. Source degeneration

Using feedback theory, the equivalent transconductance of this stage can be computed. It gives:

$$g_{m\_\deg} = \frac{g_m}{1 + g_m Z_{\deg}}. \tag{III.33}$$

Hence, for $g_m.Z_{deg}>>1$, it can be approximated to

$$g_{m\_\deg} \approx \frac{1}{Z_{\deg}}, \tag{III.34}$$

which is very interesting since the transconductance can then be set by a single impedance. Resistors are usually used but they increase noise (as demonstrated in APPENDIX D). Indeed, the noise power is proportional to Z_{deg}. That is why inductances are preferred. Feedbacks making use of transistors are used as well.

III.2.d Dynamic Source Degeneration Technique

In [III.1] and [III.7], the dynamic source degeneration technique, which is an active source degeneration, is described. The schematic of this linearization technique is depicted in Figure 113. The red-circled transistors act as equivalent resistors which linearize the differential pair.

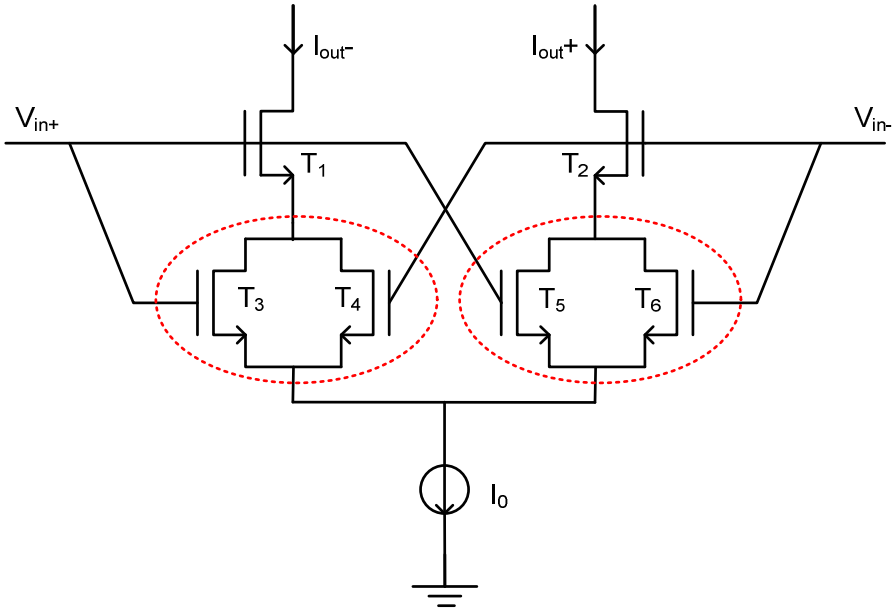

Figure 113. Schematic of the dynamic source degeneration technique

Figure 205 shows the linearization of the transconductance for various transistor sizes. The degeneration consists in reducing the g_m value in order to be more linear. Hence, though very high linearity level can be reach for small g_m values, the method is not appropriate for 10mS or more transconductances values.

Moreover, since this technique is an active degeneration of the MOS differential pair, noise is increased as described for the resistive MOS common-source circuit.

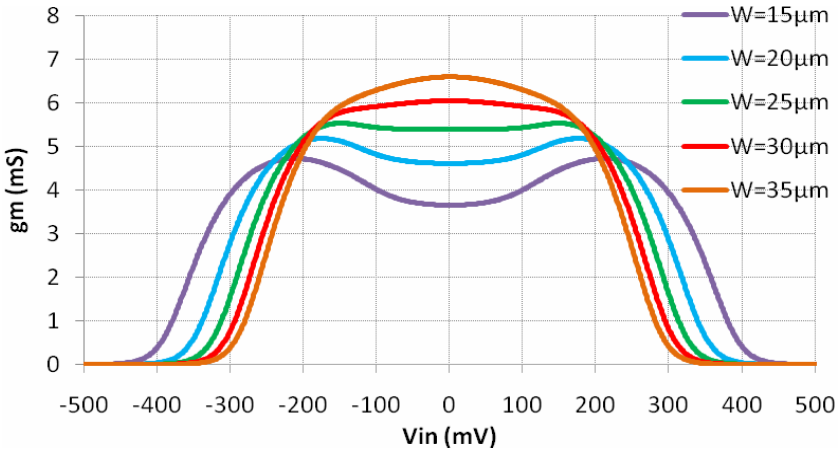

Figure 114. Transconductance linearization by dynamic source degeneration

III.2.e Unbalanced Differential Pairs Technique

Reference [III.8] reports the use of unbalanced differential pairs, as illustrated in Figure 115, in order to linearize the resulting transconductance. This method is known as **multi-*tanh*** for BiCMOS technologies and may also be used with CMOS technologies.

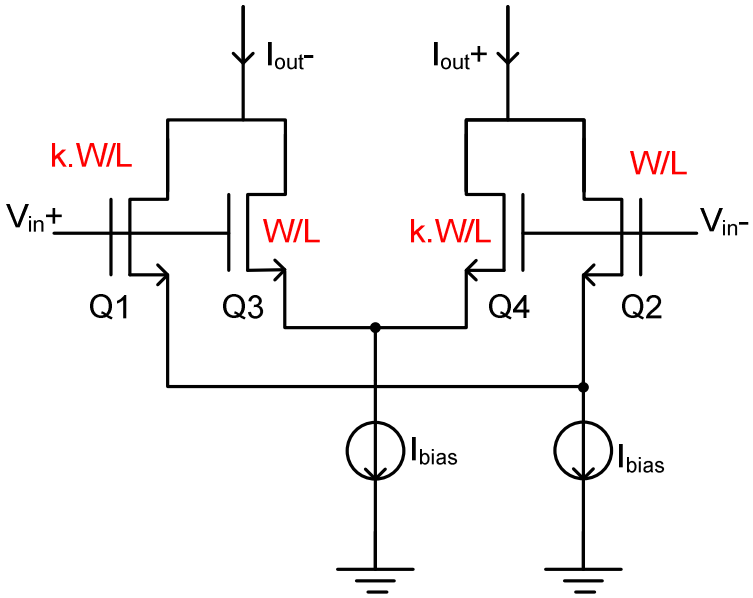

Figure 115. Unbalanced CMOS differential pairs

For a well-chosen *k* factor, the resulting current of the two parallel differential pair is highly linear. Figure 116 shows that the resulting g_m is linear on a wider range than Q1-Q2 and Q3-Q4 differential pairs. However, the final g_m is smaller than the sum of all individual g_m.

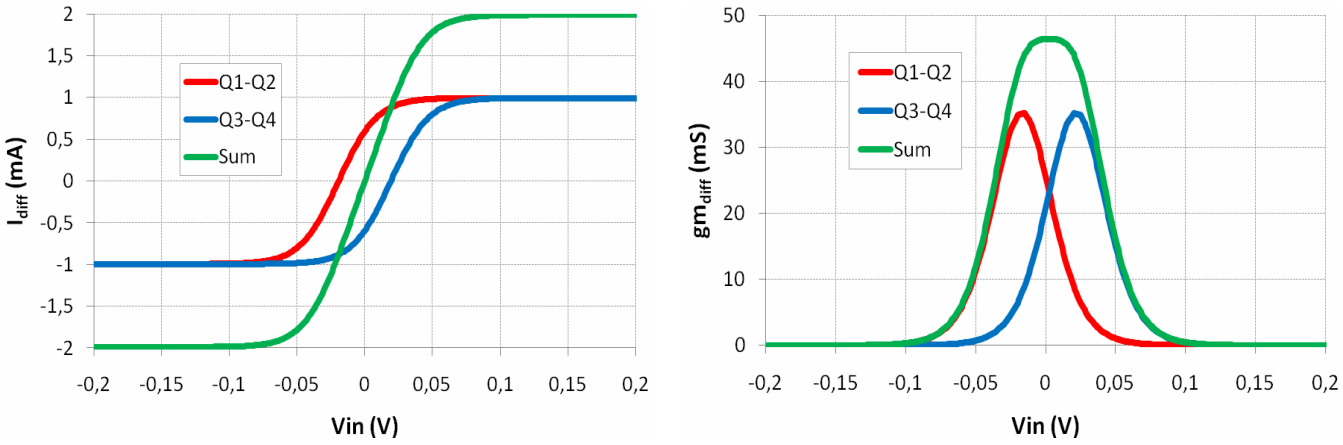

Figure 116. Linearization of the transconductance by unbalanced differential pairs

Furthermore, it is also possible to add several differential pairs in order to enhance the linearization range. This method is described in [III.9] for BiCMOS technologies.

III.2.f FDA//PDA technique

Reference [III.10] introduces the Multiple Gated Transistors (MGTR) technique. It makes use of a fully-differential amplifier (FDA) in parallel of a pseudo-differential amplifier (PDA), as shown in Figure 117.

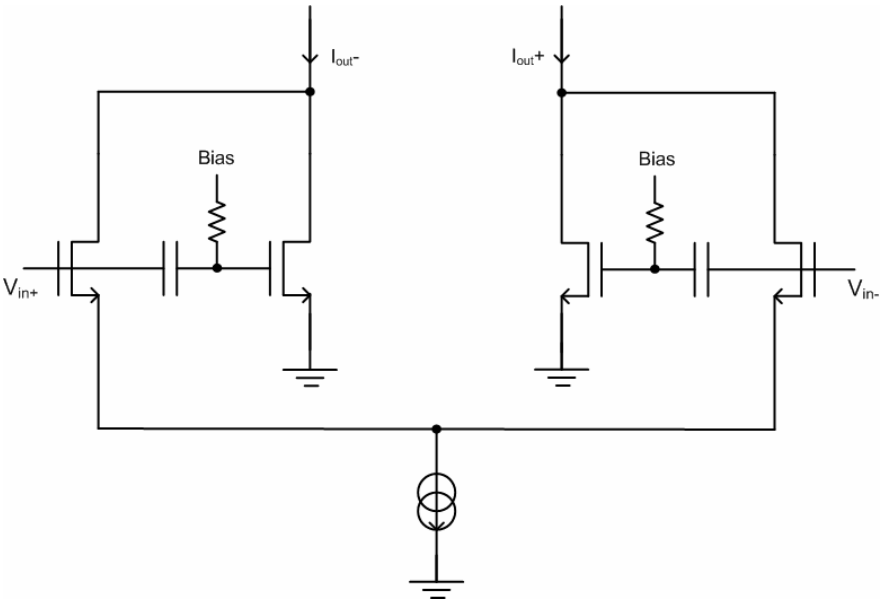

Figure 117. FDA // PDA Gm-cell design

The output differential current I_{md} from a MOS FDA is a function of the bias current I_0 and of the differential input voltage E_{md}, as demonstrated in APPENDIX D:

$$I_{md} = \frac{1}{2}\beta E_{md}\sqrt{\frac{4I_0}{\beta} - E_{md}^2} \tag{D.35}$$

where $\beta = \mu C_{ox}\frac{W}{L}$.

Developing this expression with a Taylor series up to the third order leads to:

$$I_{md} \approx \alpha E_{md} - \gamma E_{md}^3 \tag{D.36}$$

with α and γ being constant terms. Thus, the current from the FDA has a negative third order term.

Due to the bias in the sub-threshold region, the differential output current I_{md} of a MOS PDA is given by:

$$I_{md} = \lambda e^{\frac{E_{md}}{\nu}} \tag{D.37}$$

λ and ν being two constant terms.

Developing up to the third order gives:

$$I_{md} \approx aE_{md} + bE_{md}^3 \tag{D.38}$$

Indeed, since the study is carried out in differential mode, second order terms are neglected.

Hence, the combination of the exponential current from the PDA, which has a positive third order term, with the current from the FDA may lead to a cancellation of the third order terms under specific conditions. The output current of the transconductor is then linearized, as it may be observed in Figure 118.

The drain current I_d of a MOS biased in weak inversion and in the saturation region is given by:

$$I_d \approx 2\beta U_T^2 e^{\frac{V_{GS}-V_{th}}{U_T}} \tag{D.39}$$

where $V_{GS} - V_{th}$ is the input voltage and U_T the thermal voltage.

This equation highlights a strong dependency of the current versus the gate-source voltage. The biasing of the PDA should then be very accurate. The presence of β in the equation also underlines the importance of the W/L ratio on the current. Thus, the impact of process and mismatch variations will have to be studied more accurately later.

However, power consumption remains the same since almost no current is added by the PDA stage, biased in the sub-threshold region. The resulting transconductance of these two parallel pairs is equal to the FDA one but it is linear on a wider range, as depicted in Figure 118. Hence, noise and gain stay unchanged.

In the example below, the FDA MOS size is 16µm/0.28µm, minimal gate length is not used to limit Flicker noise, while the PDA MOS size is 50µm/0.28µm. The corresponding currents are 1mA for the FDA while the PDA draws about 6µA. Thanks to this technique it is possible to get a high g_m to minimize noise and to optimize linearity. Currents and g_m of both amplifiers and of the sum are plotted on Figure 118.

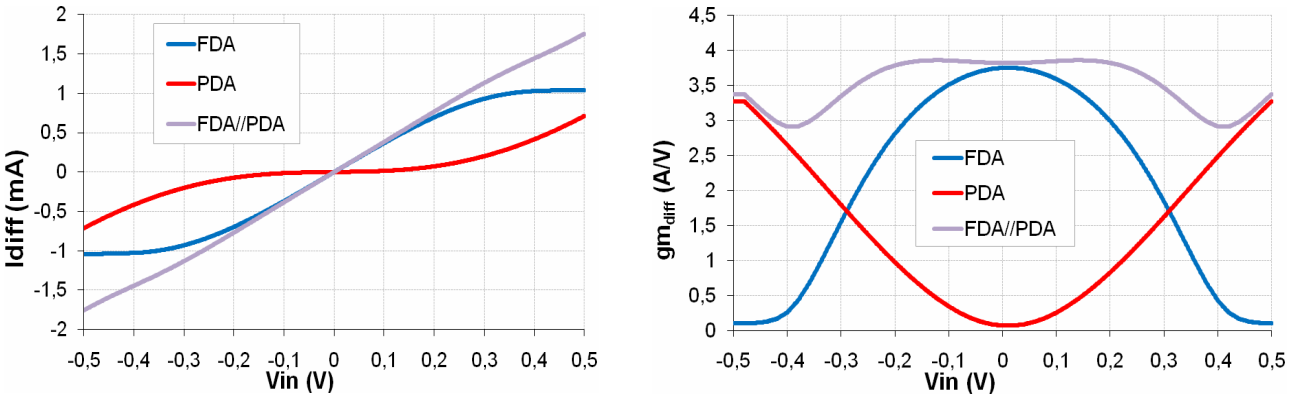

Figure 118. Transconductance linearization by MGTR

However, Figure 119 shows that this high linearity level is reached on a linearity peak for the PDA bias. As soon as the PDA bias drifts from its original value, the IIP3 of the Gm-cell is drastically reduced.

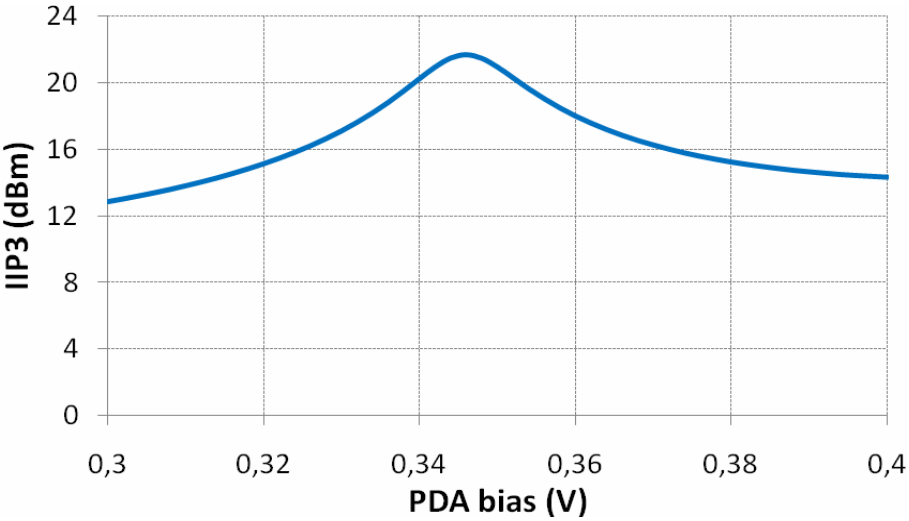

Figure 119. Transconductance linearization by MGTR

III.2.g Transconductance Linearization Techniques Comparison

Table 8 summarizes the linearity performances obtained using the different linearization techniques, as well as the advantages and drawbacks of each. To make quantitative comparisons, performances are simulated at 100MHz. The Gm-cells are studied with a capacitive load C_L (see Figure 120) which depends on the g_m value to keep the same $\frac{g_m}{C}$ ratio.

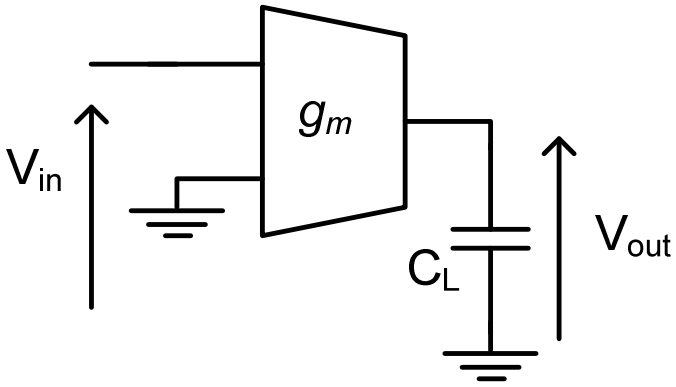

Figure 120. Gm-cell test bench

The Gm-cell DC voltage gain is set close to 22.5dB as explained further. Hence, all g_m, r_0 and C parameters are equal or comparable. Furthermore, at 100MHz, it should be underlined that the Gm-cell voltage gain is close to 0dB.

Table 8. Comparison of the transconductance linearization techniques

Technique	IIP3 and Noise Performances	Advantages	Drawbacks
Current Increase	***3dBm for 3.6mS*** ***Difficult to obtain higher g_m***	Simple technique	Power consumption Low linearity
Source Degeneration	***14dBm for 10mS*** ***8.3 10^{-18} V^2/Hz***	Simple technique	Linearity versus noise trade-off
Dynamic Source Degeneration	***16dBm for 9mS*** ***13.3 10^{-18} V^2/Hz*** ***21dBm for 2.5mS*** ***9.7 10^{-18} V^2/Hz***	High linearity	Linearity versus noise trade-off
Unbalanced Differential Pairs	***7dBm for 10.7mS*** ***9.6 10^{-18} V^2/Hz***	Linearity versus noise trade-off	Power consumption Noise increase
MGTR	***21dBm for 10mS*** ***6.5 10^{-18} V^2/Hz***	Very high linearity Power consumption Noise	Linearity peak

The MGTR technique shows the best performances. However, the linearity presents a peak versus the PDA bias that may be very sharp, as it will be discussed later on. Hence, the sensitivity to this bias will have to be taken into account when linearizing Gm-cells by this means.

In the following, second order Gm-C filters using the best two linearization techniques, dynamic source degeneration and MGTR, will be designed and compared.

III.3 Filter Implementations and Simulations

III.3.a Generalities

III.3.a.i Focus on the circuit

The proposed RF filters have been designed with ***TSMC 65nm CMOS*** process, based on BSIM4 models, using thick oxide MOS under a 2.5V supply in order to increase the input voltage swing. To allow the cascade of several Gm-cells, input and output DC voltage of the Gm-cell are set to a common value. For this purpose, in each Gm-cell, a common mode feedback is added for the control of the active load bias. The complete schematic of the filter is recalled in Figure 121.

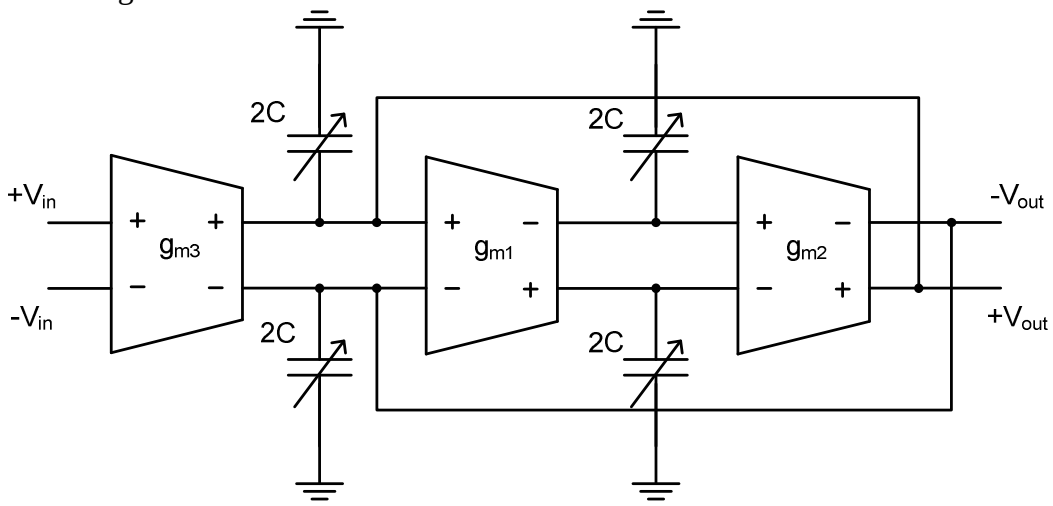

Figure 121. Proposed Differential Gm-C Filter

As far as the frequency tunability is concerned, 8 bit ***capacitors banks*** have been used, as described in Figure 122. It is composed of a main capacitor C_{fix} and of secondary capacitors that are switched in order to increase the overall capacitance.

For all capacitors banks, P1 is connected to Gm-cells output. This node is biased to 1.8V whereas the second port P2 is connected to GND.

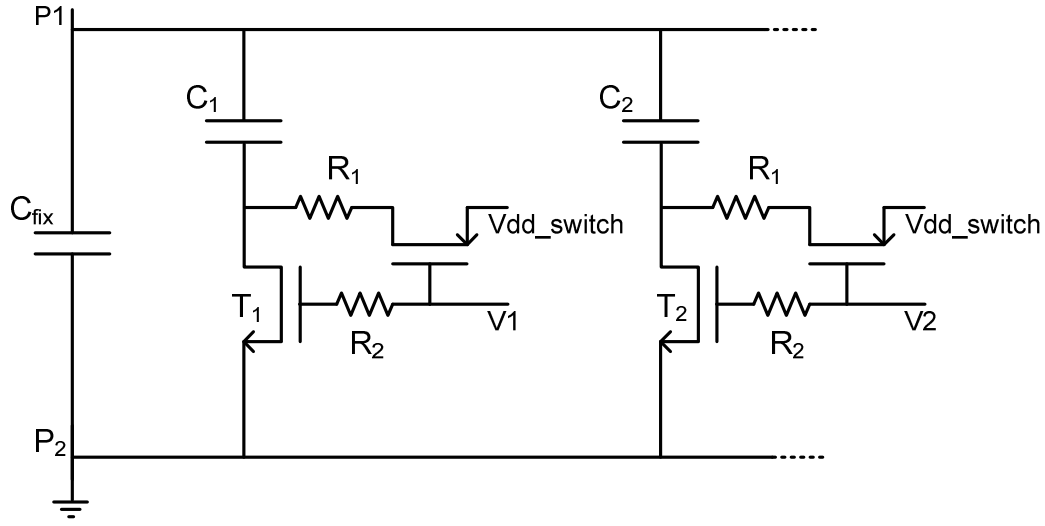

Figure 122. Capacitor banks design

Using this structure and considering the model illustrated in Figure 123 for the switches, when the switch is ON, V_{ds} is minimal so as to minimize R_{on}. Indeed, the MOS transistor is then in the triode region.

When the switch is OFF, the drain is set to a high potential V_{dd_switch} to minimize the non-linearity of the drain-bulk capacitance, also called C_{off} when dealing with switches.

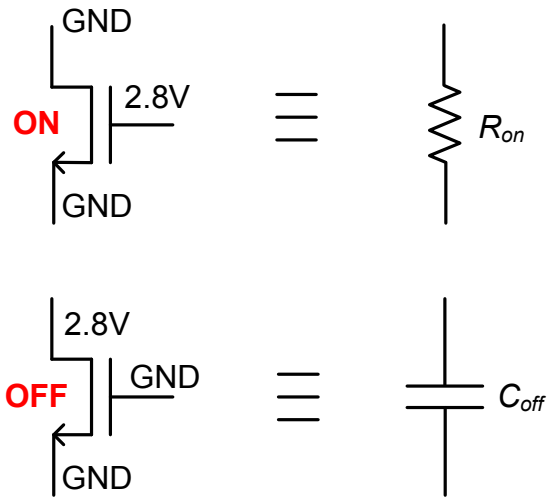

Figure 123. Model for the switches

Table 22 describes the values taken for the capacitances of the capacitor bank. C_{fix} is 3pF. The frequency step at high frequency is achieved by means of small capacitances C_1 to C_4 in order to ensure to be centered on every channel.

Table 9. Description of the capacitor bank

Bit number	C_{fix}	C_1	C_2	C_3	C_4	C_5	C_6	C_7	C_8
Capacitance (pF)	3	0.2	0.4	0.8	1.6	3.2	6.4	12.5	25

III.3.a.ii Current Source

Currents feeding the Gm-cells are provided by a bandgap and a series of current mirrors [III.1], as depicted in Figure 124.

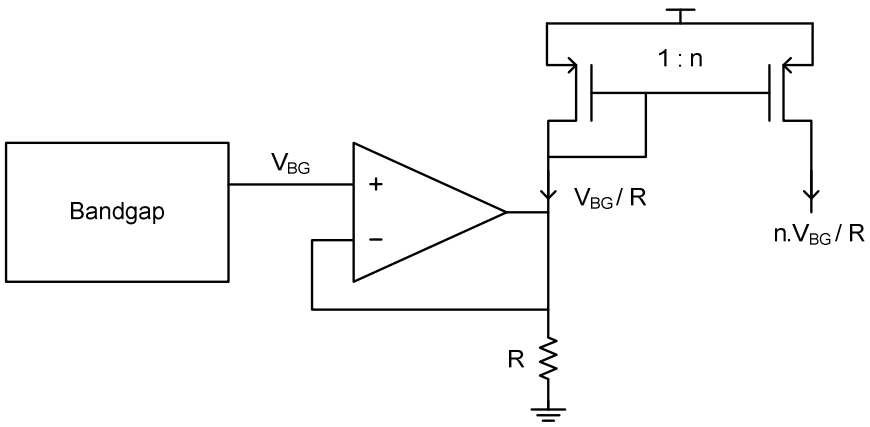

Figure 124. Current source generation

III.3.a.iii Design of the Filters

Two filters have been designed, using high-performance Gm-cells. In the previous study, two Gm-cells show interesting assets. ***Filter 1 is based on a dynamic source degeneration Gm-cell***. This simple technique exhibits an interesting trade-off noise versus linearity. ***Filter 2 is based on the MGTR technique***. This technique demonstrates the best performances. These two filters are studied in the following and then compared.

III.3.b Gm-cells with Dynamic Source Degeneration

III.3.b.i Gm-cell Design

Figure 125 depicts the design of the Gm-cell. As explained, circled in red on the figure is the dynamic source degeneration of the transconductor which is ensured here by the use of NMOS transistors T_5 to T_8.

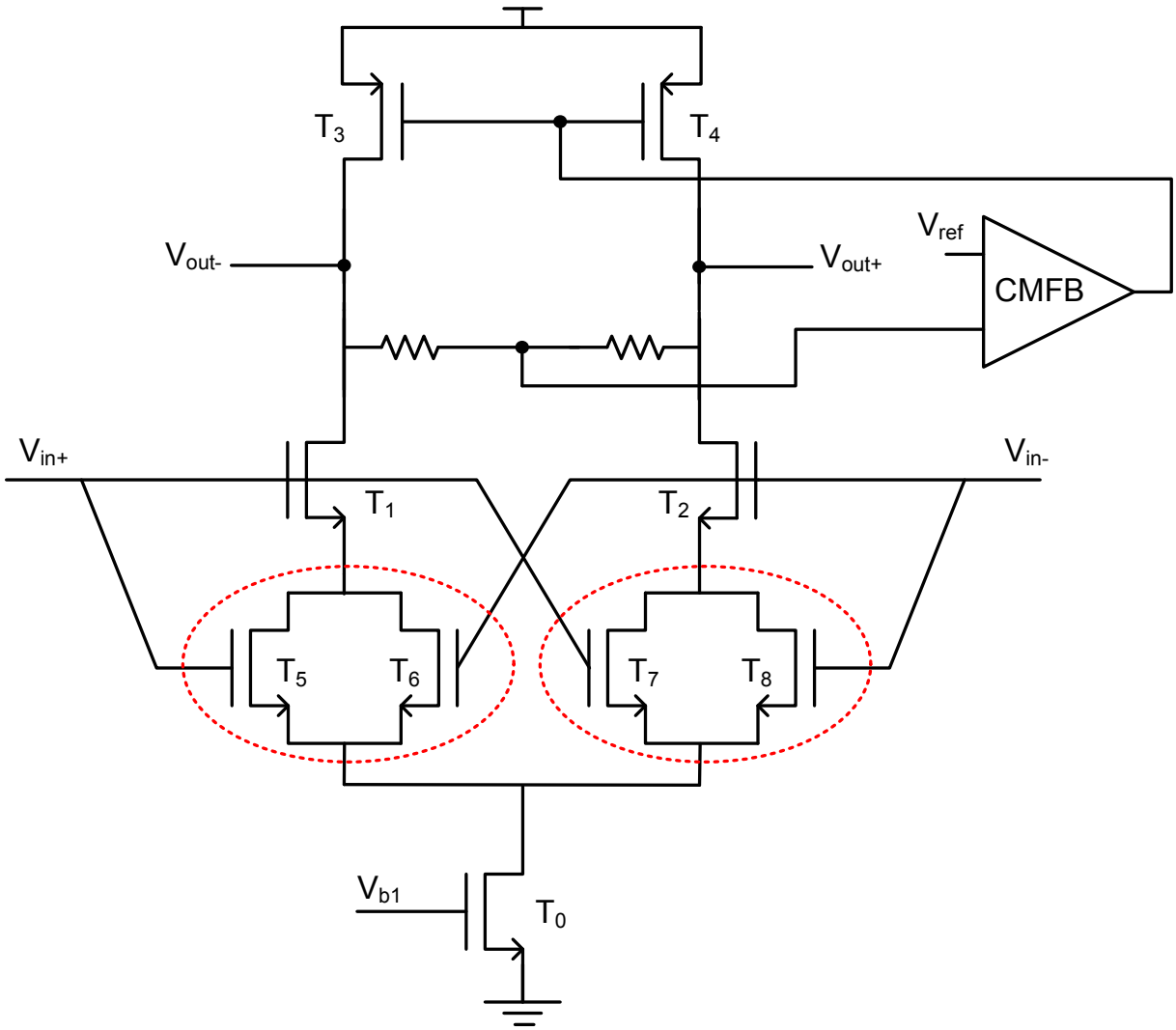

Figure 125. Gm-cell design

The dimensioning of the transistors is given in Table 10. Current consumption is 1.7mA per Gm-cell and 500µA for the CMFB.

Table 10. Gm-cell dimensioning

Transistor	W/L (µm/µm)
$T_1 - T_2$	70 / 0.5
T_5 to T_8	25 / 0.5

The resulting g_m is 2.5mS. Here it has been chosen to use a smaller transconductance than presented in Table 8 in order to reach the specified 20dBm IIP3.This is highlighted in Table 11.

Table 11. Transconductance choice

g_m (mS)	IIP3 (dBm)
2.5	21
9	16

This leads to the following DC gain and transconductance versus frequency, illustrated in Figure 126.

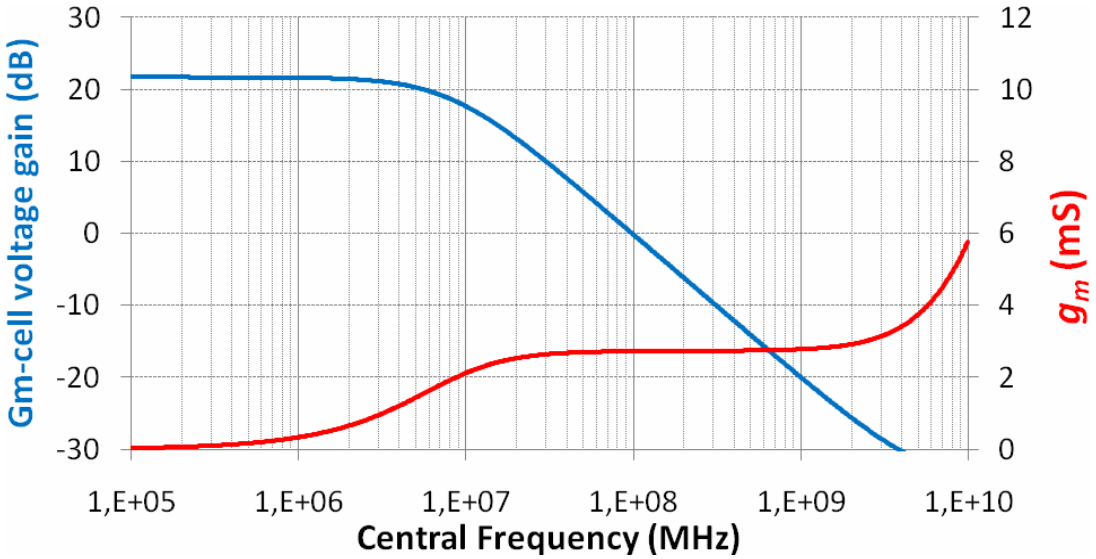

Figure 126. Gm-cell DC gain and transconductance

III.3.b.ii Simulated Filter Performances

This filter covers the range 45 – 385MHz. It provides a mean Q factor of 3.5 for a gain between 10 and 12dB as it may be seen in Figure 127.

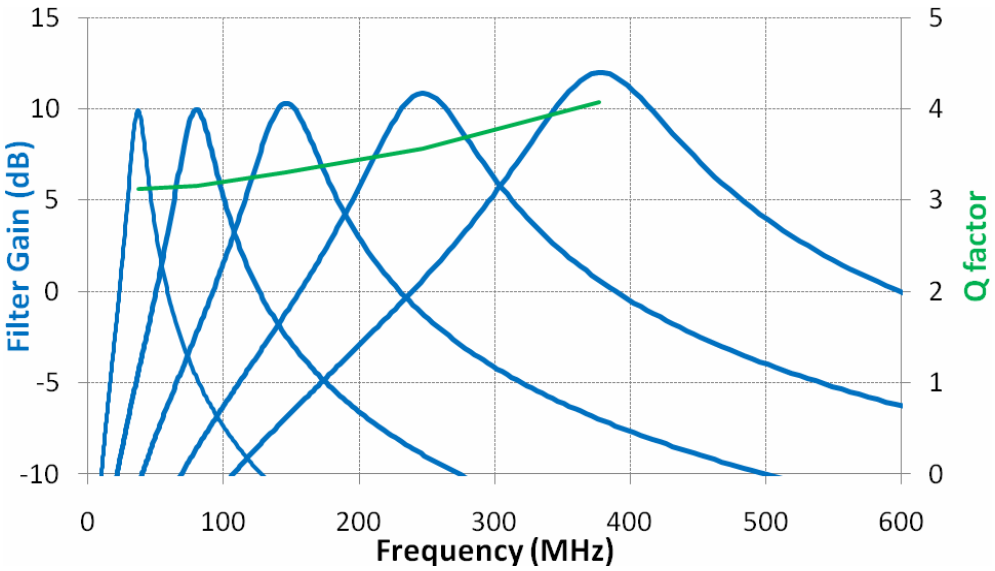

Figure 127. Filter Gain and Q-factor for various central frequencies

In-band linearity is depicted in Figure 128. IIP3 lies between 2 and -4dBm for a 18dB noise figure.

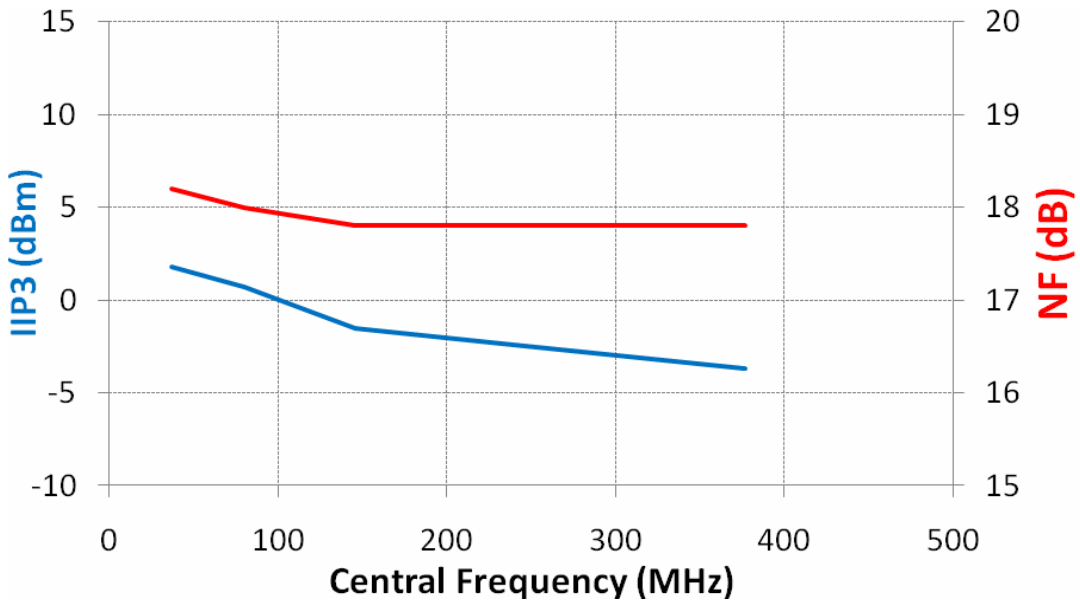

Figure 128. Filter RF performances versus central frequency

This latter graph demonstrates that the linearity of the transconductors is not high enough to ensure a high linearity for the filter. Besides, Figure 205 underlines a certain sensitivity to process and mismatch variations. Hence, this has to be compared with the second linearization technique.

III.3.c Gm-cells with MGTR

III.3.c.i Filter Design

This Gm-cell, as it may be seen in Figure 129, drains 4.5mA from the 2.5V supply.

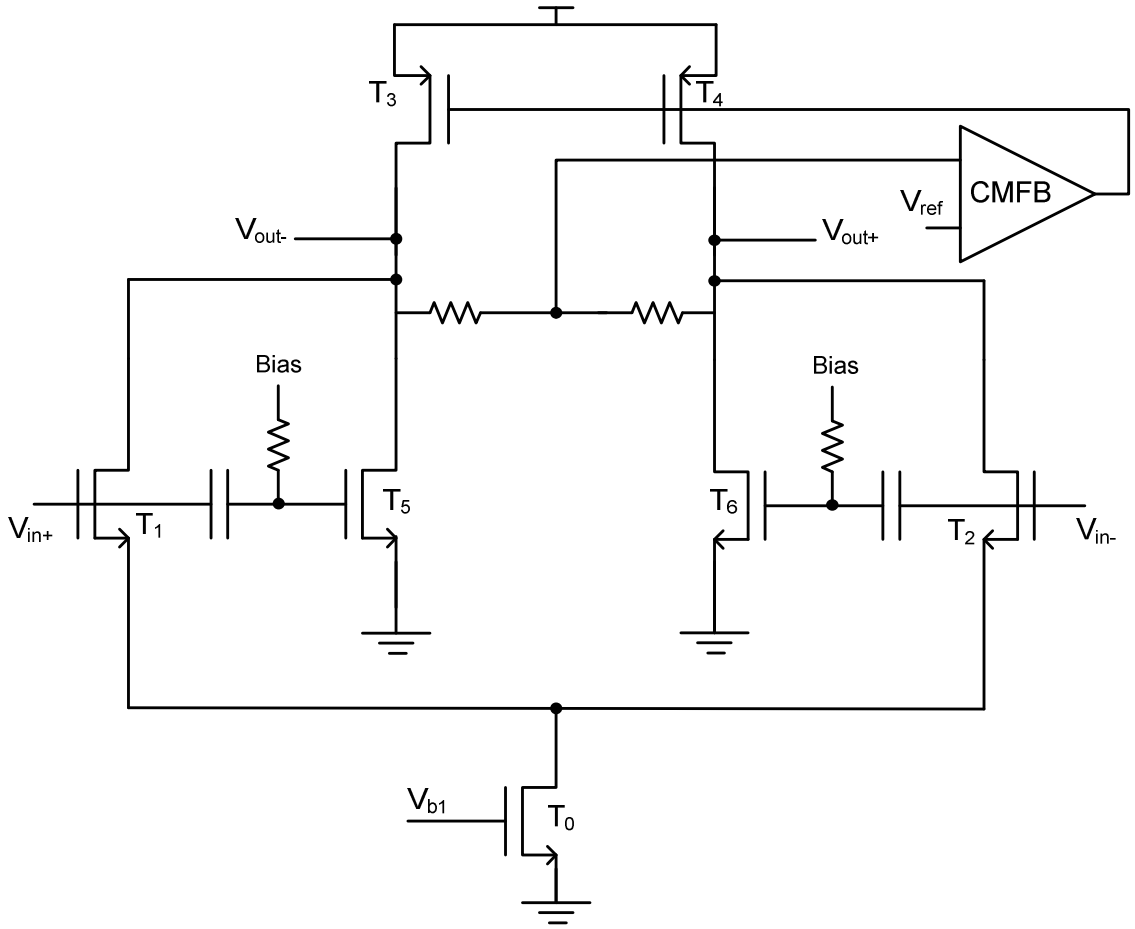

Figure 129. Gm-cell design

The dimensioning of the Gm-cell is described in Table 12. T_0 drains 4 mA in the Gm-cell while 500µA is used for the common-mode feedback (CMFB). PDA bias is set further to optimize the linearity of the Gm-cell.

Table 12. Gm-cell dimensioning

Transistor	W/L (µm/µm)
$T_1 – T_2$	32 / 0.28
$T_3 – T_4$	100 / 0.28

Figure 130 confirms the transconductance of the Gm-cell which is 10mS at the working frequency. Its voltage gain is typical of a lossy integrator. DC voltage gain is 22.5dB. Gain then decreases with frequency due to the capacitive load.

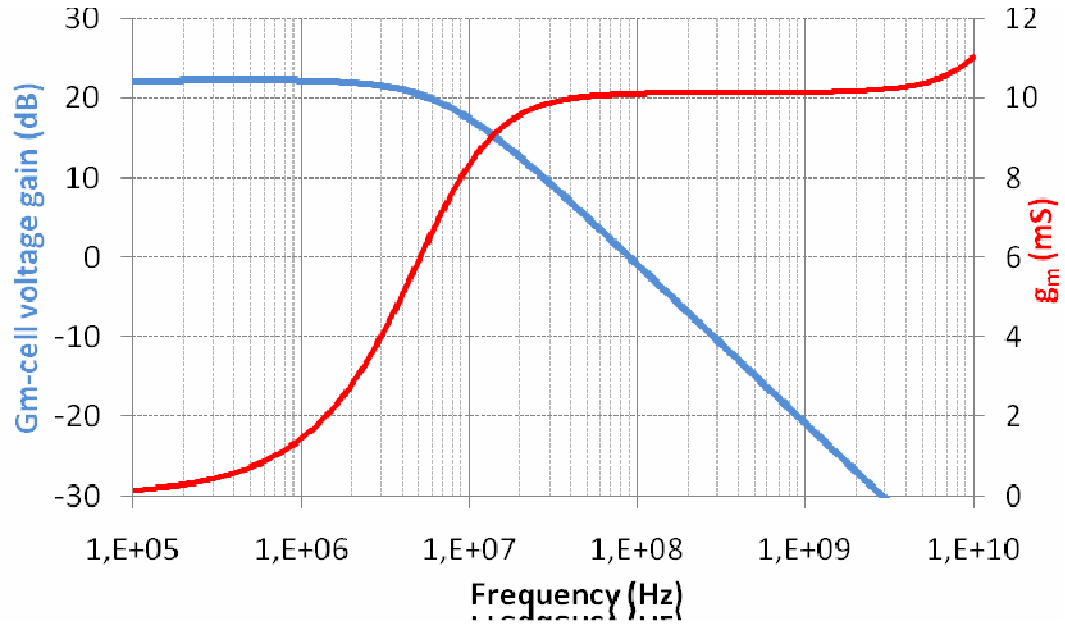

Figure 130. Gm-cell DC gain and transconductance

Figure 131 shows the loaded Gm-cell variations as a function of the voltage bias of the pseudo-differential pair. Switching-off the PDA, which corresponds to a PDA bias of 0V, the Gm-cell IIP3 is 9dBm. Disconnecting the PDA leads to a comparable value (9.4dBm). However, on a peak of linearity close to 350mV, the specified 20dBm are reached. This technique is then able to enhance the Gm-cell linearity by up to 12dB.

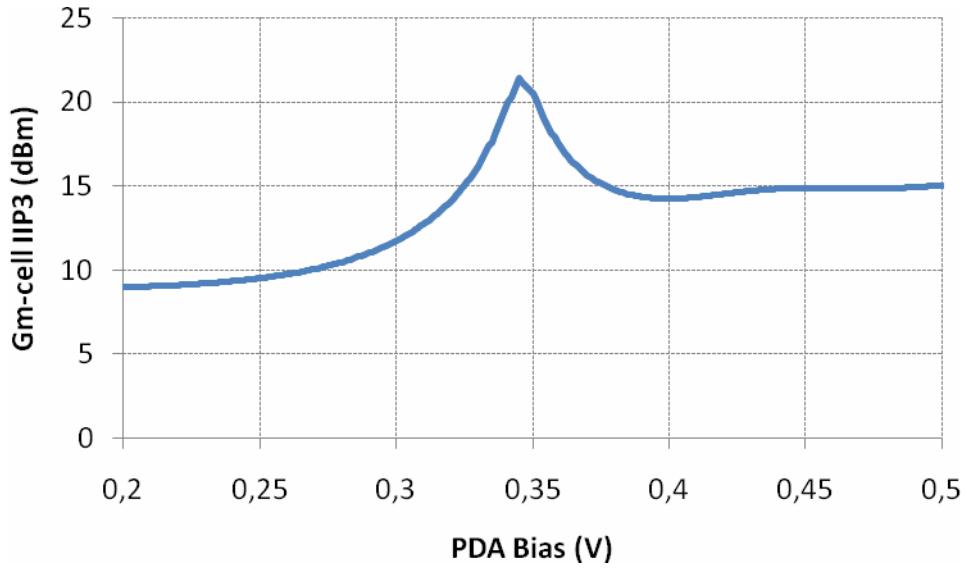

Figure 131. Gm-cell linearity versus PDA bias

Furthermore, the high sensitivity to process and mismatch issues of the MGTR technique is illustrated in Figure 132. This figure depicts the Monte-Carlo simulation results of the Gm-cell IIP3. It appears that the mean value is 19.8dBm, which is the targeted value. However, the standard deviation describes a high dispersion for 100 runs, since σ=1.5dBm. The dispersion and the sensitivity to PDA bias of each Gm-cell will result in a very sensitive filter. Robustness already appears as a limiting issue.

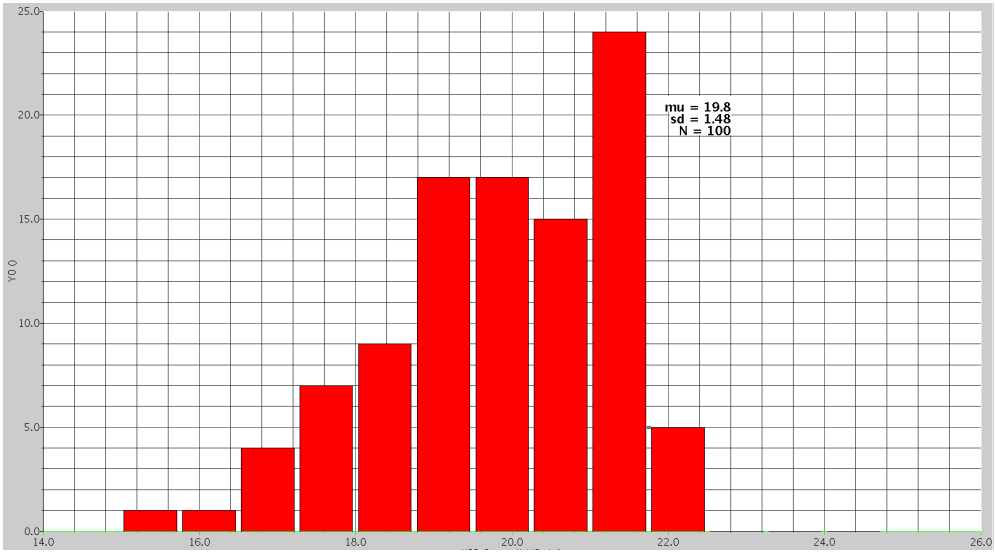

Figure 132. Monte-Carlo Simulations of the Gm-cell IIP3 for 100 runs

III.3.c.ii Filter Performances

The tuning range of Filter1 covers the full 45 to 450MHz band. A constant Q-factor of 4 is depicted in Figure 133 and guarantees a minimal harmonic rejection. Figure 134 represents the evolution of the central frequency versus the capacitance provided by the capacitor banks.

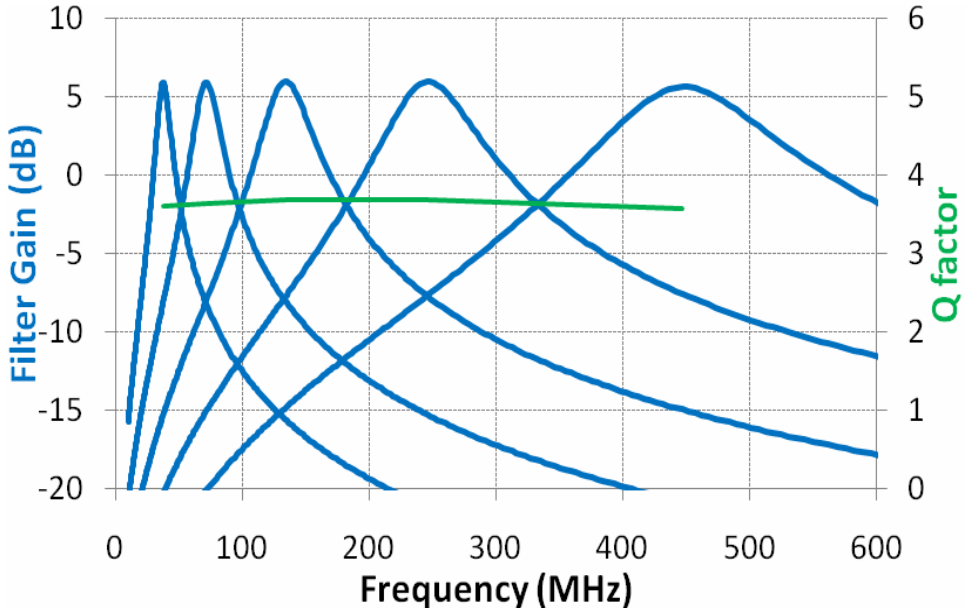

Figure 133. Filter Gain and Q-factor for various central frequencies

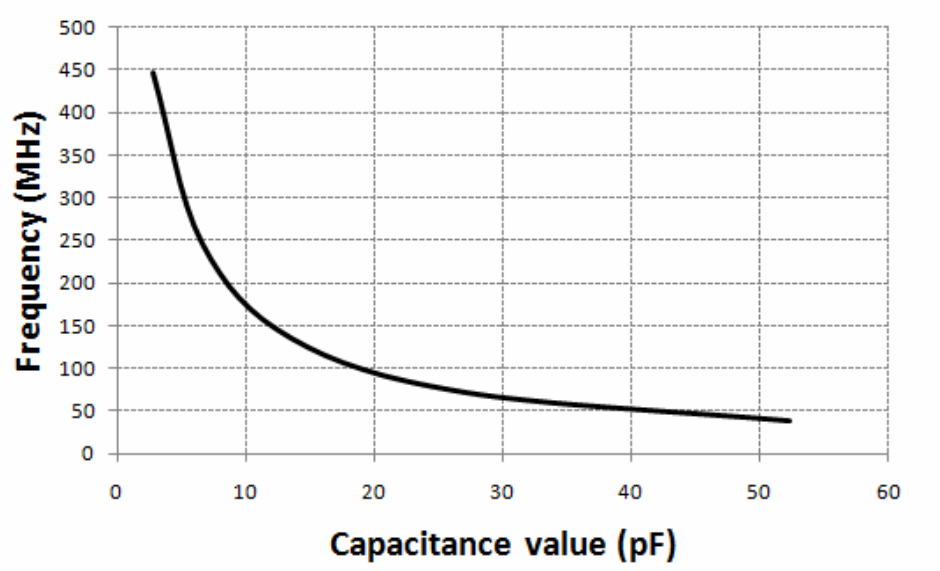

Figure 134. Central frequency variation versus capacitance values

The simulated NF on 50Ω source impedance is 16.3dB for 6dB voltage gain. The input-referred IP3 is depicted in Figure 136 and shows a high linearity above 8dBm up to 450MHz.

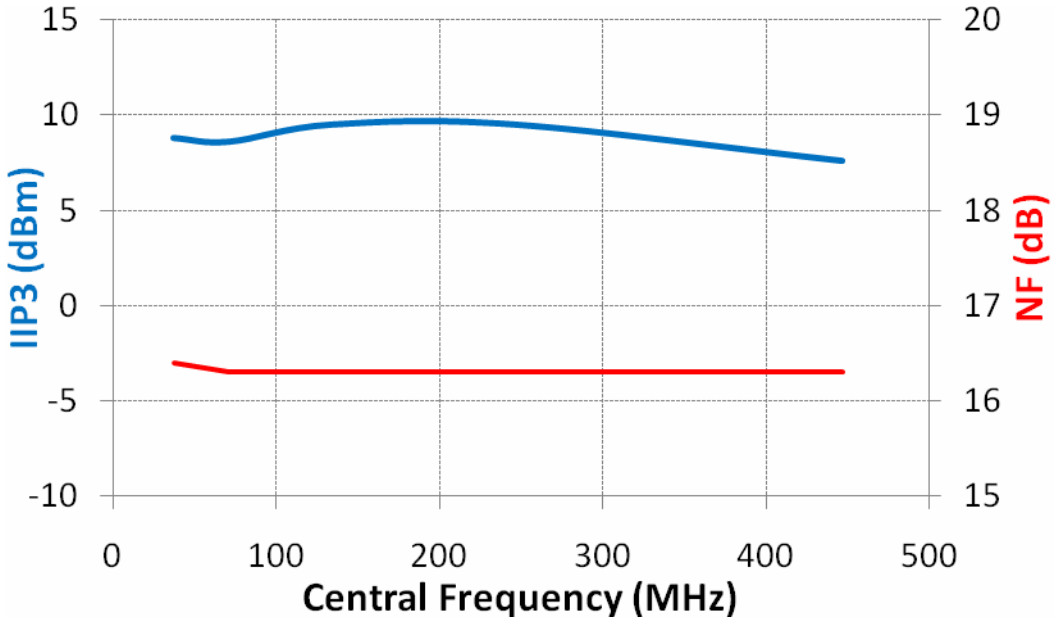

Figure 135. Filter RF performances versus central frequency

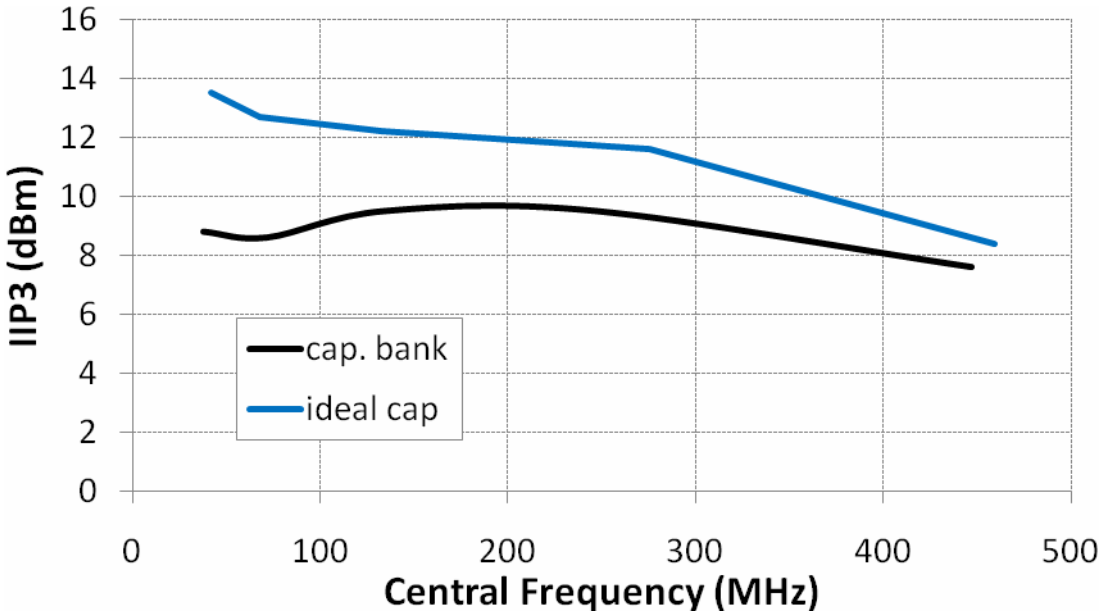

Figure 136. Filter in-band IIP3 versus central frequency

This latter graph represents the input-referred IP3 of the Gm-C filter in two cases: using ideal capacitors associated to ideal resistors modeling the switch R_{on}, or using the previously discussed capacitors banks, implemented by means of MOS capacitances. It may be observed that around 2dB are lost when implementing the capacitors banks.

It is worth adding that at low frequencies the quality factor of the filter using ideal capacitances, and so its gain, decreases. The implemented filter has been optimized, through the size of the switches, to obtain a constant Q-factor. Hence, this explains the linearity difference at 40MHz.

Table 13 summarizes the performances under process and mismatch variations. For these simulations, an ideal voltage source for the PDA has been considered. Very few variations on these parameters are observed.

Table 13. Process and Mismatch Variations

	Mean value	Sigma	Units
Central frequency	134.1	2.1	**MHz**
Bandwidth	36.4	0.7	**MHz**
Q-factor	3.7	0.1	-
Gain	6	0.35	**dB**

Figure 137 illustrates the IIP3 of the filter versus the variation of the PDA bias, set to 350mV. It can be observed that linearity is strongly degraded as soon as the bias shifts from its initial value. Indeed, a 5dBm degradation is noticed for a 5% variation. Hence, the filter requires a very accurate voltage reference. This sensitivity is the major drawback of the MGTR based Gm-C filter.

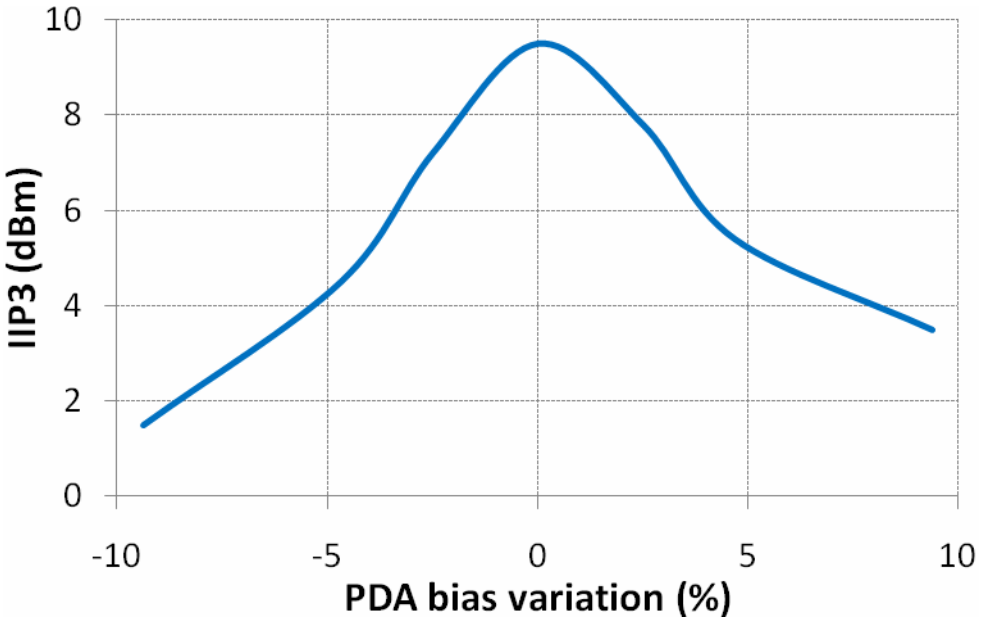

Figure 137. IIP3 versus PDA bias variation at 135MHz

Table 14 illustrates the sensitivity to process and mismatch issues of the filter linearity. Indeed, different models have been used in corners (slow, nominal and fast). In nominal, filter IIP3 is 9.9dBm whereas it is below 5dBm in the slow and fast corners.

Table 14. Linearity Process and Mismatch Variations

Corner model	Filter IIP3 @ 130MHz (dBm)
Slow-slow	4.9
Nominal	9.9
Fast-fast	4.5

III.4 Comparison of the filters

III.4.a Comparison of the Performances

Table 33 summarizes the performances obtained with the different filter and a compares them with [III.1].

Table 15. Performances Comparison

Filter	[III.1]	Filter 1	Filter 2	Units
Linearization tech.	DSD*	DSD*	MGTR	**-**
Tuning range	50 - 300	45 - 385	45 - 450	**MHz**
Q factor	6	3.5	3.7	**-**
Gain	6	10	6	**dB**
NF	20	18	16.3	**dB**
IIP3	2 to 6	-4 to 2	8 to 10	**dBm**
Power consumption	7.6	16.5	30	**mW**
Supply	1.2	2.5	2.5	**V**
CMOS Technology	130	65	65	**nm**

*DSD stands for Dynamic Source Degeneration

Filter 1 and Filter 2 present a larger tuning range than the filter reported in [III.1]. The high-end of the band is different between Filter 1 and Filter 2 due to a difference in the g_m value. Filter 1 uses a 2.5mS transconductance whereas Filter 2 uses a 10mS g_m. This difference is also visible on the NF value, which is higher when using smaller g_m, despite a higher filter gain.

As already mentioned, the linearity of Filter 1 is not high enough to compete with the other two filters. Besides, the filter gain is 4dB larger, which would involve tighter constraints on the LNA stage. Compared to reference [III.1], Filter 2 presents a higher dynamic range due both to its lower selectivity and to its particular linearization technique. This dynamic range is obtained at the cost of a higher power consumption, which also enables a larger input voltage swing (2.5V supply).

Compared to reference [III.1], Filters 1 and 2 linearity is smaller. A first possible explanation is that here, simulations have been performed with 1MHz spaced tones whereas measure in [III.1] used 10MHz spaced ones. In the latter case, the third order intermodulation products may be partially filtered out, which finally increases the intercept point value. Furthermore, in the present case, NF is lower. Hence, by means of the use of higher transconductances than in [III.1], the trade-off linearity versus noise is a bit shifted towards lower noise.

III.4.b Filter Limitations

In the following, Filter 2 has been simulated at higher frequencies in order to quantify the degradation of the performances when increasing the tuning range of the filter. Performances are summarized in Table 16.

Table 16. Filter 2 frequency limitations

Frequency Band (MHz)	Performances
40 – 240	Gain = 6dB Q = 4 IIP3 = 7 to 12.5dBm NF = 16dB 30mW
240 – 470	
470 – 750	Gain = 7-8dB Q = 4.5 IIP3 = 1dBm at 650MHz NF = 17dB 30mW ***Poor adjacent channels rejection***
750 – 1000	Gain = 8.5dB Q = 5-6 IIP3 = -0.5dBm at 1GHz NF = 17dB 30mW ***Poor adjacent channels rejection***

This table has been established using the same 10mS transconductances. Higher frequencies are reached using a smaller fixed capacitance. It comes out that Q increases with frequency, which explains the origin of the NF increase. This increase of the Q-factor is due to the higher Q-factor of the fixed capacitance compared to the Q of the other capacitances due to the R_{on} of the switch. At 650MHz and up to 1GHz, IIP3 falls down to 0dBm for a Q-factor which increases up to 6 and a NF of 17dB.

Linearity strongly decreases with frequency. Indeed, using smaller capacitances to reach higher frequencies of operation makes the C_{off} of the switches being relatively more important and this degrades the filter linearity.

Hence, the dynamic range is considerably decreased. Furthermore, a Q-factor of 6 in UHF is very poor in terms of adjacent channels rejection since N±5 channels are rejected by only 1dB.

III.5 Conclusion

Once the Gm-C second order bandpass filter topology adopted, a theoretical study has been carried out. From this study, it has been demonstrated that linearity, noise and the filter Q-factor are strongly related. In order to optimize the dynamic range of the Gm-C filter, a moderate Q has been chosen. A second choice is based on the use of Gm-cells of high transconductances to decrease the noise as much as possible. However, these high transconductances have to be linearized so that they can be associated together to obtain a highly linear Gm-C filter.

Different linearization techniques are proposed in the literature. They have been assessed in this chapter. Two of them have been used to design filters. These two filters are based on Gm-cells linearized by means of dynamic source degeneration and by multiple gated transistors. It comes out that the first filter presents a too limited linearity versus noise trade-off. The second filter exhibits a high dynamic range over a more than three octaves tuning range. However, it exhibits a high sensitivity to process and voltage variations.

Despite its interesting performances in terms of dynamic range and of power consumption, the gyrator appears to be the main source of degradation and of distortion of the signal within the Gm-C filter. Furthermore, this solution exhibits strong process and mismatch dependencies. The sensitivity and the lack of robustness of the MGTR technique lead us to take the decision not to tape out the filter as a circuit, but to carry on investigations on other high performance filtering solutions. That is why an operational amplifier based filter is analyzed in Chapter IV.

III.6 References

[III.1] Y. Sun, C. J. Jeong, I. Y. Lee, J. S. Lee, and S. G. Lee, "A 50-300-MHz low power and high linear active RF tracking filter for digital TV tuner ICs," presented at the Custom Integrated Circuits Conference (CICC), 2010 IEEE, 2010, pp. 1-4.

[III.2] A.M. Niknejad, "Oscillator Phase Noise", Integrated Circuits for Communications, University of California, Berkeley, 2009.

[III.3] Willy M. C. Sansen, *Analog Design Essentials*. Springer, 2006.

[III.4] B. Razavi, *RF Microelectronics*. Prentice-Hall, 1998.

[III.5] G. Hau, T.B. Nishimura, and N. Iwata, « A highly efficient linearized wide-band CDMA handset power amplifier based on predistortion under various bias conditions », *IEEE Transactions on Microwave Theory and Techniques*, Vol. 49,pp. 1194-1201, June 2001.

[III.6] S. Lou and H. Luong, "A Linearization Technique for RF Receiver Front-End Using Second-Order-Intermodulation Injection," *Solid-State Circuits, IEEE Journal of*, vol. 43, 2008, pp. 2404-2412.

[III.7] Y. Sun, J.-seon Lee, and S.-gug Lee, "On-chip Active RF Tracking Filter with 60dB 3rd-order Harmonic Rejection for Digital TV tuners." 2008.

[III.8] B. Gilbert, "The multi-tanh principle: a tutorial overview," *Solid-State Circuits, IEEE Journal of*, vol. 33, no. 1, pp. 2-17, 1998.

[III.9] K. Kimura, "The ultra-multi-tanh technique for bipolar linear transconductance amplifiers," *IEEE Transactions on Circuits and Systems I: Fundamental Theory and Applications*, vol. 44, no. 4, pp. 288-302, Apr. 1997.

[III.10] Tae Wook Kim and Bonkee Kim, "A 13-dB IIP3 improved low-power CMOS RF programmable gain amplifier using differential circuit transconductance linearization for various terrestrial mobile D-TV applications," *Solid-State Circuits, IEEE Journal of*, vol. 41, 2006, pp. 945-953

IV. Rauch Filtering

IV.1 Sallen-Key versus Rauch Filters

IV.1.a Towards an Operational Amplifier Based Filter

To circumvent the limitations of the Gm-C filters, operational amplifier based filters have been studied. Indeed it has been demonstrated that Gm-C filters are limited by strong degradation and distortions of the RF signal due to the gyrator. The idea behind using an OA based topology is to take advantage of both a high loop gain and a certain filtering of the signal at the input node V_A of the active component, due to the RC network. This is illustrated in Figure 138. The final purpose is to obtain a highly linear filter not compromising the noise.

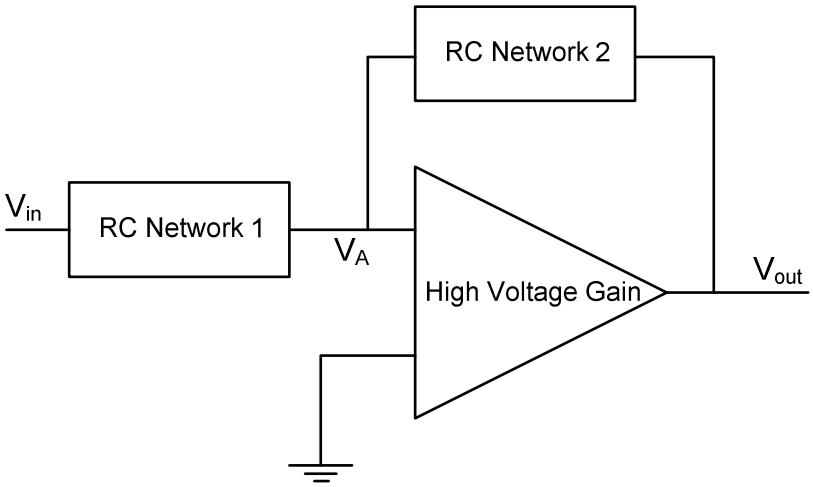

Figure 138. Principle of an OA based filter

Furthermore, to reduce the number of active and passive components in the circuit, it has been chosen to study a second order bandpass filter [IV.1]. As discussed in the introduction, a second order bandpass filter allows reaching the required specification on the RF filter stage.

Previous literature considers two main types of second order RC bandpass filters using a single wideband amplifier: ***Sallen-Key*** filters and ***Rauch*** filters. Rauch filters are also referred as *multiple feedback* structures [IV.2].

Following filters are studied with two capacitors set to a common value *C*, as shown in Figure 139, Figure 140 and Figure 142. This simplifies computations and shows interesting properties for a frequency tunable filter as it will be detailed later.

IV.1.b *Sallen-Key* Filters

The Sallen-Key second order bandpass filter is described in the literature [IV.2]. The schematic is depicted in Figure 139, where K is the voltage gain of the voltage amplifier.

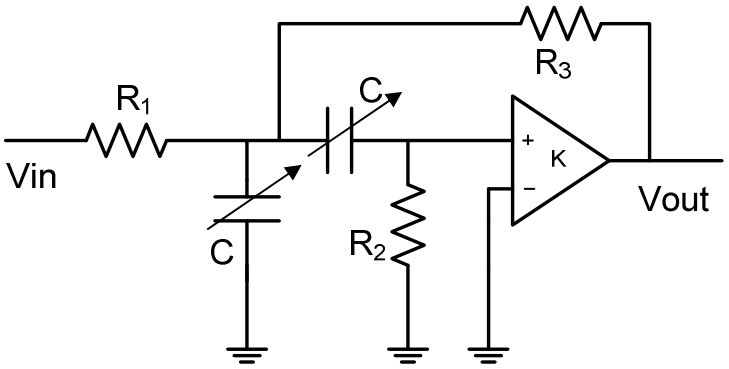

Figure 139. Sallen-Key bandpass filter schematic

The transfer function of this structure is given by:

$$H_{SK}(j\omega) = \frac{\dfrac{jC\omega KR_2}{R_1\left(\dfrac{1}{R_1}+\dfrac{1}{R_3}\right)}}{1+jC\omega\dfrac{1}{\dfrac{1}{R_2}\left(\dfrac{1}{R_1}+\dfrac{1}{R_3}\right)}\left(\dfrac{2}{R_2}+\dfrac{1-K}{R_3}+\dfrac{1}{R_1}\right)+\dfrac{(jC\omega)^2}{\dfrac{1}{R_3}\left(\dfrac{1}{R_1}+\dfrac{1}{R_2}\right)}}. \qquad \text{(IV.1)}$$

Thus, the resonant frequency is defined by

$$f_0 = \frac{1}{2\pi C}\sqrt{\frac{1}{R_3}\left(\frac{1}{R_1}+\frac{1}{R_2}\right)} \qquad \text{(IV.2)}$$

and the quality factor of this bandpass filter is:

$$Q = \frac{\sqrt{\dfrac{1}{R_3}\left(\dfrac{1}{R_1}+\dfrac{1}{R_2}\right)}}{\dfrac{1-K}{R_3}+\dfrac{1}{R_1}+\dfrac{2}{R_2}}. \qquad \text{(IV.3)}$$

Filter gain at the resonant frequency is given by:

$$Gain = \frac{K}{R_1\left(\dfrac{1-K}{R_3}+\dfrac{1}{R_1}+\dfrac{2}{R_2}\right)}. \qquad \text{(IV.4)}$$

Thus, an equation linking Q and *Gain* can be deduced:

$$Q = \frac{R_1}{K}\sqrt{\frac{1}{R_3}\left(\frac{1}{R_1}+\frac{1}{R_2}\right)}.Gain\,. \qquad \text{(IV.5)}$$

From the transfer function formula, a stability issue comes out. Indeed, the denominator should only have roots with negative real parts, so the $jC\omega$ term of this second order polynomial has to be negative as well. This leads to the condition:

$$K < \left(\frac{1}{R_1}+\frac{2}{R_2}\right)R_3 + 1. \qquad \text{(IV.6)}$$

If the voltage gain K of the amplifier does not fulfill this condition, the filter is unstable.

IV.1.c *Rauch* Filters

IV.1.c.i Negative feedback Rauch filter

In the literature, the "Rauch" filter is always described in a negative feedback configuration [IV.2], as depicted in Figure 140, where K is the voltage gain of the voltage amplifier.

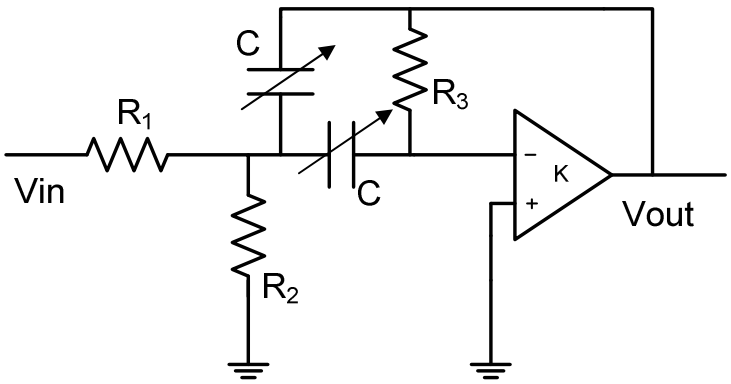

Figure 140. Negative feedback Rauch bandpass filter schematic

The transfer function of the filter can be computed, which gives:

$$H_{R-}(j\omega) = \frac{-\dfrac{jC\omega KR_3}{R_1(1+K)\left(\dfrac{1}{R_1}+\dfrac{1}{R_2}\right)}}{1+jC\omega\dfrac{1}{\dfrac{1+K}{R_3}\left(\dfrac{1}{R_1}+\dfrac{1}{R_2}\right)}\left(2\dfrac{1+K}{R_3}+\dfrac{1}{R_1}+\dfrac{1}{R_2}\right)+\dfrac{(jC\omega)^2}{\dfrac{1}{R_3}\left(\dfrac{1}{R_1}+\dfrac{1}{R_2}\right)}} \qquad \text{(IV.7)}$$

The quality factor of such a circuit is given by the formula:

$$Q = \frac{(1+K)\sqrt{\frac{1}{R_3}\left(\frac{1}{R_1}+\frac{1}{R_2}\right)}}{2\frac{1+K}{R_3}+\frac{1}{R_1}+\frac{1}{R_2}}. \qquad \text{(IV.8)}$$

Major drawback of this structure is that it requires a very high gain K to reach useable Q-factors. This limits the use of this topology at RF frequencies. Figure 141 highlights, for a certain combination of passive components (R_1=50Ω, R_2=10Ω and R_3=500Ω), that gain K should be higher than 100, meaning a 40dB voltage gain, to obtain a quality factor of 2.5 or more. Such a high gain-bandwidth product (GBW) amplifier becomes very difficult to design. ***Due to a very poor selectivity versus gain trade-off, this structure has not been studied further***.

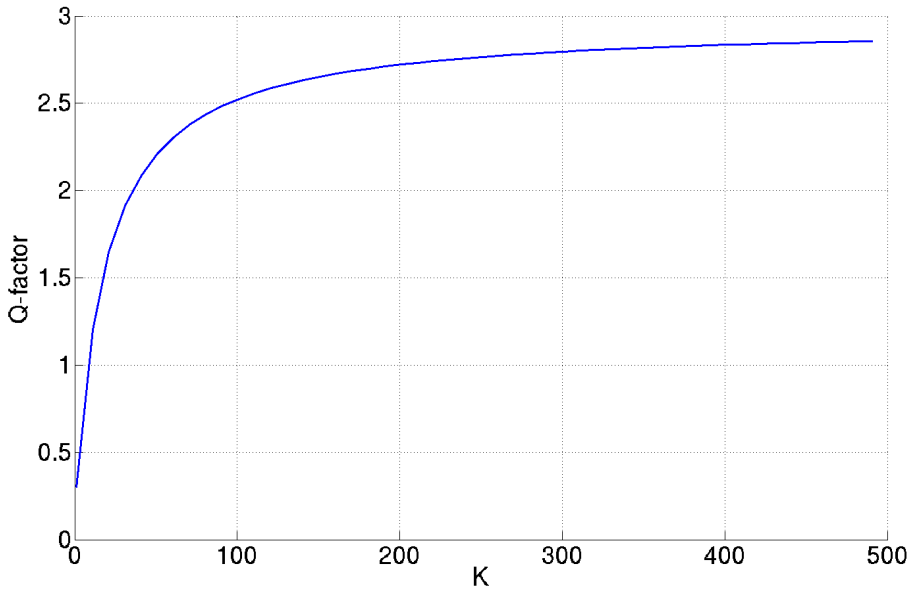

Figure 141. Q-factor of the negative feedback Rauch filter versus gain K

IV.1.c.ii Proposed positive feedback Rauch filter

The positive feedback Rauch filter is proposed, whose schematic is depicted in Figure 142, where K is the voltage gain of the voltage amplifier. It shows different trade-offs in terms of selectivity versus K and passive components values than its negative feedback counterpart.

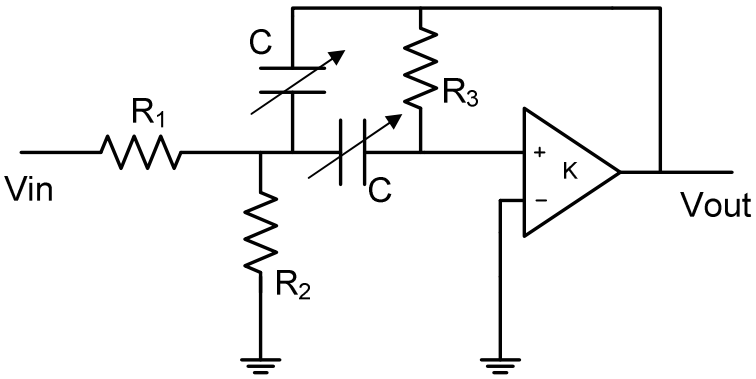

Figure 142. Positive feedback Rauch bandpass filter schematic

Hence, the filter transfer function $H_R(j\omega)$ can be computed as:

$$H_{R+}(j\omega)=\frac{\dfrac{jC\omega|K|R_3}{R_1(1-|K|)\left(\dfrac{1}{R_1}+\dfrac{1}{R_2}\right)}}{1+jC\omega\dfrac{1}{\dfrac{1-|K|}{R_3}\left(\dfrac{1}{R_1}+\dfrac{1}{R_2}\right)}\left(2\dfrac{1-|K|}{R_3}+\dfrac{1}{R_1}+\dfrac{1}{R_2}\right)+\dfrac{(jC\omega)^2}{\dfrac{1}{R_3}\left(\dfrac{1}{R_1}+\dfrac{1}{R_2}\right)}} \quad \text{(IV.9)}$$

Such a filter resonates at a central frequency determined by the passive components of the circuit

$$f_0=\frac{1}{2\pi C}\sqrt{\frac{1}{R_3}\left(\frac{1}{R_1}+\frac{1}{R_2}\right)}. \quad \text{(IV.10)}$$

The resonant frequency is similar to the Sallen-Key topology. However, in the present case, the quality factor is:

$$Q=\frac{(1-|K|)\sqrt{\dfrac{1}{R_3}\left(\dfrac{1}{R_1}+\dfrac{1}{R_2}\right)}}{2\dfrac{1-|K|}{R_3}+\dfrac{1}{R_1}+\dfrac{1}{R_2}}. \quad \text{(IV.11)}$$

The filter gain at the central frequency is given by:

$$Gain = \frac{|K|}{R_1\left(2\frac{1-|K|}{R_3}+\frac{1}{R_1}+\frac{1}{R_2}\right)} \quad \text{(IV.12)}$$

Hence, a relation between Q and *Gain* can be established as follows:

$$Q = \frac{R_1(1-|K|)}{|K|}\sqrt{\frac{1}{R_3}\left(\frac{1}{R_1}+\frac{1}{R_2}\right)}.Gain \quad \text{(IV.13)}$$

As the Sallen-Key filter, the positive feedback Rauch filter transfer function indicates a stability issue. Nevertheless, the condition is more difficult to fulfil since it requires a minimal value for K in order to keep a stable structure. Indeed, one gets:

$$K > \frac{R_3}{2}\left(\frac{1}{R_1}+\frac{1}{R_2}\right)-1 \quad \text{(IV.14)}$$

IV.1.d Comparison of the *Sallen-Key* and *Rauch* filters

Table 17 summarizes the expressions of the voltage gain and of the quality factor of the previously studied filters.

Table 17. Sum-up of the various filters parameters

Structure	Gain	Q-factor	Stability
Sallen Key	$Gain = \frac{K}{R_1\left(\frac{1-K}{R_3}+\frac{1}{R_1}+\frac{2}{R_2}\right)}$	$Q = \frac{R_1}{K}\sqrt{\frac{1}{R_3}\left(\frac{1}{R_1}+\frac{1}{R_2}\right)}.Gain$	$K < \left(\frac{1}{R_1}+\frac{2}{R_2}\right)R_3 + 1$
Negative feedback Rauch	Not computed Too low selectivity to be used at RF frequencies	$Q = \frac{(1+K)\sqrt{\frac{1}{R_3}\left(\frac{1}{R_1}+\frac{1}{R_2}\right)}}{2\frac{1+K}{R_3}+\frac{1}{R_1}+\frac{1}{R_2}}$	Always stable
Positive feedback Rauch	$Gain = \frac{\|K\|}{R_1\left(2\frac{1-\|K\|}{R_3}+\frac{1}{R_1}+\frac{1}{R_2}\right)}$	$Q = \frac{R_1(1-\|K\|)}{\|K\|}\sqrt{\frac{1}{R_3}\left(\frac{1}{R_1}+\frac{1}{R_2}\right)}.Gain$	$K > \frac{R_3}{2}\left(\frac{1}{R_1}+\frac{1}{R_2}\right)-1$

As already highlighted, the negative feedback "Rauch" is not attractive for our purposes due to its poor selectivity. In the following, only Sallen-Key and positive feedback Rauch will be compared. Moreover, for both Rauch and Sallen-Key topologies, it has been noticed that a quality factor of a few units is obtained for K values so that K<10. This is very attractive since it means using amplifiers with implementable GBW.

In the following, Rauch filter actually refers to the positive feedback structure.

For both Rauch and Sallen-Key filters, it is worth noticing that Q is independent from *C*. Hence, while K remains constant, Q also stays constant. This enables to get a constant Q-factor frequency sweep, that is to say a constant harmonics rejection.

As may be seen in Equation (IV.10), for RC filters ***the filter central frequency f_0 is proportional to 1/C*** while a passive LC circuit, made of an inductor and a variable capacitance, resonates at a central frequency proportional to $1/\sqrt{C}$. This is an interesting property for a frequency-tunable filter since the frequency tuning range is then enhanced:

$$\frac{f_{\max}}{f_{\min}} \propto \frac{C_{\max}}{C_{\min}} \tag{IV.15}$$

For these two structures, it is also noticeable to say that ***gain is required to realize the selectivity***. Now, it has to be kept in mind that the RF filter is located after a high gain LNA. Thus, considering Friis formula, the filter amplification has to be as limited as possible to take advantage of the low NF of the LNA, since the NF of the receiver is required to be very low (about 4dB nowadays). This is also explained in [IV.3]. The structure offering the best selectivity versus gain trade-off is looked for.

From formulas in Table 17, trials have been performed to find this best trade-off. Usual values used for the Sallen-Key filter are $R_1=R_3=2R_2$. Thus,

$$Gain_{SK} = \frac{K}{3-K} \tag{IV.16}$$

and

$$Q_{SK} = \frac{1}{3-K} \tag{IV.17}$$

Combining both equations leads to:

$$Q_{SK} = \frac{1+Gain_{SK}}{3} \tag{IV.18}$$

As far as the Rauch filter is concerned, it is usually used when $R_1=2R_2$ and $R_3=3R_1$. Hence, one gets:

$$Gain_R = \frac{3K}{11-2K} \tag{IV.19}$$

So,

$$K = \frac{11Gain_R}{3+2Gain_R} \tag{IV.20}$$

Thus, one can replace K in the following last equation:

$$Q_R = \frac{3(1-K)}{11-2K} \tag{IV.21}$$

Q_{SK} and Q_R versus the filter gain ($Gain_{SK}$ and $Gain_R$) are plotted together in Figure 143. It can be noticed that Rauch filters are more selective for a same filter amplification.

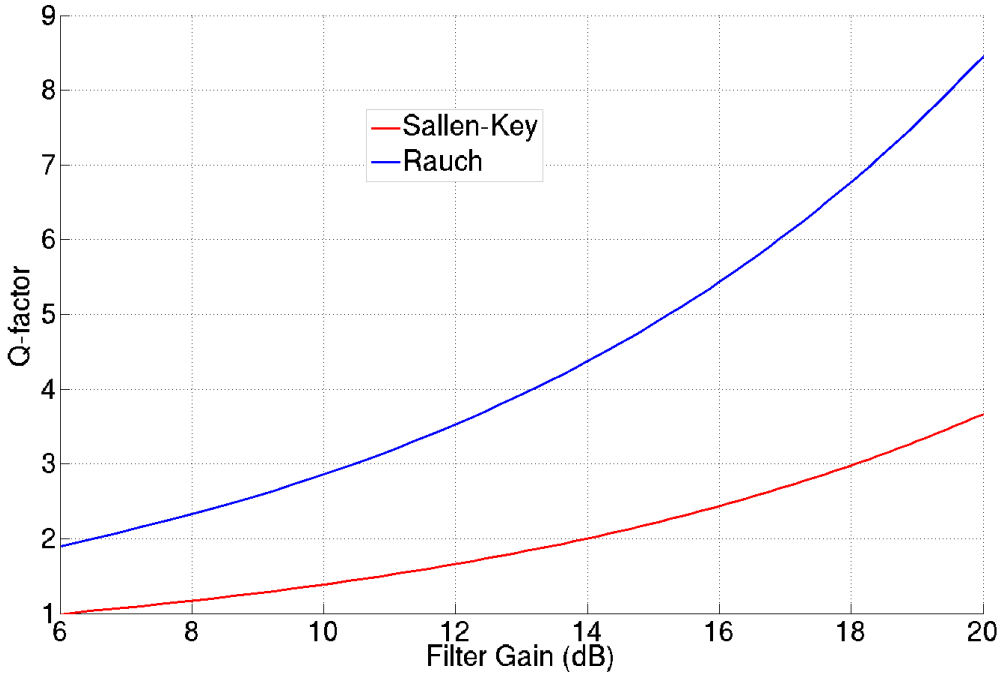

Figure 143. Q-factor versus filter gain for Rauch and Sallen-Key filters

Furthermore, a particular drawback of the Sallen-Key bandpass filter has to be pointed out. Indeed, a very high sensitivity of the Q-factor to component variations may be observed, making this structure unusable under industrial conditions. Table 18 illustrates that a 10% variation on a resistor involves more than 100% variation of the Q-factor. This is also reported in [IV.4]. The Rauch filter is less sensitive to passive component variation as it may be observed in Table 19.

Table 18. Sensitivity to passive components of the Sallen-Key filter

R_1 (Ω)	R_2 (Ω)	*R_3 (Ω)*	C (pF)	K	f_0 (MHz)	*Q-factor*
40	80	*40*	50	2,9	79,6	*12,3*
40	80	*45*	50	2,9	77,3	*3,7*
40	80	*50*	50	2,9	75,5	*2,3*

Table 19. Sensitivity to passive components of the Rauch filter

R_1 (Ω)	R_2 (Ω)	*R_3 (Ω)*	C (pF)	K	f_0 (MHz)	*Q-factor*
50	25	*135*	50	10	67,1	*2,6*
50	25	*150*	50	10	63,7	*3,0*
50	25	*165*	50	10	60,7	*3,5*

The ***high sensitivity to passive components spread limits the use of the Sallen-Key*** bandpass filter in an industrial environment. The Rauch structure allows a decrease in the sensitivity to passive components, as it will detail later on.

Besides, both ***Rauch and Sallen-Key filters present a stability issue***. The Sallen-Key stability condition is much more attractive since it mentions that K should be lower than a certain value K_{stab_SK}. The Rauch filter stability condition is $K>K_{stab\_R}$. Hence, the drop of the gain K with frequency prevents from using this filter, unless a solution is found to circumvent this issue.

Table 20 summarizes the different advantages and drawbacks of each bandpass filter.

Table 20. Comparison Sallen-Key versus Rauch filters

Structure	Advantages	Drawbacks
Sallen Key	1/C frequency tuning K<10	Gain vs Q trade-off Sensibility to passives Unstable if $K>K_{stab\_SK}$
Rauch	1/C frequency tuning Gain vs Q trade-off K<10	Unstable if $K<K_{stab}$

In the following, an original stabilization technique of the Rauch filter is introduced, which allows using the previously described properties of the filter. Indeed, this method consists in replacing the voltage gain K by a non-inverting amplifier. At the central frequency of the filter, both structures are equivalent. However, this new configuration changes the behaviour of the gain at high frequency and fulfils the stability condition.

Next section of this chapter describes optimizations and design of the structure. This study is carried out assuming that the filter is stable. Stabilization of the filter is described in the same section, after the dimensioning of the filter.

IV.2 Dimensioning the Rauch Filter

IV.2.a Choice of the Components Values

IV.2.a.i Selectivity

From Figure 143, it may be noticed that a ***quality factor of 3 can be reached for a 10dB gain filter***. It allows harmonic frequencies to be rejected by nearly 20dB (see Figure 144) and it enables to take advantage of some rejection of adjacent channels on both sides of the filter central frequency, especially at the low-end of the VHF band. Indeed, a 15dB rejection of the N+6 is obtained at 40MHz. However, such selectivity does not allow reaching the UHF range since it requires larger Q for a same adjacent selectivity.

As explained, a more selective filter would lead to higher filter amplification. To take advantage of the Friis formula, it has been chosen to limit filter gain to 10dB. Relaxing the constraints on the filter amplification by increasing the gain on the RF filter would involve more stringent constraints on the LNA noise versus gain trade-off.

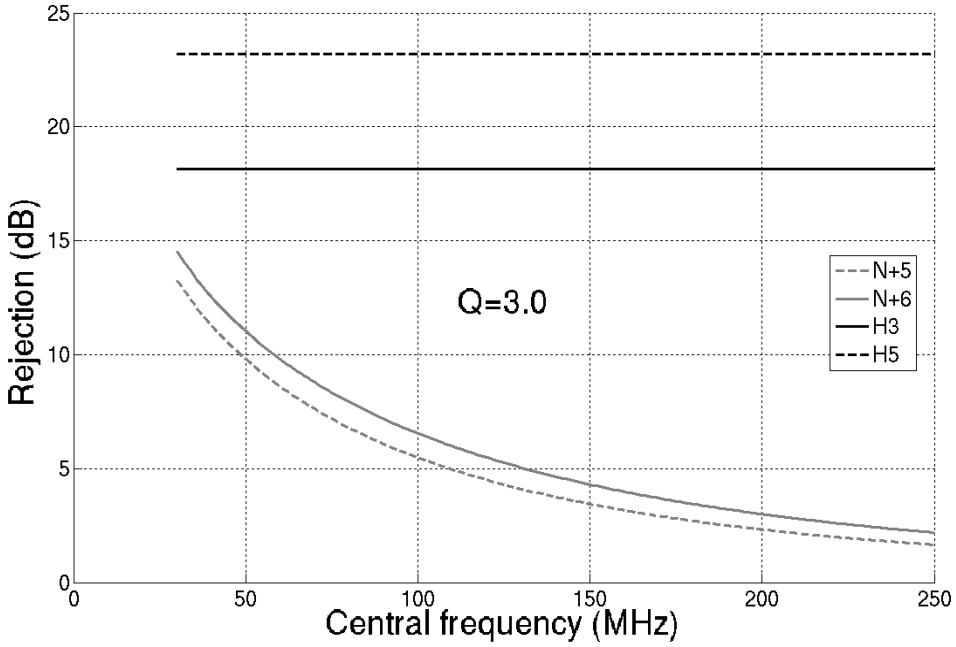

Figure 144. Harmonics and adjacent channels rejections for Q=3

IV.2.a.ii Noise Optimization

To keep noise as low as possible, all impedances values have been decreased. Indeed, since a Q-factor of 3 for a 10dB gain have been set, there is very little margin on the choice of K. The combination $R_1=2R_2$ and $R_3=3R_1$, which is often used in the literature, is the best one. A change in this combination results in an increase of the overall noise of the filter.

However, since the central frequency is proportional to $1/RC$, the use of large capacitances is required to reach the low-end of the VHF band located at 45MHz. The circuit being fully-differential, it requires a large on-chip area to realize all capacitors. Values have been summarized in Table 21.

Furthermore, it should also be taken care of the input impedance of the filter, called Z_{in} in the following. A limit of 15-20Ω has been set, which is already very low and will need a high driving capability from the LNA.

IV.2.a.iii Chosen Trade-off

Table 21 summarizes the dimensioning of the Rauch filter components.

Table 21. Passive Components Values

Component	R1	R2	R3	K	C
Value	50 Ω	25 Ω	150 Ω	10	from 12 to 84pF

IV.2.a.iv Capacitors Implementation

To enable frequency tuning, capacitors C are implemented by means of capacitors banks. MOS transistors used for the switches are supplied with Vdd_{switch}=2.8V

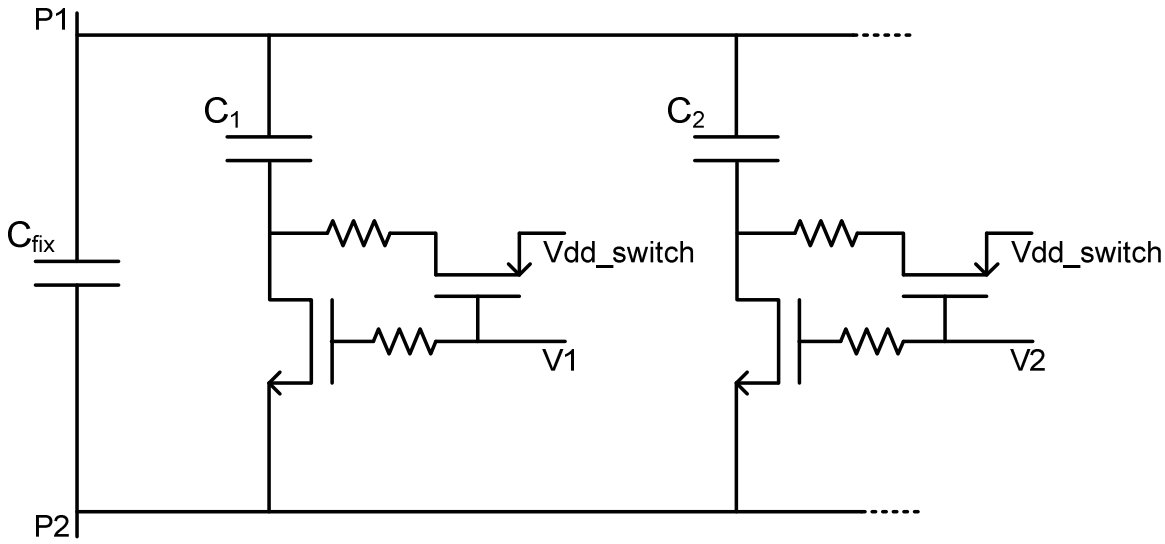

Figure 145. Capacitors banks design

For all capacitors banks, P1 is connected to R_1 and R_2. This node is set to VDD/2=1.65V. P_2 is either connected to the output, which DC voltage is close to 1.3V, or to the inverting input of the OA, stuck at GND.

As for the Gm-C filtering, this capacitor bank is composed of a main capacitor, which value is 12pF. Then, switch-controlled capacitors may be added in parallel to this main capacitor. There are 8 switchable capacitors, starting from 280fF for the smallest one, up to 36pF for the largest one. From one bit to the next one, the capacitance is doubled as shown in Table 22. To keep a constant capacitance Q-factor, MOS switches have sizes which also double. The smallest one is 5µm/0.25µm.

Table 22. Description of the capacitor bank

Bit number	0	1	2	3	4	5	6	7
Capacitance (pF)	0.28	0.56	1.12	2.24	4.48	8.96	17.92	35.84

These 8 control bits together create a control byte code, called *Dtune*, between 0 and 255. Figure 146 shows the evolution of the central frequency according to Dtune.

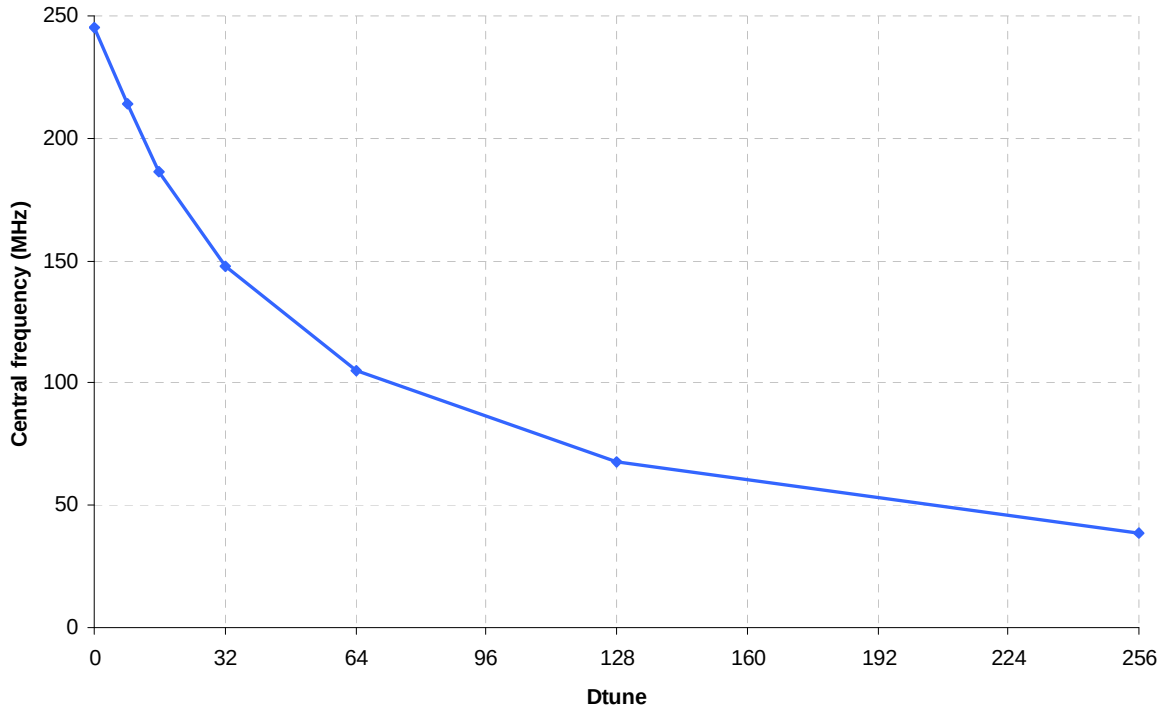

Figure 146. Central frequency of the filter versus Dtune

IV.2.b Innovative Implementation of Gain K

IV.2.b.i Open-loop Gain and Stability

As explained, the positive feedback Rauch filter is unstable for small amplifier gain K values $0<K<K_{stab}$. At high frequencies, due to a finite gain-bandwidth product, the drop of the gain K leads to the system instability, as may be seen in Figure 147. Hence, no selectivity can be achieved.

The use of a non-inverting amplifier, as described in Figure 148, prevents K from entering this unstable area (as seen in Figure 147).

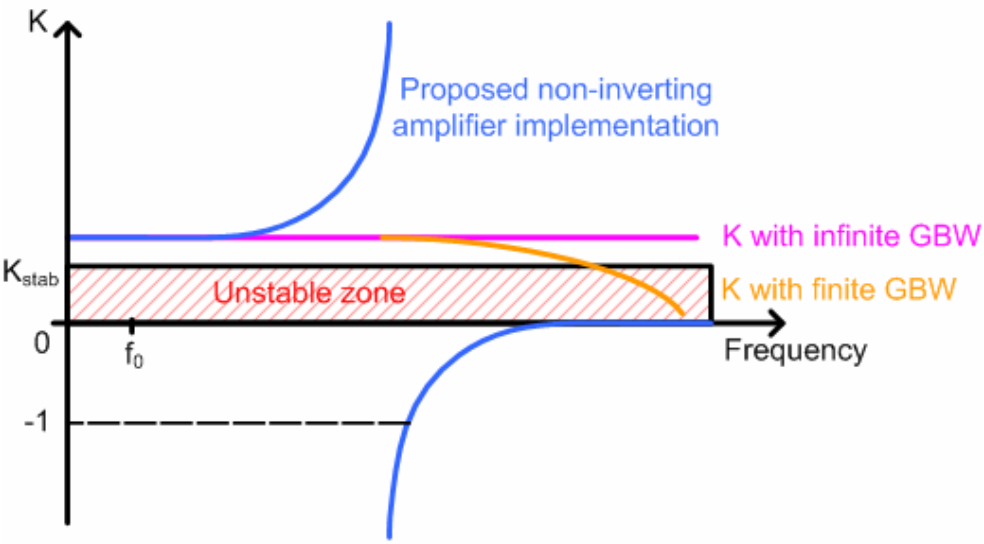

Figure 147. Frequency evolution of the open-loop gain K

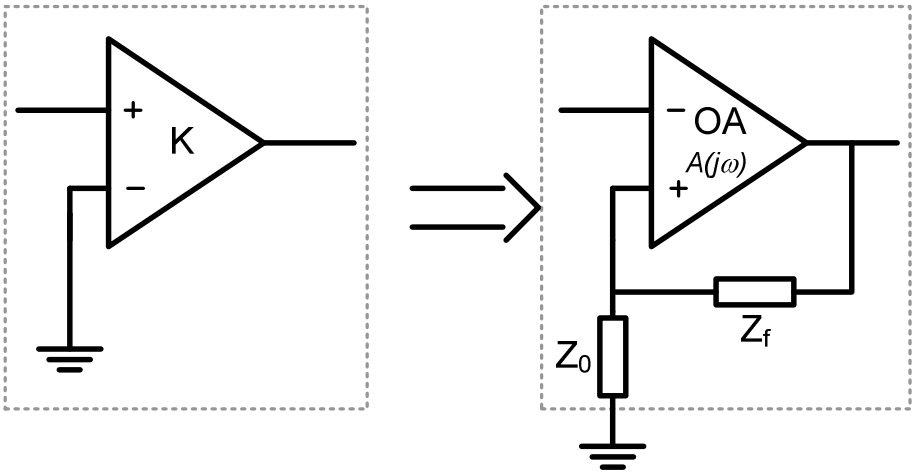

Figure 148. Proposed non-inverting amplifier implementation of gain K

The expression of K,

$$K(j\omega)=\frac{A(j\omega)\left(Z_0+Z_f\right)}{A(j\omega)Z_0-\left(Z_0+Z_f\right)}, \qquad \text{(IV.22)}$$

shows that the sign of K changes. However it happens when K becomes very high, *i.e.* when the filter transfer function (see Equation (IV.9)) becomes independent from K.

Nevertheless, gain K can take the value -1. At this point, the transfer function is:

$$H(K=-1)=\frac{R_2}{R_1+R_2}, \qquad \text{(IV.23)}$$

which leads to a filter gain rise that may be observed on Figure 149. In these condition, peaking reaches -9.5dB. This rise can be rejected further in frequency increasing the OA gain-bandwidth product, as it may be observed in Figure 150.

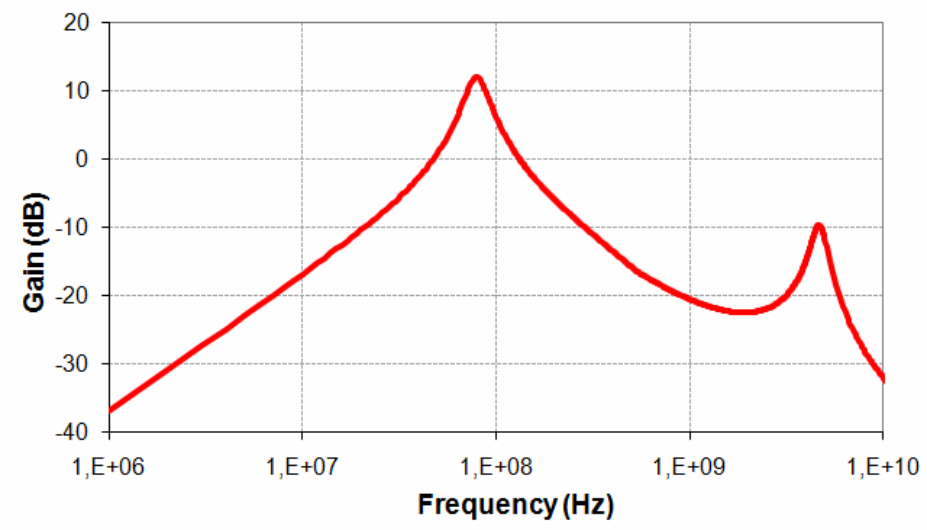

Figure 149. Filter peaking gain

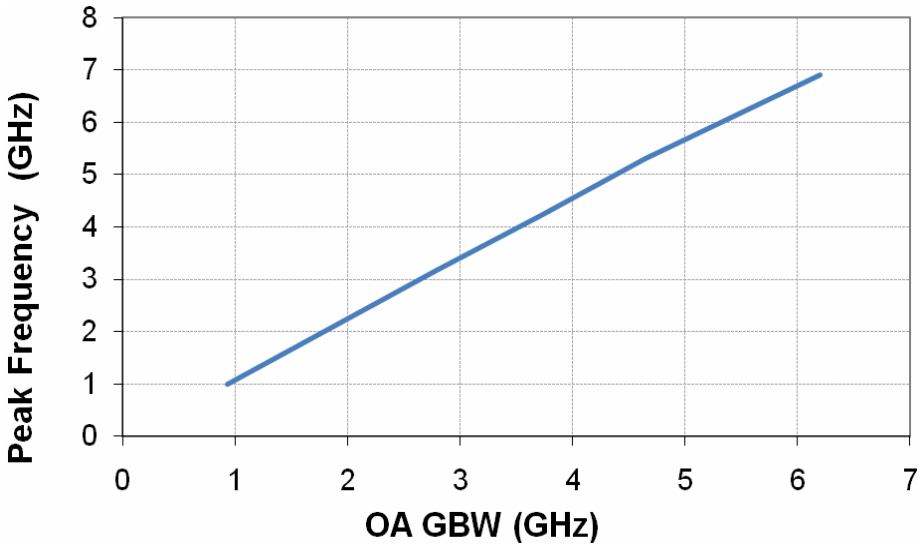

Figure 150. Peak frequency versus OA GBW

Z_0 and Z_f have to be high enough so that the output current of the OA flows through the RC network of the Rauch filter and not in the non-inverting feedback. Indeed, the

resulting gain K, constituted of the OA, Z_0 and Z_f, have to remain stable all over the frequency tuning range of the filter.

Given the expression of K,

$$K(j\omega) = \frac{A(j\omega)(Z_0 + Z_f)}{A(j\omega)Z_0 - (Z_0 + Z_f)} = \frac{1}{\frac{Z_0}{Z_0 + Z_f} - \frac{1}{A(j\omega)}}, \quad \text{(IV.24)}$$

it also appears that $A(j\omega)$ have to be as high as possible to ensure a stable value of K.

Besides, the use of capacitances instead of resistors to implement Z_0 and Z_f enables to increase the impedances and to optimize noise since they are lossless elements. As it may be observed in Table 23, NF of the filter is lowered by more than 1dB compared to equivalent resistor values. Capacitances are computed using for instance:

$$C_f = \frac{1}{2\pi f Z_f}, \quad \text{(IV.25)}$$

knowing that simulations are run at f=100MHz.

Table 23. Noise Figure of the Filter according to the nature of Z_0 and Z_f

Nature of Z_0 and Z_f	NF at 100MHz (dB)	Component Values
Resistors	15.8	R_0=150Ω, R_f=800Ω
Capacitors	14.7	C_0=10.5pF, C_f=2pF

IV.2.b.ii Stability Margins

Stability has been checked by an open-loop study carried out with *Middlebrook*'s method [IV.5]. It consists in opening the two loops by a switch which is ON only to set DC biasing in the circuit, as depicted in Figure 151.

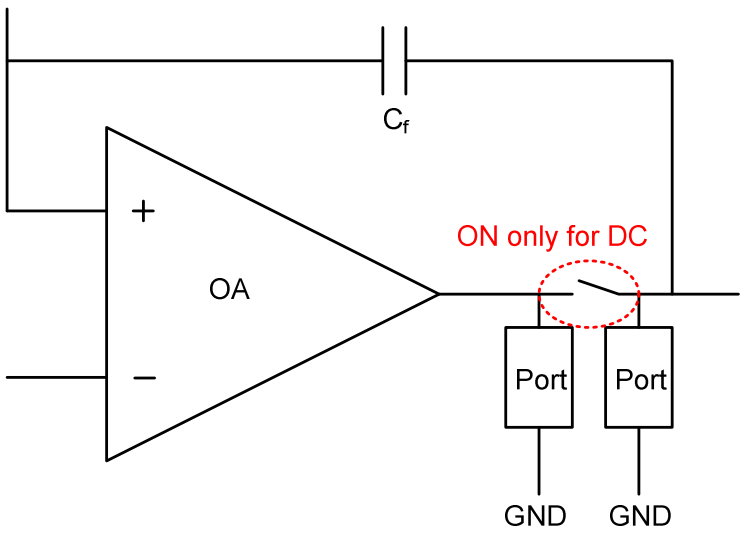

Figure 151. Open-loop Study Test-Bench

Loop gain *LG* and phase *LP* can be computed with the following formulas [IV.6]:

$$LG = 20\log\left(\frac{S_{21}-S_{12}}{1-\left(S_{11}.S_{22}-S_{21}.S_{12}\right)-2.S_{12}}\right) \quad \text{(IV.26)}$$

and

$$LP = phase\left(\frac{S_{21}-S_{12}}{1-\left(S_{11}.S_{22}-S_{21}.S_{12}\right)-2.S_{12}}\right). \quad \text{(IV.27)}$$

In the following, gain and phase margins (respectively GM and PM) are then deduced from these two expressions [IV.7] since:

$$GM = \left|0dB - LG_{LP=-180°}\right| \quad \text{(IV.28)}$$

and

$$PM = \left|-180 + LP_{LG=0dB}\right|. \quad \text{(IV.29)}$$

To ensure the stability of the system, an open-loop study has been carried out, taking into account parasitics effects. Large margins have been taken in nominal case, so that stability margins stay acceptable in worst cases (45MHz, -20°C, 3V supply and process dispersion). These margins, specified in Table 24, are crucial to ensure a robust industrialization.

Table 24. Stability margins specifications

Filter Specifications	Nominal case	Worst case	Unit
PM	50	40	**deg**
GM	15	10	**dB**

IV.2.b.iii Operational Amplifier Specifications

Table 25 summarizes the specifications set on the OA design. As said, GBW has to be as high as possible to ensure that the transfer function second peaking takes place at very high frequency. A specification of 4GHz has been set.

Furthermore, an OA voltage gain higher than 30dB is required so that gain K remains stable all over the frequency tuning range, as it has been observed previously.

The output impedance Z_{out} is very important as well since it degrades the filter quality factor when non zero. The specification on this parameter has been set to 2.5Ω.

Table 25. Sum-up of the OA specifications

OA Specifications	Value	Unit
Gain at operating frequency	>30	**dB**
Z_{out}	2.5	**Ω**
GBW	4	**GHz**

IV.3 Choice of the Technology and Design of the Rauch Filter

IV.3.a Operational Amplifier Design in 65nm CMOS

IV.3.a.i Possible OA Designs and Performances

To design the specified operational amplifier using a 65nm CMOS technology, a two stage topology has been chosen. It consists in a differential pair (T_1-T_2) with an active load (T_3-T_4) to create high gain, and an output follower (T_5) to provide low output impedance, as illustrated in Figure 152.

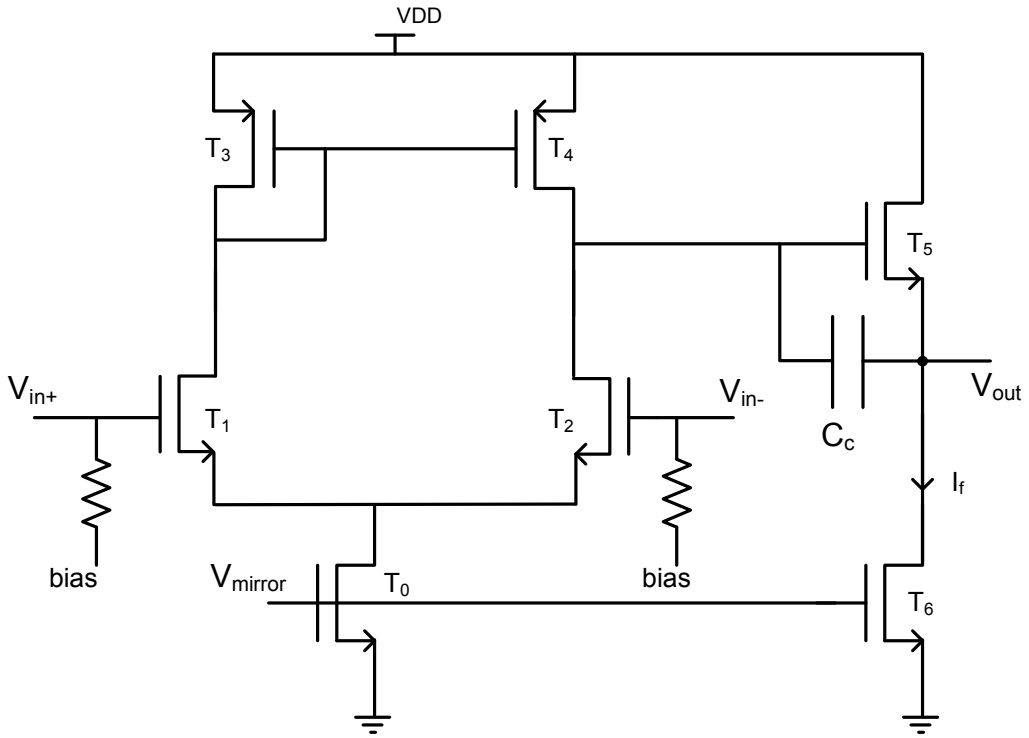

Figure 152. Schematic of the OA in CMOS

The use of 5mA in the differential pair with 250µm/0.28µm T_1 and T_2 gives g_m=22.5mS. This poor transconductance leads to a limited OA voltage gain of 15dB as depicted in Figure 153. Cascode topologies allow increasing the voltage gain but not reaching the specifications, as illustrated in Figure 153.

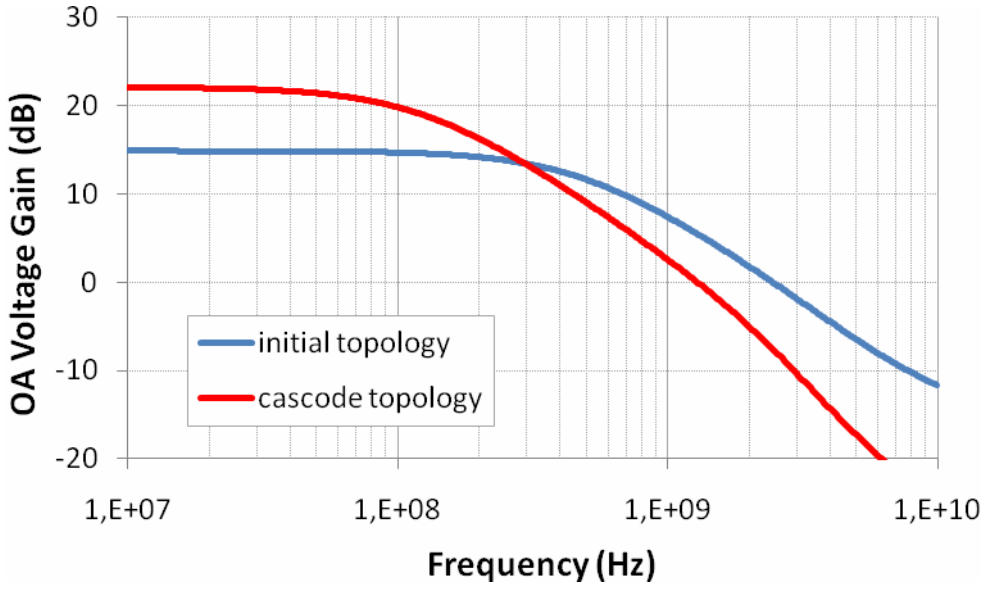

Figure 153. OA voltage gain versus frequency in CMOS

IV.3.a.ii Impact on Filter Performances

Table 26 summarizes the performances of the Rauch filter designed in 65nm CMOS, using the initial topology of the OA design.

Table 26. 65nm CMOS Rauch Filter Performances

	Rauch Filter	**Units**
f_0 Tuning Range	45 – 240	MHz
Q-factor	3	-
Filter Gain at f_0	10	dB
NF	17.5	dB
In-band IIP3	3 to 2	dBm
Supply	2.5	V
Consumption	117	mW
Technology	65nm CMOS	-

This table underlines that the performances of such a filter are strongly limited by the poor OA gain.

IV.3.a.iii Interests of a BiCMOS Technology

A BiCMOS technology is able to offer a higher transconductance in the differential pair stage for a same current, as well as a high voltage gain, due to a higher g_m/I than in CMOS technologies. Hence, it may be possible to obtain the required 30dB voltage gain using a simple OA topology.

Another interest in using NXP BiCMOS technology relies in the possibility to use MIM (Metal-Insulator-Metal) capacitors. These capacitors, which use metal levels 5 and 6 separated by a high-κ material, exhibit several advantages such as a high Q-factor and a good linearity. This is very interesting to obtain high quality capacitors banks which do not degrade or limit the linearity of the filter. Indeed, the 65nm TSMC CMOS technology available at NXP only allows the use of MOS capacitors characterized by a very high density of integration but also a higher sensitivity to bias and process variations.

IV.3.b Operational Amplifier Design in 0.25µm BiCMOS

IV.3.b.i Initial Design

OA design in BiCMOS is also based on a two stages topology, as depicted in Figure 154. As said, a high gain-bandwidth product is required, as well as a high linearity level. Current in the differential pair is set to 5mA. For the initial OA design, the follower is built by means of a single transistor.

It is worth adding that for decoupling, only one C_{dc} capacitor connected to V_{in-} is required since C_f, located in the feedback, also acts as a decoupling capacitor for V_{in+}.

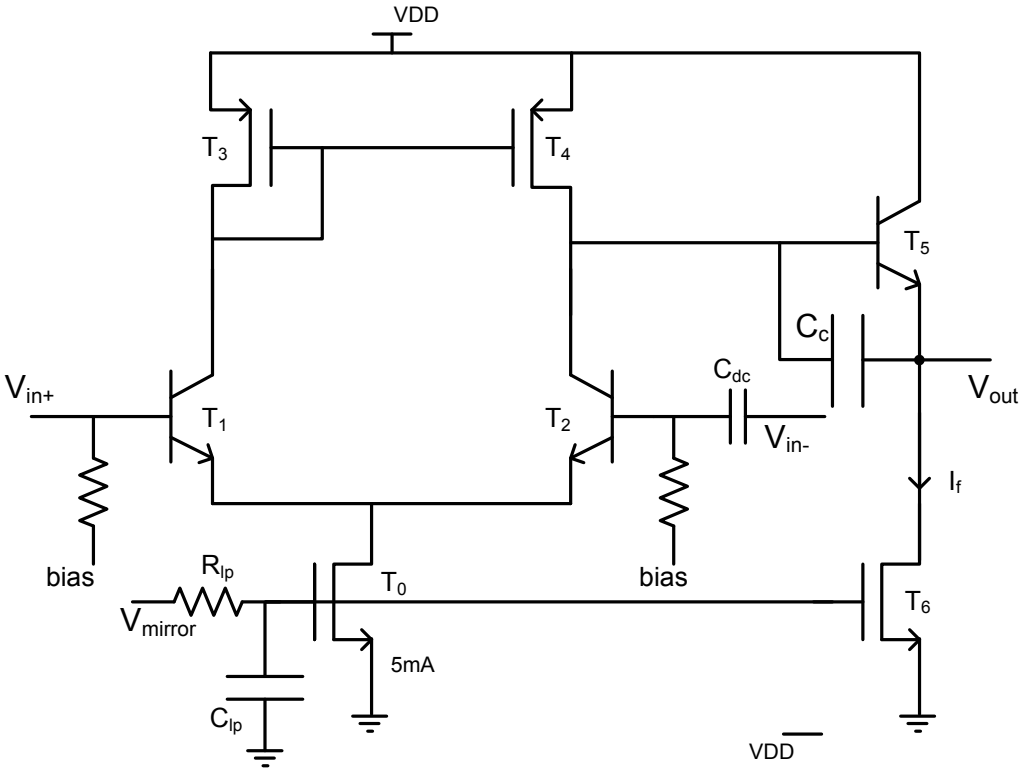

Figure 154. Initial schematic of the OA in BiCMOS

Filtering in the mirror, by means of an RC low-pass filter, has also been performed to prevent bandgap noise amplification. Components values are C_{lp}=4pF and R_{lp}=30kΩ so that f_c=1.3MHz.

The output follower is required to be very linear and to present a very low output resistance, to keep a good filter Q-factor. Indeed, when the output resistance increases, the quality factor of the filter decreases. That is why power consumption is needed.

Figure 155 shows the OIP3 of the filter versus OA follower current at 40MHz with a Q-factor of 3. This study has been performed using an output follower being a single bipolar transistor in common-collector configuration with a MOS current source. This graph demonstrates that lower current consumption through the follower directly results in lower linearity. Since the Rauch filter takes advantage of a high linearity level, it has been chosen a 12mA current in this stage. Note that Figure 155 was plotted with a differential pair fed by 3mA, and not 5mA as in the final schematic.

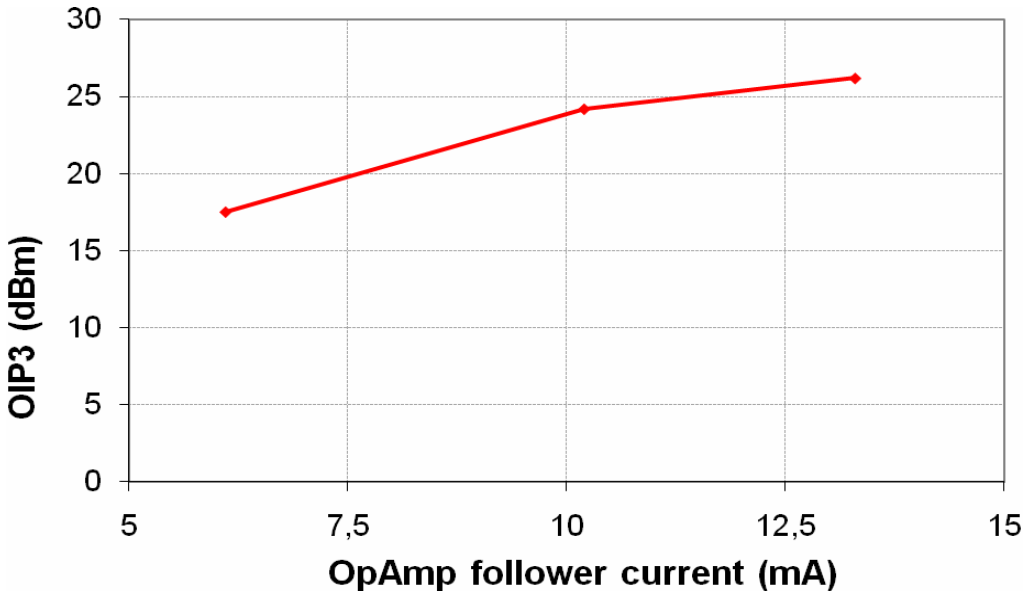

Figure 155. Linearity of the Filter versus follower current I_f

IV.3.b.ii Analysis of the Follower Stage

To enhance linearity, a feedback loop has been added to the single transistor follower, as depicted in Figure 156.

As detailed in APPENDIX D, this feedback loop increases the small signal current flowing through the load R_L by a factor (β_7+1). This allows reducing the distortions of the emitter-follower, enhancing the linearity of this stage.

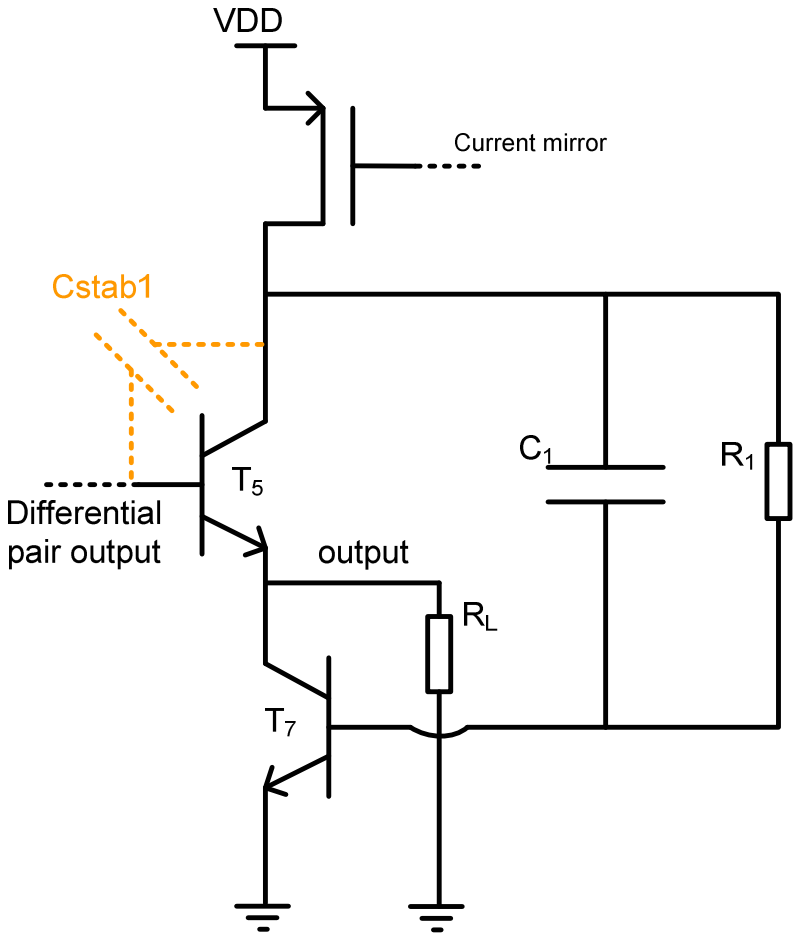

Figure 156. Feedback loop on the follower to increase linearity

Figure 157 shows that linearity is enhanced by 3 to 4dB when implementing the feedback loop on the follower.

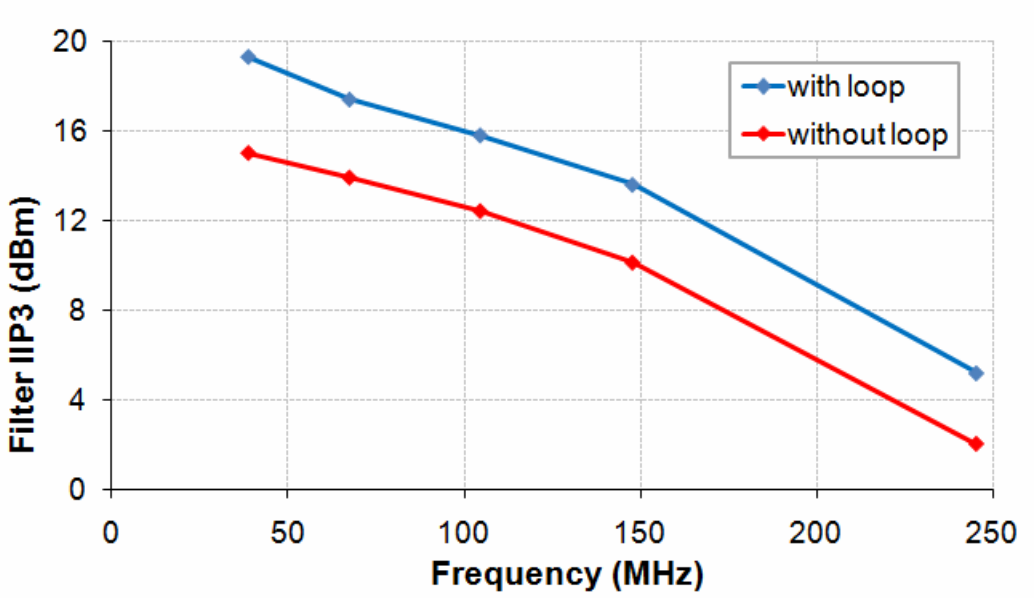

Figure 157. Enhancement of the linearity of the filter by a feedback loop on the follower stage

However, this feedback makes the filter become unstable. Indeed, the loop introduces a new pole in system transfer function. Thus, a -90° phase shift appears in closed loop operation, making the phase going below the critical -180° phase and the phase margin being negative. To ensure stability, a zero is introduced by means of capacitor C_{stab1}, which is put in parallel of the collector-base junction.

Figure 158 shows the results of a PZ analysis. It represents poles and zeros in the complex plane. This is a parametric analysis with C_{stab1} as parameter. When C_{stab1} is small, the real part of a pole is positive proving that the circuit is unstable. When Cs_{tab1} increases, the real part of the pole becomes negative, reaching the area where the circuit is stable.

Hence, there is a minimal value for C_{stab1} so that the circuit becomes stable, and the higher C_{stab1}, the higher the stability margins. However, C_{stab1} decreases the operational amplifier gain at high frequencies. As explained, a lower amplifier gain directly means lower linearity, thus showing a trade-off between stability versus linearity.

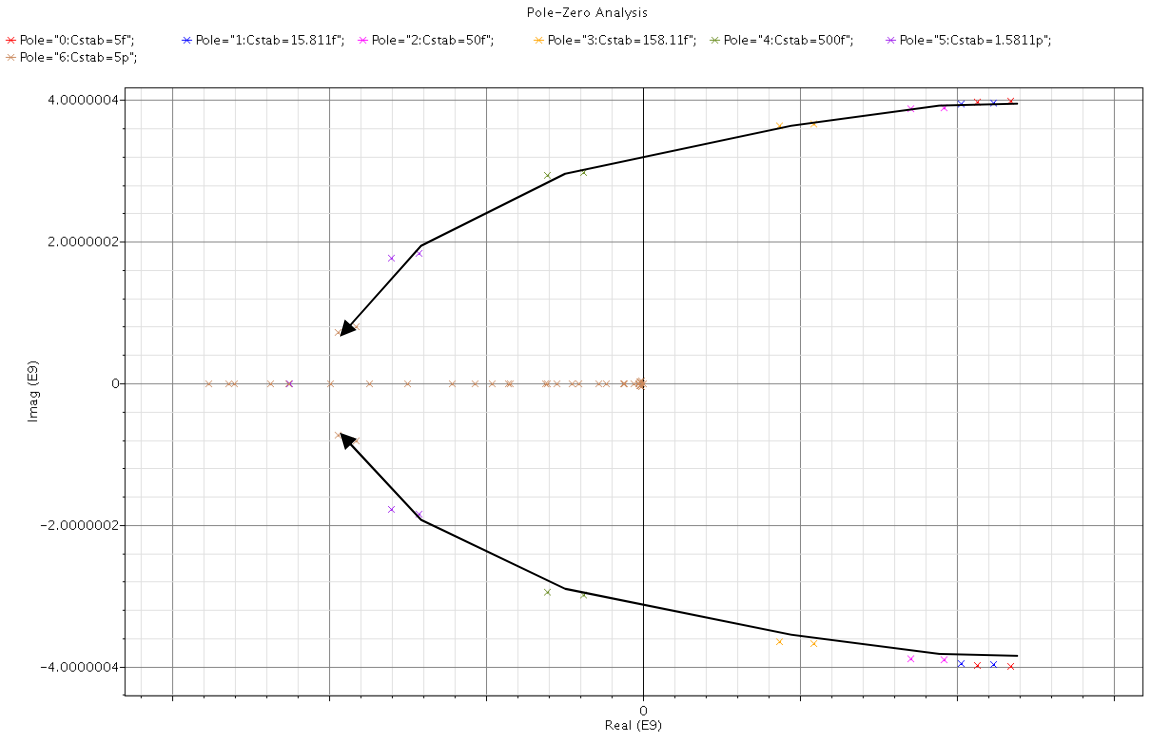

Figure 158. Location of the poles and zeros of the Rauch filter transfer function when C_{stab1} varies

IV.3.b.iii Enhancement of the Stability Margins

From the schematic simulations of the stability margins, it appears that phase and gain margins are below the specifications. That is why a second capacitor C_{stab2} has been added to increase these phase and gain margins, as it may be seen in Figure 159. This capacitor is placed between the emitters of the differential pair and the ground.

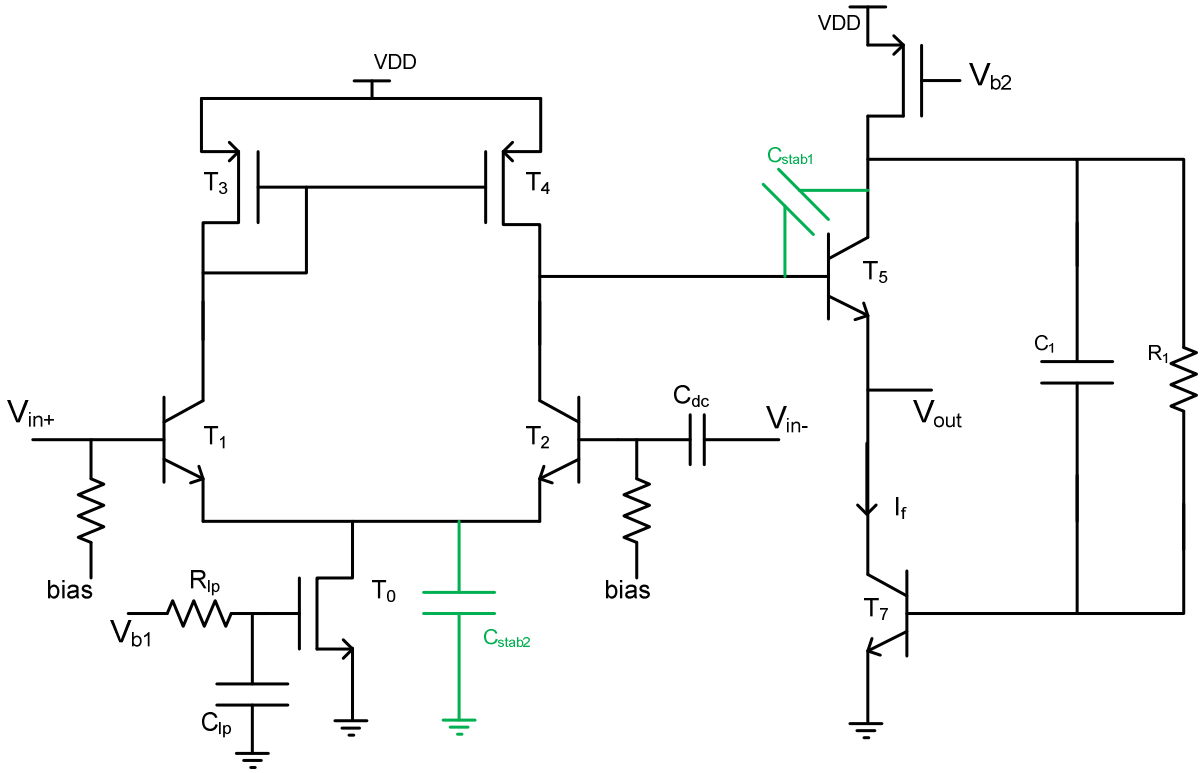

Figure 159. Final operational amplifier schematic

Figure 160 illustrates the gain and the phase of the OA without C_{stab2} and then with C_{stab2}=5pF. This capacitor introduces a zero in the transfer function of the OA. This allows increasing the phase when OA gain is close to 0dB, thus increasing the phase margin to -180° [IV.7]. C_{stab2} value is tuned so as to obtain sufficient gain and phase margins.

Table 27 has been built using schematic simulations and describes the enhancement of the stability margins, especially for PVT worst cases (-20°C and 3V supply as it may be seen later on), reaches +18° of phase margin and +6dB of gain margin. This is very important to ensure the reliability of the circuit in an industrial environment.

GM and PM are 3dB and 8° above the specification to ensure the robustness specifications when taking into account process and mismatch dispersion as well as the parasitics.

However, the major drawback of this solution is the degradation of the common-mode rejection. Indeed, at high frequency of operation, the circuit progressively becomes pseudo-differential. Measures of the common-mode rejection have been carried out. The filter rejects the common-mode by 13dB at 68MHz and by 11dB at 180MHz. These values correlate with simulations.

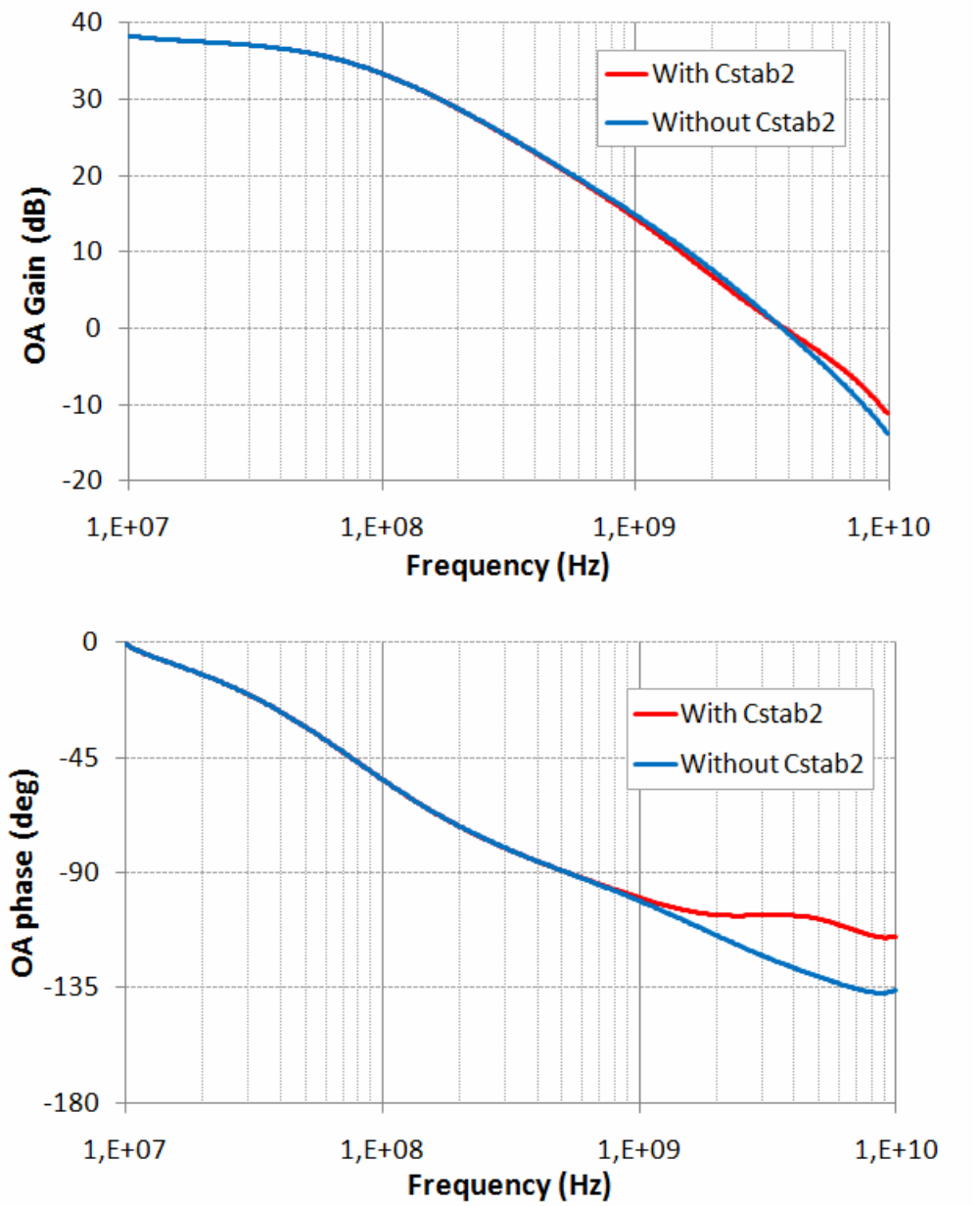

Figure 160. OA Gain and phase versus frequency when implementing Cstab2

Table 27. Stability margins enhancement by means of C_{stab2} (nominal process, -20°C, 3V supply)

Stability simulations	PM (deg)	GM (dB)
Specification	40	10
Without C_{stab2}	30.5	7.2
With C_{stab2}	48.7	13.1

IV.3.b.iv OA Performances

As it may be seen in Figure 161, the OA maximum gain is 38.3dB. Gain is higher than 30dB in up to nearly 200MHz. The gain-bandwidth product of the OA is 3.75GHz due to a high transconductance. Indeed, g_m=82.5mS. Furthermore, C_{stab2} guarantees sufficient stability margins at the cost of a decrease of the GBW.

As far as Z_{out} is concerned, the current flowing through the output follower ensures getting the required 2.5Ω.

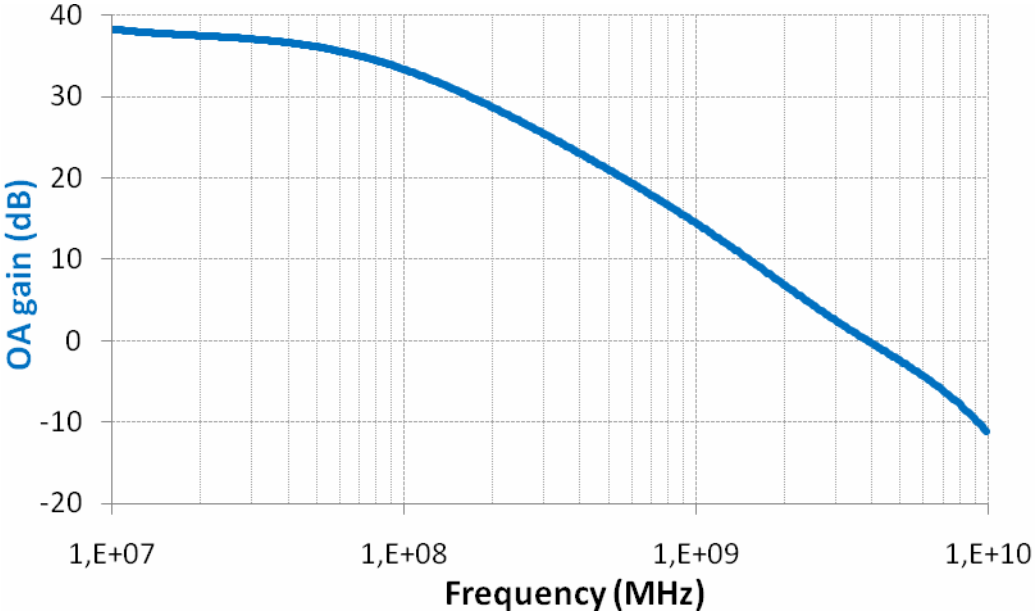

Figure 161. OA gain versus frequency

IV.3.c Implemented Filter and Test Bench

IV.3.c.i Implemented Filter

Implemented filter uses a differential configuration, as illustrated in Figure 162. Thus, the two R_2 are assembled in a two times R_2 value single resistance.

To avoid a buffer stage having a very large output decoupling capacitor, R_1=50Ω uses the impedance of the input signals generator. This simplifies the design and part of the measurement setup.

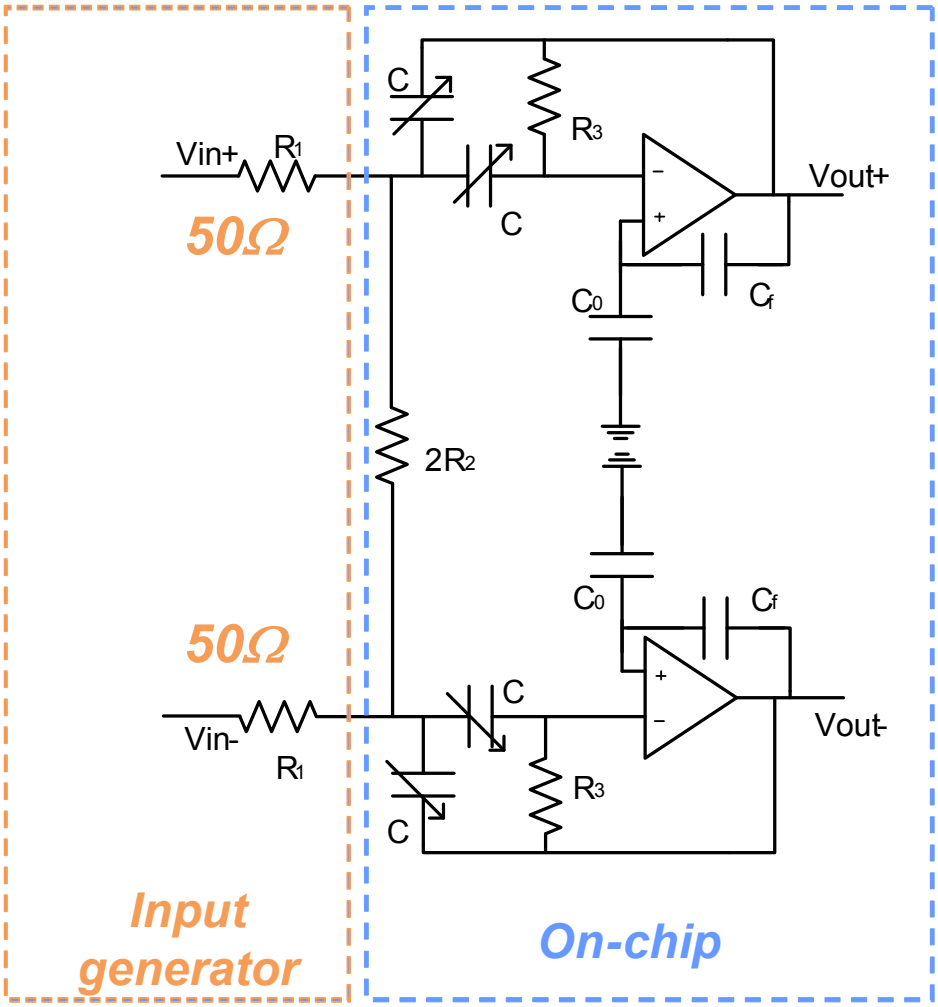

Figure 162. On-chip implemented differential filter

IV.3.c.ii Simulation Test Bench

The simulation test bench uses a 100Ω port, so R_1=50Ω per path realizing R_1. It also includes a model of the wire bondings (1nH in series with 200mΩ) for the package modelling. A 5nF decoupling capacitor and ESD diodes (from the pads) are added to achieve the schematic shown in Figure 163.

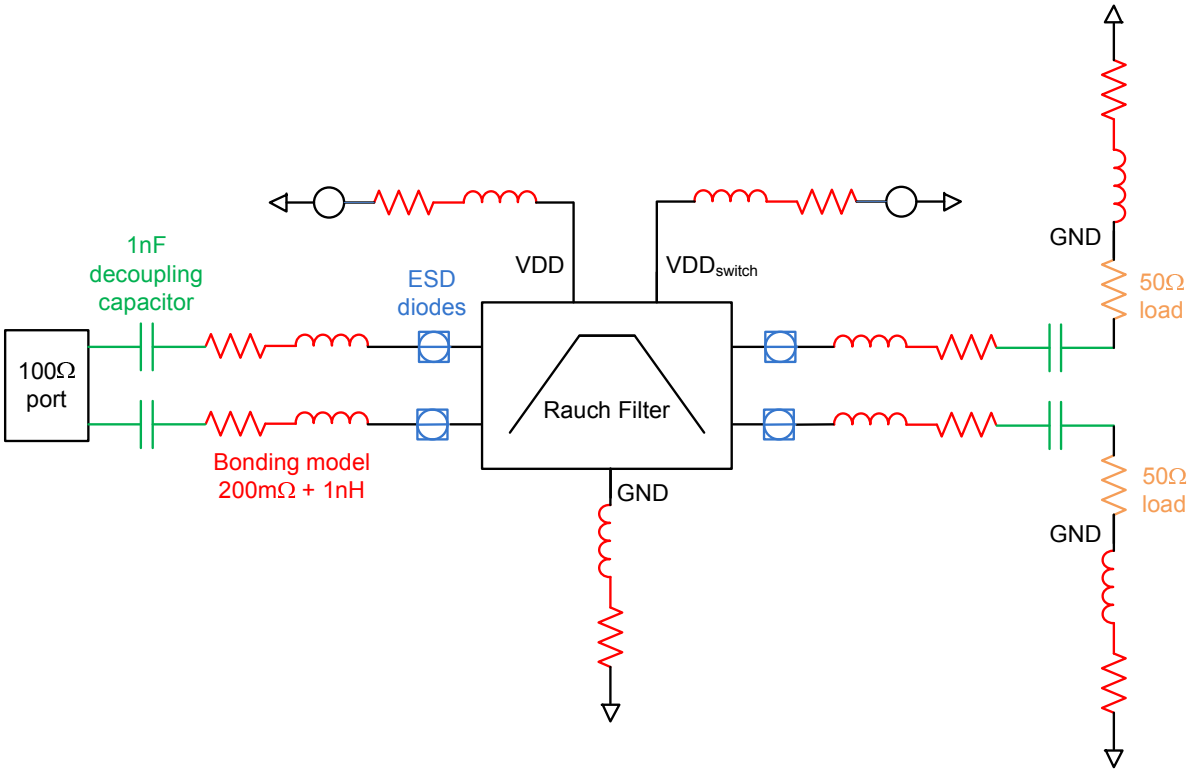

Figure 163. Main test bench

IV.3.d Filter Layout

IV.3.d.i Capacitors banks

Figure 164 shows the layout of the capacitors bank cell. On the left, in M5-M6, is the main capacitor. Switched capacitors are put next to one another and share a node (the M6 rail on the top). For instance, last capacitor is made of four equal capacitors put in parallel.

The circuitry to connect these capacitors, resistors and MOS, appears below. On top, in green M3, appear the 8 bits to control the bloc.

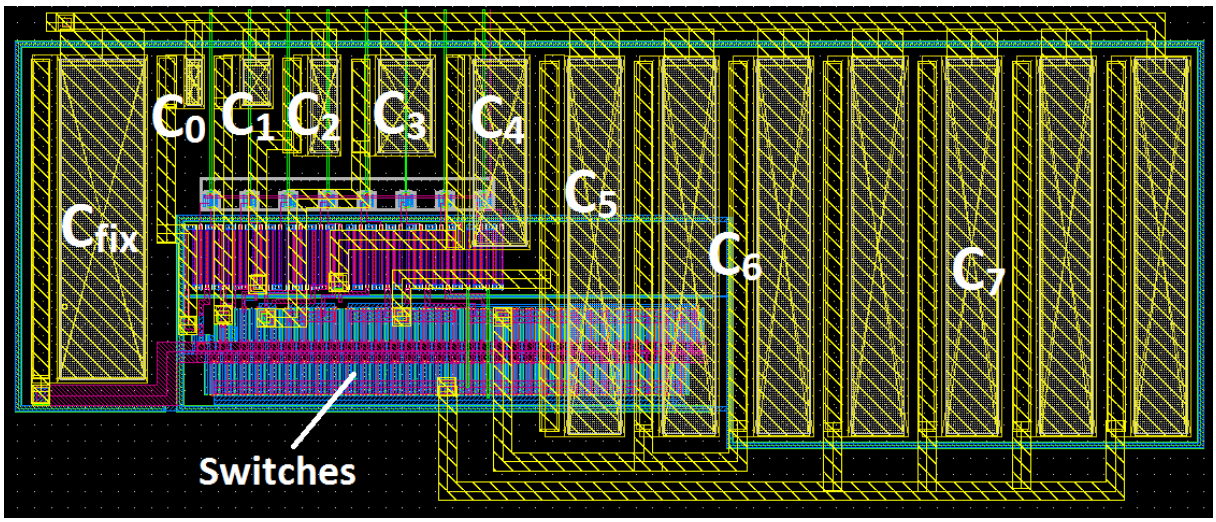

Figure 164. Layout of one capacitor bank

IV.3.d.ii Operational Amplifier

Figure 165 depicts the layout of the OA cell. On the left are two vertical transistors which make the differential pair. The third large vertical transistor is the output follower.

On the top are all PMOS transistors creating mirrors. NMOS of the current sources are located at the bottom of the layout cell.

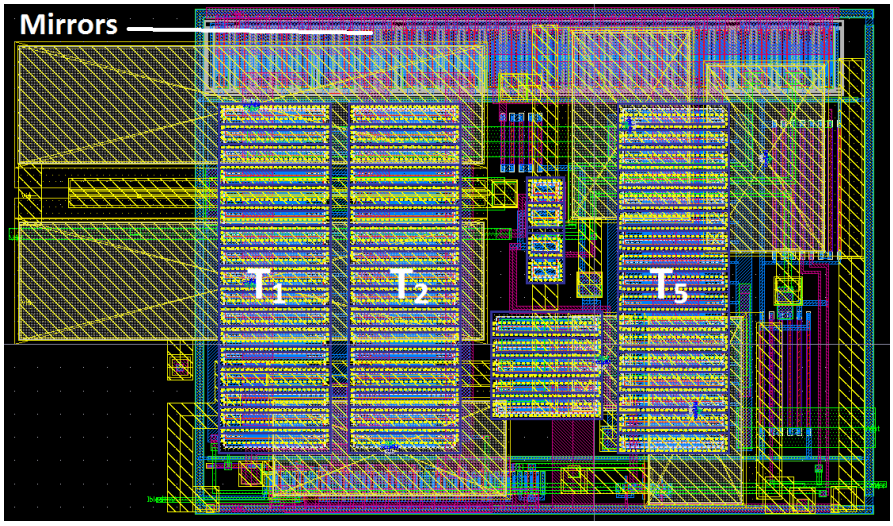

Figure 165. Layout of one OA cell

IV.3.d.iii Filter top view

Assembling all the previous blocks gives the *filter_top* cell, illustrated in Figure 166. A symmetrical structure is kept between the two paths. Supply rails are added to feed the filter with VDD and GND. The 8 bits to control switches are made accessible to be able to easily connect them to the digital part of the chip.

The filter itself is 640µm × 520µm, not taking into account the voltage and current references. The DC bias current is 47mA under 3.3V supply.

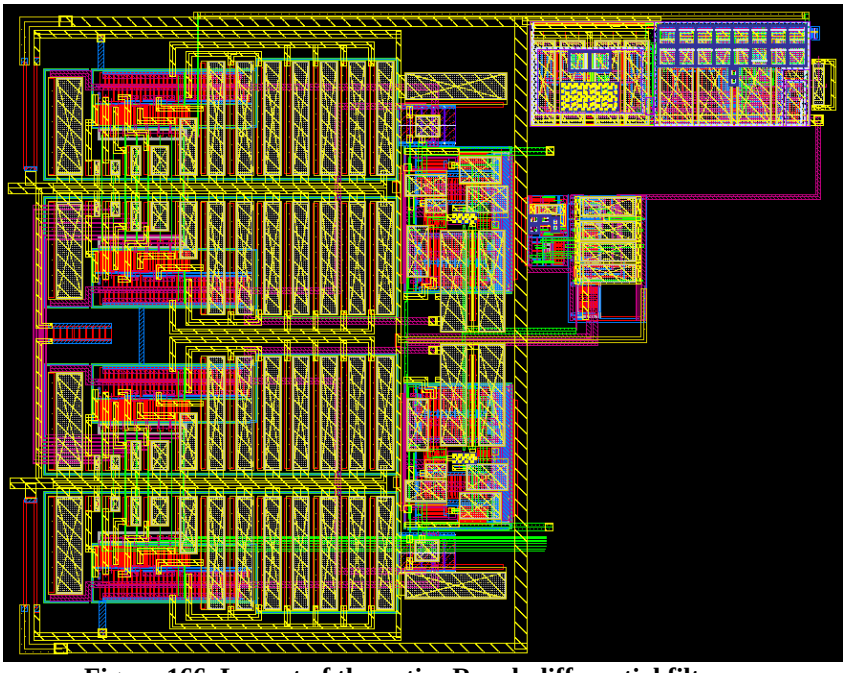

Figure 166. Layout of the entire Rauch differential filter

IV.3.e Filter Chip

Figure 167 depicts the die microphotograph of the final chip. The different blocks can be recognized quite easily.

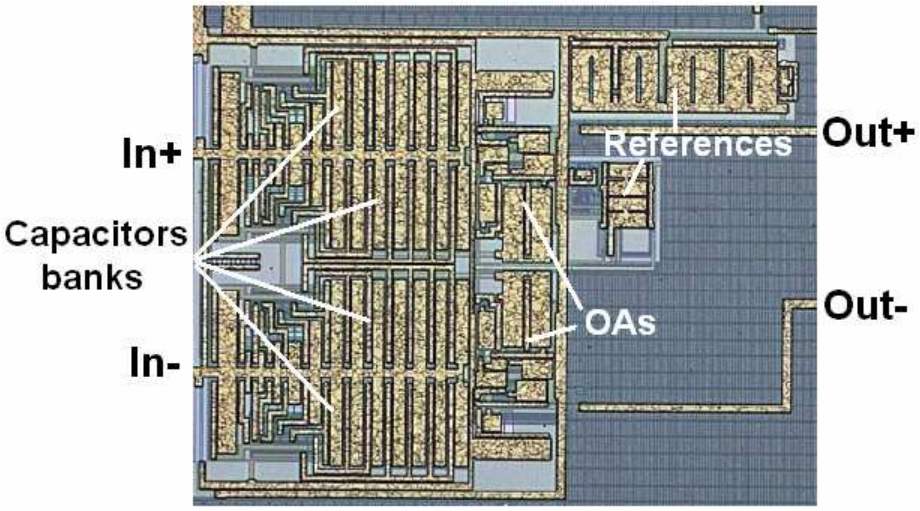

Figure 167. Rauch filter chip photograph

IV.3.f Post-layout Robustness Simulations

Following performances are the results of simulations after extraction of the parasitic due to the layout of the filter.

IV.3.f.i Final Extraction Performances

Figure 168, Figure 169 and Figure 170 describe the PVT variations of the filter Q-factor, gain and noise figure. From these graphs, one can notice the strong influence of the temperature since, as an example, Q varies (at 100MHz) from 2.5 for 120°C to 3.5 for -20°C. This is a consequence of designing an RC based structure. Indeed, resistors show strong temperature variations.

As far as the supply voltage dependency is concerned, a 10% variation of the nominal value show limited effects on these parameters, demonstrating the robustness of the design.

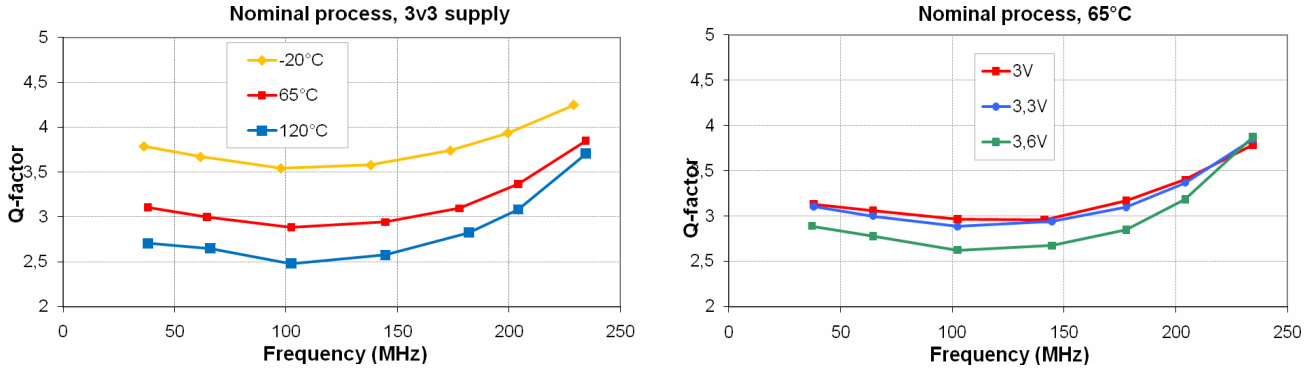

Figure 168. PVT variations of the filter Q-factor

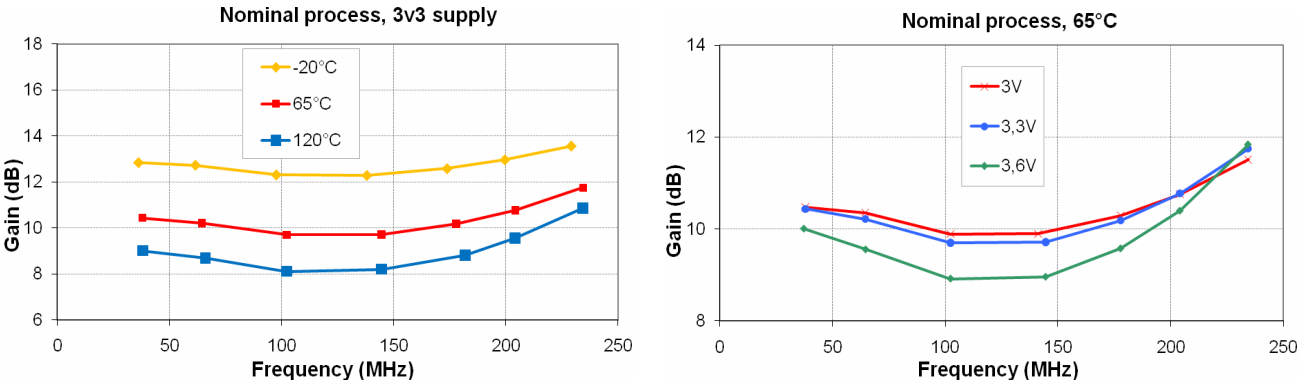

Figure 169. PVT variations of the filter gain

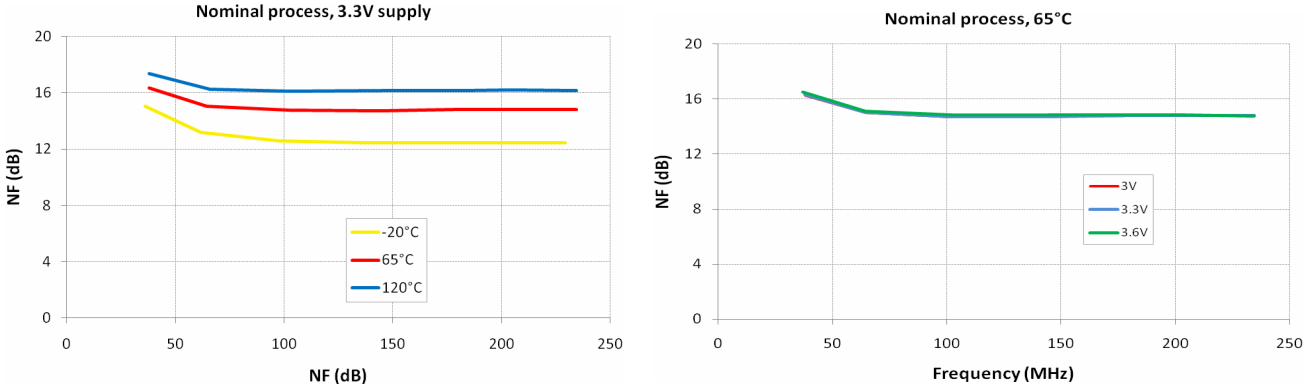

Figure 170. PVT variations of the filter NF

As far as linearity is concerned, simulations with extracted parasitic require a very large amount of memory use to be run. The two in-band tones (see APPENDIX B) need to be more and more spaced when frequency increases so as to limit the computation time, but this also results in approximations. That is why linearity simulations were only run under nominal conditions (65°C, nominal process, 3.3V supply) as it may be seen in Figure 171.

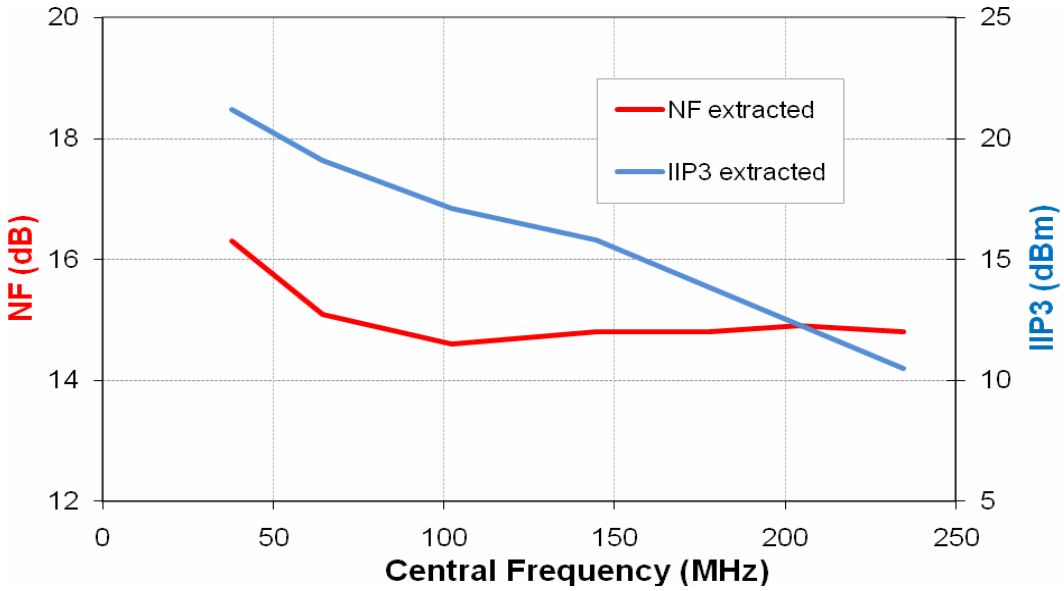

Figure 171. NF and IIP3 versus f_0 under nominal conditions

IV.3.f.ii Post-layout Stability Simulations

As explained, to ensure the reliability of the filter from an industrial point of view, it is important to keep sufficient gain and phase margins. From Figure 172 and Figure 173, it comes out that the worst case for the stability happens when temperature is -20°C and supply is 3V.

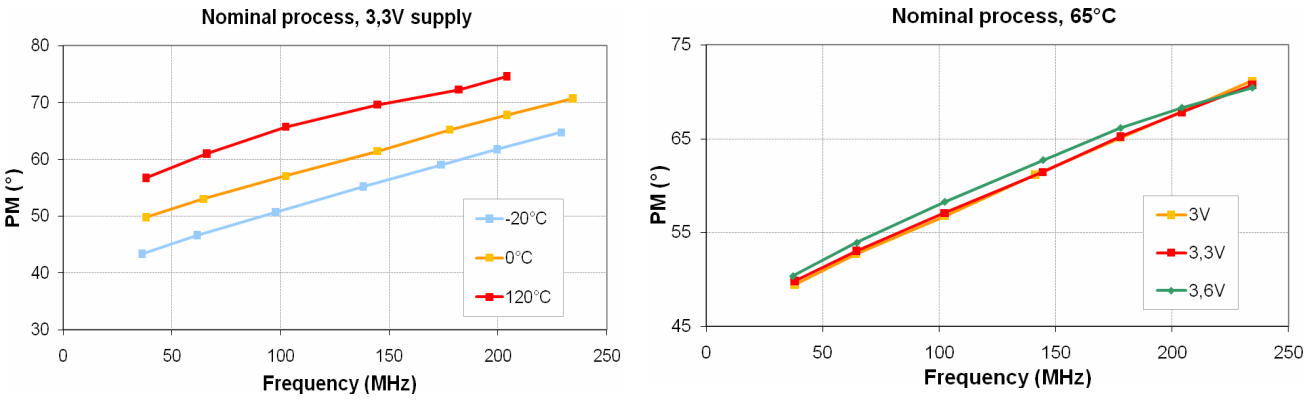

Figure 172. PVT variations of the Phase Margin

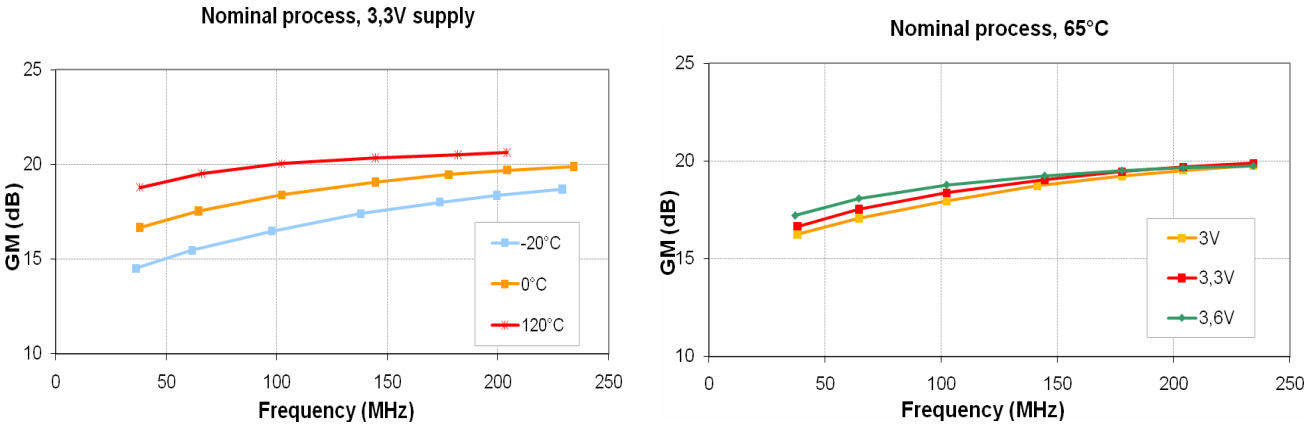

Figure 173. PVT variations of the Gain Margin

Table 28 describes the mean value μ and the standard deviation σ, obtained by100 runs of Monte Carlo simulations at 100MHz central frequency, under 65°C and 3.3V supply. Considering a 3σ deviation, one gets PM>52° and GM>17dB, which ensures the stability of the system.

Table 28. Monte Carlo Simulations (65°C, 3.3V supply, process and mismatch)

100 runs	**mean value**	**standard deviation**	**Unit**
PM	57.8	1.8	**deg**
GM	18.8	0.5	**dB**

IV.4 Rauch Filter Performances: Measurements versus Simulations

IV.4.a Measurements Bench

To measure the test chip IC of the Rauch filter, the following setup has been used, as it may be seen in Figure 174. Hybrids ensure the single-to-differential conversion of the signal.

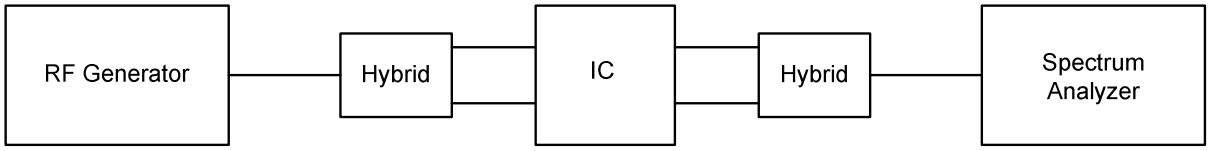

Figure 174. Filter gain versus frequency

IV.4.b Measurements Results

The frequency response of the filter is measured at different central frequencies as illustrated in Figure 175. The tuning range of the filter covers frequencies from 45 up to 240MHz.

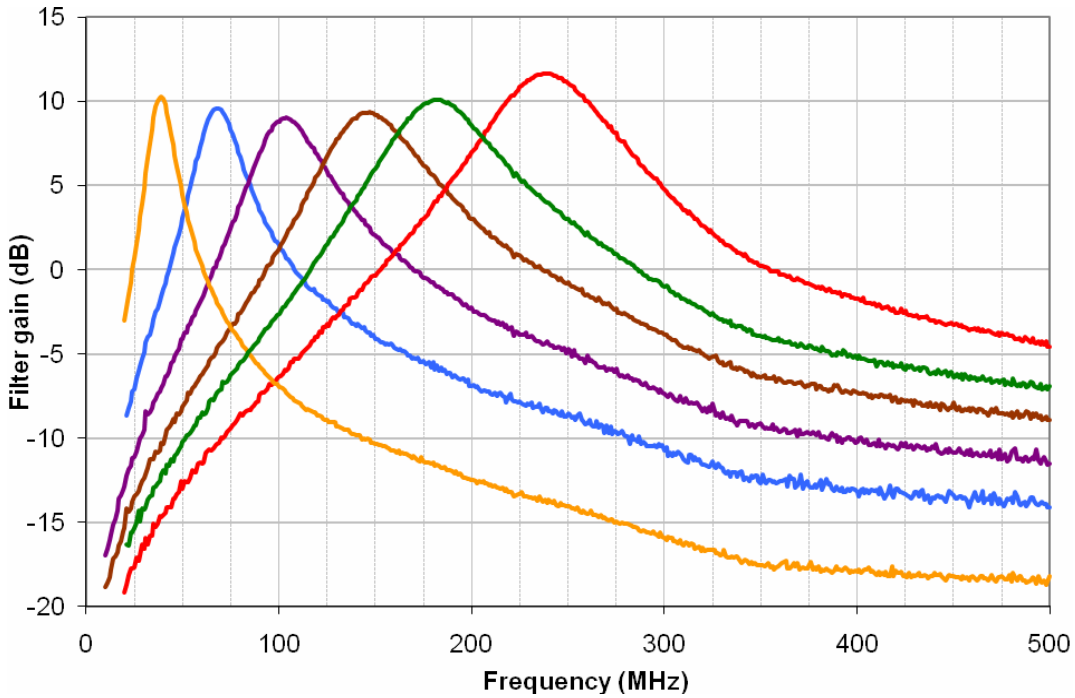

Figure 175. Filter gain versus frequency

As specified, a mean Q-factor of 3 for a 10dB voltage gain is shown on Figure 176.

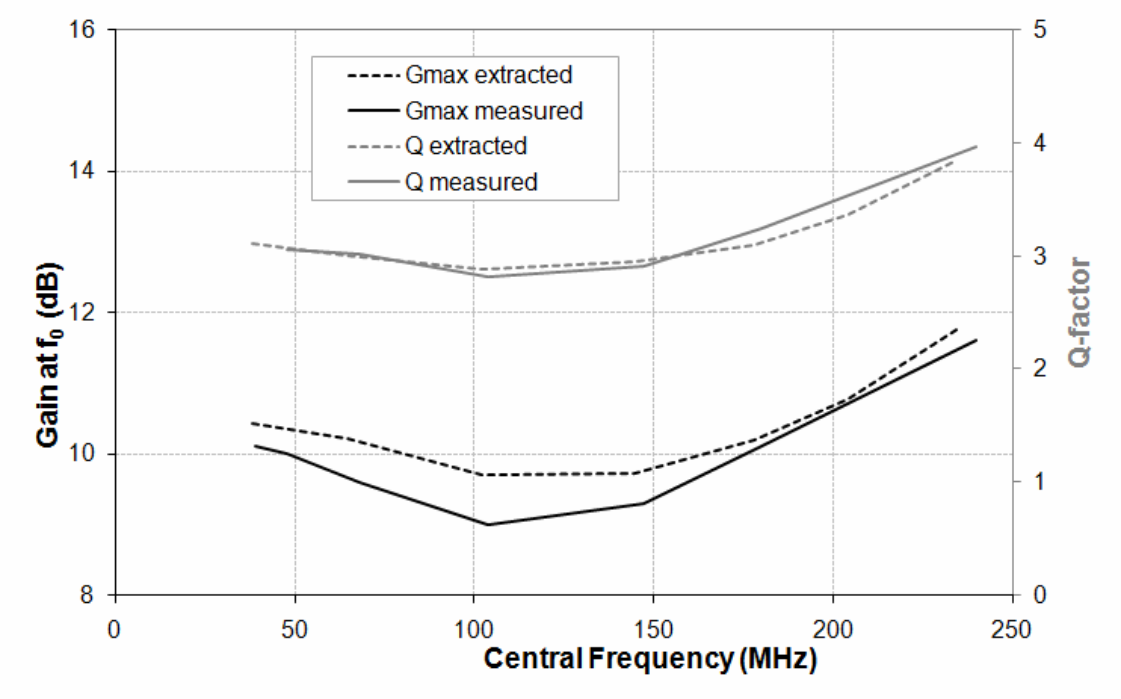

Figure 176. Q and maximum gain versus central frequency

NF on 50Ω source impedance R_1 is 15dB, and in-band IIP3 stays above 9dBm, as shown on Figure 177. Measurements are in line with the expected dynamic range. This filter, using 3.3V, allows a -5.5dBm maximum input power to be supported without degrading performances (Figure 178). Hence, the filter is able to keep its high RF performances even when handling a large signal swing from the LNA output.

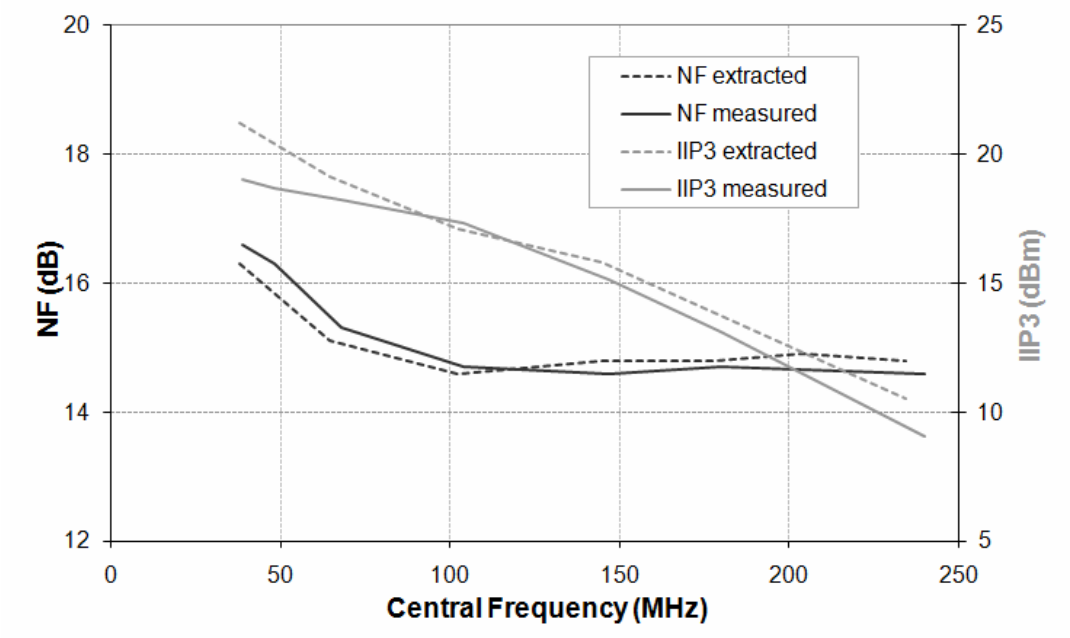

Figure 177. NF and IIP3 versus central frequency

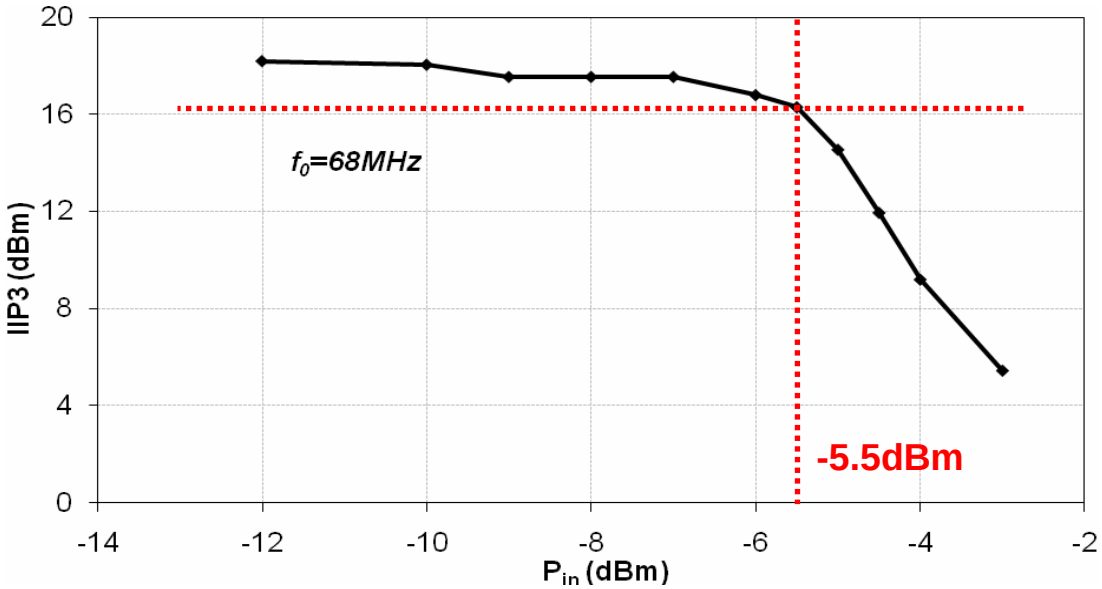

Figure 178. IIP3 versus input power P_{in}

In-band linearity has been measured using two tones within the bandwidth of the filter. Hence, the intermodulation products are not filtered out. In addition, measurements with out-of-band tones swept in the spectrum have been performed as shown on Figure 179. Out-of band IIP3 exhibits linearity performances that have been correlated with in-band IIP3 and the filter selectivity. This enables the quantification of the strong interferers impact on linearity and it also shows that the active part of the filter does not limit linearity.

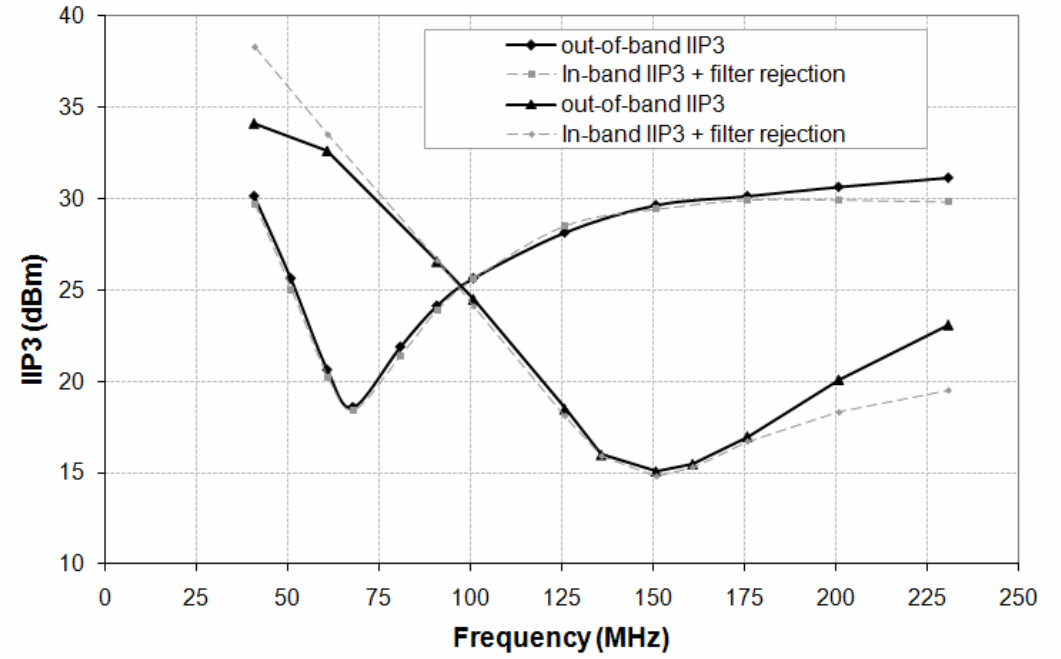

Figure 179. Out-of-band linearity compared with in-band linearity when taking into account the filter rejection, for f_0=68MHz and for f_0=147MHz

As described in introduction, the Rauch filter exhibits a peaking in the GHz range. This peaking has been measured and can be observed in Figure 180. This peaking takes place at 2.47GHz and takes the value -9.5dB. The value of -9.5dB corresponds to the value of the transfer function for gain K = -1. This takes the value -9.5dB.

$$H(K=-1)=\frac{R_2}{R_1+R_2}. \qquad \text{(IV.30)}$$

However, this peaking was expected at higher frequencies, close to 4GHz according to Figure 150. This shift towards lower frequencies is certainly due to capacitive parasitic.

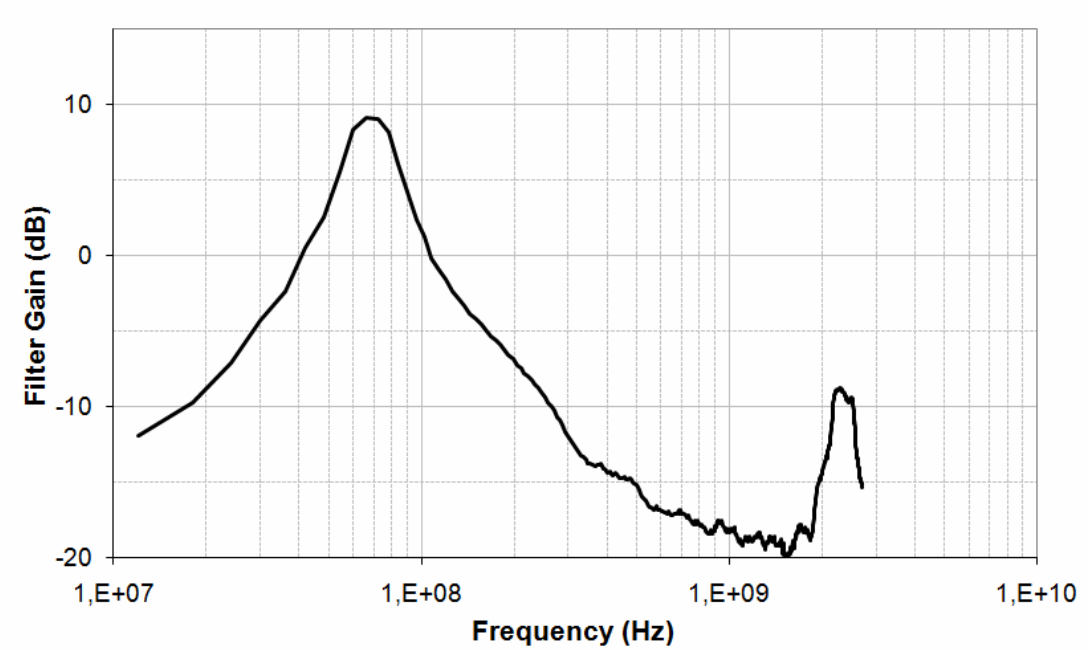

Figure 180. Filter peaking at 2.47 GHz (-9.5dB)

IV.4.c Performances Sum-up

The filter ensures the high RF performances required for a silicon TV tuner, while keeping a large input voltage swing for the proposed selectivity, by power consumption increase.

Table 29. Sum-up of the Rauch filter performances

	Rauch Filter	Units
f_0 Tuning Range	45 - 240	MHz
Q-factor	3	-
Filter Gain at f_0	10	dB
NF	15	dB
In-band IIP3	19 to 9	dBm
Max. Input Power	-5.5	dBm
Supply	3.3	V
Consumption	155	mW
Technology	BiCMOS 0.25µm	-

IV.5 Frequency Limitations

As said, the Rauch filter has originally been designed to be tunable between 45 and 240MHz. The use of this filter at higher operating frequencies results in using the OA with a reduced voltage gain. Indeed, due to its finite GBW, the gain of the OA decreases with frequency [IV.7].

Furthermore, a lower OA gain leads to a higher K and so to a Q-factor enhancement since

$$K(j\omega) = \frac{A(j\omega)\left(Z_0 + Z_f\right)}{A(j\omega)Z_0 - \left(Z_0 + Z_f\right)}. \qquad \text{(V.31)}$$

Indeed, the fixed capacitor decrease to 6pF in the capacitors banks so that the central frequency increases as well leads to a Q factor of 6 at 450MHz, and to a gain of 15dB. Q is enhanced due to a lower OA gain. Moreover, due to this smaller voltage gain, the input RF signal is more subject to distortions from the OA. This is why IIP3 strongly decreases as frequency increases. At 450MHz, in this configuration, IIP3 falls down to -3dBm.

One possibility to counter the change in the value of K is to implement a tunable capacitor C_f (or C_0) in order to keep K constant. This partially fights the drop of the OA gain and gives the results described in Table 30 where 5dBm IIP3 (for 10dB gain) are obtained at 450MHz for a 3.5 Q factor value.

Last point preventing us from using the Rauch structure at higher frequencies is the ***trade-off selectivity versus filter gain***. As explained in introduction, a more demanding selectivity is required in UHF in order to reject adjacent channels in a sufficient way. This is only possible increasing the gain of the filter. However, this solution would require amplifying less on the front-end LNA and it would result in challenging noise constraints on this LNA as well [IV.3].

Table 30. Frequency Limitations of the Rauch Filter

<table>
<tr><th>Frequency Band</th><th>Rauch BiCMOS 0.25µm</th><th>Rauch 65nm CMOS</th></tr>
<tr><td>40 - 240 MHz</td><td>MEASURES
G=10dB Q=3
IIP3=9 to 19dBm
NF=15 to 16,5dB
155mW</td><td>SIMULATIONS
G=10dB, Q=3
IIP3=3 to 2 dBm
NF=17,5dB
@70MHz</td></tr>
<tr><td>240 - 470 MHz</td><td>SIMULATIONS
linearity falls down in frequency due to OA frequency limitation
G=10dB Q=3,5
NF=15dB
IIP3 down to 5dBm @ 450MHz
if switches on C0
G=10dB Q=3,5</td><td rowspan="3">OpAmp limits linearity
N+6 selectivity too low</td></tr>
<tr><td>470 - 750 MHz</td><td rowspan="2">OpAmp limits linearity
N+6 selectivity too low</td></tr>
<tr><td>750 - 1000 MHz</td></tr>
</table>

IV.6 Conclusion

As explained, major limitation of Gm-C circuits is the strong degradation of the RF signal through the gyrator. That is why RC structures have been investigated. Their ability to handle large signal swings and their principle, based on a high voltage gain operational amplifier, make them attractive solutions to handle a high dynamic range RF selectivity.

A theoretical study leads us to a Rauch topology, which uses an innovative positive feedback to ensure stability. Optimizations have been carried out to obtain the highest dynamic range while keeping a Q-factor of 3.

Hence, a low noise and highly linear RF tunable bandpass filter has been designed in BiCMOS 0.25µm. It provides the specified Q-factor of 3 over the 45-240MHz band, with IIP3 above 9dBm and a NF of 15dB. The high RF performances of the filter implementation, with 155mW power consumption, give the perspective of the full integration of the RF selectivity function in a silicon TV tuner over more than two octaves of the VHF band.

IV.7 References

[IV.1] Y. Tsividis and J. O. Voorman, *Integrated continuous-time filters: principles, design, and applications*. IEEE Press, 1993.

[IV.2] T. Kugelstadt, “Active filter design techniques,” in *Op Amps for Everyone: Design Reference*, R. Mancini, Ed. Boston, MA: Newnes, pp. 271–281.

[IV.3] Zhiqiang Gao, Jianguo Ma, Mingyan Yu, and Yizheng Ye, “A Fully Integrated CMOS Active Bandpass Filter for Multiband RF Front-Ends,” *Circuits and Systems II: Express Briefs, IEEE Transactions on*, vol. 55, no. 8, pp. 718-722, 2008.

[IV.4] McVey, P.J., "Sensitivity in some simple RC active networks," *Electrical Engineers, Proceedings of the Institution of*, vol.112, no.7, pp.1263-1269, July 1965.

[IV.5] R.D. Middlebrook, “The General Feedback Theorem: A Final Solution for Feedback Systems”, *IEEE Microwave Magazine*, Application Note, volume 7, no. 2, pp. 50-63, April 2006.

[IV.5] M. Bernard, A. Daubeenfeld, T. Kervaon and S. Robert, “Middlebrook’s method for loop gain simulations”, NXP Internal report, January 2005.

[IV.7] Willy M. C. Sansen, *Analog Design Essentials*. Springer, 2006.

V. A Perspective for Future Developments

V.1 N-path Filtering Principle

N-path filtering is a method, already described in the sixties and in the eighties [V.1 and V.2], which uses the lack of reverse isolation of passive mixers to perform impedance transforms. A revival of interest for this technique occurs in 2010-2011 and exhibits promising results for the full integration of RF filtering.

To explain the principle of N-path filtering, let's consider a ***switched capacitor*** low-pass filter, whose cut-off frequency is called f_{LP}. Such filter consists in sampling the signal at a given sampling frequency f_c. Figure 181 depicts its amplitude response A_{SCLP}. Aliasing at f_c suggests using a low pass filter to create a bandpass one. However, Nyquist theorem prevents sampled-data filters from processing input signal whose frequency is higher than half the sampling frequency.

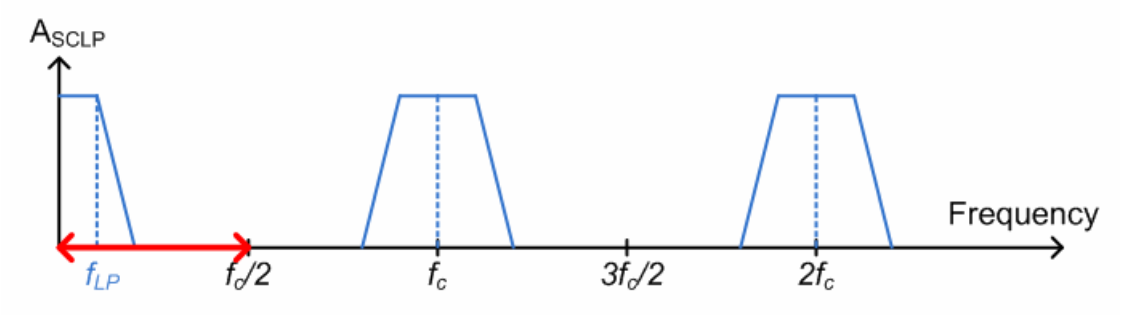

Figure 181. Amplitude response of an SC low-pass filter

It is then only possible to use the bandpass characteristic when the Nyquist range, depicted in red on Figure 181 and on Figure 183, is large enough. Hence, the number of samples per period has to be increased. This is possible introducing additional paths, as illustrated in Figure 182 for a 4-path configuration. N similar time invariant lowpass networks and 2N mixer driven by time/phase shifted versions of clock *p(t)* and *q(t)*. This architecture allows transferring a lowpass characteristic to a bandpass with the center frequency determined by the mixing frequency.

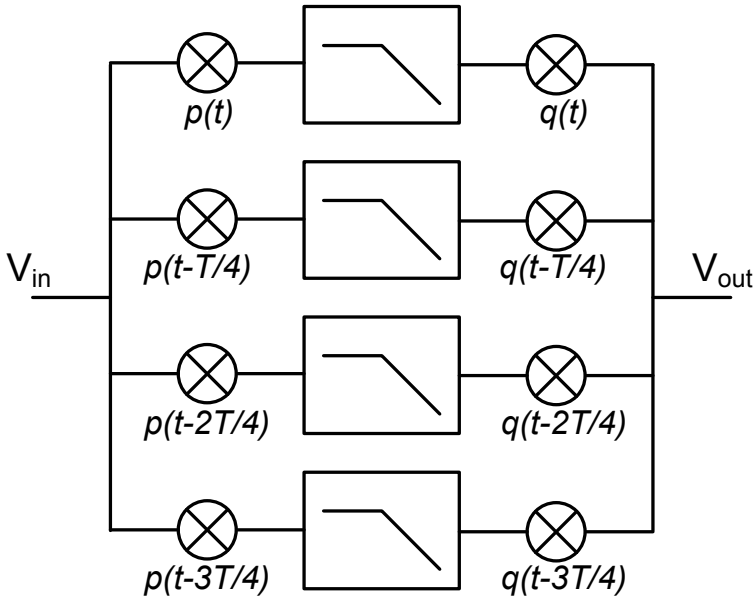

Figure 182. 4-path structure

A 4-path filter, for instance, consists in four parallel identical filter cells which are cyclically sampled with a clock frequency. A bandpass filter centered at the clock frequency f_c can then be used. Hence, frequency tuning means tuning the sampling frequency.

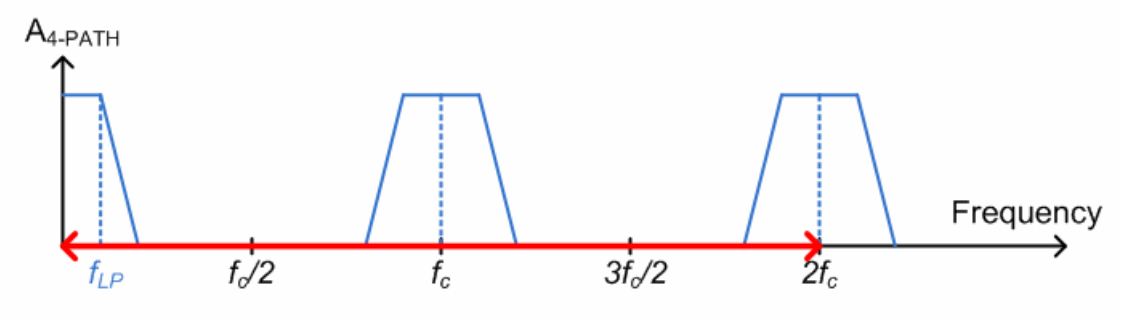

Figure 183. Amplitude response of a 4-path filter

As explained in [V.3] and depicted in Figure 184.a, mixers are realized by means of switches driven by multiphase clocks. Low pass filters are simply implemented with an RC network. Since a resistor is a memory-less element, it can be shared by all paths and shifted in front of them. Furthermore, the first set of switches can also implement the function of the second set of switches, if V_{out} is tapped between the resistor and the switches, as illustrated in Figure 184.b and detailed in [V.3].

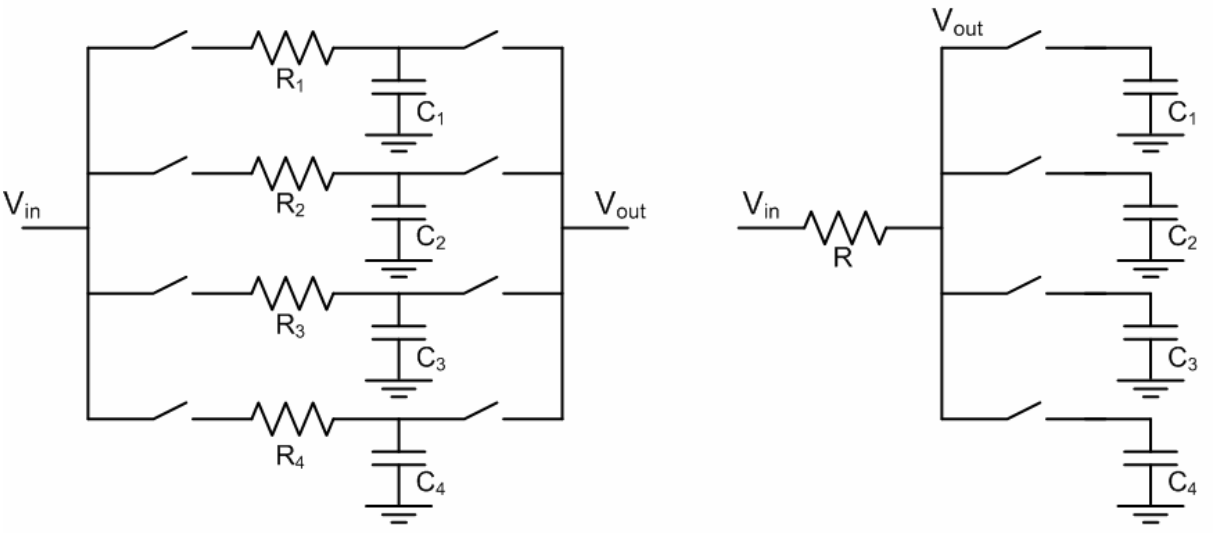

Figure 184. Switched-RC 4-path filter (a) and the simplified version (b)

The filter bandwidth is determined by a baseband low-pass filter. Indeed, due to the lack of reverse isolation, the passive mixer constituted by the switches frequency-translates the baseband impedance to RF. Therefore, very small cut-off frequencies can be achieved and, by up-conversion at the sampling frequency, create a highly selective bandpass filter whose central frequency is controlled by the clock frequency.

In the following, simulations are run in a 4-path configuration to describe and quantify the impact of all parameters.

V.2 4-path Filter Simulations

V.2.a 4-path Filter Architecture

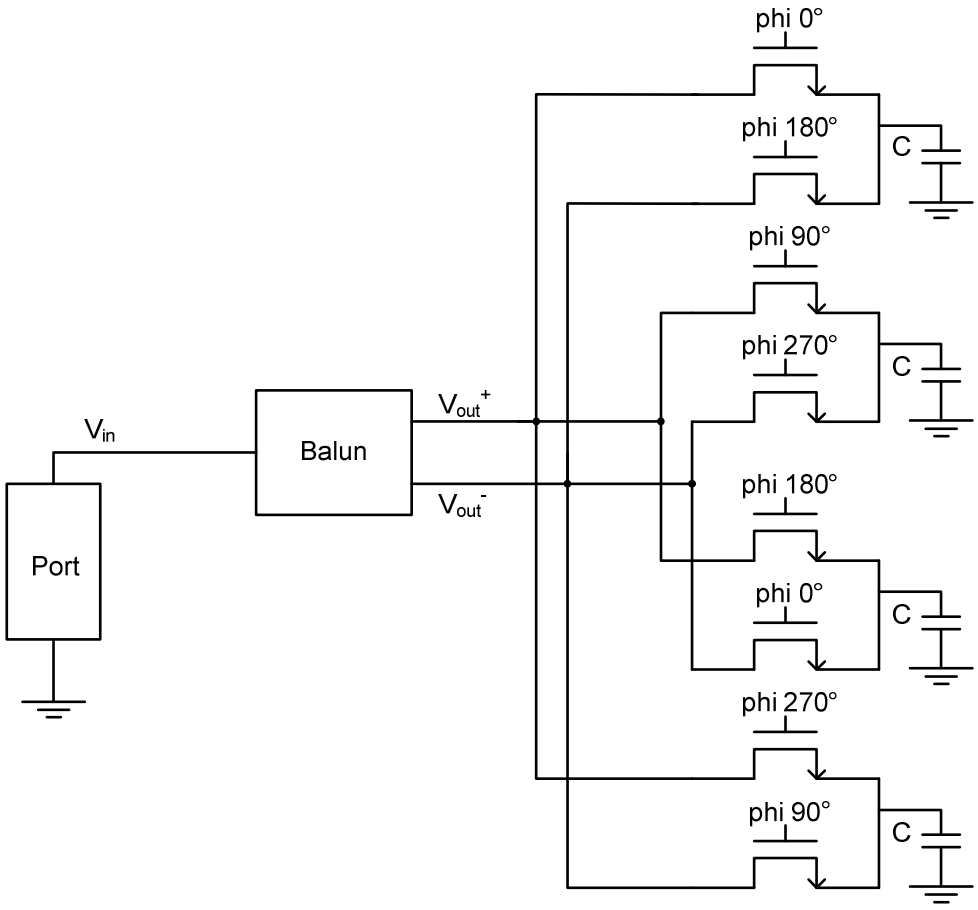

Figure 185. Simulated 4-path filter

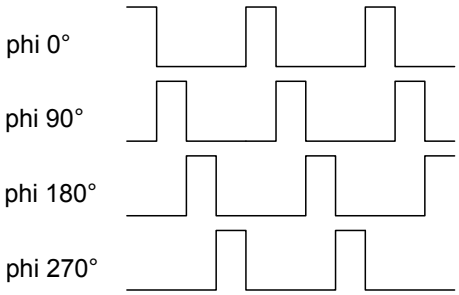

Figure 186. Non-overlapped 25% duty-cycle clocks

This 4-path filter architecture presented in Figure 185 uses a non-overlapped 25% duty-cycle clock depicted in Figure 186. It also cancels the even harmonics of the switching frequency due to anti-phase switching of the differential input. To simplify, it has been chosen to perform first simulation trials with a 4-path (N=4) architecture. With an N-phase high-Q BPF, the closest folding frequency is shifted to $(N-1)^{th}$ harmonic, which can be pushed to high frequency by using a large N value. However, "although folding frequencies are moved to higher frequencies, the input impedance seen from the RF side is equal to the baseband impedance shifted to the LO frequency and all of its odd harmonics, along with scaling factors that resemble to *sinc* function with respect to the harmonic number" [V.4].

V.2.b Selectivity and Main Parameters

For first simulations, switches size is 100/0.06 and capacitors are 66pF, as described in [V.5]. Clock frequency f_{clk} is 250MHz and the differential output signal, which exhibits a quality factor of 5, is plotted versus frequency in Figure 187.

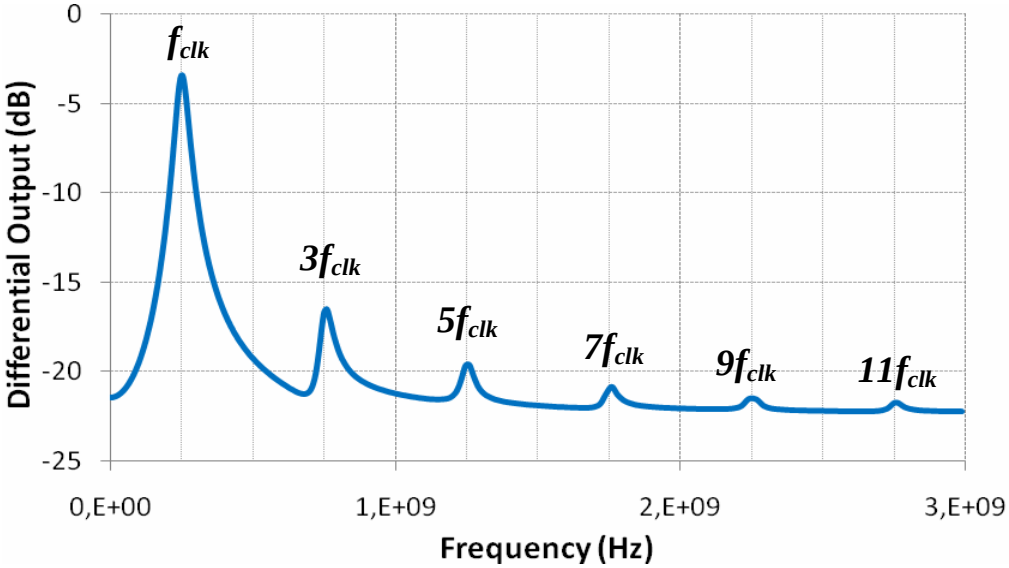

Figure 187. Output signal versus frequency with f_{clk}=250MHz

As expected, the closest folding appears at 3×250=750MHz and higher frequency foldings are located at odd multiples of the clock frequency.

Maximum rejection is 19dB for a -3dB gain at the central frequency. In the literature, it is demonstrated that maximum rejection is limited by the R_{on} switch resistance which has to be very small with respect to source resistance R. Larger switch size than 100/0.06 can then be used to enhance maximum rejection as it may be observed in Figure 188. However, this means larger parasitic capacitors, which affect the tuning range and clock leakage, and also require more clock power to drive the switches [V.5].

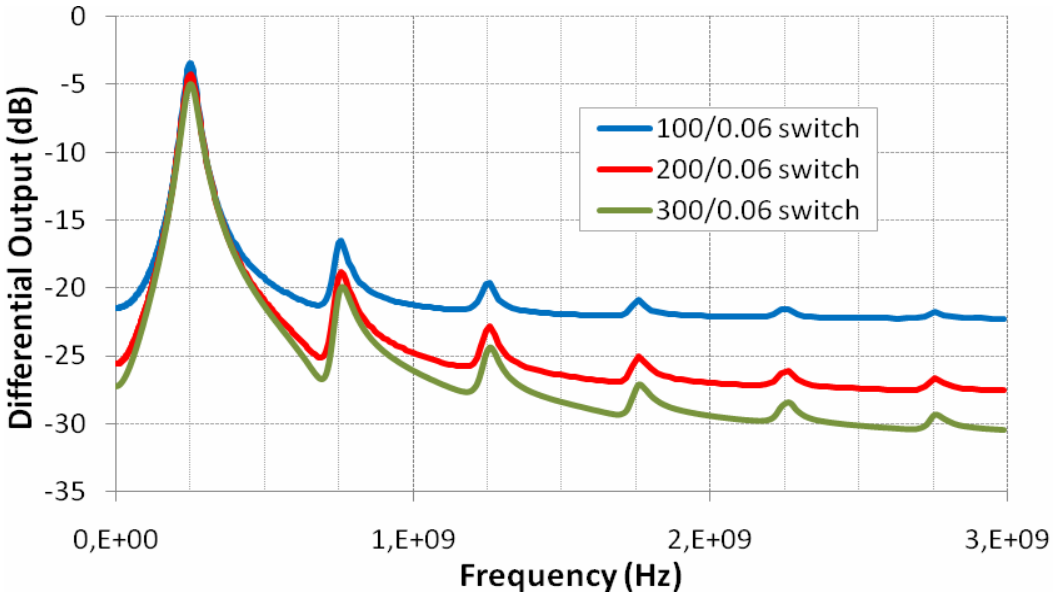

Figure 188. Enhancement of the maximum rejection reducing the R_{on} of the switches

The frequency tunability is ensured tuning the clock frequency. This may be observed in Figure 189.

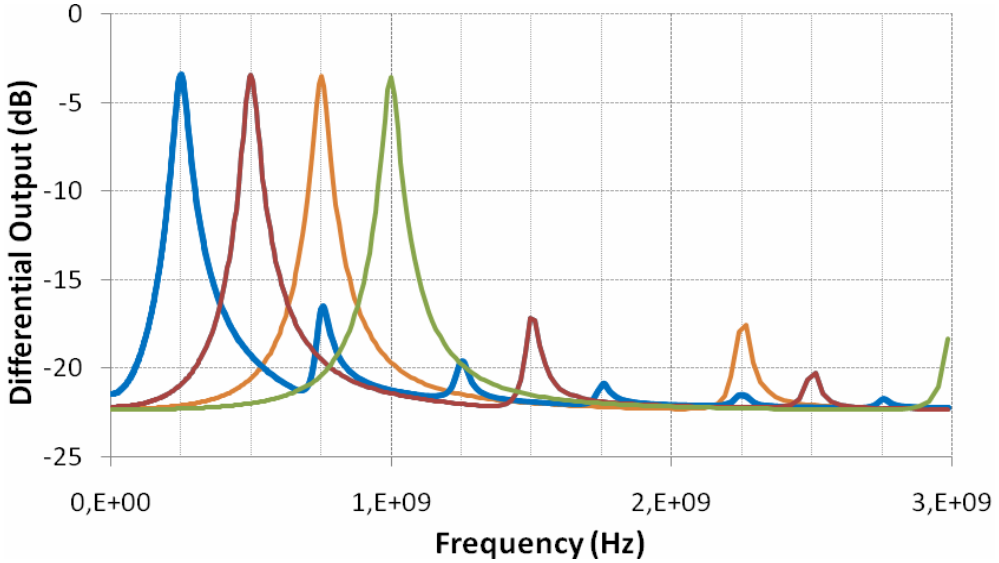

Figure 189. Frequency tuning of the 4-path filter

As far as selectivity is concerned, the bandwidth of the filter is adjusted tuning the RC constant of the baseband low-pass filter. The higher the RC constant, the smaller the bandwidth. Figure 190 depicts the output signal obtained for various C values between 10 and 100pF.

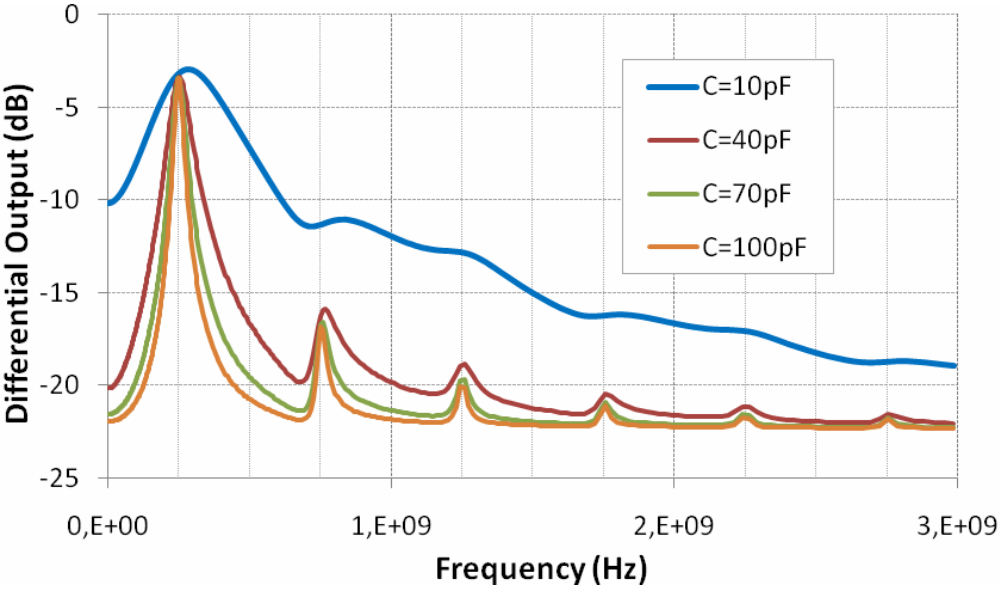

Figure 190. Selectivity tuning of the 4-path filter

Another important parameter to analyze is the duty cycle of the clock, which is 25% in the nominal case. Trials have been performed to quantify the effect of a 20% and a 30% duty cycle clock. Simulation results are plotted in Figure 191.

In reference [V.5] is presented the computation of the equivalent input impedance of the N-path filter. Hence, from the formula it is clear that when the duty cycle is smaller than 1/N, all switches are OFF periodically for some time and the output signal of the filter then simply tracks the input signal. It results in smaller insertion loss at the central frequency of the filter. Indeed, -2dB gain is obtained for 20% duty cycle against -3.5dB for 25% duty cycle.

A duty cycle higher than 1/N results in undesired charge sharing since two switches can be ON at the same time. The shape of the filter is totally destructed due to large insertion loss (-13dB in Figure 191).

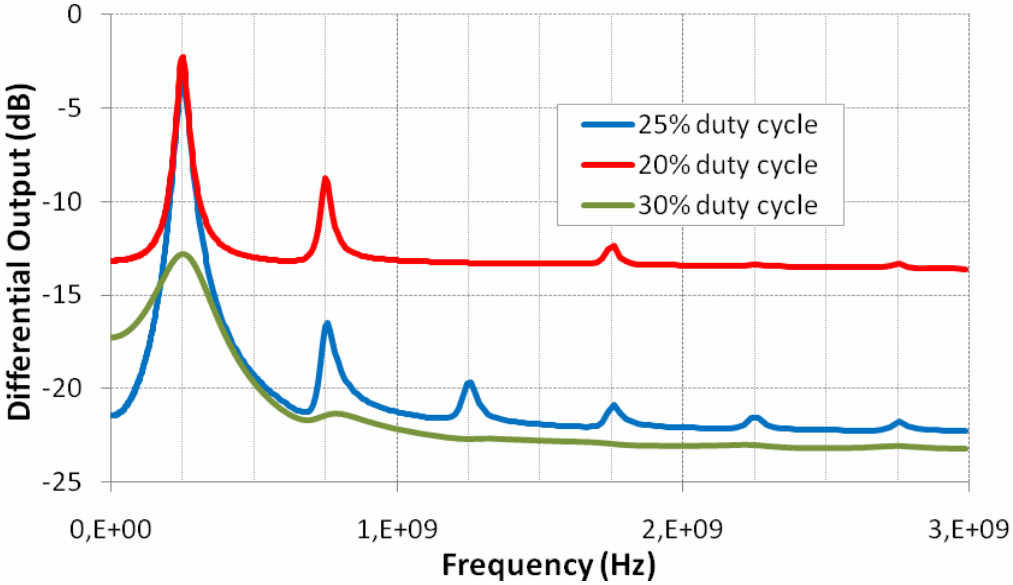

Figure 191. Impact of the duty cylce

V.2.c RF Performances

As explained in [V.5], most output noise power is due to thermal noise of the source and switch resistances. Moreover, noise foldings from around the harmonics of f_{clk} have to be taken into account. Noise figure values below 5dB are reported, where noise is mainly caused by the noise folding of noise coming from the source resistance [V.5].

As far as linearity is concerned, it is determined by the switch sizes and the implemented capacitors. That is why very high linearity levels and 1dB compression points are reported in the literature (see Table 31).

Reference [V.6] details the impact of diverse imperfection sources which may degrade the performances of an N-path filter. These imperfections have four main sources:

- ***LO phase noise***, which causes reciprocal down-conversion to on top of the desired signal;
- ***Second order non-linearity of the switches in presence of mismatch***, which can fold an amplitude modulated blocker to on top of the desired signal;
- ***Quadrature inaccuracy of the duty cycle***, which involves an image folding to on top of the desired signal;
- ***Thermal noise of the switches***, since harmonics down-conversion increases thermal noise contribution.

V.3 State-of-the-Art

V.3.a 4-path Filtering State-of-the-Art

References [V.3 and V.5] report measurement results of very high RF performances using the structure in Figure 185, with NF below 5dB with IIP3 higher than 14dBm, for a Q factor between 3 and 29. However, due to aliasing, maximum rejection is limited to 15dB. The results in this paper are summarized in Table 31. It is worth highlighting that an external balun is used for the single to differential conversion. In this table, the maximum rejection is defined by the difference between the gain at f_{clk} and the gain between two folding frequencies.

Table 31. Sum-up of 4-path filter performances

	[V.5]	**Units**
f_0 Tuning Range	100 – 1000	MHz
Q-factor	3 to 29 *(BW=35MHz)*	-
Filter Gain at f_0	-2	dB
Maximum rejection	15	dB
NF	3 to 5	dB
In-band IIP3	14 to 21	dBm
P_{1dB}	2	dBm
Consumption	2 to 16	mW
Active area	0.07	mm^2
Technology	65nm CMOS	-

V.3.b An Innovative Fully-integrated Architecture

As explained in these papers, “most integrated receivers nowadays are *zero* or *low-IF* (Figure 192.a), and benefit from a simple structure and a high level of integration as *image rejection* is not a major concern, and *channel selection* is performed by low-frequency low-pass filters”. However, these filters consist of RC networks which do not scale with the technology. Besides “constraints such as 1/f noise or second order non-linearity demand large device sizes for the IF blocks, exacerbating the scalability issue” [V.7]. A *superheterodyne* architecture does not experience these issues since it uses IF but it requires external filters for image rejection and channel selection, as illustrated in Figure 192.b.

To circumvent the scalability issue of zero or low-IF architectures and to achieve the same level of integration, references [V.6] and [V.7] propose an architecture with a high IF (110MHz), similar to a superheterodyne receiver, where image and blockers are progressively filtered throughout the receiver chain by means of *frequency-translated* filters derived from the original N-path filtering concept. This may be observed in Figure 192.c.

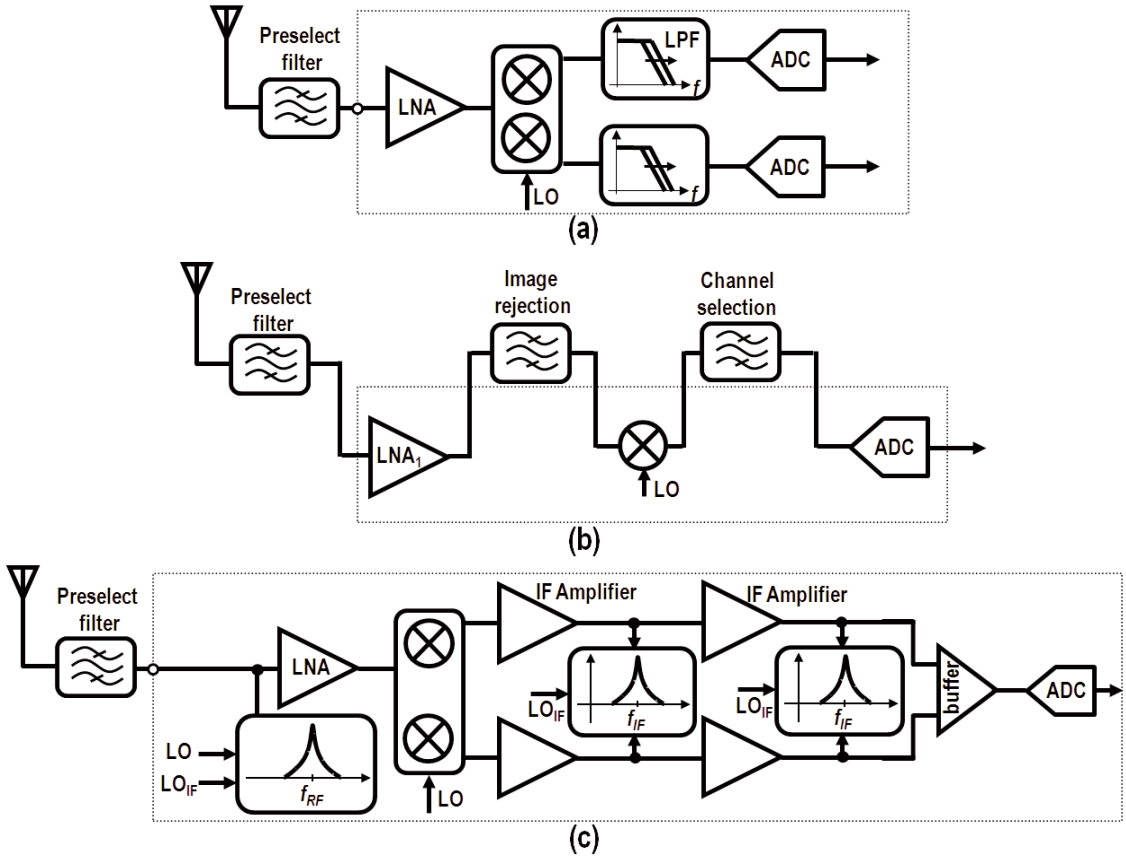

Figure 192. Zero-IF architecture (a), Conventional heterodyne receiver (b) and reported heterodyne receiver architecture (c) [V.7]

The performances of this Rx chain are presented in Table 32.

Table 32. Sum-up of RF front-end performances with a high-Q 4-path RF filter

	[V.7]	Units
Tuning Range	1.8 to 2	GHz
IF frequency	110	MHz
Maximum gain	55	dB
NF at max gain	2.8	dB
In-band IIP3 at max gain	-8.5	dBm
N+6 rejection with RF filter ON	47	dB
Current Consumption	13.5	mA
Active area	0.76	mm^2
Technology	65nm CMOS	-

V.4 Conclusion

In this chapter, it has been demonstrated that N-path filtering exhibits promising assets in order to handle the RF selectivity of TV tuners. These assets are high RF performances (NF below 5dB and IIP3 above 14dBm are reported) over a very wide frequency tuning range, such as a decade (100-1000MHz). Despite a limited harmonic frequencies rejection, small bandwidth can be achieved keeping excellent RF performances. This harmonics rejection can also be enhanced using a higher N factor or using better switches. Hence, CMOS technology scaling is possible.

In the literature, new RF front-end architectures are proposed to take full advantage of the assets of N-path filtering [V.8 and V.9]. These architectures without LNA, where the N-path filter is directly connected to the antenna, present promising results with very high linearity (>11dBm IIP3) and interesting NF (<6.5dB). That is why N-path filtering is a promising perspective to the present work on RF filtering.

V.5 References

[V.1] L.E. Franks and I.W. Sandberg, "An alternative approach to the realizations of network functions: N-path filter," *Bell Syst. Tech. J.*, pp. 1321-1350, 1960.

[V.2] D. C. von Grunigen, R. P. Sigg, J. Schmid, G. S. Moschytz, and H. Melchior, "An integrated CMOS switched-capacitor bandpass filter based on N-path and frequency-sampling principles," *IEEE Journal of Solid-State Circuits*, vol. 18, no. 6, pp. 753-761, Dec. 1983.

[V.3] A. Ghaffari, E. A. M. Klumperink, and B. Nauta, "A differential 4-path highly linear widely tunable on-chip band-pass filter," in *2010 IEEE Radio Frequency Integrated Circuits Symposium (RFIC)*, 2010, pp. 299-302.

[V.4] A. Mirzaei, H. Darabi, and D. Murphy, "Architectural Evolution of Integrated M-Phase High-Q Bandpass Filters," *IEEE Transactions on Circuits and Systems I: Regular Papers*, vol. PP, no. 99, pp. 1-1, 0.

[V.5] A. Ghaffari, E. A. . Klumperink, M. C. . Soer, and B. Nauta, "Tunable High-Q N-Path Band-Pass Filters: Modeling and Verification," *IEEE Journal of Solid-State Circuits*, vol. 46, no. 5, pp. 998-1010, May 2011.

[V.6] A. Mirzaei and H. Darabi, "Analysis of Imperfections on Performance of 4-Phase Passive-Mixer-Based High-Q Bandpass Filters in SAW-Less Receivers," *IEEE Transactions on Circuits and Systems I: Regular Papers*, vol. 58, no. 5, pp. 879-892, May 2011.

[V.7] A. Mirzaei, H. Darabi, and D. Murphy, "A low-power process-scalable superheterodyne receiver with integrated high-Q filters," in *Solid-State Circuits Conference Digest of Technical Papers (ISSCC), 2011 IEEE International*, 2011, pp. 60-62.

[V.8] C. Andrews and A. C. Molnar, "A passive-mixer-first receiver with baseband-controlled RF impedance matching, <6dB NF, and >27dBm wideband IIP3," in *Solid-State Circuits Conference Digest of Technical Papers (ISSCC), 2010 IEEE International*, 2010, pp. 46-47.

[V.9] M. Soer, E. Klumperink, Z. Ru, F. E. van Vliet, and B. Nauta, "A 0.2-to-2.0GHz 65nm CMOS receiver without LNA achieving >11dBm IIP3 and <6.5 dB NF," in *Solid-State Circuits Conference - Digest of Technical Papers, 2009. ISSCC 2009.*

IEEE International, 2009, pp. 222-223,223a.

VI. Conclusion

Context of the PhD thesis

This PhD thesis work took place in the TV reception domain. Indeed, NXP Semiconductors currently designs TV tuners for different standards such as analog TV, digital TV or cable TV. These spectra cover a wide frequency range from 45MHz to 1002MHz, with channel widths of 6 to 8MHz according to the standard.

To obtain a high quality reception, the TV tuner has to handle the RF off-air or cable signal. The role of the tuner is to amplify and to select the desired channel among all the received ones. This has to be performed with as little degradation and distortion as possible. Indeed, the wanted channel is then transmitted to the demodulator and the cleaner the signal, the fewer the demodulation errors. That is why the TV tuner should present high RF performances. In particular, it is required to be low noise, to be able to manage weak wanted signals, and highly linear, to be able to manage strong interferers which may degrade the quality of the reception.

Within the tuner architecture, an RF filter is located between the front-end low noise amplifier and the mixer. This RF filter realizes the first selectivity step of the tuner. It allows rejecting harmonic frequencies due to the downconversion of the RF signal at LO odd harmonic frequencies when mixing. Furthermore, this RF filter also allows the rejection of adjacent channels for the international standard compliance (Nordig or ATSC A/74 for instance). It also enables to reject non-TV signals like the FM bands (88-108MHz) which act as interferers. Specifications have been set on these different rejections as well as on the tuning range of the filter, in order to quantify the requirements.

Currently the RF filters of NXP tuners are realized by means of LC resonators with several off-chip inductors. Due to the technological trend which aims at integrating the whole tuner on-chip (the so called *fully-integrated silicon tuner*), alternative integrated solutions, and in particular active topologies, are looked for. Hence, the impact and the opportunities of technology on fully-active solution have to be quantified. Besides, a primary focus is set on low-VHF bands since the inductances at this frequency (~100nH) prevent from any integration on-chip. From these issues, the problematic of the present PhD thesis has been determined and set to:

Limitations & Opportunities of Active Circuits for the Realization of a High Performance Frequency Tunable RF Selectivity for TV Tuners

RF selectivity challenges

In this thesis, several topologies have been assessed. The purpose is to find which one best suits the abacus created with the rejections specifications of the RF filter. It comes out that the second order bandpass topology is the best. It actually needs few components which make it an attractive structure for easy tunability. Moreover, it is also possible to tune the quality factor Q of such a filter. Q describes the selectivity of the filter and is defined as the ratio of the central frequency by the -3dB bandwidth. The higher the quality factor, the more selective the filter.

Once the topology chosen, the literature has been assessed to find most appropriate solutions. First, LC passive filters have first been studied as a comparison basis to active solution studied further. A figure-of-merit has also been introduced to handle fair comparisons with current state-of-the-art. As far as fully-active structures are concerned, the literature mainly considers Gyrator-C and Gm-C filters. Gyrator-C filters consist in emulating an inductive behaviour at RF frequencies by a gyrator, allowing the replacement of inductors by active counterparts. Gm-C filters actually consist in synthesizing a transfer function by means of integrators, and so of Gm-cells. For simple topologies such as the second order bandpass, these two kinds of filter may lead to the same structure.

Gm-C filters

The studied Gm-C filter structure is based on an analogy with a parallel LC resonator where the inductor is replaced by a gyrator. Tuning the gyrator value and tuning the capacitance in parallel, a large tuning range is obtained compared to a passive LC filter. The theoretical study of noise and linearity limitations leads to the choice of a moderate quality factor since as soon as Q increases, RF performances are strongly degraded. This study also demonstrates that high RF performances are required on all Gm-cells. It has been chosen to use large transconductance values (2.5 and 10mS) in order to decrease the overall noise of the filter. However, such transconductances have to be linearized to reach the linearity specification set on the Gm-cell.

Several transconductor linearization techniques from the literature have been assessed. Only two of them exhibit an interesting linearity versus noise trade-off: the Dynamic Source Degeneration (DSD) which is also used in the literature for a TV reception RF filter [VI.1], and Multiple Gated Transistors (MGTR) which show the most promising results at the Gm-cell level. Gm-C filters based on Gm-cells designed with these linearization techniques have been simulated in 65nm CMOS technology. Table 33 summarizes the obtained performances compared to literature results. The filter with MGTR-based Gm-cells presents the best performances. For 6dB gain and a Q-factor close to 4, it exhibits an IIIP3 above 8dBm up to 450MHz, with a 16dB NF. However, this structure appears to be very sensitive to bias as well as process and mismatch variations, where a robust solution is required for our applications. That is why no test-chip has been realized based on this architecture.

Table 33. Performances Comparison

Filter	[VI.1]	Filter 1	Filter 2	Units
Linearization tech.	DSD*	DSD*	MGTR	**-**
Tuning range	50 - 300	45 - 385	45 - 450	**MHz**
Q factor	6	3.5	3.7	**-**
Gain	6	10	6	**dB**
NF	20	18	16.3	**dB**
IIP3	2 to 6	-4 to 2	8 to 10	**dBm**
Power consumption	7.6	16.5	30	**mW**
Supply	1.2	2.5	2.5	**V**
CMOS Technology	130	65	65	**nm**

From the Gm-C filters design, it comes out that the main limitation of the performance is the gyrator. Indeed, the RF signal undergoes strong distortion and degradation when flowing through the active inductor. It has also been assessed the ability of the Gm-C filter to be used at higher frequencies. However, linearity is strongly degraded as soon as frequency increases. This is due to the use of smaller capacitances in the capacitors banks ensuring the frequency tuning. Indeed, the switch capacitances non-linearity of the switches becomes non negligible compared to the classically capacitances. Furthermore, a selectivity of 4 in UHF only rejects adjacent channels by 1dB or less. A higher Q is demanded but enhancing the quality factor would result in higher NF.

Rauch filters

To overcome Gm-C limitations due to the signal flowing through the gyrator, operational amplifier (OA) based filters are investigated. The purpose is to take advantage of both a high loop gain and a filter response introduced by to the RC network. Hence, we are aiming at designing a highly linear filter while not compromising noise at the same time.

However, RC filters are more selective at high gain. Among the structures found in the literature, the positive feedback Rauch topology presents the highest selectivity for a given gain. It also presents limited sensitivity to passive components, making it a more robust solution. It has been chosen to limit the filter gain to 10dB, which corresponds to a quality factor of 3 when optimizing the dimensioning of the Rauch filter. Indeed, if the gain on the RF filter stage is too high, this would result in very high noise constraints on the LNA.

The positive feedback Rauch filter is unstable under a certain condition. An innovative solution has been proposed to stabilize the filter, based on a non-inverting operational amplifier, which prevents from fulfilling this instability condition. Specifications on the operational amplifier have then been set to obtain the best performances and choose the technology. The choice of the technology turns to 0.25µm BiCMOS instead of 65nm CMOS due to the higher OA voltage gain. Stability margins have then been taken to ensure the robustness of the circuit. It has then be realized on a test-chip and measured in a laboratory.

Measurements show a perfect agreement with the post-layout simulations. As specified, a quality factor of 3 is obtained for 10dB gain. As summarized in Table 34, NF is 15dB whereas IIP3 is higher than 9dB up to 240MHz. IIP3 is 19dBm at 45MHz, which demonstrates the highly linear characteristic of the filter. The tuning range is limited to 240MHz due to the drop of the gain of the OA which strongly degrades the linearity performances of the filter. Moreover, a Q of 3 at higher frequencies would reject by less than 1dB the adjacent channels.

Table 34. Sum-up of the Rauch filter performances

	Rauch Filter	**Units**
f_0 Tuning Range	45 - 240	MHz
Q-factor	3	-
Filter Gain at f_0	10	dB
NF	15	dB
In-band IIP3	19 to 9	dBm
Max. Input Power	-5.5	dBm
Supply	3.3	V
Consumption	155	mW
Technology	BiCMOS 0.25µm	-

Comparison of the Proposed Filters

As said, a figure-of-merit has been proposed in the introduction to compare RF filters results with state-of-the art literature ones. This FOM is defined as:

$$FOM1 = 10^{\frac{IIP3-NF}{10}} . Q_{moy} . f_{\max} . TR \qquad \text{(VI.1)}$$

where *TR* is the frequency tuning range.

It can also take into account the power consumption P_{DC} of the filter.

$$FOM2 = \frac{10^{\frac{IIP3-NF}{10}} . Q_{moy} . f_{\max} . TR}{P_{DC}} \qquad \text{(VI.2)}$$

Table 35 summarizes the performances obtained with the Gm-C and the Rauch filter. These two filters are compared to the most significant paper dealing with a fully active frequency tunable bandpass filter for TV tuners [VI.1].

Table 35. Performances Comparison

	[VI.1]	**Gm-C Filter 2**	**Rauch Filter**	**Units**
Topology	Gm-C (DSD)	Gm-C (MGTR)	Rauch	**-**
IIP3	4	9	14	**dBm**
NF	20	16	15	**dB**
Q_{moy}	6	3.7	3	**-**
f_{max}	300	450	240	**MHz**
TR = f_{max}/f_{min}	6	10	6	**-**
Power consumption	7.6	30	155	**mW**
Technology	130nm CMOS	65nm CMOS	0.25µm BiCMOS	**-**
Supply	1.2	2.5	3.3	**V**
Measures / Simu.	Measurements	Simulations	Measurements	**-**
FOM1	***271***	***3100***	***3430***	**-**
FOM2	***35***	***103***	***22***	**-**

It is worth highlighting that *FOM1* is the highest for the Rauch filter. Compared to the literature, the Gm-C filter designed with the MGTR technique also shows a high FOM1. Hence, this means that the Rauch filter exhibits the best RF performances versus selectivity trade-off all over the frequency tuning range.

When taking into account the power consumption, the proposed Gm-C filters shows the best figure. However, process issues when implementing this solution on silicon may strongly degrade the measured results. Reference [VI.1] and the Rauch filter then present comparable FOM2 results. The Rauch filter is optimized in terms of noise and linearity whereas the filter in [VI.1] is optimized for low power consumption. Besides, it has been chosen a 3.3V supply for the Rauch to enhance the input power of the filter while keeping the specified performances. With a 1.2V supply, this input power is then reduced.

Future improvements of the Gm-C would consist in working on the Gm-cell linearity versus noise trade-off. Perspectives on the Rauch filter mainly concern the improvement of the operational amplifier design in order to increase the bandwidth above 30dB voltage gain.

Conclusion and Perspectives

Two fully active frequency tunable bandpass filters have been simulated, and one of them measured. The results presented all along this PhD thesis open the perspective of the full integration of the silicon TV tuner over at least the first two octaves of the VHF band, leading to the emergence of the first fully-integrated silicon TV tuner.

An encouraging perspective for future developments is the study of N-path filters which exhibit a wide tuning range for high RF performances and high selectivity. However, these topologies may require the modification of the front-end architecture of the tuner to be used. This may involve important changes on the specifications of each block constituting the front-end architecture to finally allow reaching targeted tuner NF and harmonic rejection for instance.

Reference

[VI.1] Y. Sun, C. J. Jeong, I. Y. Lee, J. S. Lee, and S. G. Lee, “A 50-300-MHz low power and high linear active RF tracking filter for digital TV tuner ICs,” presented at the Custom Integrated Circuits Conference (CICC), 2010 IEEE, 2010, pp. 1-4.

French Conclusion

Après avoir introduit le contexte de cette thèse ainsi que les spécifications requises en matière de filtrage RF pour un récepteur TV, différentes topologies répondant à ces spécifications ont été étudiées dans une seconde partie. L'objectif a été de trouver laquelle répond le mieux aux besoins de réjections définis en introduction. Il apparaît que la structure passe bande du second ordre est la meilleure. Elle requiert un minimum d'éléments, ce qui la rend intéressante pour l'accord en fréquence. De plus, il est possible de régler le facteur de qualité Q du résonateur utilisé pour le filtrage. Q décrit la sélectivité du filtre et correspond au rapport de la fréquence centrale par la bande passante à -3dB. Plus le facteur de qualité est grand, plus le filtre est sélectif.

Une fois la topologie choisie, une étude de la littérature a été menée pour trouver la solution la plus appropriée pour la réaliser. D'abord, les filtres LC passifs ont été étudiés comme base de comparaison pour les filtres actifs. Une figure de mérite a également été proposé pour réaliser des comparaisons justes avec les résultats de l'état de l'art. En ce qui concerne les structures purement actives, la littérature décrit principalement les filtres Gyrator-C et Gm-C. Les filtres Gyrator-C consistent en fait à émuler un comportement inductif aux fréquences RF grâce à un gyrateur et ainsi de rendre possible le remplacement d'inductance par un remplaçant purement actif. Les filtres Gm-C consistent eux à synthétiser une fonction de transfert par l'intermédiaire d'intégrateurs, et donc de cellules Gm. Pour des topologies relativement simples comme un passe bande du second ordre, ces deux sortes de filtres peuvent mener à une même structure.

La structure du filtre Gm-C est basée sur une analogie avec un résonateur parallèle LC où l'inductance est simplement remplacée par un gyrateur. En réglant la valeur du gyrateur et la capacité qui lui est associée en parallèle, une large plage d'accord en fréquence est obtenue en comparaison d'un filtre LC classique. L'étude théorique des limitations de ce filtres en termes de bruit et de linéarité ont mené au choix d'un factor de qualité modéré car dès que Q augmente, les performances RF sont fortement dégradées. Cette étude montre aussi que de bonnes performances RF sont requises sur les cellules Gm. Il a alors été choisi d'utiliser des valeurs de transconductance de 2.5 et 10mS pour diminuer le bruit de filtre résultant. Cependant, de telles transconductances ont besoin d'être linéarisées pour atteindre les spécifications requises sur les cellules Gm.

Différentes méthodes de linéarisation proposées dans la littérature ont été évaluées. Seules deux présentent un compromis linéarité – bruit intéressant. Ces deux méthodes ont été utilisées pour simuler des filtres en CMOS 65nm. La seconde méthode de linéarisation mène aux meilleurs résultats sur le filtre. Les simulations montrent des résultats encourageants. Pour un facteur de qualité de 4 sur la bande 45-450MHz, le NF est de 16dB et l'IIP3 est supérieur à 8dBm. Cependant cette structure s'avère très sensible à la polarisation ainsi qu'aux variations de procédés, alors qu'une solution robuste est recherchée pour nos applications. C'est pourquoi aucune puce n'a été réalisée.

A partir des designs de filtres Gm-C, il apparaît que la principale source de limitation des performances est le gyrateur. En effet, le signal subit de fortes distorsions et dégradations dans cette structure. L'utilisation à plus hautes fréquences de ces filtres a également été

étudiée. Il s'avère que la linéarité est fortement dégradée dès que la fréquence augmente. Cela est dû à l'utilisation de plus faibles capacités dans les bancs de capacités permettant l'accord en fréquences. En effet, les capacités non-linéaires des commutateurs deviennent alors de moins en moins négligeables en comparaison de la capacité utile. De plus, un facteur de qualité de 4 en UHF ne permet la réjection des canaux adjacent que d'1dB maximum. Enfin, une sélectivité plus importante est requise en UHF mais cela mènerait à l'augmentation du NF du filtre.

Pour dépasser les limitations des filtres Gm-C dues au signal passant dans le gyrateur, des structures à amplificateurs opérationnels ont été investiguées. L'objectif est de profiter du fort gain de boucle et d'un certain filtrage, grâce au réseau RC, au nœud qui correspond à l'entrée du composant actif. Ainsi on a recherché à designer un filtre fortement linéaire tout en ne compromettant pas le bruit.

Cependant les filtres RC sont plus sélectifs à fort gain. Parmi les structures proposées par la littérature, la topologie de Rauch en rétroaction positive présente la meilleure sélectivité pour un gain donné. Sa sensibilité à la valeur des composants passifs est aussi réduite comparée à d'autres structures. Par ailleurs, il a été choisi de limiter à 10dB le gain du filtre, ce qui correspond à un facteur de qualité de 3 en optimisant le dimensionnement du filtre de Rauch. En effet, si le gain du filtre RF était trop important, cela résulterait en de très fortes contraintes de bruit sur l'amplificateur faible bruit situé en amont.

Le filtre de Rauch est stable à condition d'avoir un gain d'amplificateur de tension supérieur à une valeur critique. Cette structure n'est donc a priori pas utilisable ainsi car avec un produit gain – bande passante finie, cette condition n'est plus réalisée. Cependant, une solution originale a été proposée dans ce manuscrit, basée sur un amplificateur non-inverseur pour réaliser le gain en tension. Cette solution innovante empêche le gain en tension ainsi créé de tomber dans la zone d'instabilité. Le filtre a été implémenté en BiCMOS 0.25µm, car le CMOS 65nm ne permet pas d'obtenir un gain d'amplificateur opérationnel assez élevé. Des marges de stabilité ont par ailleurs été prises pour assurer la robustesse du circuit. Le test-chip a ensuite été mesuré au laboratoire.

Les mesures montrent un accord parfait avec les simulations post-layout. Comme spécifié, on obtient un facteur de qualité de 3 pour 10dB de gain sur la bande 45 – 240MHz. Le NF du filtre est de 15dB alors que l'IIP3 est compris entre 19 et 9dBm. La bande d'accord est limitée à 240MHz car la chute de gain de l'amplificateur opérationnel implique une forte dégradation de la linéarité pour des fréquences plus élevées. Comme pour le Gm-C, la sélectivité à plus haute fréquence est trop limitée pour envisager l'élargissement de la bande d'accord.

Ainsi, deux types de filtres ont été proposés pour obtenir une intégration totale de la fonction de filtrage RF d'un récepteur TV. Les résultats obtenus permettent d'envisager l'intégration totale du récepteur TV sur silicium sur au moins les deux premières octaves.

APPENDIX A

A.1 Available Power and Available Gain

In order to define correctly the noise generated by a system, the available power of a certain signal and the available power gain of the system under study [A.1 and A.2].

A.1.a Available Input and Output Powers

Available Input Signal

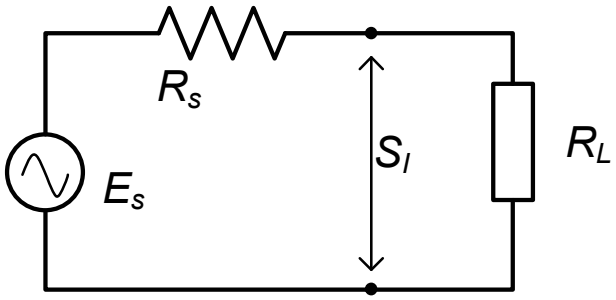

Figure 193. Available Input Signal

The available input signal power S_I is the power that *would* be extracted from a signal source by a load conjugately matched to the output of the source. Figure 193 depicts how this available input signal power can be defined, by means of the formula:

$$S_I = \frac{E_S^2}{4R_S} \qquad \text{(A.1)}$$

S_I only depends on the characteristics of the source. In particular, it is independent of the impedance of the actual load R_L. For a load $R_L \neq R_S$, the delivered power is less than the available power but the available power is still S_I.

Available Output Signal

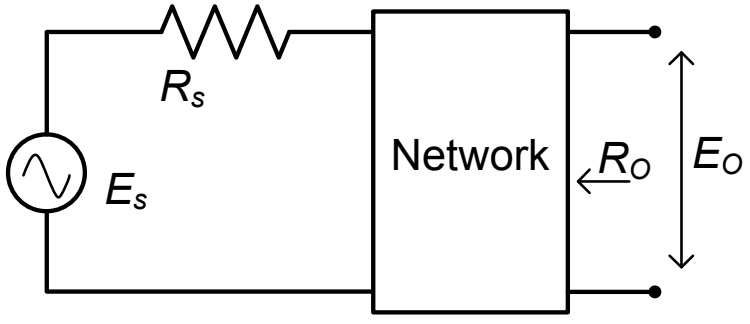

Figure 194. Available Output Signal

The available output signal power S_O is the power that *would* be extracted by a load conjugately matched to the output of the network. Figure 194 illustrates how the available output signal power can be defined, using the formula:

$$S_O = \frac{E_O^2}{4R_O} \qquad \text{(A.2)}$$

It is worth noticing that S_0 only depends on the characteristics of the network and its signal source, and of the impedance match at its input. In particular, S_0 is independent of the load of the network.

A.1.b Available Gain

The available power gain is defined [A.1] by the following formula, which is applicable to both active and passive devices:

$$G = \frac{S_O}{S_I} \tag{A.3}$$

It is worth noticing that G is independent of impedance match at the output, but is dependent on impedance match at the input. As a consequence, the available gain is maximum when the source is matched to the input.

A.2 The Various Origins of Noise

A.2.a Origins of Noise

There are three main origins of noise in electronic systems [A.3].

Thermal noise comes from the thermal Brownian motion of electrons, or any other charged particles, in an electrical component like a resistor for instance. This kind of noise is proportional to the absolute temperature. Indeed, since there would be no motion at the absolute zero temperature, this would mean the absence of noise.

Thermal noise power are given by the following formulas:

$$v_n^2 = 4kTRB \tag{A.4}$$

$$i_n^2 = 4kT\frac{1}{R}B \tag{A.5}$$

where, k is the Boltzmann constant, T the absolute temperature given in Kelvin, B the effective noise bandwidth and R the resistance of the material in Ω.

Shot noise originates from the corpuscular nature of the energy transport. The finite number of charged particles, electrons for example, creates a quantized random current flow which can be described by a Poisson distribution. It can be demonstrated that it gives the following shot noise power:

$$i_n^2 = 2qI_dB \tag{A.6}$$

Flicker noise is a low-frequency phenomenon, also called "1/f noise". It is due to conductivity variations of the material where the current flows, like the presence of contaminants and of defects in the crystal structure of the semiconductor material. The equivalent noise power is given by:

$$i_n^2 = K\frac{I^\alpha}{f^\beta}B \tag{A.7}$$

K being a constant, α and β being coefficients.

A.2.b Available Input and Output Noise Powers

Input noise N_I is defined as the thermal noise generated in the resistance of the signal source. The available noise power from a resistor is then:

$$N_I = \frac{v_n^2}{4R} = kTB \tag{A.8}$$

The available output noise can also be defined and will be referred as N_O in the following.

A.3 Signal-to-Noise Ratio

These different types of noise together create a background noise power. This unwanted noise can degrade or mask a desired signal. To characterize this degradation, the Signal to Noise Ratio, called *SNR* in the following, is defined [A.4]. Taken at the input, the SNR_{in} is defined as the ratio between the available signal power S_I at the input and the available input noise N_I:

$$SNR_{in} = \frac{S_I}{N_I} \tag{A.9}$$

Taken at the output, SNR_{out} is defined as the ratio of the available output power S_O by the available output noise N_O, which includes amplified input noise.

$$SNR_{out} = \frac{S_O}{N_O} \tag{A.10}$$

Hence, signal quality is characterized by the final output SNR. A low SNR_{out} corresponds to a signal strongly corrupted by noise.

A.4 Noise Factor and Noise Figure

The noise factor is defined [A.1] as the ratio of the SNR at the input and of the SNR at the output:

$$F = \frac{S_I / N_I}{S_O / N_O} = \frac{N_O}{GN_I} = \frac{N_O}{GkT_0B} = \frac{GkT_0B + N_R}{GkT_0B} \tag{A.11}$$

where N_R is the noise added by the receiver.

It is worth highlighting that, for the definition of the noise factor, N_I is expressed as:

$$N_I = kT_0B \tag{A.12}$$

where T_0 is a standard temperature which value is 290°K.

In electronics NF, which stands for Noise Figure, is also used. It has the following formula:

$$NF = 10\log(F) \tag{A.13}$$

A.5 Friis' Formula

In case of multistage systems, as it may be seen in Figure 195, the total noise factor can be computed as a function of the noise factors F_i and the gains G_i of each bloc, provided that the chain of quadripoles is conjugately matched at all interfaces. This equation is known as the Friis' formula [A.1].

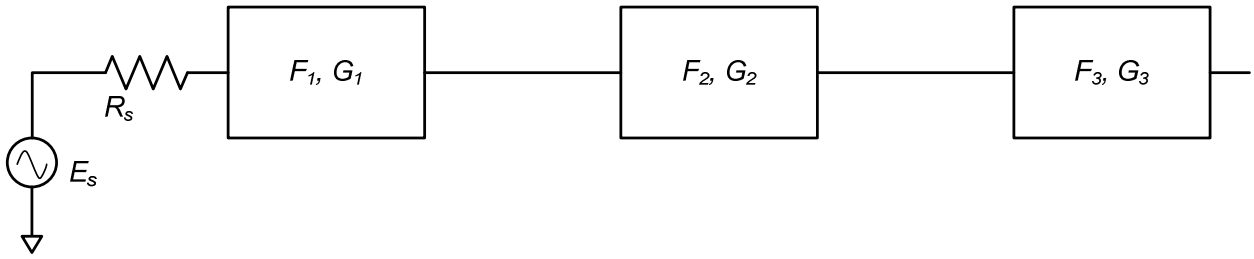

Figure 195. Multistage System

$$F_{total} = F_1 + \frac{F_2 - 1}{G_1} + \frac{F_3 - 1}{G_1 G_2} + \frac{F_4 - 1}{G_1 G_2 G_3} + \ldots \qquad \text{(A.14)}$$

The Friis' formula underlines how critical for noise the first stage of a receiver chain is. Indeed, to lower the total noise factor of the chain, the most efficient solution is to increase the gain and to lower the noise factor of the first stage.

A.6 Noise Measurements

To measure the NF of the filter, the popular ***Y-factor method*** is used [A.5 and A.6]. It consists in using an ENR (Excess Noise Ratio) source. In the present case, a noise diode has been used. It actually is a Zener diode under a high DC voltage (28V). According to the working frequency, the ENR of such a diode is standard and can be found in a table.

The diode is directly connected to the input of the filter as shown in Figure 1. The output of the filter is then connected to the spectrum analyzer.

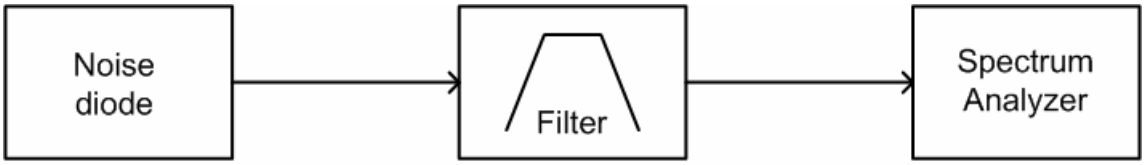

Figure 196. NF Measurement

The noise source is successively turned on and off, by turning on and off the DC voltage. The change in the output noise power density is measured with help of the spectrum analyzer.

The formula to calculate the noise figure is given by:

$$NF = 10\log\left(\frac{10^{\frac{ENR}{10}}}{10^{\frac{Y}{10}}-1}\right) \qquad \text{(A.15)}$$

in which *ENR* is given in a table and *Y* is the difference between the output noise power density when the noise source is on and off.

The major advantage of this technique is that is can measure a wide range a NF in a simple way. It is also able to measure it at any frequency regardless of the device under test gain. However, when measuring very high NF, error could be large.

A.7 References

[A.1] Friis, H.T., Noise Figures of Radio Receivers, Proc. Of the IRE, July 1944, pp 419-422.

[A.2] R.J. Mohr, “Mohr on Receiver Noise, Characterization, Insights and Surprises”, IEEE Microwave Theory & Techniques Society Tutorial, 2010.

[A.3] S. Amiot, “Intégration des Récepteurs TV, du transistor à la télévision”, cours Supélec, 2007.

[A.4] “Fundamentals of RF and Microwave Noise Figure Measurements”, Agilent Technologies, Application Note 57-1, August 2010.

[A.5] “Three Methods of Noise Figure Measurement”, Maxim, application note 2875, Nov. 2003.

[A.6] “Noise Figure Measurement Accuracy – The Y-factor Method”, Agilent Technologies, Application Note 57-2, May 2010.

APPENDIX B

B.1 General Considerations

B.1.a "Single-tone" input signal

Though classical electronic components such as amplifiers are considered as linear elements for small signals, they have non-linear transfer characteristics. On Figure 197 are shown the theoretical transfer characteristic of an amplifier as well as its simulated one. It consists in a linear zone between two saturated portions. Let's consider

$$x(t) = X\cos(\omega t) = X\cos\phi \qquad \text{(B.1)}$$

For $|X| < X_{max}$, the response to a sinusoidal input remains sinusoidal since the transfer characteristic is linear. In the frequency domain, a single frequency tone in both input and output is then obtained.

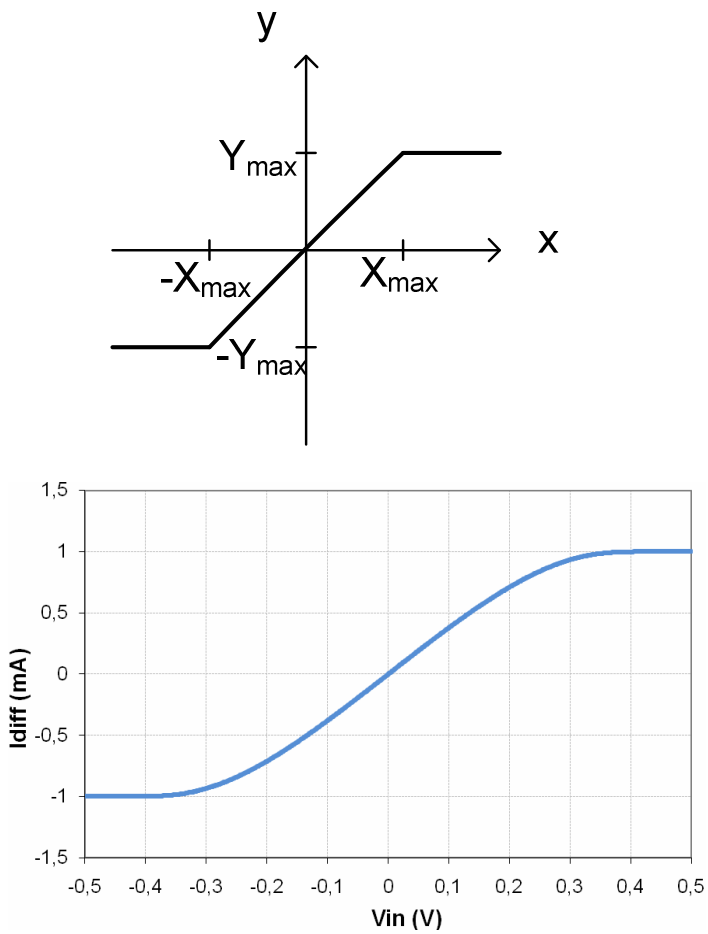

Figure 197. Theoretical and simulated saturated gain of an amplifier

Now, if $|X| > X_{max}$, the input signal will be subject to saturation in the amplifier. The output signal will no longer be sinusoidal since the sine edges are cut. Thus discontinuities will lead to harmonics in the frequency domain. This phenomenon is called ***distortion***.

To estimate the influence of the distortion on a system, let's expand, for small signal, the non-linear response with a Taylor series:

$$y = k_0 + k_1 x + k_2 x^2 + k_3 x^3 + \ldots \quad \text{(B.2)}$$

Introducing the previously defined input signal, we get:

$$y = Y_0 + Y_1 \cos\phi + Y_2 \cos(2\phi) + Y_3 \cos(3\phi) \quad \text{(B.3)}$$

With:

$$Y_0 = k_0 + \frac{1}{2} k_2 X^2 + \ldots \quad \text{(B.4)}$$

$$Y_2 = \frac{1}{2} k_2 X^2 + \ldots \quad \text{(B.5)}$$

$$Y_1 = k_1 X + \frac{3}{4} k_3 X^3 + \ldots \quad \text{(B.6)}$$

$$Y_3 = \frac{1}{4} k_3 X^3 + \ldots \quad \text{(B.7)}$$

If the system were perfectly linear and without offset, only k_1 would remain among all k_is, since this factor corresponds to the gain of the system.

For a non-linear system, the amplitude of the fundamental Y_1 is changed with the addition of a cubic term. Thus Y_1 can be either smaller or larger than that obtained with a linear system. It is referred as an expansive characteristic when $k_3>0$ and to a compressive characteristic when $k_3<0$. Figure 198 shows how compression points are deduced, which correspond to a 1dB deviation of the non-linear characteristic with respect to the linear one.

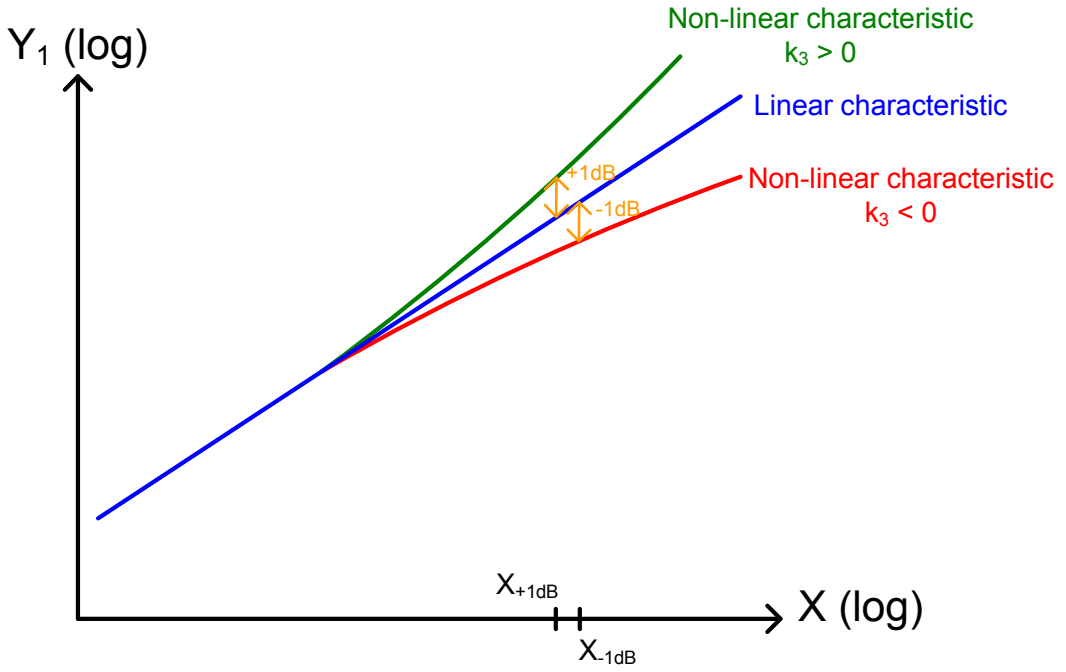

Figure 198. Expansion and compression point at 1dB

B.1.b “Duo-tone” input signal

Now, still considering a non-linear system with the polynomial characteristic defined as:

$$y = k_0 + k_1 x + k_2 x^2 + k_3 x^3 + \ldots \tag{B.8}$$

Assuming the case of a signal composed of ***two sinusoidal waves***:

$$x(t) = X_1 \cos(\omega_1 t) + X_2 \cos(\omega_2 t) = X_1 \cos(\phi_1) + X_2 \cos(\phi_2)\,. \tag{B.9}$$

The output signal is obtained combining these last two equations. Let’s have a look at the result term by term. The linear term is given by:

$$k_1 x = k_1 X_1 \cos(\phi_1) + k_1 X_2 \cos(\phi_2)\,. \tag{B.10}$$

Then, the amplitudes of the sinusoidal waves are merely multiplied by the gain k_1.

$$k_2 x^2 = k_2 \left[X_1 \cos(\phi_1) + X_2 \cos(\phi_2)\right]^2 \tag{B.11}$$

$$k_2 x^2 = k_2 \left[X_1^2 \cos^2(\phi_1) + 2 X_1 X_2 \cos(\phi_1)\cos(\phi_2) + X_2^2 \cos^2(\phi_2)\right] \tag{B.12}$$

Thus,

$$k_2 x^2 = \underbrace{\frac{k_2 X_1^2}{2} + \frac{k_2 X_2^2}{2}}_{\text{constant term}} + \underbrace{\frac{k_2 X_1^2}{2}\cos(2\phi_1) + \frac{k_2 X_2^2}{2}\cos(2\phi_2)}_{\text{second harmonics}} + \underbrace{k_2 X_1 X_2 \left[\cos(\phi_1 + \phi_2) + \cos(\phi_1 - \phi_2)\right]}_{\text{Second order intermodulation products}} \tag{B.13}$$

These different terms are plotted versus frequency in Figure 199.

It is worth noticing that a constant term is present at DC. There are also second order harmonic frequencies, but what is interesting to highlight is the presence of second order intermodulation products. Indeed, the output signal contains two equal amplitude components for which the frequencies are the sum and the difference of the input frequency. They are called ***second order intermodulation products*** *(IM2).*

Now, let's have a look to the cubic term.

$$k_3 x^3 = k_3 \left[X_1 \cos(\phi_1) + X_2 \cos(\phi_2) \right]^3 \tag{B.14}$$

$$k_3 x^3 = k_3 \left[X_1^3 \cos^3(\phi_1) + 3X_1^2 X_2 \cos^2(\phi_1)\cos(\phi_2) + 3X_1 X_2^2 \cos(\phi_1)\cos^2(\phi_2) + X_2^3 \cos^3(\phi_2) \right] \tag{B.15}$$

Thus,

$$\begin{aligned}
k_3 x^3 &= \frac{3k_3}{2}\left(X_1 X_2^2 + \frac{X_1^3}{2} \right)\cos(\phi_1) + \frac{3k_3}{2}\left(X_1^2 X_2 + \frac{X_2^3}{2} \right)\cos(\phi_2) \quad \Big\} \text{ fundamental} \\
&+ \frac{k_3 X_1^3}{4}\cos(3\phi_1) + \frac{k_3 X_2^3}{4}\cos(3\phi_2) \quad \Big\} \text{ 3rd harmonics} \\
&+ \frac{3k_3 X_1^2 X_2}{4}\left[\cos(2\phi_1 + \phi_2) + \cos(2\phi_1 - \phi_2) \right] \\
&+ \frac{3k_3 X_1 X_2^2}{4}\left[\cos(2\phi_2 + \phi_1) + \cos(2\phi_2 - \phi_1) \right] \quad \Big\} \text{ 3rd order IM products}
\end{aligned} \tag{B.16}$$

These different terms are also plotted versus frequency in Figure 199.

This latter equation clearly shows that third order non-linearity produces a fundamental component as well as third order harmonic frequencies. Moreover, we can notice the presence of ***third order intermodulation products*** at $2f_1 + f_2$, $2f_2 + f_1$, $2f_1 - f_2$ and $2f_2 - f_1$.

When f_1 and f_2 are close, the components at frequencies $2f_1 - f_2$ and $2f_2 - f_1$ can be particularly bothersome because they are very close to initial frequencies.

Figure 199 illustrates the spectrum which is composed of second and third order intermodulation products and also of harmonic frequencies.

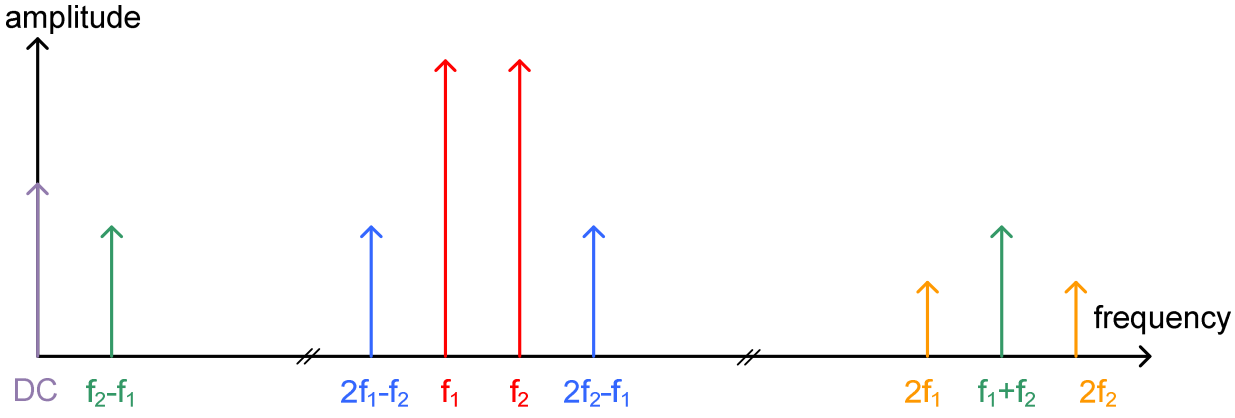

Figure 199. Output spectrum of a two-tone input signal transformed by a non-linear system

B.1.c Intercept Point Definition

Now let's consider the case where $X_1 = X_2 = V_{in}$. The average input power P_{in} and its corresponding level are given by [B.1]:

$$L_{in} = 10\log\left(\frac{P_{in}}{1mW}\right) = 10\log\left(\frac{V_{in}^2}{2R_{in}1mW}\right). \quad \text{(B.17)}$$

Given the gain G of the system, the output level of the linear term is equal to:

$$L_{out1} = 10\log\left(\frac{P_{out1}}{1mW}\right) = 10\log\left(\frac{GP_{in}}{1mW}\right) = L_{in} + G_{dB}. \quad \text{(B.18)}$$

Now, given that:

$$G = \frac{V_{out}^2}{2R_L}.\frac{2R_{in}}{V_{in}^2} = \frac{(k_1 V_{in})^2}{V_{in}^2}\frac{R_{in}}{R_L} = k_1^2.\frac{R_{in}}{R_L}. \quad \text{(B.19)}$$

The amplitude of the third order intermodulation product leads to the following average output power:

$$P_{out3} = \frac{\left(\frac{3}{4}k_3 V_{in}^3\right)^2}{2R_L}. \quad \text{(B.20)}$$

Doing some calculations, one can obtain:

$$L_{out3} = 10\log\left(\frac{\left(\frac{3}{4}k_3 V_{in}^3\right)^2}{2R_L.1mW}\right) = 3L_{in} + K_{dB}, \quad \text{(B.21)}$$

K_{dB} being a constant term.

L_{out1} and L_{out3} as a function of L_{in} are plotted on Figure 200. Because of compression and higher-order IM products, the intercept point (IP3) between the two curves is theoretical. However, the fictive intercept point can be projected on the abscissa (giving the input IP3 called *IIP3*) or on the ordinates (leading to the output IP3 called *OIP3*).

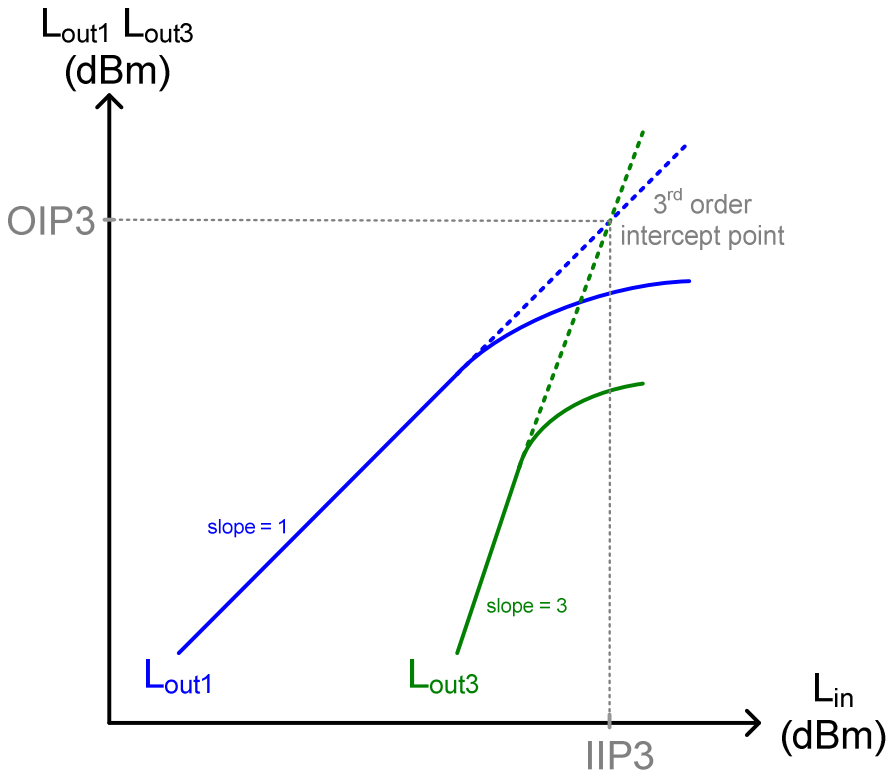

Figure 200. Third order intercept points definitions

The second order intercept point (IP2) can be defined in the same manner, with a slope equals to 2. IIP2 and OIP2 are the equivalent of IIP3 and OIP3.

B.1.d Example

Let's consider a differential pair made with bipolar transistors as depicted in Figure 201.

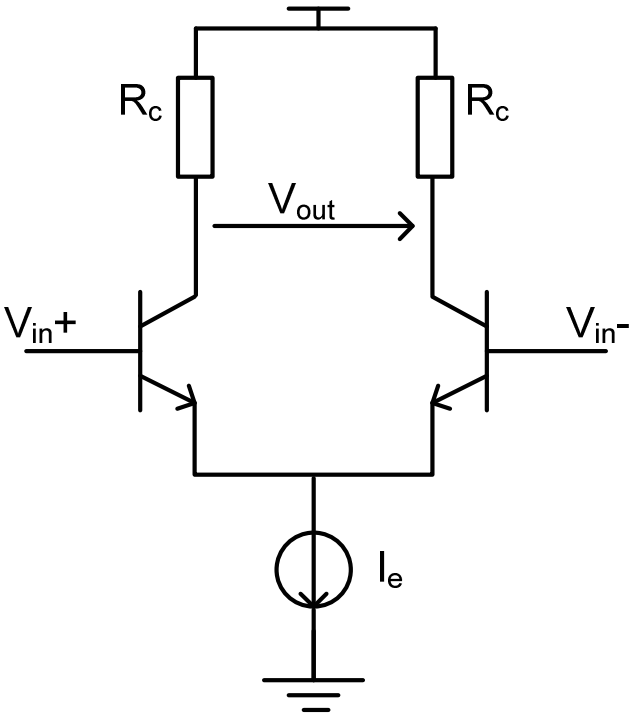

Figure 201. Differential pair

The output voltage is then given by :

$$V_{out} = RI_e \tanh\left(\frac{V_{in}}{2U_T}\right) \tag{B.22}$$

Developing this expression leads to:

$$V_{out} = RI_e\left(\frac{V_{in}}{2U_T} - \frac{V_{in}^3}{24U_T^3}\right) \tag{B.23}$$

Hence,

$$k_1 = \frac{R_c I_e}{2U_T} \tag{B.24}$$

$$k_3 = -\frac{R_c I_e}{24U_T^3} \tag{B.25}$$

Thus, one gets:

$$IIP3 = \sqrt{\frac{4}{3}\left|\frac{k_1}{k_3}\right|} = 4U_T \tag{B.26}$$

B.2 RF Filter Linearity Measurements

In the following, it is assumed that the RF filter has a unity gain. If it were not the case, intercept point values would have to be corrected by the gain of the filter. This chapter aims at presenting how linearity has been measured in the laboratory [B.2].

B.2.a In-band IIP3 measurement

To measure the in-band input referred third order intercept point, two closely-spaced tones are applied within the bandwidth of the filter. As explained, these two tones create intermodulation products. IIP3 can then be related to the difference between the wanted signal level and the intermodulation products levels by the following equation:

$$IIP3 = \frac{IMR_3}{2} + P_{in\_2tones} \qquad \text{(B.27)}$$

where P_{in_2tones} is the power level of the two applied tones.

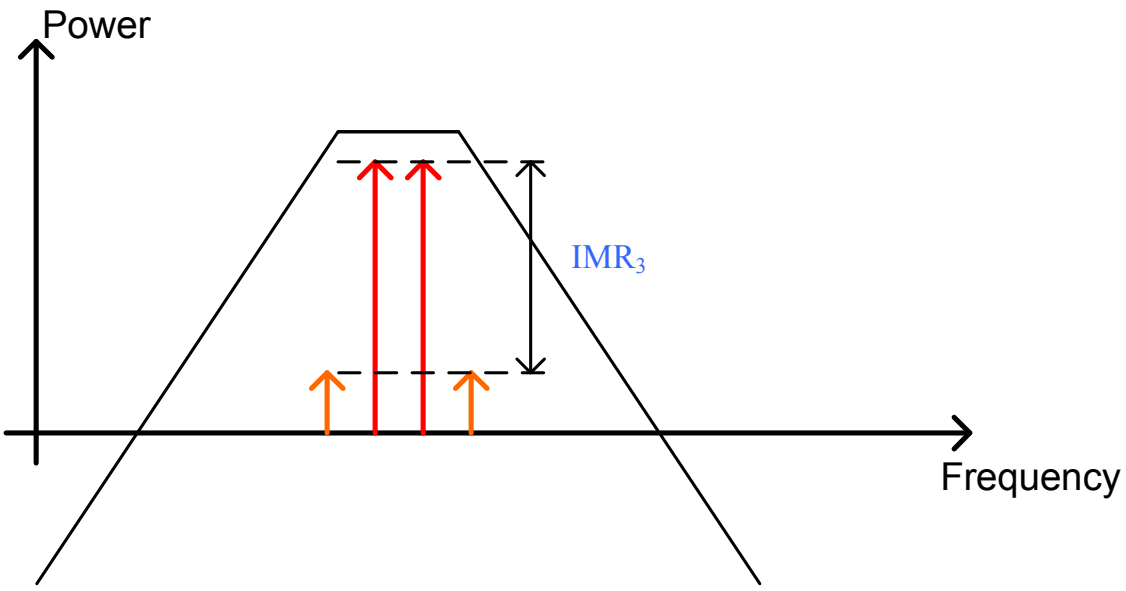

Figure 202. Measurement of the in-band IIП3

B.2.b Out-of-band IIP3 measurement

To measure the out-of-band input referred third order intercept point, two tones are applied at high frequencies (f_1 and f_2), close to one another. The RF filter is centred on the wanted signal at f_{wanted}. The two far-away tones transfer some modulation to the wanted signal, which will result in two tones close to f_{wanted} and on each side of it. As before, the IIP3 can be related to the difference between the wanted signal level and the modulated tone.

$$IIP3 = \frac{\Delta X_{\text{mod}} + 6}{2} + P_{in\_unwanted} \tag{B.28}$$

where $P_{in\_unwanted}$ is the power level of the two applied tones.

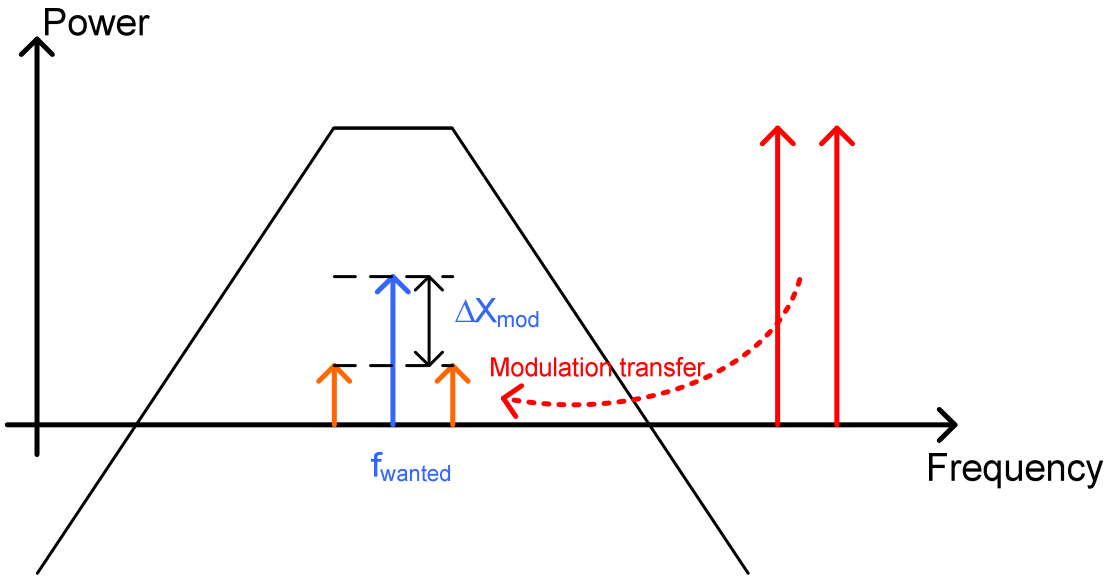

Figure 203. Measurement of the out-of-band IIП3

B.2.c IIP2 measurement

To measure the input referred second order intercept point, two tones are applied at low (f_1) and high (f_2) frequencies. The RF filter is centred on f_{wanted}, and the tones frequencies are chosen so that the intermodulation product (at f_2-f_1) is very close to the wanted signal. A quite low power level of the wanted signal is chosen in order to allow a good measurement of the second order intermodulation ratio IMR_2, depicted on Figure 204, which is the level difference between the level of the intermodulation product and the level of the wanted channel. The IMR_2 level is related to the two interferer tones levels, which have to be specified.

There is a direct relation between IMR_2 and IIP2:

$$IIP2 = IMR_2 + P_{in\_wanted}\,, \tag{B.29}$$

where $P_{InputTone}$ is the input tone power level.

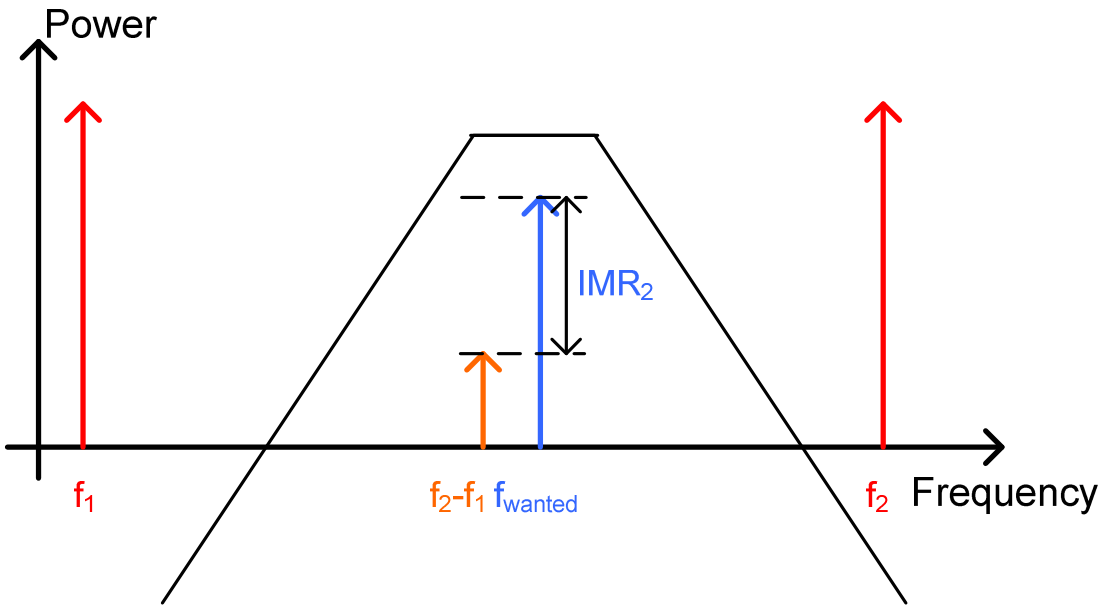

Figure 204. Measurement of IMR_2

B.3 References

[B.1] C. Dehollain, *RF Electronics lecture*, EPFL, 2008.

[B.2] K. Kundert, “Accurate and Rapid Measurement of IP2 and IP3”, The Designers Guide Community, *www.designersguide.org*.

APPENDIX C

The following tables sum up the main characteristics of tunable filters found in the literature. They have been sorted chronologically and references are given further.

Note that in the column nature of the filter, the acronyms FD stands for “fully-differential”, SS for “single to single” and PD for “pseudo-differential”.

If a case is left blank in the table, no description/indication is given in the paper.

C.1 Gyrator-C filtering

year	Ref.	f0 (MHz)	BW (MHz)	Q	gain (dB)	Order	IIP3 (dBm)	NF (dB)	techno	node (µm)	conso (mW)	nature	supply V	realization
2000	[C.1]	625 - 1680		~ 33	35		-30	5,5	CMOS	0,5	24,3	SS		simu
2000	[C.1]	625 - 1680		12 - 300	31,4	2	-31	5,5	CMOS	0,5	24,3	SS		simu
2000	[C.2]	720 - 1030		~ 31	20	2	-30		CMOS	0,35	12	FD	2	simu
2002	[C.3]	2400 - 2600	20 - 200	~ 36		4	6,2	47	CMOS	0,35	1	FD	2	simu
2002	[C.3]	2400 - 2600	20 - 200	~ 70		6	-8,75	48	CMOS	0,35	1	FD	2	simu
2003	[C.4]	400 - 1100		2 - 80	-15	2	-15	32	CMOS	0,35		FD		chip
2004	[C.5]	400 - 1100		2 - 80	-15	2	-15	32	CMOS	0,35		FD		chip
2005	[C.6]	1600 - 2450	12 - 80	30 - 200		4	-4		CMOS	0,25	5,1	FD	1,8	simu
2005	[C.7]	1800 - 2450	12 - 80	30 - 200		4	-4		CMOS	0,25				
2005	[C.8]	400 - 2400	20 - 300	50 - 125	40	4			CMOS	0,25	4,5	SS	2,5	simu

year	Ref.	f0 (MHz)	BW (MHz)	Q	gain (dB)	Order	IIP3 (dBm)	NF (dB)	techno	node (µm)	conso (mW)	nature	supply V	realization
2006	[C.9]	500 - 1300	11,5	~ 60	1	2	-26	8,5	CMOS	0,35	274	SS	5	simu
2006	[C.10]	880 - 3720				2			CMOS	0,18	26			simu
2006	[C.11]	700 - 2000	~ 65	22 - 53	20	2		6	BiCMOS	0,25	81	FD	2,7	simu
2007	[C.12]	2000 - 2900		~ 80		2			CMOS	0,18	4	SS	1,5	
2008	[C.13]	600 - 2400		6 - 2000		2			CMOS	0,18	1	FD	1,8	simu
2008	[C.14]	600 - 2400		6 - 2000		2			CMOS	0,18	1	FD	1,8	simu
2008	[C.15]	880 - 1100	~ 20			2		17	BiCMOS					simu
2008	[C.16]	1920 - 3820	~ 60		6	2		18	CMOS	0,18	10,8		1,8	chip

C.2 Gm-C Filtering

year	Ref.	f0 (MHz)	BW (MHz)	Q	gain (dB)	Order	IIP3 (dBm)	NF (dB)	techno	node (µm)	conso (mW)	nature	supply V	realization
1999	[C.17]	559 - 970		1,2-400	15,7		-12,4	6	CMOS	0,5	52,5	SS		simu
1999	[C.18]	10 - 100							BiCMOS	0,29				
2000	[C.19]	3.5 - 70	0,2	150		6	-10	17	CMOS		120		2,5	chip
2000	[C.20]	400 - 2300	250	5	-20		-12	15	BiCMOS		65	FD	5	chip
2001	[C.21]	54 - 74		60		4	-9,25		CMOS	0,35				chip
2001	[C.22]	6 - 15		50					CMOS	0,8			1,4	chip
2001	[C.23]	0,05 - 2,1			0,6	3			CMOS	0,8	1,73	FD	1,8	chip
2002	[C.24]	80 - 200				4			CMOS	0,35				chip
2003	[C.25]	1,5 - 12				6	7,2		CMOS	0,18	15	FD	1,8	Chip
2004	[C.26]	0,3 - 32		4-500			8		CMOS	0,8			2	Chip
2005	[C.27]	1 - 100			13,5	6	2	17,0	CMOS	0,09	13,5			
2005	[C.28]	42 - 215				3			CMOS	0,35	3,8	PD	2	simu
2005	[C.29]	10 - 126		6	0	2			CMOS	0,18	5,2		1,8	simu

year	Ref.	f0 (MHz)	BW (MHz)	Q	gain (dB)	Order	IIP3 (dBm)	NF (dB)	techno	node (µm)	conso (mW)	nature	supply V	realization
2005	[C.30]	1,5 - 50				5			CMOS	0,25			3,3	simu
2008	[C.31]	287 - 860	15		10	8	7	30	CMOS	0,13	8,6	FD		simu
2008	[C.31]	48 - 287	11		10	2	7	30	CMOS	0,13	8,6	FD		simu
2009	[C.32]	50 - 300			0	3	16,9	14	CMOS	0,18	72	FD	1,8	chip
2010	[C.33]	70 - 280			0				CMOS	0,13	21	FD	1,5	chip
2010	[C.34]	50 - 300	8 - 50		6	2	5	20	CMOS	0,13	7,6	FD	1,2	chip
2011	[C.35]	48 - 780	15 - 60	3-13		8	-5	24	CMOS	0,13	36	FD	1,2	chip

C.3 Rm-C filtering

year	Ref.	f0 (MHz)	BW (MHz)	Q	gain (dB)	Order	IIP3 (dBm)	NF (dB)	techno	node (µm)	conso (mW)	nature	supply V	realization
1995	[C.36]	124 - 218,7		~ 2,5					CMOS		9,44	FD	2,5	
2001	[C.37]	41 - 178			20	2	-5	15	CMOS	0,5	14	FD	2	chip

C.4 LC filtering with passive components

year	Ref.	f0 (MHz)	BW (MHz)	Q	gain (dB)	Order	IIP3 (dBm)	NF (dB)	techno	node (µm)	conso (mW)	nature	supply V	realization	inductor
1999	[C.38]	895 - 995		~ 25		2		5,9	CMOS	0,6	9,3	SS	2,7	chip	
2002	[C.39]	700 - 1200				2			BiCMOS	0,8	9		2		
2003	[C.40]	1940 - 2210	~ 53,8	~ 40		2			CMOS	0,35	5		1,3	chip	spiral
2004	[C.41]	980 - 1090		5 - 180	16	2		13	CMOS	0,35	15,5	SS		chip	spiral
2005	[C.42]	2100 - 3500	~ 148				1	15	CMOS	0,18	12,7		1,8	simu	
2007	NXP Hybrid+	42 - 870				2	10	8	BiCMOS						discrete
2010	[C.43]														

C.5 References

C.5.a Gyrator-C filtering

[C.1] Y. Chang, J. Choma, and J. Wills, "The design and analysis of a RF CMOS bandpass filter," *Circuits and Systems, 2000. Proceedings. ISCAS 2000 Geneva. The 2000 IEEE International Symposium on*, 2000, pp. 625-628 vol.2.

[C.2] Yue Wu, M. Ismail, and H. Olsson, "A novel CMOS fully differential inductorless RF bandpass filter," *Circuits and Systems, 2000. Proceedings. ISCAS 2000 Geneva. The 2000 IEEE International Symposium on*, 2000, pp. 149-152 vol.4.

[C.3] A. Thanachayanont, "Low voltage low power CMOS inductorless RF bandpass filter with high image rejection capability," *Circuits and Systems, 2002. MWSCAS-2002. The 2002 45th Midwest Symposium on*, 2002, pp. III-548-51 vol.3.

[C.4] Yue Wu, Xiaohui Ding, M. Ismail, and H. Olsson, "RF bandpass filter design based on CMOS active inductors," *Circuits and Systems II: Analog and Digital Signal Processing, IEEE Transactions on*, vol. 50, 2003, pp. 942-949.

[C.5] Yue Wu, Xiaohui Ding, M. Ismail, and H. Olsson, "CMOS active inductor and its application in RF bandpass filter," *Radio Frequency Integrated Circuits (RFIC) Symposium, 2004. Digest of Papers. 2004 IEEE*, 2004, pp. 655-658.

[C.6] Zhiqiang Gao, Mingyan Yu, Yizheng Ye, and Jianguo Ma, "Wide Tuning Range of A CMOS RF Bandpass Filter For Wireless Applications," *Electron Devices and Solid-State Circuits, 2005 IEEE Conference on*, 2005, pp. 53-56.

[C.7] Zhiqiang Gao, Jianguo Ma, Mingyan Yu, and Yizheng Ye, "A CMOS RF tuning wide-band bandpass filter for wireless applications," *SOC Conference, 2005. Proceedings. IEEE International*, 2005, pp. 79-80.

[C.8] Zhiqiang Gao, Jianguo Ma, Yizheng Ye, and Mingyan Yu, "Large tuning band range of high frequency filter for wireless applications," *Circuits and Systems, 2005. ISCAS 2005. IEEE International Symposium on*, 2005, pp. 384-387 Vol. 1.

[C.9] V. Stornelli, G. Ferri, G. Leuzzi, and A. De Marcellis, "A tunable 0.5-1.3 GHz CMOS 2nd order bandpass filter with 50Ω input-output impedance matching," *Circuits and Systems, 2006. ISCAS 2006. Proceedings. 2006 IEEE International Symposium on*, 2006, p. 4 pp.

[C.10] K. Allidina and S. Mirabbasi, "A widely tunable active RF filter topology," *Circuits and Systems, 2006. ISCAS 2006. Proceedings. 2006 IEEE International Symposium on*, 2006, p. 4 pp.

[C.11] Z. Sassi, "Etude et Conception De Structures De Filtrage Actif Radiofréquence Intégrées En Technologie CMOS et BiCMOS pour application à la téléphonie cellulaire", Université de Limoges, école doctorale science technologie santé, faculté des sciences et techniques, 2006.

[C.12] R. Weng and R. Kuo, "An ω0-Q Tunable CMOS Active Inductor for RF Bandpass Filters," *Signals, Systems and Electronics, 2007. ISSSE '07. International Symposium on*, 2007, pp. 571-574.

[C.13] C. Andriesei, L. Goras, and B. Delacressoniere, "Active RF bandpass filter with wide frequency tuning range," *Semiconductor Conference, 2008. CAS 2008. International*, 2008, pp. 397-400.

[C.14] C. Andriesei, L. Goras, and F. Temcamani, "Negative resistance based tuning of an RF bandpass filter," *Circuits and Systems for Communications, 2008. ECCSC 2008. 4th European Conference on*, 2008, pp. 83-86.

[C.15] S. Del Re, G. Leuzzi, and V. Stornelli, "A new approach to the design of high dynamic range tunable active inductors," *Integrated Nonlinear Microwave and Millimetre-Wave Circuits, 2008. INMMIC 2008. Workshop on*, 2008, pp. 25-28.

[C.16] Zhiqiang Gao, Jianguo Ma, Mingyan Yu, and Yizheng Ye, "A Fully Integrated CMOS Active Bandpass Filter for Multiband RF Front-Ends," *Circuits and Systems II: Express Briefs, IEEE Transactions on*, vol. 55, 2008, pp. 718-722.

C.5.b Gm-C filtering

[C.17] Yuyu Chang, J. Choma, and J. Wills, "A 900 MHz active CMOS LNA with a bandpass filter," *Mixed-Signal Design, 1999. SSMSD '99. 1999 Southwest Symposium on*, 1999, pp. 33-36.

[C.18] N. Rao, V. Balan, R. Contreras, J. Chern, and Y. Wang, "A 150 MHz continuous-time seventh order 0.05° equiripple linear phase filter," *Circuits and Systems, 1999. ISCAS '99. Proceedings of the 1999 IEEE International Symposium on*, 1999, pp. 664-666 vol.2.

[C.19] J. van der Tang, D. Kasperkovitz, and A. Bretveld, "A 65 mW, 0.4-2.3 GHz bandpass filter for satellite receivers," *Custom Integrated Circuits Conference, 2000. CICC. Proceedings of the IEEE 2000*, 2000, pp. 383-386.

[C.20] Y. Choi and H. Luong, "A high-Q and wide-dynamic-range CMOS IF bandpass filter for monolithic receivers," Circuits and Systems, 2000. Proceedings. ISCAS 2000 Geneva. The 2000 IEEE International Symposium on, 2000, pp. 144-147 vol.2.

[C.21] H. Elhallabi, Y. Fouzar, and M. Sawan, "High frequency CMOS Gm-C bandpass filter with automatic on-chip tuning," *Electronics, Circuits and Systems, 2001. ICECS 2001. The 8th IEEE International Conference on*, 2001, pp. 823-826 vol.2.

[C.22] F. Munoz, A. Torralba, R. Carvajal, and J. Ramirez-Angulo, "Tunable CMOS low-voltage linear transconductor and its application to HF GM-C filter design," *Circuits and Systems, 1999. 42nd Midwest Symposium on*, 1999, pp. 826-829 vol. 2.

[C.23] J. De Lima and C. Dualibe, “A linearly tunable low-voltage CMOS transconductor with improved common-mode stability and its application to gm-C filters,” *Circuits and Systems II: Analog and Digital Signal Processing, IEEE Transactions on*, vol. 48, 2001, pp. 649-660.

[C.24] Mingdeng Chen, J. Silva-Martinez, S. Rokhsaz, and M. Robinson, “A 2-Vpp 80-200-MHz fourth-order continuous-time linear phase filter with automatic frequency tuning,” *Solid-State Circuits, IEEE Journal of*, vol. 38, 2003, pp. 1745-1749.

[C.25] Shinichi Hori, Tadashi Maeda, hitoshi Yano, Noriaki Matsuno, Keiichi Numata, Nobuhide Yoshida, Yuji Takahashi, Tomoyuki Yamase, R. Walkington, and H. Hikaru, “A widely tunable CMOS Gm-C filter with a negative source degeneration resistor transconductor,” *Solid-State Circuits Conference, 2003. ESSCIRC '03. Proceedings of the 29th European*, 2003, pp. 449-452.

[C.26] R. Carvajal, J. Galan, A. Torralba, F. Munoz, and J. Ramirez-Angulo, “1.33 mW, 2 V CMOS continuous-time bandpass filter with two decades of centre frequency tuning range and high Q,” *Circuits, Devices and Systems, IEE Proceedings* -, vol. 152, 2005, pp. 456-464.

[C.27] M. Elmala, B. Carlton, R. Bishop, and K. Soumyanath, “A highly linear filter and VGA chain with novel DC-offset correction in 90nm digital CMOS process,” *VLSI Circuits, 2005. Digest of Technical Papers. 2005 Symposium on*, 2005, pp. 302-303.

[C.28] A. Otin, C. Aldea, and S. Celma, “Low voltage LC-ladder Gm-C low-pass filters with 42-215 MHz tunable range,” *Circuit Theory and Design, 2005. Proceedings of the 2005 European Conference on*, 2005, pp. I/245-I/248 vol. 1.

[C.29] E. Lebel, A. Assi, and M. Sawan, “Field programmable Gm-C array for wide frequency range bandpass filter applications,” *Circuits and Systems, 2005. ISCAS 2005. IEEE International Symposium on*, 2005, pp. 1952-1955 Vol. 3.

[C.30] T. Tanaka, Sungwoo Cha, S. Shimizu, T. Ida, H. Ishihara, T. Matsuoka, K. Taniguchi, A. Sugimori, and H. Hihara, “A widely tunable Gm-C filter using tail current offset in two differential pairs,” *Circuits and Systems, 2005. ISCAS 2005. IEEE International Symposium on*, 2005, pp. 812-815 Vol. 1.

[C.31] Y. Sun, J. Lee, and S. Lee, “On-chip Active RF Tracking Filter with 60dB 3rd-order Harmonic Rejection for Digital TV tuners,” 2008.

[C.32] Kuduck Kwon, Hong-Teuk Kim, and Kwyro Lee, “A 50–300-MHz Highly Linear and Low-Noise CMOS $Gm{hbox{-}}C$ Filter Adopting Multiple Gated Transistors for Digital TV Tuner ICs,” *Microwave Theory and Techniques, IEEE Transactions on*, vol. 57, 2009, pp. 306-313.

[C.33] W. Li, H. Yumei, and H. Zhiliang, “70-280 MHz 21 mW 53 dB SFDR Gm-C filter,” *Electronics Letters*, vol. 46, no. 17, pp. 1187 -1188, Aug. 2010.

[C.34] Y. Sun, C. J. Jeong, I. Y. Lee, J. S. Lee, and S. G. Lee, “A 50-300-MHz low power and high linear active RF tracking filter for digital TV tuner ICs,” *Custom Integrated Circuits Conference (CICC)*, 2010 IEEE, 2010, pp. 1-4.

[C.35] Y. Sun, C. J. Jeong, S. K. Han, and S. G. Lee, “CMOS on-chip active RF tracking filter for digital TV tuner ICs,” *Electronics Letters*, vol. 47, no. 6, pp. 407-409, Mar. 2011.

C.5.cRm-C filtering

[C.36] P. Lu, C. Wu, and M. Tsai, “VHF bandpass filter design using CMOS transresistance amplifiers ,” *Circuits and Systems, 1993., ISCAS '93, 1993 IEEE International Symposium on*, 1993, pp. 990-993 vol.2.

[C.37] Y. Cheng, J. Gong, and C. Wu, “New CMOS 2 V low-power IF fully differential Rm-C bandpass amplifier for RF wireless receivers,” *Circuits, Devices and Systems, IEE Proceedings* -, vol. 148, 2001, pp. 318-322.

C.5.d LC filtering with passive components

[C.38] S. Bantas, Y. Papananos, and Y. Koutsoyannopoulos, “CMOS tunable bandpass RF filters utilizing coupled on-chip inductors,” *Circuits and Systems, 1999. ISCAS '99. Proceedings of the 1999 IEEE International Symposium on*, 1999, pp. 581-584 vol.2.

[C.39] A. Worapishet, S. Ninyawee, and M. Chongcheawchamnan, “Enhanced tuneable coupled inductor for ultra-wide variable centre frequency LC filters,” *Circuits and Systems, 2002. APCCAS '02. 2002 Asia-Pacific Conference on*, 2002, pp. 355-358 vol.1.

[C.40] F. Dulger, E. Sanchez-Sinencio, and J. Silva-Martinez, “A 1.3-V 5-mW fully integrated tunable bandpass filter at 2.1 GHz in 0.35-μm CMOS,” *Solid-State Circuits, IEEE Journal of*, vol. 38, 2003, pp. 918-928.

[C.41] S. Bantas and Y. Koutsoyannopoulos, “CMOS active-LC bandpass filters with coupled-inductor Q-enhancement and center frequency tuning,” *Circuits and Systems II: Express Briefs, IEEE Transactions on*, vol. 51, 2004, pp. 69-76.

[C.42] J. Nakaska and J. Haslett, “A CMOS quality factor enhanced parallel resonant LC-tank with independent Q and frequency tuning for RF integrated filters,” *System-on-Chip for Real-Time Applications, 2005. Proceedings. Fifth International Workshop on*, 2005, pp. 96-100.

[C.43] Y. Kanazawa, Y. Fujimoto, and K. Iizuka, “A 130M to 1GHz digitally tunable RF LC-tracking filter for CMOS RF receivers,” pp. 469-472, Nov. 2008.

APPENDIX D

D.1 MOS Differential Pair

The following study is based on computations that may be found in [D.1] and [D.2].

D.1.a Transfer Characteristic

Let's consider the MOS differential pair depicted in Figure 205. It is also assumed that M_1 and M_2 are in the strong inversion regime and in saturation mode.

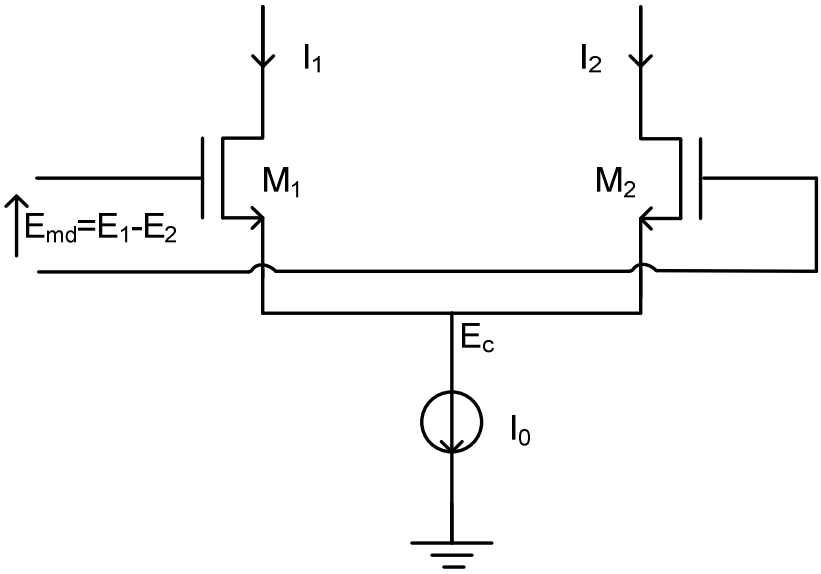

Figure 205. Simplified Transconductor

Assuming that

$$\beta = \mu C_{ox} \frac{W}{L} \tag{D.1}$$

and the same β for M_1 and M_2, currents I_1 and I_2 are given by:

$$I_1 = \frac{1}{2}\beta\left(E_1 - E_c - V_{th}\right)^2 \tag{D.2}$$

$$I_2 = \frac{1}{2}\beta\left(E_2 - E_c - V_{th}\right)^2 \tag{D.3}$$

Hence,

$$\sqrt{I_1} = \sqrt{\frac{1}{2}\beta}\left(E_1 - E_c - V_{th}\right) \tag{D.4}$$

$$\sqrt{I_2} = \sqrt{\frac{1}{2}\beta}\left(E_2 - E_c - V_{th}\right) \tag{D.5}$$

It is also considered the differential current I_{md}, defined as follows:

$$I_{md} = I_{d1} - I_{d2} \tag{D.6}$$

$$I_{d1} = \frac{I_0 + I_{md}}{2} \tag{D.7}$$

$$I_{d2} = \frac{I_0 - I_{md}}{2} \tag{D.8}$$

Given that the differential input voltage is

$$E_{md} = E_1 - E_2, \tag{D.9}$$

this gives:

$$\sqrt{I_1} - \sqrt{I_2} = E_{md}\sqrt{\frac{1}{2}\beta} \tag{D.10}$$

$$I_1.I_2 = \frac{1}{4}\left(I_0^2 - I_{md}^2\right) \tag{D.11}$$

Now, let's consider

$$\left(\sqrt{I_1} - \sqrt{I_2}\right)^2 = I_1 + I_2 - 2\sqrt{I_1}\sqrt{I_2} = I_0 - 2\sqrt{I_1}\sqrt{I_2} \tag{D.12}$$

Combining last three equations, one gets:

$$\left(E_{md}\sqrt{\frac{1}{2}\beta}\right)^2 = I_0 - \sqrt{I_0^2 - I_{md}^2} \tag{D.13}$$

Then,

$$\left(I_0 - \left(E_{md}\sqrt{\frac{1}{2}\beta}\right)^2\right)^2 = I_0^2 - I_{md}^2 \tag{D.14}$$

Developing this expression leads to:

$$\boxed{I_{md} = \frac{1}{2}\beta E_{md}\sqrt{\frac{4I_0}{\beta} - E_{md}^2}} \tag{D.15}$$

Hence, for small signals, the transconductance can be approximated to:

$$g_m \approx \beta(V_{GS} - V_{th}) \tag{D.16}$$

D.1.b Linearity Computation

Normalizing the latter equation to the effective gate voltage, defined as

$$X = \frac{E_{md}}{\sqrt{\frac{I_0}{\beta}}} = \frac{E_{md}}{V_{GS} - V_{th}}, \tag{D.17}$$

one gets

$$\boxed{y = \frac{I_{md}}{I_0} = X\sqrt{1 - \frac{X^2}{4}}} \tag{D.18}$$

for $|X| \leq \sqrt{2}$.

Hence, developing up to the third order, this leads to

$$y \approx X - \frac{X^3}{8}. \tag{D.19}$$

Thus, it gives:

$$\frac{\partial^3 y}{\partial X^3} = -\frac{3}{4}. \tag{D.20}$$

To compute *IIP3*, it is needed:

$$IM3 = \frac{g_3}{g_1} = \frac{3}{32}X^2. \tag{D.21}$$

Given that

$$IIP3 = \frac{V_{in}}{\sqrt{IM3}}, \tag{D.22}$$

one obtains:

$$\boxed{IIP3 = 4\sqrt{\frac{2}{3}}(V_{GS} - V_{th})} \tag{D.23}$$

D.2 MOS Degenerated Common-Source Circuit

Figure 206 depicts the schematic of a degenerated MOS transistor. The equivalent transconductance of this stage is given by [D.1]:

$$g_{m,eq} = \frac{g_m}{1 + Z_{\deg}\left(g_m + \frac{1}{r_0}\right)} \approx \frac{1}{Z_{\deg}} \text{ if } Z_{deg} \text{ is large enough} \tag{D.24}$$

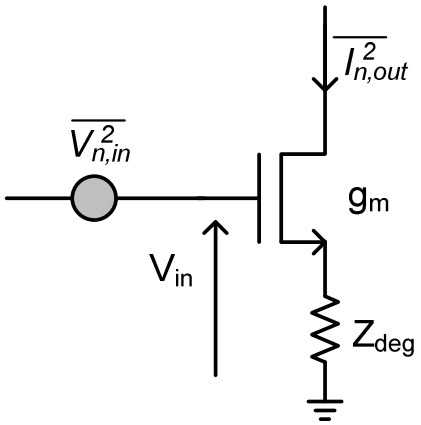

Figure 206. Degenerated MOS transistor

The equivalent input noise power of such a circuit can be computed. First let's compute the output noise current, which is:

$$I_{n,out} = \frac{g_m V_n}{1 + g_m Z_{\deg}} \tag{D.25}$$

Now, assuming only thermal noise, one can obtain :

$$\overline{V}_{n,in}^2 = 4kT\frac{2}{3g_m}\left(1 + g_m Z_{\deg}\right) \tag{D.26}$$

Hence, noise increases as Z_{deg} increases.

D.3 Linearity Enhancement of an Emitter-Follower

D.3.a Initial Linearity

Let's consider the emitter follower illustrated in Figure 207.

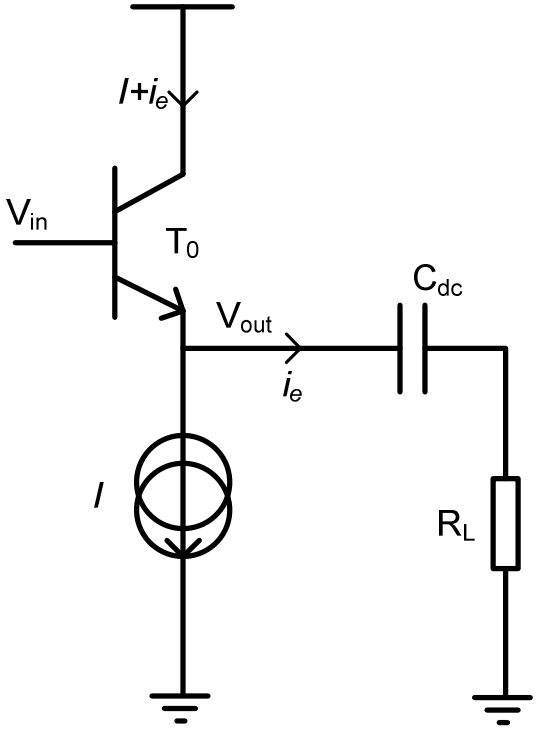

Figure 207. Emitter Follower Schematic

Assuming that collector and emitter currents are equal, the current flowing through the load R_L can be approximated to i_e. Hence [D.2]:

$$i_e = \frac{v_{out}}{R_L} \tag{D.27}$$

Then, considering a biasing current I, the output can be computed by:

$$V_{out} + v_{out} = V_{in} + v_{in} - U_T \ln\left(\frac{I + i_e}{I_s}\right) \tag{D.28}$$

Computing, this leads to:

$$V_{out} + v_{out} = V_{in} + v_{in} - U_T \ln\left(\frac{I + \frac{v_{out}}{R_L}}{I_s}\right) \tag{D.29}$$

Thus

$$V_{out} + v_{out} = V_{in} + v_{in} - U_T \ln\left(1 + \frac{v_{out}}{R_L I}\right) + U_T \ln\left(\frac{I_s}{I}\right) \tag{D.30}$$

Now, DC biasing leads to

$$V_{out} = V_{in} + U_T \ln\left(\frac{I_s}{I}\right), \tag{D.31}$$

which simplifies equation (D.30).

Since the term $\frac{v_{out}}{R_L I}$ is close to 0, it is possible to develop Equation (D.31) with a Taylor series, which gives:

$$v_{in} = v_{out} + U_T\left[\frac{v_{out}}{R_L I} - \frac{1}{2}\left(\frac{v_{out}}{R_L I}\right)^2 + \frac{1}{3}\left(\frac{v_{out}}{R_L I}\right)^3 + o\left(\left(\frac{v_{out}}{R_L I}\right)^3\right)\right] \tag{D.32}$$

Hence

$$v_{in} \approx \left(1 + \frac{U_T}{R_L I}\right)v_{out} - \frac{1}{2}\frac{U_T}{(R_L I)^2}v_{out}^2 + \frac{1}{3}\frac{U_T}{(R_L I)^3}v_{out}^3 \tag{D.33}$$

This expression is of the form

$$v_{in} = a v_{out} + b v_{out}^2 + c v_{out}^3 \tag{D.34}$$

and we are looking for a solution of the type

$$v_{out} = A v_{in} + B v_{in}^2 + C v_{in}^3 \tag{D.35}$$

to compute the IIP3 of the emitter-follower stage.

This leads to:

$$v_{in} = a\left(A v_{in} + B v_{in}^2 + C v_{in}^3\right) + b\left(A v_{in} + B v_{in}^2 + C v_{in}^3\right)^2 + c\left(A v_{in} + B v_{in}^2 + C v_{in}^3\right)^3 \tag{D.36}$$

Limiting to third order terms, we obtain:

$$v_{in} = aA v_{in} + \left(aB + bA^2\right)v_{in}^2 + \left(aC + cA^3\right)v_{in}^3 \tag{D.37}$$

Identifying the two sides of this equation gives a system:

$$aA = 1 \tag{D.38}$$

$$aC + cA^3 = 0 \tag{D.39}$$

Hence

$$A = \frac{1}{a} = \frac{1}{1 + \frac{U_T}{R_L I}} = \frac{R_L I}{U_T + R_L I} \tag{D.40}$$

and

$$C = -\frac{c}{a^4} = -\frac{U_T}{3(R_L I)^3}\left(\frac{R_L I}{U_T + R_L I}\right)^4 = -\frac{U_T R_L I}{3(U_T + R_L I)^4} \ . \tag{D.41}$$

This leads to:

$$v_{out} \approx \frac{R_L I}{U_T + R_L I} v_{in} + B v_{in}^2 - \frac{U_T R_L I}{3(U_T + R_L I)^4} v_{in}^3 \tag{D.42}$$

Now

$$IIP3 = \sqrt{\frac{4}{3}\left|\frac{a}{c}\right|} \tag{D.43}$$

And so

$$\boxed{IIP3 = 2\sqrt{\frac{\left(U_T + R_L I\right)^3}{U_T}}} \tag{D.44}$$

D.3.b Enhancement by Means of a Feedback Loop

Let's consider the emitter follower illustrated in Figure 208, which is constituted of a feedback loop by means of transistor T_1.

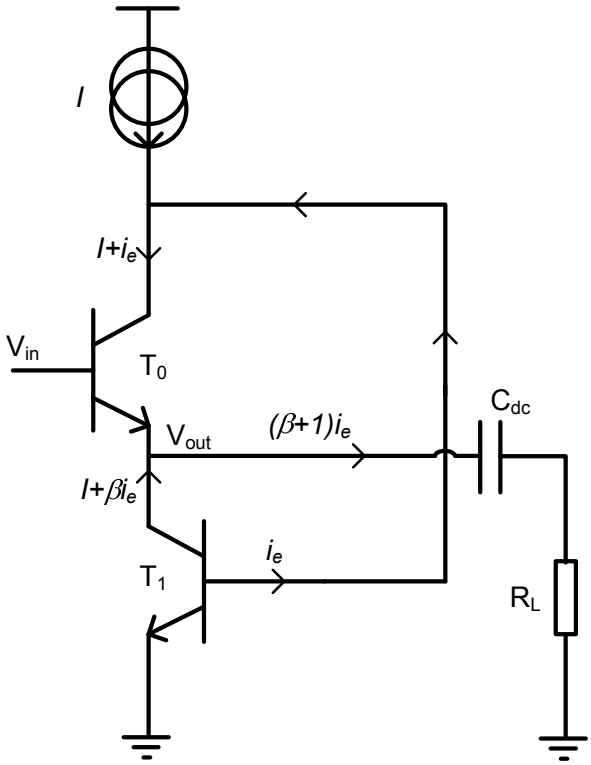

Figure 208. Emitter Follower with Feedback Loop Schematic

Assuming that collector and emitter currents are equal, the current flowing through the load R_L can be approximated to i_e. Hence:

$$(\beta + 1) i_e = \frac{v_{out}}{R_L} \tag{D.45}$$

It is also assumed that biasing current flows mainly through T_0 and T_1.
Then, considering a biasing current I, the output can be computed by:

$$V_{out} + v_{out} = V_{in} + v_{in} - U_T \ln\left(\frac{I + i_e}{I_s}\right) \tag{D.46}$$

Computing, this leads to:

$$V_{out} + v_{out} = V_{in} + v_{in} - U_T \ln\left(\frac{I + \frac{v_{out}}{(\beta+1)R_L}}{I_s} \right) \tag{D.47}$$

The method used to find the IIP3 of the emitter-follower leads to the linearity with the feedback loop with almost the same computations:

$$\boxed{IIP3 = 2\sqrt{\frac{(U_T + (\beta+1)R_L I)^3}{U_T}}} \tag{D.48}$$

Comparing equation (D.44) and (D.48), it has been demonstrated that IIP3 is enhanced by the current gain β of transistor T_1.

D.4 References

[D.1] B. Razavi, *Design of Analog CMOS Integrated Circuits*. McGraw-Hill, 2001.

[D.2] Paul R. Gray, Paul J. Hurst, Stephen H. Lewis, and Robert G. Meyer, *Analysis and Design of Analog Integrated Circuits (fourth edition)*, John Wiley & sons, Inc. 2001.

Personal Bibliography

International Conferences

[SJ.1] S. Jolivet, S. Amiot, D. Lohy, B. Jarry, and J. Lintignat, “A 45–470MHz Gm-C tunable RF bandpass filter for TV tuners designed in 65nm CMOS,” in *New Circuits and Systems Conference (NEWCAS), 2011 IEEE 9th International*, 2011, pp. 13-16.

[SJ.2] S. Jolivet, S. Amiot, O. Crand, S. Bertrand, B. Jarry, and J. Lintignat, “A High Dynamic Range Fully-Active 45-240MHz Tunable RF Bandpass Filter for TV Tuners,” in *European Solid-State Circuits Conference (ESSCIRC), 2011 IEEE 37th International*, 2011, pp. 315-318.

National Conference

[SJ.3] S. Jolivet, S. Amiot, B. Jarry, and J. Lintignat, “Filtre RF passe-bande de type "Rauch" accordable en fréquences pour les récepteurs TV,” *Journées Nationales Micro-ondes (JNM),* 2011.

Table of Figure

Table of tables

Résumé :

La présente thèse étudie les limitations et les opportunités résultant de l'utilisation de circuits purement actifs comme alternative aux circuits passifs classiques pour la réalisation d'un filtrage RF pour récepteur TV. Ce filtrage RF doit être accordable en fréquence, sélectif et à hautes performances en termes de bruit et de linéarité. Après étude de l'état de l'art, deux structures de filtres ont été étudiées plus en détails et simulées, sur une topologie passe bande du second ordre qui est celle qui répond le mieux à nos spécifications. Les filtres Gm-C proposés ont des performances intéressantes mais limitées car le gyrateur dégrade le signal RF. Un filtre de Rauch est proposé par ailleurs avec le but de créer un filtre hautement linéaire pour augmenter la dynamique. Une rétroaction originale permet l'utilisation de ce filtre avec un bon compromis sélectivité – amplification, ainsi que de très bonnes performances RF. Ce filtre a été réalisé sur silicium et mesuré en laboratoire, menant à une très bonne corrélation des résultats. Enfin, les deux structures proposées ont été comparées à l'état de l'art de la littérature grâce à une figure de mérite. Une perspective intéressante à ce travail est également introduite à travers les filtres *N-path*, qui fournissent des résultats encourageants mais qui nécessitent un remaniement de l'architecture du récepteur TV.

Mots clés : Filtre actif, Filtre Gm-C, Filtre de Rauch, Filtre accordable en fréquence, Linéarisation de Transconducteurs, CMOS 65nm, BiCMOS 0,25µm, Récepteurs TV.

Limitations & Opportunities of Active Circuits for the Realization of a High Performance Frequency Tunable RF Selectivity for TV Tuners

Abstract :

The present manuscript studies the limitations and the opportunities resulting in using fully-active circuits as an alternative to classical passive solutions for the realization of an RF filtering for TV tuners. This RF filtering has to be frequency tunable, selective and high performances in terms of noise and linearity. After the study of the state-of-the-art, two structures of filter are studied in details and simulated on a second order bandpass topology which best fulfills the required specifications. Proposed Gm-C filters have interesting performances but are limited by the gyrator which is the main source of degradation of the RF signal in this structure. A Rauch filter is also proposed with the purpose of designing a highly linear filter to increase the dynamic range. An original feedback allows using this filter with a good selectivity – gain trade-off, as well as high RF performances. This filter has been integrated on silicon and measured in laboratory, leading to perfect agreement with simulations. Proposed Gm-C and Rauch structures are compared to state-of-the-art results from the literature by means of an innovative figure-of-merit. An interesting perspective to this work is proposed though the study of N-path filters which exhibit encouraging results but may require important changes in the TV tuner architecture to be used at full potential.

Keywords : Active filter, Gm-C filter, Rauch filter, Frequency Tunable filter, Transconductor linearization, 65nm CMOS, 0.25µm BiCMOS, TV tuners.